Optimizing drug delivery in oncology using imaging and therapeutic ultrasound

Josanne Sophia de Maar

OPTIMIZING DRUG DELIVERY IN ONCOLOGY USING IMAGING AND THERAPEUTIC ULTRASOUND

Josanne Sophia de Maar

Optimizing drug delivery in oncology using imaging and therapeutic ultrasound

Optimale medicijnverdeling bij kanker met behulp van beeldvorming en therapeutisch ultrageluid

(met een samenvatting in het Nederlands)

Proefschrift

ter verkrijging van de graad van doctor aan de
Universiteit Utrecht
op gezag van de
rector magnificus, prof.dr. H.R.B.M. Kummeling,
ingevolge het besluit van het college voor promoties
in het openbaar te verdedigen op

donderdag 26 januari 2023 des middags te 12.15 uur

door

Josanne Sophia de Maar

geboren op 3 maart 1992
te Groningen

Promotoren:
Prof. dr. E. van der Wall
Prof. dr. C.T.W. Moonen

Copromotoren:
Dr. R.H.R. Deckers
Dr. B.B.M. Suelmann

Beoordelingscommissie:
Prof. dr. S.C. Linn
Prof. dr. S. Siesling
Prof. dr. H.J. Bloemendal
Prof. dr. R. de Bree
Prof. dr. ir. C.A.T. van den Berg

TABLE OF CONTENTS

Voor mijn opa's, voor de blik van de dokter en het perspectief van de patiënt

INTRODUCTION AND THESIS OUTLINE

INTRODUCTION

In the recent years much progress has been made in cancer treatment. Besides the traditional therapies such as chemotherapy, surgery and radiotherapy, targeted therapy and immunotherapy are increasingly being used and have clearly contributed to the improved outcome of patients with cancer.

Overall, survival of patients with cancer in the Netherlands is improving [1]. However, better survival rates have not been observed equally between cancer types. A well-known explanation is phenotypic heterogeneity in tumours and their micro-environment, which has genetic and non-genetic causes [2]. Because of this, some (parts of) tumours or their metastases are intrinsically less sensitive to a certain therapy. In addition, heterogeneity in the distribution of drugs can be part of the problem. Differences in drug distribution between patients (e.g. pharmacokinetic differences), but also between organs within patients and even within regions of a single tumour or metastasis, contribute to a heterogeneous treatment effect [3-5]. Furthermore, as patients survive longer, long term side effects of the treatments become increasingly relevant [6-9].

This thesis is based on two central concepts.

First, an effective drug is only effective when it reaches the right location at the right dose.

Second, a treatment can be defined as optimal when maximal efficacy is joined by minimal toxicity.

With these concepts in mind, this thesis investigates two methods using therapeutic ultrasound.

    I.   **MR-HIFU hyperthermia** combined with **temperature sensitive liposomes** containing chemotherapy

    II.   **Ultrasound and microbubble therapy**

Both interventions aim to optimize local drug delivery, in order to obtain a maximum therapeutic effect at the target locations, while minimizing healthy tissue damage (toxicity). To bring these therapies from studies in cells (*in vitro*) to patients, clinical trials in veterinary patients can help pave the road to clinical human translation. Obtaining detailed information on patient characteristics using imaging, but also by learning from data of previous patients, could help to further optimize targeted therapy and personalize cancer treatment.

In this introduction, the background and mechanisms behind these two therapeutic ultrasound approaches will be described briefly, as well as the patient populations we expect will benefit from these therapies. Finally, an outline of the chapters in this thesis will be provided.

Ultrasound

Ultrasound is known for its application in imaging. During ultrasound (US) imaging, pulses of ultrasound waves (with a frequency above 20 kHz) are send through tissue. The waves reflect on the demarcation between two types of tissues (with different acoustic impedance) and echoes are detected and converted to a grayscale image which makes distinction between tissues possible [10]. In contrast-enhanced ultrasound (CEUS), gas containing particles (ultrasound contrast agents) are administered to obtain additional information on vascularization or delineation of body cavities. The contrast is caused by the large difference in acoustic properties between liquid (e.g. blood or lymph) and gas, and because the ultrasound pulses cause oscillation of the contrast agent [10-12].

In this thesis, we use ultrasound not just for imaging, but also to enhance local drug delivery. In this setting we use the term therapeutic ultrasound. Two examples of therapeutic ultrasound are MR-guided high intensity focused ultrasound (MR-HIFU) and ultrasound in combination with microbubbles (USMB therapy).

Magnetic resonance-guided high intensity focused ultrasound

MR-HIFU is a truly non-invasive treatment modality, that combines magnetic resonance imaging (MRI) and high intensity focused ultrasound (HIFU) to warm up tissues or to create mechanical effects. In HIFU, transmitted ultrasound waves are focused into one specific point, which has an effect similar to focusing light with a magnifying glass to burn leaves. In the focus point the intensity will be very high and the tissue starts to warm up. Depending on the treatment goal, a tumour can be heated to 55-70°C (thermal tissue ablation) [13-15] or to 40-43 °C (mild local hyperthermia, which we investigate in this thesis) [16-18].

HIFU is commonly performed with magnetic resonance guidance: MRI is used to control which part of the patient is heated (i.e. treatment planning) and MR thermometry measures temperature simultaneously (i.e. treatment guidance) [19].

Ultrasound and microbubble therapy

The second method of therapeutic ultrasound applied in this thesis is ultrasound and microbubble (USMB) therapy. Microbubbles are ultrasound contrast agents: gas-filled particles, 1-10 μm in diameter, with a biocompatible shell generally made of phospholipids or proteins [20, 21]. Examples of microbubbles approved for clinical CEUS are SonoVue (which contains sulphur hexafluoride (SF6) gas), Definity and Optison (both containing perfluorocarbons). In addition to its role in CEUS imaging, the combination of ultrasound and microbubbles has the potential to locally enhance the delivery of drugs. When exposed to low-intensity ultrasound, microbubbles will oscillate, which is called stable cavitation. Microbubbles exposed to higher intensities will collapse violently, called inertial cavitation. Both types of cavitation induce a number of effects, collectively known as sonopermeation, which can improve drug delivery to tumour tissue. These effects include formation of pores in cell membranes (sonoporation), enhanced endocytosis and increased vascular

permeability [22, 23]. Furthermore, both increased and decreased perfusion after USMB have been described [24].

Nanomedicine and lyso-thermosensitive liposomal doxorubicin

To improve local drug delivery, MR-HIFU induced hyperthermia can be combined with (temperature-sensitive) nanomedicine. Nanomedicine aims to improve the balance between efficacy and safety of drugs by targeting drug-loaded nanometre scale particles specifically to tumours [25]. These nanomedicines include polymeric nanoparticles, liposomes, micellar nanoparticles, protein nanoparticles and inorganic and metallic nanoparticles. A small number of nanomedicines are currently used in the clinic, such as pegfilgrastim (PEGylated G-CSF protein), liposomal doxorubicin, liposomal irinotecan and nab-paclitaxel (albumin-bound paclitaxel nanoparticles) [26, 27]. Liposomes are nanoparticles which consist of a phospholipid bilayer with an aqueous core [28]. In this thesis, we propose the use of the nanomedicine lyso-thermosensitive liposomal doxorubicin (LTLD, also known as ThermoDox), containing the drug doxorubicin. The composition of the phospholipid bilayer makes the liposome temperature sensitive and suitable for heat-triggered release of doxorubicin. The cytotoxic (chemotherapy) drug doxorubicin is frequently used for the treatment of a wide range of cancers, including breast cancer. LTLD is administered intravenously. When heated to 40-42 °C, LTLD releases doxorubicin in the blood stream within seconds [29-31]. In this way, a high concentration of doxorubicin can be achieved in a heated tumour (3-25 fold higher than with conventional doxorubicin in small animals [32-34]). At normal body temperature (circa 37 °C), doxorubicin slowly leaks from the liposome, and after two hours all of the doxorubicin is released [29]. Without heating, LTLD leads to a similar biodistribution [35, 36] and antitumour efficacy [30, 33] compared to conventional doxorubicin. Several tumour heating methods have been used in combination with LTLD, also in clinical studies [37-41]. In this thesis we propose a study of magnetic resonance-guided high intensity focused ultrasound (MR-HIFU) induced hyperthermia.

Patient populations in this thesis

The methods to improve drug delivery investigated in this thesis are proposed for two groups of patients. The first group consists of patients with *de novo* metastatic breast cancer (MBC) or "*de novo* stage IV", for whom we have designed a clinical trial of LTLD plus MR-HIFU hyperthermia. Because this is the first in-human trial to evaluate this combined treatment, we considered that evaluating safety and feasibility in a study population without a curative intent was most feasible and in line with common practice in phase I trials. However, we expect that future patients with earlier stage breast cancer will benefit from the combination of LTLD plus MR-HIFU hyperthermia in the setting of neoadjuvant chemotherapy. Applying this treatment in the neoadjuvant setting could lead to more complete pathological responses, possibilities for less extensive, or even without surgery,

increase the amount of radically removed tumours and possibly decrease local recurrence rates. If safety and feasibility are sufficiently proven in patients with *de novo* MBC, we will proceed with a clinical trial in the neoadjuvant setting.

The second group contains patients with head and neck cancer, where we think USMB therapy could provide a benefit in patients with locally advanced tumours in whom radical surgery often is difficult or disfiguring. In these patients USMB could potentially facilitate radical surgery with less local morbidity and, by obtaining cancer-free margins, also reduce the risk of local recurrences. In order to bridge the gap from *in vitro* results to clinical patients we performed a study in the third population described below: veterinary patients with the feline equivalent of head and neck cancer.

1. *De novo metastatic breast cancer*

In the Netherlands, yearly around 14,500 patients are diagnosed with invasive breast cancer [42]. Around 5% present with *de novo* MBC: these patients have distant metastases at the time of their primary breast cancer diagnosis [43]. In the majority of patients diagnosed with metastatic (stage IV) disease, the metastases are diagnosed in the years that follow their breast cancer diagnosis, so called metachronous MBC. When patients present with *de novo* MBC, the question arises what the best approach will be in dealing with both the local breast tumour and the distant metastases. Although many studies have suggested that local treatment of the breast tumour in patients with *de novo* MBC would provide a survival benefit [44-46], recent randomized studies have refuted this [47, 48]. Usually, these patients are treated with palliative systemic treatment such as chemotherapy, endocrine therapy or targeted therapy. Because they have both local disease (in the breast) and distant metastases (elsewhere) patients with *de novo* MBC make a valuable study population to evaluate both the local and the systemic efficacy and toxicity of new therapies (such as LTLD plus MR-HIFU hyperthermia).

2. *Head and neck cancer*

Head and Neck Squamous Cell Carcinoma (HNSCC) affects approximately 3,000 new patients yearly in the Netherlands[49]. This group of cancers is located in the head and neck region (for example in the mouth, nose, larynx or pharynx). Most patients present with locally advanced disease [50, 51], where primary surgery is often not an option, because the tumour cannot be removed completely or because surgery would create unacceptable local damage. Combinations of chemotherapy, targeted or immunotherapy and radiotherapy are being used [52]. Despite treatment with combined modalities, up to half of the patients develop local recurrences, which are in most cases incurable [53, 54]. Moreover, treatment is associated with undesired acute and long-term toxicity [8, 9, 55]. The predominance of locally advanced disease and local recurrences emphasizes the

need for improved local therapy, while minimizing local and systemic side effects. For this reason we hypothesize that optimizing local drug delivery using therapeutic ultrasound could benefit these patients.

3. Feline oral squamous cell carcinoma

Since there are many pathophysiologic and genetic similarities between head and neck cancer in humans and in cats, feline oral squamous cell carcinoma (FOSCC) patients are a valuable model to bridge the gap between *in vitro* and small animal studies and human patients with head and neck cancer [56-58]. An additional advantage towards clinical translation is that due to the size of cats, it is possible to use the same clinical equipment used in humans, while for small animal experiments often dedicated equipment is necessary.

FOSCC is very common in aged cats, 10% of all tumours diagnosed in cats are oral tumours, of which 61.2% is squamous cell carcinoma[59]. Cats are often presented in an advanced stage of disease [60]. As in human HNSCC, cancer is often locally invasive and most cats succumb to local disease progression [58, 61].

Standard of care treatment options of oral squamous cell carcinoma in cats are similar to those in humans. Surgery is performed if possible and adjuvant radiotherapy can be added if resection is known or suspected to be incomplete. Primary radiation therapy, with palliative or curative intent, is an alternative in non-resectable disease, which can be combined with chemotherapy as a radiosensitizer [62-64]. Supportive care alone is also common and results in a median overall survival time of approximately 1.5 months. [65].

OUTLINE OF THE THESIS

In **part 1 (chapter 1)** we discuss heterogeneity in drug distribution, which can occur on many scales, ranging from differences in pharmacokinetics and -dynamics between patients to heterogeneity within a single tumour, all potentially leading to a heterogeneous treatment effect (i.e. therapy heterogeneity). We reviewed the role of imaging to evaluate this heterogeneity in the setting of nanomedicine. These imaging techniques can be used to visualize nanoparticle distribution, drug distribution and characteristics of the tumour environment, that influence therapy heterogeneity and thus efficacy. Imaging can help to evaluate therapy effect in a (pre)clinical setting, better understand underlying mechanisms leading to heterogeneity, select patients for personalized treatment and evaluate the effect of methods that aim to address therapy heterogeneity.

In **part 2 and 3** we discuss two of these methods, with the goal to decrease therapy heterogeneity and thus to optimize drug distribution. Both methods use therapeutic ultrasound to increase local drug deposition without increasing side effects. **Part 2**

concerns the combination of MR-HIFU hyperthermia and temperature sensitive liposomes with doxorubicin used in patients with breast cancer. **Chapter 2** provides more insight into the study population of the clinical trial described in chapter 3: patients with *de novo* metastatic breast cancer. Data from the Netherlands Cancer Registry (NCR) were analysed, to compare characteristics, survival and treatment between patients with *de novo* and metachronous MBC in the period 2008-2018. **Chapter 3** describes the design of a phase I clinical trial which will investigate the combination of lyso-thermosensitive liposomal doxorubicin (LTLD, ThermoDox) and Magnetic Resonance guided High Intensity Focused Ultrasound (MR-HIFU). This trial was designed to evaluate safety, tolerability and feasibility of this combination treatment in patients with *de novo* MBC, in whom both local and systemic efficacy and toxicity of the treatment can be monitored. During palliative chemotherapy, conventional doxorubicin will be replaced by intravenous LTLD and the primary tumour in the breast will be warmed by MR-HIFU hyperthermia.

Part 3 discusses therapeutic ultrasound and microbubbles (USMB therapy) to improve drug distribution and illustrates imaging applications of USMB. We hypothesize that USMB therapy could improve treatment for patients with head and neck cancer, as they often have local problems in the primary tumour region. Increasing drug delivery locally without increasing systemic side effects could be beneficial. This part describes the steps that we took to bring this therapy further to the clinic, from *in vitro* to a veterinary trial. In **chapter 4** we investigated the potential of a clinical ultrasound system and clinically available microbubbles to perform USMB *in vitro* and to enhance local chemotherapy effect. **Chapter 5** describes a veterinary clinical trial in cats with feline oral squamous cell carcinoma. These cats, with otherwise limited treatment options, were treated with the combination of bleomycin (chemotherapy) and ultrasound and microbubbles (USMB therapy). During the trial, perfusion of the tumour was evaluated before and after USMB therapy with contrast-enhanced ultrasound, as well as tumour progression, survival duration and owner reported quality of life of the cats. **Chapter 6** is a review concerning new developments in imaging for sentinel node biopsy in patients with head and neck cancer. Several techniques can be used to identify the lymph node with the highest change of metastasis based on lymphatic flow and proximity to the primary tumour (the sentinel node). If that lymph node does not contain metastasis, it is considered unlikely that other lymph nodes do. The procedure can help select which patient needs extensive therapy to improve survival, and in which patient this can be omitted, thereby avoiding associated side effects. One of the imaging methods discussed is contrast-enhanced lymphosonography. In this setting ultrasound and microbubbles are not used as therapy but for contrast-enhanced ultrasound imaging of lymphatic flow and accumulation in lymph nodes.

REFERENCES

1. Siesling S, Visser O, Aarts MJ, Verhoeven RHA, Aben KKH, Dinmohamed AG, van Dijk B, van der Aa M, Louwman M, Lemmens VEPP (2019) [Fight against cancer in the Netherlands: current state of affairs] [Article in Dutch]. Ned Tijdschr Geneeskd 163:D4150.

2. Marusyk A, Almendro V, Polyak K (2012) Intra-tumour heterogeneity: a looking glass for cancer? Nat Rev Cancer 12(5):323-334. https://doi.org/10.1038/nrc3261

3. Minchinton AI, Tannock IF (2006) Drug penetration in solid tumours. Nat Rev Cancer 6(8):583-592. https://doi.org/10.1038/nrc1893

4. Tredan O, Galmarini CM, Patel K, Tannock IF (2007) Drug resistance and the solid tumor microenvironment. J Natl Cancer Inst 99(19):1441-1454. https://doi.org/10.1093/jnci/djm135

5. Garattini S, Fuso Nerini I, D'Incalci M (2018) Not only tumor but also therapy heterogeneity. Ann Oncol 29(1):13-18. https://doi.org/10.1093/annonc/mdx751

6. Schmielau J, Rick O, Reuss-Borst M, Kalusche-Bontemps EM, Steimann M (2017) Rehabilitation of Cancer Survivors with Long-Term Toxicities. Oncol Res Treat 40(12):764-771. https://doi.org/10.1159/000485187

7. Haidinger R, Bauerfeind I (2019) Long-Term Side Effects of Adjuvant Therapy in Primary Breast Cancer Patients: Results of a Web-Based Survey. Breast Care (Basel) 14(2):111-116. https://doi.org/10.1159/000497233

8. Nilsen ML, Belsky MA, Scheff N, Johnson JT, Zandberg DP, Skinner H, Ferris R (2020) Late and Long-Term Treatment-Related Effects and Survivorship for Head and Neck Cancer Patients. Curr Treat Options Oncol 21(12):92. https://doi.org/10.1007/s11864-020-00797-x

9. Buchberger AMS, Strzelczyk EA, Wollenberg B, Combs SE, Pickhard A, Pigorsch SU (2021) Report on Late Toxicity in Head-and-Neck Tumor Patients with Long Term Survival after Radiochemotherapy. Cancers (Basel) 13(17). https://doi.org/10.3390/cancers13174292

10. Perera RH, Hernandez C, Zhou H, Kota P, Burke A, Exner AA (2015) Ultrasound imaging beyond the vasculature with new generation contrast agents. Wiley Interdiscip Rev Nanomed Nanobiotechnol 7(4):593-608. https://doi.org/10.1002/wnan.1326

11. Leen E, Averkiou M, Arditi M, Burns P, Bokor D, Gauthier T, Kono Y, Lucidarme O (2012) Dynamic contrast enhanced ultrasound assessment of the vascular effects of novel therapeutics in early stage trials. Eur Radiol 22(7):1442-1450. https://doi.org/10.1007/s00330-011-2373-2

12. Schinkel AF, Kaspar M, Staub D (2016) Contrast-enhanced ultrasound: clinical applications in patients with atherosclerosis. Int J Cardiovasc Imaging 32(1):35-48. https://doi.org/10.1007/s10554-015-0713-z

13. Kim YS, Keserci B, Partanen A, Rhim H, Lim HK, Park MJ, Kohler MO (2012) Volumetric MR-HIFU ablation of uterine fibroids: role of treatment cell size in the improvement of energy efficiency. Eur J Radiol 81(11):3652-3659. https://doi.org/10.1016/j.ejrad.2011.09.005

14. Hurwitz MD, Ghanouni P, Kanaev SV, Iozeffi D, Gianfelice D, Fennessy FM, Kuten A, Meyer JE, LeBlang SD, Roberts A, et al. (2014) Magnetic resonance-guided focused ultrasound for patients with painful bone metastases: phase III trial results. J Natl Cancer Inst 106(5). https://doi.org/10.1093/jnci/dju082

15. Hsiao YH, Kuo SJ, Tsai HD, Chou MC, Yeh GP (2016) Clinical Application of High-intensity Focused Ultrasound in Cancer Therapy. J Cancer 7(3):225-231. https://doi.org/10.7150/jca.13906

16. Chu W, Staruch RM, Pichardo S, Tillander M, Kohler MO, Huang Y, Ylihautala M, McGuffin M, Czarnota G, Hynynen K (2016) Magnetic Resonance-Guided High-Intensity Focused Ultrasound Hyperthermia for Recurrent Rectal Cancer: MR Thermometry Evaluation and Preclinical Validation. Int J Radiat Oncol Biol Phys 95(4):1259-1267. https://doi.org/10.1016/j.ijrobp.2016.03.019

17. Bing C, Patel P, Staruch RM, Shaikh S, Nofiele J, Wodzak Staruch M, Szczepanski D, Williams NS, Laetsch T, Chopra R (2019) Longer heating duration increases localized doxorubicin deposition and therapeutic index in Vx2 tumors using MR-HIFU mild hyperthermia and thermosensitive liposomal doxorubicin. Int J Hyperthermia 36(1):196-203. https://doi.org/10.1080/02656736.2018.1550815

18. Zhu L, Partanen A, Talcott MR, Gach HM, Greco SC, Henke LE, Contreras JA, Zoberi I, Hallahan DE, Chen H, et al. (2019) Feasibility and safety assessment of magnetic resonance-guided high-intensity focused ultrasound (MRgHIFU)-mediated mild hyperthermia in pelvic targets evaluated using an in vivo porcine model. Int J Hyperthermia 36(1):1147-1159. https://doi.org/10.1080/02656736.2019.1685684

19. de Poorter J (1995) Noninvasive MRI thermometry with the proton resonance frequency method: study of susceptibility effects. MRM 34:359-367.

20. Chong WK, Papadopoulou V, Dayton PA (2018) Imaging with ultrasound contrast agents: current status and future. Abdom Radiol (NY) 43(4):762-772. https://doi.org/10.1007/s00261-018-1516-1

21. Frinking P, Segers T, Luan Y, Tranquart F (2020) Three Decades of Ultrasound Contrast Agents: A Review of the Past, Present and Future Improvements. Ultrasound Med Biol 46(4):892-908. https://doi.org/10.1016/j.ultrasmedbio.2019.12.008

22. Deprez J, Lajoinie G, Engelen Y, De Smedt SC, Lentacker I (2021) Opening doors with ultrasound and microbubbles: Beating biological barriers to promote drug delivery. Adv Drug Deliv Rev 172:9-36. https://doi.org/10.1016/j.addr.2021.02.015

23. Snipstad S, Sulheim E, de Lange Davies C, Moonen C, Storm G, Kiessling F, Schmid R, Lammers T (2018) Sonopermeation to improve drug delivery to tumors: from fundamental understanding to clinical translation. Expert Opin Drug Deliv 15(12):1249-1261. https://doi.org/10.1080/17425247.2018.1547279

24. Snipstad S, Vikedal K, Maardalen M, Kurbatskaya A, Sulheim E, Davies CL (2021) Ultrasound and microbubbles to beat barriers in tumors: Improving delivery of nanomedicine. Adv Drug Deliv Rev 177:113847. https://doi.org/10.1016/j.addr.2021.113847

25. Allen TM, Cullis PR (2004) Drug delivery systems: entering the mainstream. Science 303:1818-1822.

26. Bobo D, Robinson KJ, Islam J, Thurecht KJ, Corrie SR (2016) Nanoparticle-Based Medicines: A Review of FDA-Approved Materials and Clinical Trials to Date. Pharm Res 33(10):2373-2387. https://doi.org/10.1007/s11095-016-1958-5

27. Giodini L, Re FL, Campagnol D, Marangon E, Posocco B, Dreussi E, Toffoli G (2017) Nanocarriers in cancer clinical practice: a pharmacokinetic issue. Nanomedicine 13(2):583-599. https://doi.org/10.1016/j.nano.2016.07.012

28. Bangham AD, Standish MM, Watkins JC (1965) Diffusion of univalent ions across the lamellae of swollen phospholipids. J Mol Biol 13:238-252.

29. Al-Jamal WT, Al-Ahmady ZS, Kostarelos K (2012) Pharmacokinetics & tissue distribution of temperature-sensitive liposomal doxorubicin in tumor-bearing mice triggered with mild hyperthermia. Biomaterials 33(18):4608-4617. https://doi.org/10.1016/j.biomaterials.2012.03.018

30. Needham D, Anyarambhatla G, Kong G, Dewhirst MW (2000) A new temperature-sensitive liposome for use with mild hyperthermia: characterization and testing in a human tumor xenograft model. Cancer Res 60:1197-1201.

31. Needham D, Dewhirst MW (2001) The development and testing of a new temperature-sensitive drug delivery system for the treatment of solid tumors. Adv Drug Deliv Rev 53:285-305.

32. Ponce AM, Viglianti BL, Yu D, Yarmolenko PS, Michelich CR, Woo J, Bally MB, Dewhirst MW (2007) Magnetic resonance imaging of temperature-sensitive liposome release: drug dose painting and antitumor effects. J Natl Cancer Inst 99(1):53-63. https://doi.org/10.1093/jnci/djk005

33. Kong G, Anyarambhatla G, Petros WP, Braun RD, Colvin M, Needham D, Dewhirst MW (2000) Efficacy of Liposomes and Hyperthermia in a Human Tumor Xenograft Model: Importance of Triggered Drug Release. Cancer Res 60:6950-6957.

34. Li L, ten Hagen TL, Hossann M, Suss R, van Rhoon GC, Eggermont AM, Haemmerich D, Koning GA (2013) Mild hyperthermia triggered doxorubicin release from optimized stealth thermosensitive liposomes improves intratumoral drug delivery and efficacy. J Control Release 168(2):142-150. https://doi.org/10.1016/j.jconrel.2013.03.011

35. Ranjan A, Jacobs GC, Woods DL, Negussie AH, Partanen A, Yarmolenko PS, Gacchina CE, Sharma KV, Frenkel V, Wood BJ, et al. (2012) Image-guided drug delivery with magnetic resonance guided high intensity focused ultrasound and temperature sensitive liposomes in a rabbit Vx2 tumor model. J Control Release 158(3):487-494. https://doi.org/10.1016/j.jconrel.2011.12.011

36. Staruch RM, Ganguly M, Tannock IF, Hynynen K, Chopra R (2012) Enhanced drug delivery in rabbit VX2 tumours using thermosensitive liposomes and MRI-controlled focused ultrasound hyperthermia. Int J Hyperthermia 28(8):776-787. https://doi.org/10.3109/02656736.2012.736670

37. Zagar TM, Vujaskovic Z, Formenti S, Rugo H, Muggia F, O'Connor B, Myerson R, Stauffer P, Hsu IC, Diederich C, et al. (2014) Two phase I dose-escalation/pharmacokinetics studies of low temperature liposomal doxorubicin (LTLD) and mild local hyperthermia in heavily pretreated patients with local regionally recurrent breast cancer. Int J Hyperthermia 30(5):285-294. https://doi.org/10.3109/02656736.2014.936049

38. Poon RT, Borys N (2011) Lyso-thermosensitive liposomal doxorubicin: an adjuvant to increase the cure rate of radiofrequency ablation in liver cancer. Future Oncol 7(8):937-945.

39. Tak WY, Lin SM, Wang Y, Zheng J, Vecchione A, Park SY, Chen MH, Wong S, Xu R, Peng CY, et al. (2017) Phase III HEAT study adding Lyso-Thermosensitive Liposomal Doxorubicin to Radiofrequency Ablation in patients with unresectable hepatocellular carcinoma lesions. Clin Cancer Res 24(1):73-83. https://doi.org/10.1158/1078-0432.CCR-16-2433

40. Lyon PC, Gray MD, Mannaris C, Folkes LK, Stratford M, Campo L, Chung DYF, Scott S, Anderson M, Goldin R, et al. (2018) Safety and feasibility of ultrasound-triggered targeted drug delivery of doxorubicin from thermosensitive liposomes in liver tumours (TARDOX): a single-centre, open-label, phase 1 trial. Lancet Oncol 19(8):1027-1039. https://doi.org/10.1016/s1470-2045(18)30332-2

41. Gray MD, Lyon PC, Mannaris C, Folkes LK, Stratford M, Campo L, Chung DYF, Scott S, Anderson M, Goldin R, et al. (2019) Focused Ultrasound Hyperthermia for Targeted Drug Release from Thermosensitive Liposomes: Results from a Phase I Trial. Radiology 291(1):232-238. https://doi.org/10.1148/radiol.2018181445

42. IKNL (2021) Breast cancer in the Netherlands, trends 1989 - 2020 based on data from the Netherlands Cancer Registry [Flyer IKNL, title translated from Dutch]. https://iknl.nl/getmedia/fe459c3a-c561-40de-b740-fff15997f020/IKNL-Folder-Borstkanker-2020.pdf. Accessed 15 February 2022

43. Ruiterkamp J, Ernst MF, de Munck L, van der Heiden-van der Loo M, Bastiaannet E, van de Poll-Franse LV, Bosscha K, Tjan-Heijnen VC, Voogd AC (2011) Improved survival of patients with primary distant metastatic breast cancer in the period of 1995-2008. A nationwide population-based study in the Netherlands. Breast Cancer Res Treat 128(2):495-503. https://doi.org/10.1007/s10549-011-1349-x

44. Khan SA (2016) Surgical Management of de novo Stage IV Breast Cancer. Semin Radiat Oncol 26(1):79-86. https://doi.org/10.1016/j.semradonc.2015.08.004

45. Headon H, Wazir U, Kasem A, Mokbel K (2016) Surgical treatment of the primary tumour improves the overall survival in patients with metastatic breast cancer: A systematic review and meta-analysis. Mol Clin Oncol 4(5):863-867. https://doi.org/10.3892/mco.2016.778

46. Soran A, Ozmen V, Ozbas S, Karanlik H, Muslumanoglu M, Igci A, Canturk Z, Utkan Z, Ozaslan C, Evrensel T, et al. (2018) Randomized Trial Comparing Resection of Primary Tumor with No Surgery in Stage IV Breast Cancer at Presentation: Protocol MF07-01. Ann Surg Oncol 25(11):3141-3149. https://doi.org/10.1245/s10434-018-6494-6

47. Tsukioki T, Shien T, Doihara H (2020) Effect of local surgery on outcomes of stage IV breast cancer. Translational Cancer Research 9(8):5102-5107. https://doi.org/10.21037/tcr.2020.01.60

48. Khan SA, Zhao F, Goldstein LJ, Cella D, Basik M, Golshan M, Julian TB, Pockaj BA, Lee CA, Razaq W, et al. (2022) Early local therapy for the primary site in de novo stage IV breast cancer: results of a randomized clinical trial (EA2108). Journal of Clinical Oncology JCO2102006. https://doi.org/https://doi.org/10.1200/JCO.21.02006

49. IKNL (2022) Incidence head and neck cancer [Title translated from Dutch]. https://doi.org/https://iknl.nl/kankersoorten/hoofd-halskanker/registratie/incidentie. Accessed 1 April 2022

50. Braakhuis BJ, Leemans CR, Visser O (2014) Incidence and survival trends of head and neck squamous cell carcinoma in the Netherlands between 1989 and 2011. Oral Oncol 50(7):670-675. https://doi.org/10.1016/j.oraloncology.2014.03.008

51. van der Kamp MF, van Dijk BAC, Plaat BEC, van der Laan B, Halmos GB (2021) To what extent has the last two decades seen significant progress in the management of older patients with head and neck cancer? Eur J Surg Oncol 47(6):1398-1405. https://doi.org/10.1016/j.ejso.2021.01.014

52. Chow LQM (2020) Head and Neck Cancer. N Engl J Med 382(1):60-72. https://doi.org/10.1056/NEJMra1715715

53. Leeman JE, Li JG, Pei X, Venigalla P, Zumsteg ZS, Katsoulakis E, Lupovitch E, McBride SM, Tsai CJ, Boyle JO, et al. (2017) Patterns of Treatment Failure and Postrecurrence Outcomes Among Patients With Locally Advanced Head and Neck Squamous Cell Carcinoma After Chemoradiotherapy Using Modern Radiation Techniques. JAMA Oncol 3(11):1487-1494. https://doi.org/10.1001/jamaoncol.2017.0973

54. Rohde M, Rosenberg T, Pareek M, Nankivell P, Sharma N, Mehanna H, Godballe C (2020) Definition of locally recurrent head and neck squamous cell carcinoma: a systematic review and proposal for the Odense-Birmingham definition. Eur Arch Otorhinolaryngol 277(6):1593-1599. https://doi.org/10.1007/s00405-020-05953-5

55. Szturz P, Wouters K, Kiyota N, Tahara M, Prabhash K, Noronha V, Adelstein D, Van Gestel D, Vermorken JB (2019) Low-Dose vs. High-Dose Cisplatin: Lessons Learned From 59 Chemoradiotherapy Trials in Head and Neck Cancer. Front Oncol 9:86. https://doi.org/10.3389/fonc.2019.00086

56. Supsavhad W, Dirksen WP, Martin CK, Rosol TJ (2016) Animal models of head and neck squamous cell carcinoma. Vet J 210:7-16. https://doi.org/10.1016/j.tvjl.2015.11.006

57. Cannon C (2015) Cats, Cancer and Comparative Oncology. Veterinary Sciences 2(3):111-126. https://doi.org/10.3390/vetsci2030111

58. Wypij JM (2013) A naturally occurring feline model of head and neck squamous cell carcinoma. Patholog Res Int 2013:502197. https://doi.org/10.1155/2013/502197

59. Stebbins KE, Morse CC, Goldschmidt MH (1989) Feline Oral Neoplasia: A Ten-Year Survey. Vet Pathol 26:121-128.

60. Martin CK, Tannehill-Gregg SH, Wolfe TD, Rosol TJ (2011) Bone-invasive oral squamous cell carcinoma in cats: pathology and expression of parathyroid hormone-related protein. Vet Pathol 48(1):302-312. https://doi.org/10.1177/0300985810384414

61. Bostock DE (1972) The prognosis in cats bearing squamous cell carcinoma. J small Anim Pract 13:119-125.

62. Sabhlok A, Ayl R (2014) Palliative radiation therapy outcomes for cats with oral squamous cell carcinoma (1999-2005). Vet Radiol Ultrasound 55(5):565-570. https://doi.org/10.1111/vru.12157

63. Withrow SJ, Vail DM. Withrow and MacEwen's small animal clinical oncology. United States: Saunders Elsevier; 2007. 846 p.

64. Biller B, Berg J, Garrett L, Ruslander D, Wearing R, Abbott B, Patel M, Smith D, Bryan C (2016) 2016 AAHA Oncology Guidelines for Dogs and Cats. J Am Anim Hosp Assoc 52:181-204.

65. Hayes AM, Adams VJ, Scase TJ, Murphy S (2007) Survival of 54 cats with oral squamous cell carcinoma in United Kingdom general practice. J Small Anim Pract 48(7):394-399. https://doi.org/10.1111/j.1748-5827.2007.00393.x

PART I
Introduction of relevant concepts
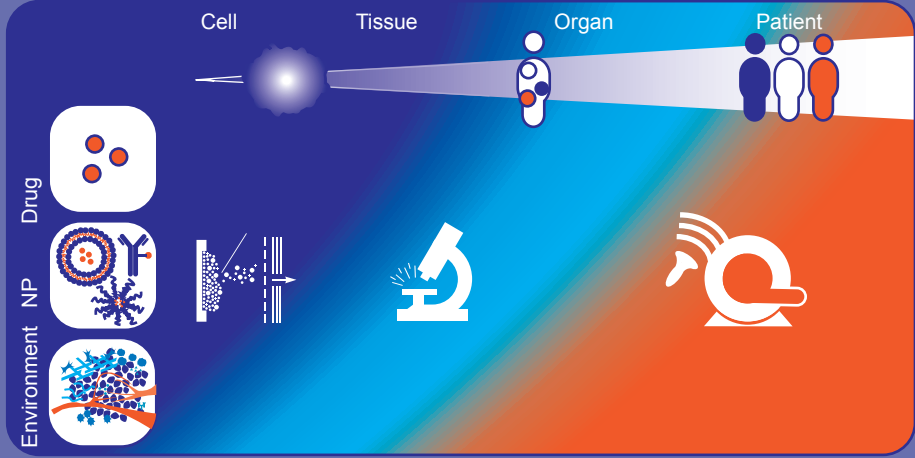
1

SPATIAL HETEROGENEITY OF NANOMEDICINE INVESTIGATED BY MULTISCALE IMAGING OF THE DRUG, THE NANOPARTICLE AND THE TUMOUR ENVIRONMENT

Josanne Sophia de Maar[1], Alexandros Marios Sofias[2], Tiffany Porta Siegel[3], Rob J. Vreeken[3,4],Chrit Moonen[1], Clemens Bos[1], Roel Deckers[1]

[1] Division of Imaging and Oncology, University Medical Center Utrecht, Utrecht University, the Netherlands
[2] Department of Circulation and Medical Imaging, Faculty of Medicine and Health Sciences, Norwegian University of Science and Technology (NTNU), Trondheim, Norway
[3] The Maastricht Multimodal Molecular Imaging Institute (M4I), Division of Imaging Mass Spectrometry, Maastricht University, Maastricht, the Netherlands
[4] Janssen Research & Development, Beerse, Belgium

ABSTRACT

Genetic and phenotypic tumour heterogeneity is an important cause of therapy resistance. Moreover, non-uniform spatial drug distribution in cancer treatment may cause pseudo-resistance, meaning that a treatment is ineffective because the drug does not reach its target at sufficient concentrations. Together with tumour heterogeneity, non-uniform drug distribution causes "therapy heterogeneity": a spatially heterogeneous treatment effect. Spatial heterogeneity in drug distribution occurs on all scales ranging from interpatient differences to intratumour differences on tissue or cellular scale. Nanomedicine aims to improve the balance between efficacy and safety of drugs by targeting drug-loaded nanoparticles specifically to tumours. Spatial heterogeneity in nanoparticle and payload distribution could be an important factor that limits their efficacy in patients. Therefore, imaging spatial nanoparticle distribution and imaging the tumour environment giving rise to this distribution could help understand (lack of) clinical success of nanomedicine. Imaging the nanoparticle, drug and tumour environment can lead to improvements of new nanotherapies, increase understanding of underlying mechanisms of heterogeneous distribution, facilitate patient selection for nanotherapies and help assess the effect of treatments that aim to reduce heterogeneity in nanoparticle distribution.

In this review, we discuss three groups of imaging modalities applied in nanomedicine research: non-invasive clinical imaging methods (nuclear imaging, MRI, CT, ultrasound), optical imaging and mass spectrometry imaging. Because each imaging modality provides information at a different scale and has its own strengths and weaknesses, choosing wisely and combining modalities will lead to a wealth of information that will help bring nanomedicine forward.

INTRODUCTION

In 2015, 17.5 million people were diagnosed with cancer globally and its incidence is increasing. Although the prognosis of most cancer types has improved, still 8.7 million people died of cancer in that year [1]. Rather than a single disease, 'cancer' comprises of a diverse collection of diseases. A high degree of heterogeneity in tumour genotype, phenotype and behaviour (including responsiveness to therapy) exists not only between tumour types, but also between tumours of the same histological type in different patients [2], between primary and metastatic tumours in the same patient , within a patient's tumour that is developing over time [3] and even within a single tumour at one moment [2, 4-10]. The genetic and non-genetic causes of tumour heterogeneity have been reviewed in detail elsewhere. This heterogeneity is an important cause of therapy resistance [3, 11-14] and in some cancer types an association between the degree of intratumoural heterogeneity and a worse prognosis has been found [15-17]. This stresses the importance of evaluating disease heterogeneity and the need for personalized treatment.

Therapy heterogeneity
Therapy heterogeneity, a spatially heterogeneous treatment effect, is another important source of variability between patients and between tumours within an individual. Spatial heterogeneity in drug distribution contributes to therapy heterogeneity and can lead to pseudoresistance: the treatment does not have the desired effect, not because of cellular or genetic mechanisms of resistance, but because the drug simply does not reach all tumour cells at a high enough concentration [18-20]. Moreover, unintended accumulation of drugs in healthy tissue may lead to increased toxicity [18]. Furthermore, heterogeneity in spatial distribution of drugs can generate distinct microenvironments within the tumour, causing intra- and intertumour heterogeneity and, ultimately, influencing clinical outcome.

Spatial heterogeneity of nanomedicine
Heterogeneous drug distribution occurs for drugs of all sizes. In this review we will focus on its impact in the field of nanomedicine. Nanomedicines are sub-micron size drug delivery systems, which are designed to improve the drug delivery to tumours while reducing systemic side effects [21]. Several principles for drug targeting to tumours are described in literature [22]: passive targeting (mainly relying on the enhanced permeability and retention (EPR) effect [23, 24]), active targeting (using carriers decorated with tumour-specific targeting antibodies) or triggered release (drug release from nanocarriers in response to heat, ultrasound or light) [25]. Regardless of the targeting method, nanomedicine has to overcome several physiological barriers before reaching the targeted tumour cells, which may very likely introduce therapy heterogeneity [26].

Scales of heterogeneity

As reviewed by Garattini et al., heterogeneous drug distribution leading to therapy heterogeneity can occur on many scales [18]. On each scale different factors influence the distribution of the nanoparticle and drug.

On patient scale, the inter-patient variability of nanomedicine pharmacokinetics (PK) is influenced by many factors such as age, gender, body composition, prior treatments, and drug-drug interactions [27]. For a number of liposomal nanoparticles, it has been shown that the PK variability of nanoparticles is greater than that of the corresponding small molecule drugs [28]. Clearance of most nanoparticles occurs mainly via the mononuclear phagocyte system (MPS, also known as the reticuloendothelial system) through uptake by circulating and tissue-homing phagocytic cells, primarily in the liver and spleen [29]. One explanation for interpatient differences is that MPS function is affected by age, gender and inflammation [30]. Comorbidity affecting renal function or hepatic function could in turn diminish renal clearance or hepatobiliary excretion of certain nanoparticles. On the other hand, the presence of tumours in the liver increased the clearance of a liposomal campthothecin analogue [31]. Furthermore, due to the accelerated blood clearance (ABC) phenomenon, a second dosage of polyethylene glycol (PEG)ylated nanoparticles is cleared more rapidly, leading to additional inter and intra patient differences [32].

Also on the organ and tumour scale, many factors can contribute to heterogeneity in nanoparticle and drug distribution between different tumours in an individual patient. Accumulation of nanoparticles is tumour type and organ dependent [33]. Tumour locations with limited perfusion or specific barriers such as the blood brain barrier [34] or blood retina barrier [35] can hinder nanoparticle and drug accumulation. A large variation in EPR effect exists between tumour types, sizes and locations, most likely related to variability in tumour blood vessel architecture and function [26, 36]. Likewise, preclinical small animal tumour models generally overestimate the EPR effect compared to tumours in patients, which complicates clinical translation of nanomedicine [37]. Moreover, differences in composition of the tumour microenvironment (including immune cell infiltration, pericyte coverage of the endothelium, density of the extracellular matrix, hypoxia and interstitial fluid pressure (IFP) can lead to intertumour heterogeneity in nanoparticle accumulation and treatment effect [3, 37-40].

Finally, on tissue and cellular scale, there are numerous causes for heterogeneity in drug and nanoparticle distribution within a single tumour. These intratumour differences relate among other things to endothelial cell gaps across the vessel wall, perfusion, extracellular matrix composition and immune cell presence (e.g. tumour associated macrophages, TAM) [3, 19, 38]. Variable endothelial gaps (ranging from one to hundreds of nanometers) result in non-uniform extravasation of nanoparticles into the tumour [41]. Heterogeneity in tumour perfusion will cause non-uniform transport of nanoparticles and nutrients to different parts of the tumour and introduce local variance in oxygenation and tumour pH [19, 38].

Role of imaging to evaluate spatial heterogeneity of nanomedicine

Some nanomedicine formulations are currently used in the clinic [42, 43], but overall the success of nanomedicine has been modest [44-46]. Spatial heterogeneity in distribution of nanoparticles could be an important factor limiting the efficacy in patients and therefore the acceptance of nanotherapy in the clinic. Better understanding of the extent and impact of therapy heterogeneity from cellular to patient scale may increase the success of nanomedicine in clinical practice.

Many imaging methods are available to visualize at a variety of scales the three main factors (i.e. nanoparticle distribution, drug distribution and tumour environment) that influence spatial therapy heterogeneity and thus efficacy. These methods can be used to:

1. Evaluate the effect of the therapy in a preclinical setting, to facilitate the development of new treatments.
2. Improve understanding of the underlying mechanisms that lead to heterogeneous distribution of nanoparticles and drugs.
3. Select patients and predict their treatment response for a personalized treatment plan: which patient likely benefits from a certain therapy and in which patient is adaptation of therapy necessary?
4. Evaluate the effect of methods that aim to address therapy heterogeneity, such as modulating the tumour microenvironment, hyperthermia or sonopermeation [19, 47, 48].

Scope

Over the last years, several excellent review papers on imaging in nanomedicine were published focusing on imaging the biodistribution of nanoparticles [49], imaging labelled nanoparticles [50-52], the role of imaging to evaluate treatments that alter nanoparticle delivery [47], imaging nanoparticles as companion diagnostics [53, 54], or clinical applications of imaging in the field of nanomedicine [55-57]. In this review we will provide a non-exhaustive overview of imaging methods used in the field of nanomedicine, which visualize spatial distribution of nanoparticles or drugs or factors contributing to heterogeneity on different scales, i.e. patient, organ/tumour and tissue/cellular scale. For each method, we will highlight the three main aspects that can be imaged: the drug, the nanoparticle and the tumour (micro-) environment. We will focus on three groups of imaging modalities. A summary of the modalities and their strengths and limitations is presented in Table 1. First we will discuss non-invasive clinical imaging methods, because of their direct usability in clinical translation of nanomedicine. Subsequently, we will elaborate on the most commonly used preclinical modality optical imaging as it is the most frequently employed imaging modality to investigate the interplay between drug, nanoparticle and environment. Optical imaging can be a non-invasive technique in the preclinical setting, while it is invasive clinically. Finally we will discuss mass spectrometry imaging (MSI), an invasive but promising and versatile label-free method for monitoring

drug distribution and effect. Our goal is to show how imaging can provide information on all aspect that influence nanotherapy and in this way will help clinical and preclinical researchers to improve the effectiveness of nanotherapies and translate their use to cancer patients.

NUCLEAR IMAGING: SCINTIGRAPHY/SPECT/PET

Nuclear imaging techniques, namely scintigraphy, Single-Photon Emission Computed Tomography (SPECT) and Positron Emission Tomography (PET) provide highly sensitive quantitative information about the distribution of an administered radiopharmaceutical. They are often combined with CT (SPECT/CT or PET/CT) to add anatomical information and perform attenuation correction. Since the spatial resolution is lower than that of MRI, CT and US imaging, clinical PET and SPECT are mainly informative on patient and organ scale. In the preclinical setting, high-resolution PET and SPECT techniques demonstrate expansion to the tissue scale [58], which is nicely represented by the study of Wang et al. showing the heterogeneous spatial distribution of radiolabelled multi-walled carbon nanotubes in mouse brains with high-resolution SPECT [59].

Currently, the metabolic activity measured with ^{18}F-fluorodeoxyglucose (FDG-) PET/CT is widely used in the clinic for diagnosis and monitoring therapy response. Traditionally several parameters are analysed for diagnosis and prognosis, including maximum standardized uptake values (SUVmax), peak standardized uptake values (SUVpeak), metabolic tumour volume (MTV), and total lesion glycolysis (TLG). Recently, intratumoural heterogeneity of baseline ^{18}F-FDG uptake measured by PET texture analysis has been introduced as new predictive and prognostic factor for neoadjuvant chemotherapy [60-63].

Imaging the nanoparticle

Nuclear imaging has already gained widespread acceptance in the management of cancer using standard chemotherapeutic agents, but may also play an important role in the advancement of nanomedicine towards clinical practice. Historically, nuclear imaging is used to image the distribution of radiolabelled nanoparticles on the patient and organ/tumour scale [47, 49-51, 56, 57]. Already in 1984, Lopez et al. used scintigraphy to track the distribution of Tc-99-m labelled liposomes in cancer patients on organ scale [64]. More recently, studies have used nuclear imaging of radiolabelled nanoparticles as a companion diagnostic to predict treatment response to drug containing nanoparticles or for directly visualizing the distribution of labelled therapeutic nanoparticles [65-69]. The latter approach is nicely illustrated by a clinical study in nineteen HER2-positive metastatic breast cancer patients [69]. HER2-targeted PEG-liposomes containing doxorubicin were administered together with a ^{64}Cu-labelled tracer dose of the same liposomes and their

distribution was imaged by PET/CT. This study was able to demonstrate and quantify the EPR effect in patients and found that tumour liposome concentrations were similar to those found preclinically. Heterogeneity in nanoparticle distribution on the patient and tumour scale was observed and an association was found between the amount of ^{64}Cu-labelled liposome uptake in the tumour and the overall tumour response and progression free survival [69]. Recently, Miedema et al. used PET/CT to track [89]Zr-labelled docetaxel nanoparticles in five patients with various tumour types and observed uptake of the nanoparticles in 35% of the tumours, which they attributed to the EPR effect. Heterogeneous patterns of accumulation were seen on patient and organ scale [70].

Imaging the tumour environment

Furthermore, clinical studies with different tracers are being conducted to extend the use of nuclear imaging to gaining insight into the different aspects of tumour physiology, such as proliferation (e.g. ^{18}F-fluorothymidine (FLT-PET) [71-73]), hypoxia (e.g. ^{18}F-fluoromisonidazole (F-MISO)-PET [55, 74, 75]) and angiogenesis (e.g. with radiolabelled arginine-glycine-aspartic acid (RGD) peptide tracers [76] or vascular endothelial growth factor expression [76, 77]).

Other tracers visualize expression of receptors that can be targeted by drugs (e.g. ^{18}F-fluoroestradiol (FES-) PET [78, 79], human epidermal growth factor receptor 2 (HER2-) PET or SPECT [80]), demonstrate suitability for targeted therapy (e.g. response prediction to tyrosine kinase inhibitors in non-small cell lung cancer [76, 81]), or image tumour specific markers (e.g. prostate specific membrane antigen (PSMA-) PET [82, 83] and radiolabelled somatostatin analogues for neuroendocrine tumours [84, 85]).

Nuclear imaging methods create the possibility to combine imaging of nanoparticle distribution with imaging of characteristics of the tumour environment. A good example of this is the ZEPHIR trial [86], which was able to characterize tumour and therapy heterogeneity on the patient and tumour scale, based on pre-treatment HER2-PET/CT with [89]Zr-trastuzumab and FDG-PET/CT after just one treatment cycle. These two types of PET imaging where used to characterize distribution of the nanoparticle (trastuzumab in T-DM1) and the tumour environment (FDG uptake). In metastatic breast cancer patients, who all had HER2 positive disease on biopsy, the combination of early metabolic response on FDG-PET (significant reduction in FDG uptake in >50% of the tumour load) and positive [89]Zr-trastuzumab uptake (>50% of the tumour load) on the HER2-PET could predict treatment response to the antibody-drug conjugate (ADC) trastuzumab-emtansine (T-DM1) (Fig. 1A) [86]. A preclinical immunohistochemistry study has shown that trastuzumab distribution is also very heterogeneous on the tissue scale and that a large amount of HER2 receptors are never reached by trastuzumab [87]. The ZEPHIR study demonstrates that the inherent problems of characterising the tumour environment by tissue biopsies (i.e. sampling error and overlooking intra- and intertumour heterogeneity) can be circumvented through the use of nuclear imaging.

Imaging the drug

Depending on the nanoparticles' release characteristics, imaging nanoparticle distribution might not necessarily reflect the distribution of encapsulated drugs and thus provide an incomplete view of drug distribution. To avoid the shortcomings of imaging the nanoparticle, the chemotherapeutic drug camptothecin and a photosensitizing agent were conjugated and labelled with ^{64}Cu. In this way, the distribution of the drug conjugate could be imaged even after release from the polymeric nanoparticle. This study showed that a higher amount of the ^{64}Cu-labelled photosensitizing agent was delivered to the tumour when it was conjugated to camptothecin. Accordingly, nanoparticles containing the combination more efficiently inhibited tumour growth than nanoparticles containing either the photosensitizer or camptothecin [88]. Attempts have been made to distinguish the distribution of nanoparticles from the distribution of drugs with nuclear imaging. For example, Lamichhane et al. combined PET and SPECT to image [111In]-Liposomes and the encapsulated [^{18}F]-Fluorinated Carboplatin separately on organ scale. A similar distribution was found for both drug and carrier, with the highest accumulation in the spleen and liver. (Fig. 1B) [89].

MAGNETIC RESONANCE IMAGING

Because of the lack of radiation, its high spatial resolution and excellent soft tissue contrast**.** Magnetic resonance imaging (MRI) is widely used in daily clinical practice for tumour diagnosis, characterisation and response evaluation. MRI is increasingly being investigated in image-guided therapy such as MR-guided radiotherapy (MR-LINAC) [90] and MR-guided High Intensity Focused Ultrasound (MR-HIFU) [91, 92]. Several MRI techniques have been used in nanomedicine research, to characterize the tumour environment and to image the distribution of nanoparticles or (model) drugs on organ/tumour and tissue scale [47, 49, 50, 55, 56, 93].

Imaging the tumour environment

Tumour vascular development and density, as well as perfusion and hypoxia, are key regulators of nanoparticle distribution and nanotherapy effect. Dynamic Contrast Enhanced (DCE-) MRI has been used in clinical trials to evaluate the effect of antivascular treatment on perfusion and vascular permeability [94, 95]. Preclinically, Baker et al. used MRI and histopathology to evaluate factors of the tumour environment that contribute to therapy heterogeneity on tissue level. Distribution of trastuzumab was very heterogeneous. However, area's with little trastuzumab did not correspond with areas that were poorly vascularized [96]. More specifically related to nanomedicine, Activin receptor-like kinase 5 (ALK5) inhibition with A-83-01 was shown to increase accumulation of liposomal Gadolinium (Gd) diethylenetriaminepentaacetic acid

(DTPA) on dynamic MRI [97]. Restricted diffusion on diffusion weighted imaging (DWI) correlates with the cell density of a tumour [98, 99], while Blood Oxygenation Level Dependent (BOLD-) and Tissue Oxygenation Level-Dependent (TOLD-) MRI quantify tumour oxygenation [100, 101]. Hypoxic regions inherently have impaired transport of molecules and in addition hypoxia alters key cellular process such as energy metabolism and cellular receptor uptake and signalling, that can affect both intracellular uptake and efflux of nanomedicine [102].

Imaging the nanoparticle

Iron-oxide nanoparticles have been approved as MRI contrast agent for clinical use. However, they can also function as companion diagnostic or as (imageable) drug delivery systems [103]. For example, Ramanathan et al. conducted a clinical pilot study where they used feromoxytol (FMX) iron nanoparticles (also known as superparamagnetic iron oxide particles, SPION) to predict the deposition of nanoliposomal irinotecan. They showed a correlation between FMX-MRI and tumour response [104]. This companion diagnostic approach could lead to improved patient selection and personalized treatment. Alternatively, tracking the distribution of therapeutic nanoparticles could help with response prediction and early adaptation of a treatment plan. For example Hsu et al. could track the uptake of iron oxide nanoparticles conjugated to tyrosine kinase inhibitor erlotinib at tissue scale, and observed that the particle induced tumour inhibition in non-small cell lung cancer-bearing mice (Fig. 1C) [105]. Also other MRI contrast agents such as manganese and gadolinium have been incorporated in nanoparticles to create paramagnetic nanoparticles that can be imaged with MRI [106, 107]. For instance, Nitta et al. used Gd-dendron modified liposomes to evaluate intratumoural microvasculature with MRI and found a clear difference in vessel architecture between two tumour models. In addition, increased leakage of the liposomes into the tumour tissue was observed after anti-angiogenic sunitinib treatment [108].

Imaging model drugs

Moreover, MRI contrast agents have been encapsulated in nanoparticles as model drugs, to visualize and quantify drug release triggered by temperature, pH or ultrasound sensitive nanoparticles using MRI [93, 109]. Onuki et al. combined two MRI contrast agents to visualize the nanoparticle distribution as well as content release in mice on tissue scale. The mice were treated with poly(D,L-lactide-*co*-glycolide) nano/microspheres, encapsulated with gadolinium-DTPA, SPIONs and the chemotherapeutic drugs 5-fluorouracil. *In vivo*, release of gadolinium-DTPA was seen from 30 minutes after intravenous injection, in the same tumour regions where most of the nanospheres had accumulated [110]. Using MR contrast agents as a model drug is a convenient way to visualize *in vivo* drug release and spatial distribution at tumour and tissue scale. However, these MR contrast agents may influence the stability of nanoparticle [111] and interact

with the co-loaded drug. Furthermore, the tissue distribution of the MR contrast agent and the co-loaded drug may not correspond due to different physicochemical properties of both molecules.

COMPUTED TOMOGRAPHY

Computed tomography (CT) imaging is very commonly used in the clinic for diagnostic purposes and response evaluation after treatment. More recently, it was shown that CT could derive tumour transport properties in patients with pancreatic cancer that correlated with gemcitabine incorporation, pathological response, and oncologic outcome [112]. Yoon et al. showed that CT texture features, as a non-invasive imaging biomarker for the identification of intratumoural heterogeneity, correlated with survival rate in gastric cancer [63].

Imaging the tumour environment

The added value of CT imaging for nanomedicine through identifying tumour transport properties was already shown in the preclinical setting. Dynamic Contrast Enhanced (DCE) CT has been used in several studies to measure the intratumoural perfusion, permeability and the accumulation of CT contrast agent-containing nanoparticles in mice [49, 113-116]. Since intratumoural perfusion is associated with liposome accumulation, DCE-CT could be useful to select patients more likely to respond to treatment with liposomal drugs [117]. Correlations were found between distribution of interstitial fluid pressure, tumour perfusion and the intratumoural accumulation of iohexol-containing liposomes imaged with CT on tissue scale (Fig. 1D) [118]. Spectral CT is another promising technique to image therapy heterogeneity on tissue scale, since it can provide high-resolution imaging and quantification of various components of the tumour microenvironment by taking advantage of differences in their energy-dependent attenuation [119]. Spectral CT has already been utilized to monitor vascular and tumour response to vascular endothelial growth factor (VEGF-) inhibitors in rabbits [120] and to assess angiogenesis clinically [121]. Related to nanomedicine, both tumour vasculature and tumour retention of liposomes has been imaged simultaneously with spectral CT, by administering iodine and Gd liposomes at different intervals before CT imaging [116].

Imaging the nanoparticle

In addition to imaging a contrast agent encapsulated in a nanoparticle, CT can also be utilized to image metallic nanoparticles with a high attenuation of x-rays [49, 122]. For example Mao et al. used CT to image the distribution of gold nanoparticle clusters containing doxorubicin on tissue scale and found that the nanoparticles accumulated mostly in the periphery of the tumour [123]. Because vessels in the tumour periphery are

actually on average less permeable than in the tumour core, these results suggest that EPR is not the only factor in play. Extravasation into the core might, among other factors, be hampered by tumour perfusion and the interstitial tumour matrix [26]. In another study, CT imaging showed that hollow bismuth subcarbonate nanotubes, assembled from ultrasmall nanoclusters and loaded with doxorubicin for chemoradiotherapy, had an increased circulation time and exhibited a stronger EPR effect in mice compared to non-assembled ultrasmall nanoclusters [124].

ULTRASOUND IMAGING

Ultrasound (US) is a low-cost, radiation-free and patient-friendly clinical imaging method that is mostly used for tumour diagnosis and image-guided biopsies. The introduction of contrast-enhanced ultrasound (CEUS), i.e. using microbubbles as ultrasonographic contrast agents, has extended the application of ultrasound in many fields due to improved image quality and new information that cannot be obtained with standard US [125, 126].

Imaging the tumour environment

CEUS can provide anatomical as well as functional information about the vasculature of the tumour (micro-) environment [127-131]. As an example, CEUS with poly (butyl cyanoacrylate)-based microbubbles has been used to image the degree of vascularisation on tumour scale in mice, which was correlated with the degree of EPR-mediated accumulation of a polymeric drug carrier [132]. Moreover, Rojas et al. used targeted sub-micron phase-change contrast agents (liquid perfluorocarbon droplets, that contrary to microbubbles can also provide extravascular contrast) to image angiogenic vessels and perfusion in rats [133].

Tumour environment modelling treatments to improve nanoparticle delivery have been investigated using CEUS. Changes in tumour physiology (i.e. vessel fraction and blood flow) measured by US imaging after collagenase treatment corresponded with changes in IFP, therefore US imaging can be used as an earlier marker of tumour response [134]. Fibrinolytic therapy decompressed blood vessels and improved tumour perfusion was observed with CEUS. Probably related to these physiological changes, the anticancer efficacy of nanoparticle-encapsulated paclitaxel and the penetration of liposomal doxorubicin improved by fibrinolytic therapy [135]. IFP can also be measured directly by US elastography [136].

Recent advances in US imaging such as ultrafast ultrasound and super-resolution techniques provide also information on microvascular properties [137]. Ultrafast Doppler imaging is capable of visualizing the heterogeneous tumour vasculature over time in 3-D with high sensitivity and spatial resolution (80 μm) [138, 139]. Super-resolution

ultrasound imaging technology allows vascular imaging at even higher spatial resolution (~10 µm) [140]. These techniques have already been used for detailed visualization of tumour microvascular morphology [141], characterization of tumour perfusion on tissue scale (Fig. 1E) [142] and monitoring of early tumour response to an angiogenesis inhibiting drug [143] and will soon be of great value for prediction of nanotherapy heterogeneity and response.

Imaging the nanoparticle
In addition to imaging the tumour environment, the distribution of nanoparticles can be imaged by US, using echogenic nanoparticles [144] (e.g. nanobubbles [145, 146], echogenic liposomes [147], polymeric gas-containing nanoparticles [148-150] or combining ultrasound contrast agents with nanoparticles through simultaneous administration or the use of nanoparticle-coated microbubbles [151-153]. Besides the benefits associated with imaging of nanoparticle distribution, ultrasound and microbubbles can improve the therapeutic effect of a drug or nanoparticle through a number of mechanisms, summarized as 'sonopermeation' [154].

Imaging the drug
Although drugs cannot be imaged directly with ultrasound, drug distribution can be visualized. To achieve this, Ektate et al. developed low-temperature sensitive echogenic liposomes, loaded with doxorubicin and perfluoropentane. Tumour hyperthermia led to increased US contrast in mice, which was correlated with increased doxorubicin delivery [147]. Min et al. used a different approach and administered doxorubicin-loaded calcium carbonate polymeric nanoparticles to tumour-bearing mice. In an acidic environment, such as a tumour, the nanoparticles released their doxorubicin load and simultaneously produced carbon dioxide nanobubbles through hydrolysis, which made ultrasound imaging of release at tumour scale possible [155].
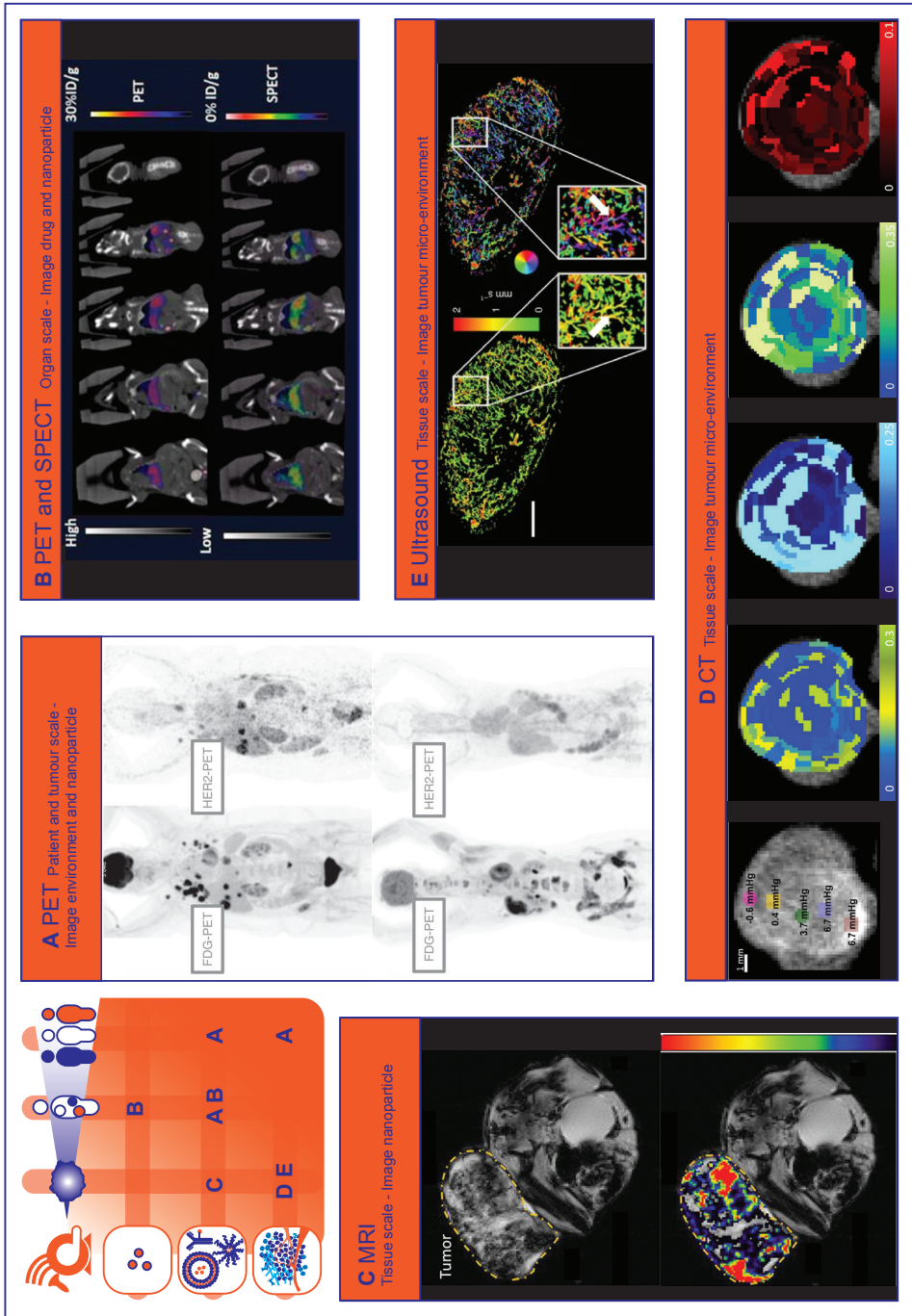
Figure 1 [Legend on the next page]

Figure 1. Non-invasive clinical methods to image spatial heterogeneity of nanomedicine

(A) Patterns of HER2–PET/CT confronted with FDG–PET/CT, Maximum intensity projection. Lesion uptake was considered pertinent when visually higher than blood pool. **Top**: dominant part of tumour load showed tracer uptake. Lung, liver and bone involvement seen of FDG-PET: not all lung lesions are seen on HER2-PET. **Bottom**: entire tumour load lacked tracer uptake. Liver and bone involvement seen on FDG-PET are not seen on HER2PET. *(Adapted with permission from [86], copyright 2016 Oxford University Press on behalf of the European Society for Medical Oncology)*

(B) *In vivo* computed tomography (CT), positron emission tomography (PET)/CT, and SPECT/CT images of a nude mouse injected with 14 MBq of [^{18}F]-FCP encapsulated [^{111}In]-Liposome through tail vein injection 1 h post-administration. Coronal images. Both PET/CT and SPECT/CT images show the uptake of [^{18}F]-FCP encapsulated in [^{111}In]-Liposome in the liver and spleen. Both images correspond to each other in the uptake profile, demonstrating the feasibility of dual-tracer imaging from a single nano-construct. (*Adapted with permission from [89], copyright 2017 MDPI*)

(C) MR T2* images of CL1-5-F4/NF-κB-*luc2*-xenograft-bearing mice treated with erlotinib-conjugated iron oxide nanoparticles. Voxelwise estimates of the intratumoural iron concentration derived from changes in the ΔR2* signal ($P < 0.0001$), which correlates to the amount of intratumoural erlotinib content. **Top**: T2* weighted MR image. **Bottom**: T2*-weighted MR image with color-coded overlay of voxelwise estimates of intratumoural iron concentration *(Adapted with permission from [105], copyright 2018 Elsevier)*

(D) A panel of images showing point-based measurements of IFP overlaid on the intratumoural distribution of CT-liposomes in an orthotopic tumour. Images from **left to right** represent: interstitial Fluid Pressure (IFP); permeability; perfusion; interstitial volume fraction; plasma volume fraction. The coloured circles and corresponding numbers represent the region of interest (ROI) locations, ROI size used for point-based analysis, and measured IFP. Predominantly peripheral CT-liposome enhancement was observed, with some heterogeneous accumulation within the central tumour region. Metrics of perfusion were spatially heterogeneous, but tended to increase towards the tumour periphery. *(Adapted with permission from [118], copyright 2015 Elsevier)*

(E) Motion model ultrasound localization microscopy (mULM). Super-resolution ultrasound images of an A431 tumour provide detailed information on the microvascular architecture including insights into vascular connectivity and the number of vascular branching points (see arrows in magnifications). Functional information such as MB velocities (**left** image) and MB flow directions (**right** image; color-coding illustrating the direction of flow according to the coloured circle) can be determined for each individual vessel and evaluated together with the morphological characteristics. Scale bar=1mm. *(Adapted with permission from [142], copyright 2018 Nature Research)*

OPTICAL IMAGING OF NANOTHERAPY HETEROGENEITY

Optical imaging modalities are used to collect a variety of information on various spatial and temporal scales [156]: from organism to molecule and from static snapshots to real-time continuous dynamic visualization [157]. These techniques are used in preclinical set-ups to provide macroscopic information at organism and organ scales (bioluminescence imaging (BLI), fluorescence imaging (FLI)) [158] or combined in tomographic set-ups to provide three-dimensional distribution profiles at organ and tissue scales (fluorescence diffuse optical tomography (fDOT), fluorescence-mediated molecular tomography (FMT)) [159, 160]. Most importantly, the possibility for high spatial and temporal resolution imaging enables tissue and (sub-)cellular scale imaging in preclinical set-ups via intravital microscopy (IVM) (confocal laser scanning microscopy (CLSM) and two-photon / multiphoton microscopy (MPM)) [161, 162]. Real-time *in vivo* optical imaging modalities are steadily substituting "old-school" *ex vivo* methodology – "dead mice tell too few tales" [163] – and, preclinically, they establish high-resolution alternatives to conventional clinical imaging modalities. In addition, supplementary *ex vivo / in vitro*

optical imaging techniques can provide supportive structural and functional information (immunohistochemistry (IHC) on tissue slices, electron microscopy (EM), flow cytometry imaging). Optical imaging is widely used in the development and evaluation of nanotherapies: molecular imaging helps unravel nanoparticles' complex *in vivo* fate [164, 165], while development of nanoparticles with multimodal-imaging potential [166-170] and state-of-the-art fluorescence-labelling strategies [171, 172] increase the amount and quality of information.

WHOLE BODY FLUORESCENCE IMAGING ON ORGANISM AND ORGAN / TUMOUR SCALE

Traditionally, macroscopic optical imaging modalities are used in preclinical small animal experimental procedures as alternatives to conventional non-terminal / non-invasive whole-body imaging modalities (PET/SPECT, MRI, CT). BLI, one of the most commonly used optical imaging techniques, allows real-time detection of protein-derived native light emission (Fig. 2A). Even though the required genetic engineering (transfection of cancer cell lines, transgenic animals) makes the technique inapplicable to wild type tumours [173], BLI remains a fast and user-friendly option to evaluate nanotherapy efficacy based on the endogenous luminescence of tumours [174-180] to verify nanoparticles' diagnostic or theranostic potential [168, 181, 182], and to combine with other imaging approaches [183]. Another extensively used preclinical imaging technique is whole body fluorescence imaging (FLI), which requires the administration of fluorescent nanoparticles or molecules (Fig. 2A). Whole body FLI allows for a two dimensional organism and organ/tumour scale evaluation of nanotherapy spatial heterogeneity. Researchers use FLI to define nanoparticles' *in vivo* release profile [184], to monitor nanoparticle tumour accumulation [185-189], to determine how specific structural characteristics of nanoparticles alter their tumour accumulation [186], to examine nanoparticles theranostic potential [170, 190-192], to evaluate the performance of nanoparticles as potential single- [193-195] or multimodal [168, 170, 196, 197] imaging probes. Despite the fact that BLI and FLI can be used to delineate solid tumours and detect fluorescent nanoparticles respectively, they fail to provide three-dimensional and deep-tissue information. This disadvantage can be surpassed by integrating fluorescence-driven tomographic techniques [159]. fDOT [173] and fluorescence molecular tomography hybridized with computed tomography (FMT-CT) [198-200] in combination with Near-infrared (NIR-) decorated nanoparticles provide additional three-dimensional spatial information (Fig. 2B).

INTRAVITAL MICROSCOPY ON TISSUE AND (SUB)CELLULAR SCALE

Recent advancements in molecular imaging revealed the dark side of the field of nanomedicine. The scepticism about the EPR effect [39], the demonstration of low targeting efficiency towards tumour cells [201], and even, surprisingly, the incrimination of nanomaterials as metastasis mediators [202] denote that nanoparticle behaviour *in vivo* is highly complex. Therefore, a deeper understanding of *in vivo* behaviour, targeting mechanisms and nanoparticles' specific engagement with cell populations (tumour, stromal, endothelial, immune cells) is essential. Extensive use of real-time imaging techniques like IVM, could potentiate our efforts to characterize the tumour microenvironment on tissue and cellular scale (Fig. 2C) and design nanotherapies with predictable and desired physicochemical and immunobiological behaviour.

Imaging the nanoparticle

Indeed, IVM can provide information regarding nanoparticles' extravasation, diffusion, and penetration into tumours (Fig. 2C). For such purpose, orange/red fluorescence-labelled nanoparticles are most commonly injected together with large molecular weight (e.g. 2 MDa) green fluorescence-labelled dextran to delineate vessels. This two-dye strategy was applied to confirm the silica nanoparticle-based delivery of small interfering ribonucleic acid (siRNA) cancer therapeutics to orthotopic MDA-MB-231 tumours [203]. Similarly, extravasation of 100 nm long circulating liposomes into melanomas in presence / absence of Tumour Necrosis Factor (TNF) co-administration was evaluated. The IVM experiment revealed TNF-mediated vessel permeabilization that led to enhanced liposome extravasation. Unsurprisingly, the TNF-derived benefit was not observed for liposomes of larger size (400, 800 nm) [204], corroborating the realization that nanoparticles much larger than 100 nm cannot extravasate. Alongside qualitative visualization, IVM was utilized for semi-quantitative analysis comparing accumulation of nanoparticles in tumours versus healthy organs [205].

Interestingly, IVM has been used to identify differences in nanoparticle diffusion to tumour sites or nanoparticle tumour targeting, and to correlate them to different physicochemical properties, providing an excellent tool for head-to-head nanoparticle comparisons. The size-dependent diffusion of nanoparticles was studied after administration of a library of small fluorescent quantum dot nanoparticles with diameters of 12, 60 and 125 nm, revealing that 12 nm nanoparticles diffused twice as far in comparison to the largest size particles [206]. Similarly, a size effect was found when attempting to target lymph node metastases with nanoparticles: of three nanoparticles with diameters of 30, 70, and 80 nm, only the smallest reached the metastasis [207]. By comparing the studies that aimed to understand the importance of the nanoparticle size in *in vivo* behaviour, a clear pattern of deeper tissue penetration by smaller nanoparticles

is revealed. In another study low (5 mol %) PEG surface density proved to contribute to a higher targeting specificity of arginylglycylaspartic acid (RGD) nanoparticles, than high (50 mol %) surface PEG density [208]. A head-to-head comparison between the extravasation of a quantum dot and a nanotube sharing similar surface coating, surface area, and charge but different geometry (spherical vs cylindrical respectively) revealed shape-dependent and tumour-dependent extravasation patterns. Of three investigated tumour models, cylindrical single-walled carbon nanotubes were found to extravasate only markedly in a human glioblastoma tumour model, while spherical quantum dots extravasated only in a colon adenocarcinoma tumour model. Surprisingly, no extravasation of either nanoparticle was observed in an ovarian adenocarcinoma tumour model [209]. Comparably, heterogeneity in extravasation patterns between these tumour models was found for RGD-decorated and control quantum dots [210]. The importance of morphology was emphasized when plateloid-shaped microparticles were found to adhere more efficiently to tumour vasculature and exhibit a higher tumour to liver accumulation ratio than cylindroid microparticles [211].

Imaging the tumour environment

In addition to addressing nanoparticle tumour targeting and accumulation profiles, IVM has been used to unravel more intricate interactions between nanoparticles and immune cells; an interesting option given the increasing appeal of cancer immunotherapy. One of the first studies providing real-time insight in the behaviour of TAM, developed magneto-fluorescent nanoparticles enabling the visualization of nanoparticle-labelled TAM on tumour/organ scale (MRI, FMT) and on tissue and cellular scale (IVM). Among other findings, TAM phagocytosed more nanoparticles than other myeloid cells, they were situated in close proximity to tumour cells and displayed low motility [212]. Since nanoparticles tend to accumulate in TAMs, the hypothesis that an increase in TAM population within the tumour microenvironment would also increase nanoparticle accumulation was tested. Application of radiation proved to increase TAM / tumour cell ratio and confirmed this hypothesis: radiation enhanced the accumulation of liposomal doxorubicin in the tumour. IVM experiments showed that the enhanced accumulation was mediated by an increase in 'vascular bursts' (bursts of extravasation of nanoparticles into the tumour tissue) for which the presence of TAM and perivascular phagocytes was required [213]. Of note, the verification that vascular bursts are a driving mechanism for enhanced accumulation of nanoparticles within a tumour, challenges the conventional EPR-effect theory about roughly homogeneously increased leakiness of tumour vasculature [214]. Another immune cell-related variable that has been tested via IVM is the nanoparticle clearance from circulation. Myeloid immune cells proved to be a significant mediator of nanoparticle clearance, as nanoparticles injected in mice pre-treated with clodronate (which causes depletion of phagocytotic cells), circulated in a significantly higher amount in the blood [215].

Given that angiogenesis is a hallmark of cancer, the attention of intravital microscopy users has been directed particularly to nanoparticle-mediated vessel wall visualization and targeting. Already in the mid '00s, a successful attempt using vascular cell adhesion molecule 1 (VCAM-1) decorated nanoparticles paved the way for future success [216]. Subsequently, the development of RGD-decorated multimodal (fluorescence and paramagnetic) quantum dots [217] or nanoemulsions [208] aimed to actively target the αvβ3 integrin receptor overexpressed by angiogenic endothelium. By comparing the above studies, we see that attaching a certain targeting peptide to a nanoparticle alters the nanoparticle's *in vivo* behaviour in a similar manner regardless of the selected nanomaterial, i.e., nanoemulsions versus quantum dots. The multimodal nature of nanoparticles allows for visualization of angiogenic endothelium and neovasculature on tumour/organ scale (MRI, FLI, BLI), tissue scale (IHC and IVM), and cellular scale (IVM) [208, 217]. Of note, IVM strategies of visualizing nanoparticles and immune cells could be expanded outside the field of nanomedicine, for cancer cell imaging [218], which could be used as complementary technique in the analysis of liquid biopsies [219] and in the assessment of tumour heterogeneity [220].

The new mechanistic and molecular insights that were obtained through IVM procedures inspired researchers to develop IVM-specialized imaging agents. Biocompatible organic dots for MPM [221], magneto-fluorescent nanoparticles [222] and fluorescent nanoprobes that detect vascular permeability [223] are among representative examples of nanoparticles aiming to increase the information obtained by imaging.

OPTICAL IMAGING OF DRUGS

Visualization of fluorescent-labelled nanoparticles and related aspects of the tumour microenvironment provide valuable information on therapy heterogeneity in nanomedicine. Imaging the administered drug itself would complete the picture. However, direct imaging of drugs remains elusive. In this respect, inherently fluorescent drugs are convenient [224, 225], and some chemotherapeutic drugs relevant to cancer research possess fluorescent properties (i.e. doxorubicin, mitoxantrone, irinotecan) [226]. The application fluorescent drugs is nicely illustrated by a study that showed colocalization of fluorescent doxorubicin with Kupffer cells outside of tumours in a liver metastasis mouse model after treatment with PEGylated liposomal doxorubicin (Fig. 2E) [225]. Another interesting study from our institution used ex-vivo fluorescence microscopy to quantify tumour tissue doxorubicin concentration and heterogeneity of doxorubicin distribution after treatment of mice with doxorubicin, PEGylated liposomal doxorubicin (Doxil) and temperature-sensitive doxorubicin liposomes (ThermoDox) at three different dosages. Heterogeneity in doxorubicin distribution was visualized on tissue scale and could be compared spatially to heterogeneous vessel perfusion, hypoxia and dividing cell fraction

in the tumour microenvironment [227]. However, *in vivo* imaging of inherently fluorescent drugs is hampered by their relatively low fluorescence quantum yield, which limits their detectability at therapeutic concentrations. Another approach could be the conjugation of fluorescent molecules to the drugs that are carried by nanoparticles, despite the fact that this could result into alternation of their properties. The conjugation of fluorescent dyes to macromolecular drugs has been successfully applied before [87, 96, 228]. In these studies the drugs had a significantly higher molecular weight than the conjugated fluorescent dye, which made their biodistribution properties, targeting specificity and efficacy less likely to be compromised by the dye. Fluorescently labelled therapeutic antibodies have already been administered to patients in early clinical studies [229-231].

TISSUE OPTICAL CLEARING

Utilization of fluorescent molecules is often restricted by factors such limited imaging depth. Therefore, more sophisticated *ex vivo* techniques like the tissue optical clearing strategies [232] have been developed to surpass these limitations [233] by reversing the tissue opacity [234]. The application of such a methodology has been successfully applied to 3D cell spheres [235], tissue samples [236, 237], intact organs [238, 239] and even entire organisms [240]. Even though most of the conducted research is performed in soft tissues and organs, e.g., the brain, the tissue optical clearing strategies appear an appealing methodology for visualizing tissues in which fluorescence signal is heavily scattered, such as the dense connective tissue [241]. Tissue clearing applications provide high quality 3D information and improved mapping of the tissue environment which is useful to investigate the nanoparticle [242-244] and drug [228] distribution at tissue, organ, and organism scale. Additionally, tissue clearing has been used as a tool to study the heterogeneity of immune cell infiltration and therapeutic response in tumour models [245]. Besides its pre-clinical use, tissue clearing methodology has been applied for microscopic assessment of clinical specimens [246].

CLINICAL TRANSLATION OF OPTICAL IMAGING

Due to the limitations in tissue penetration and size of the imageable subject, *in vivo* optical imaging is mainly constricted to preclinical applications. Clinically, optical imaging is of course widely used on *ex vivo* biopsy or surgical samples. Although this consists mostly of immune histochemistry, some work has been done to complement this with fluorescent imaging [247, 248]. To our knowledge, fluorescent imaging has not yet been applied in clinical trials using nanomedicine. However, progress has been made towards translation of the use of silica nanoparticles for intra-operative sentinel node

and tumour detection [249, 250]. In the future ex-vivo analysis of patient biopsies or surgical samples during clinical nanomedicine trials could provide detailed information on therapy heterogeneity on the tissue scale by visualizing nanoparticles, tumour microenvironment and perhaps fluorescent drugs. However, non-invasive in-vivo techniques will probably remain more appealing. Apart from nanomedicine, the clinical use of optical imaging is mostly complementary, with primary focus on intraoperative imaging [248, 251-253] and fluorescence-guided diagnosis [248, 254].

OPTOACOUSTIC IMAGING

Optoacoustic (photoacoustic) imaging is an emerging hybrid technique that combines the benefits of US and optical techniques, i.e. deep imaging depth, high spatial resolution and high contrast [255]. In optoacoustic imaging energy emitted by a pulsed laser source is absorbed by tissue causing its thermoelastic expansion, which generates ultrasound waves that can be detected with conventional ultrasound transducers [256]. The spatial resolution and imaging depth can be adapted to the scale of the preferred application domain, ranging from cellular substructures to organs with the same type of contrast [257]. Optoacoustic signal is mainly provided by endogenous molecules, such as haemoglobin (Hb), melanin, lipids, and collagen, or exogenous contrast agents such as small-molecule dyes, gold nanoparticles and liposomes [258, 259].
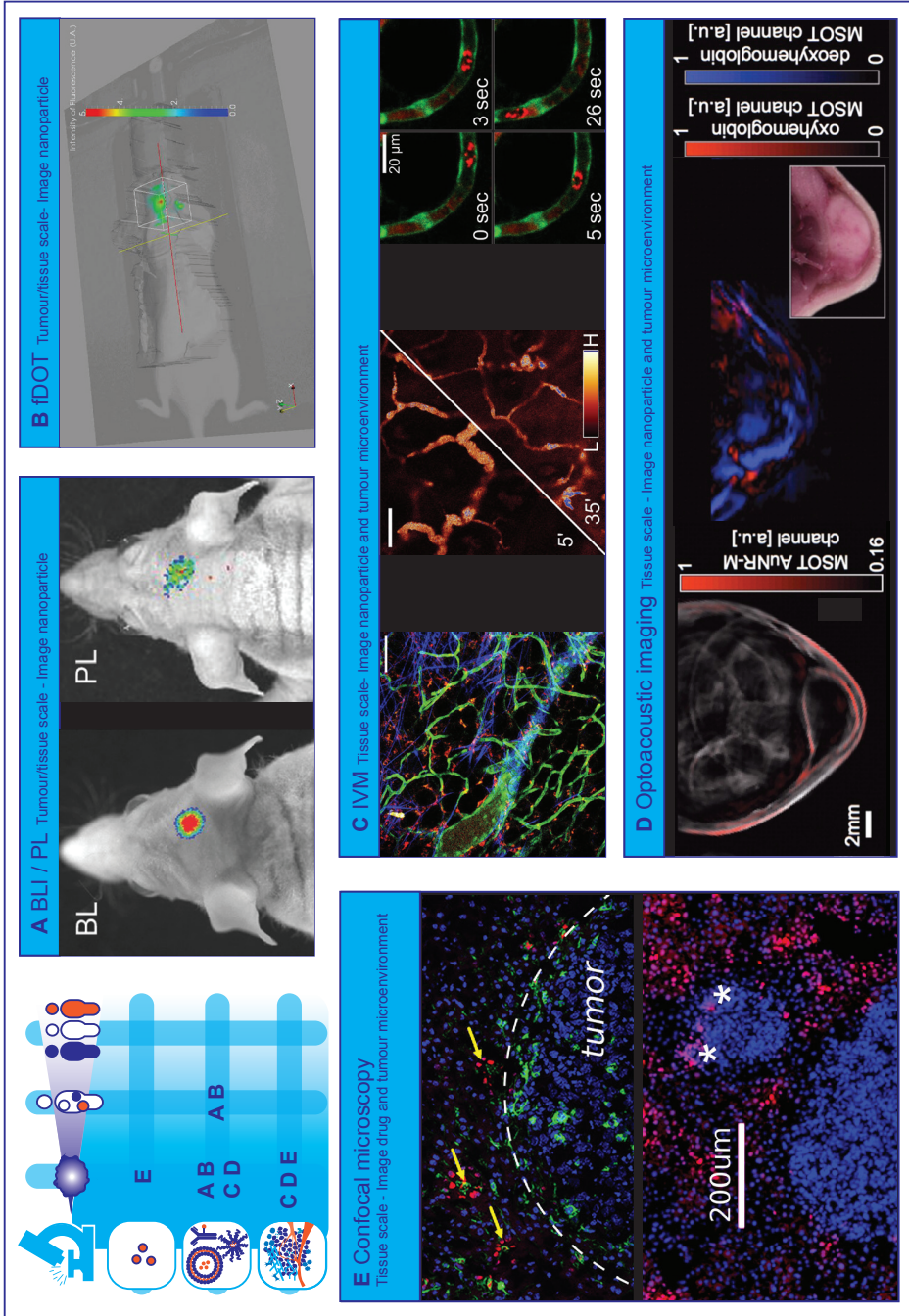
Figure 2 [Legend on the next page]

Figure 2. Optical technologies to image spatial heterogeneity of nanomedicine
(A) Combination of bioluminescence imaging (BLI) of luciferase expressing glioblastoma and photoluminescence (PL) imaging of theranostic photonic nanoparticles to verify nanoparticle tumour targeting efficacy. *(Adapted with permission from [181], copyright 2016 Wiley).*
(B) 3D fluorescence-enhanced diffuse optical tomography (fDOT) image after injection of NIR-decorated nanoparticles in tumour-bearing mouse. *(Adapted with permission from [173] copyright 2012 SPIE Digital Library).*
(C) Representative examples of real-time intravital microscopy (IVM) used to visualizing tumour microenvironment and track nanoparticles. The combination of bright-field illumination, non-linear optical imaging effects, endogenous fluorescence, and i.v. administration of fluorescent dyes contribute to a high quality tumour microenvironment characterization. **Left**: Green fluorescent protein (GFP) expressing endothelium (green) in a TIE2GFP mouse, 70 KDa TMR-dextran positive TAM (red), collagen (blue). **Middle**: Rhodamine-labelled nanoemulsions, passive diffusion on inflamed tissue over 30 min. **Right**: Atto633-labelled Doxil-like liposomes in circulation (red blur within vessel) and phagocytosed by a slow-moving circulating immune cell (red blob), GFP expressing endothelium (green) on TIE2GFP mouse (green). Scale bars 100 µm (right: 20 µm). *(A.M. Sofias and S. Hak, unpublished data).*
(D) Multispectral Optoacoustic Tomography (MSOT) images of nude mouse with A2780 tumour **Left**: gold nanorod accumulation (overlaid in red) 24 hours after injection **Right**: MSOT images of oxyhemoglobin (red) and deoxyhemoglobin (blue) distribution visualizes vasculature. *(Adapted with permission from [277], copyright 2012 Radiological Society of North America (United States))*
(E) Heterogeneity of transport and structural properties of 4T1 breast cancer metastases in mouse liver. Several magnified metastases with different sizes and the red fluorescence of extravasated doxorubicin delivered by PEGylated liposomal doxorubicin (PLD) and colocalizing (yellow arrows) with Kupffer cells (green) outside tumours; stars denote doxorubicin fluorescence in tumours, the white-dashed line indicates the tumour *boundary (Adapted with permission from [225], copyright 2018 Elsevier)*

Imaging the tumour environment

In the oncology domain the endogenous contrast is typically used to study tumour vasculature [260, 261] and oxygenation status (Hb) [262, 263] at cellular scale [264] as well as at tissue scale [265]. Whereas targeted exogenous contras agents enable the readout of a specific biological entity or process such as Epidermal Growth Factor Receptor (EGFR) expression [266] or matrix metalloproteinase activity [267]. By using multiple wavelength illumination (i.e. Multispectral Optoacoustic Tomography (MSOT)) it is possible to differentiate the contribution of different contrast agents and analyse their concentration and distribution simultaneously. In the work of Tomaszewski et al. MSOT imaging of endogenous contrast (i.e. signals from oxy- and deoxyhaemoglobin) and exogenous contrast (signals from the FDA approved organic dye indocyanine green (ICG)) allowed for the non-invasive assessment of tumour vascular function, hypoxia, and necrosis revealing a complex, yet consistent network of relationships in the tumour vascular microenvironment [262]. Okumura et al., in turn, showed the potential of photoacoustic imaging coupled with ICG for evaluating changes in tumour vascular permeability associated with antiangiogenic therapy [268]. ICG rapidly binds to albumin in plasma, becoming a macromolecule that is not able to extravasate from vessels with intact endothelium. Reduced vessel permeability after anti-VEGF therapy, perceived as photoacoustic signal decrease in the tumour, was detected before inhibition of tumour growth indicating the potential of optoacoustic imaging as early marker of therapy response. Reporter gene products such as β-galactosidase [269], tyrosinase [270, 271] and fluorescent proteins [272] have also been used to produce contrast for optoacoustic imaging. Recently, Peters et al. introduced a

new approach for creating optoacoustic imaging contrast by injecting phototrophic purple bacteria into tumours, which allowed them to monitor *in vivo* spatiotemporal changes of macrophage activity [273]. The spatiotemporal distribution and activity of macrophages are very relevant for nanomedicine since macrophages are increasingly being used for targeting nanoparticles towards tumour cells [274].

Imaging the nanoparticle

Nanocarriers not only serve as optoacoustic contrast agent, but can also act as vehicles for drugs. Several nanoparticles have been loaded with drugs and combined with optoacoustic imaging for non-invasive and real-time monitoring of biodistribution and pharmacokinetics [275, 276]. Herzog et al. used the MSOT approach to investigate the accumulation over time of long-circulating gold nanorods as well as intratumoural patterns of hemoglobin oxygenation to demonstrate imaging of the EPR effect (Fig. 2D). Higher nanorod accumulation was seen in the tumour model with a higher fraction of deoxygenated haemoglobin, although the underlying mechanism is still unclear [277]. The work by Song et al. illustrates nicely how MSOT is applied for whole-body visualization of the nanocarrier-based drugs distribution as well as the blood vessels in mice. They demonstrated that the distribution of platinum containing nanoparticles in tumours is highly vascularity-dependent, and could only access the peripheral region of the tumours [278]. Similarly, Kim et al. used bioconjugated gold nanocages as a contrast agent for quantitative molecular optoacoustic tomography of melanomas and surrounding blood vessels at microscopic scale *in vivo* [279]. These gold nanocages have already been used for triggered drug delivery [280]. Another interesting approach is to use pulsed laser irradiation, intrinsically part of optoacoustic instrumentation, as a stimulus for triggered drug release [281]. Here, low-intensity laser irradiation was used for photoacoustic imaging, while high-intensity laser irradiation induced the vaporization of perfluorohexane loaded in the nanoparticle and triggering the fast release of the co-loaded drug paclitaxel.

Imaging the drug

In order to monitor the drugs themselves using optoacoustic imaging they should exhibit NIR-absorbing properties. Unfortunately, few if any clinically prescribed drugs have strong intrinsic absorption in the NIR. As an alternative, small molecule NIR dyes are co-loaded with drugs of interest to monitor drug release and distribution [282]. An alternative approach for monitoring drug release was recently proposed by Yang et al. [283]. They developed a multifunctional nanotheranostic platform consisting of two optoacoustic imaging probes that allowed for concurrent non-invasive real-time ratiometric optoacoustic imaging of acidic tumour pH and monitoring of pH-induced drug release in living mice.[284]

PHOTOTHERMAL AND PHOTODYNAMIC THERAPY

Optical and optoacoustic imaging have frequently been combined with photothermal therapy (PTT [170, 187, 190, 285]) and photodynamic therapy (PDT [168, 188, 189]) so that the NIR excitation can be used for both imaging and therapy. The recent progress in this field was excellently reviewed by Zhu et al. [286]. In PDT a photosensitizer is administered, which is subsequently activated by external light. In PTT nanoparticles generate heat upon laser light excitation. Nanoparticles (e.g. gold nanoparticles) can act as photothermal agents while simultaneously delivering photosensitizing agents [287]. Clinical trials using these therapies have already been performed [288] and imaging the distribution of photodynamic and photothermal agents could help towards further clinical translation.

MASS SPECTROMETRY IMAGING

Mass Spectrometry Imaging (MSI) is a label free, multiplex technique that is used to visualize the molecular distribution of endogenous compounds such as metabolites[289], lipids [290, 291], proteins and peptides [292-294], as well as drugs [295, 296] and drug delivery systems [297] in biological tissues. MSI therefore has the ability to collect not only drug distribution data but also endogenous compound information related to drug-induced efficacy and toxicity on tissue and cellular scale. This technique is increasingly being used in the pharmaceutical research and development pipeline and has demonstrated its utility from early stage drug discovery to preclinical development and clinical evaluation of tumour response to treatment. MSI is used for i) localizing and quantifying drug and metabolite levels (pharmacokinetics) to study efficacy [295], ii) assessing off target drug accumulation to study toxicity [298, 299], and iii) detecting endogenous biomarkers (pharmacodynamics) for predicting and evaluating treatment response [300].

In MSI spatially defined desorption/ionization methods are used to collect sequentially mass spectra from a small region (pixel) of a tissue sample. Among the multitude of surface sampling techniques, matrix-assisted laser desorption/ionisation (MALDI) uses a laser beam for desorption/ionization of tissue-representative molecules co-crystalized in a solidified matrix; while desorption electrospray ionization (DESI) makes use of an electrically charged solvent spray and in secondary ion mass spectrometry (SIMS), a beam of high energy primary ions (e.g. Ar+, Ga+, In+) is used to release secondary ions from the sample surface. In contrast to MALDI and SIMS where the sample is analysed under vacuum, DESI is non-destructive and performed at atmospheric pressure, which renders the technique more user friendly and through appropriate solvent selection, more tuneable to increase selectivity and/or sensitivity. Depending on the ionization

method used spatial resolution, sensitivity, and the molecules that can be analysed change. Mostly, MALDI is used at 10 to 20 µm spatial resolution, whilst DESI resolution spans 50 µm till 200 µm and SIMS allows for sub-µm resolution. Sensitivity wise DESI outperforms MALDI and SIMS, partly due to increased pixel size (see spatial resolution) and partly due to improved ionization efficiency. Although sensitivity is determined by e.g. physiochemical properties of the compound, typically one requires low µg/g concentrations in the case of DESI and approx. 20 µg/g tissue for detection by MALDI and SIMS.

Imaging the drug

The number of drugs that have been detected using MSI is extensive, ranging from anti-cancer drugs (e.g. paclitaxel [301], sunitinib [302], doxorubicin [303]), antibiotics (moxifloxacin [304], polymyxin [298]), beta blocker propranolol [305] and antipsychotic drug olanzapine [306]. MALDI and DESI are mainly used to study the drug distribution at tissue scale. MALDI MSI images for example showed clearly that the distribution of paclitaxel distribution is very heterogeneous and depends on the histopathological characteristics of the different tumour models investigated (figure 3A) [307]. High performance liquid chromatography (HPLC) analysis of tumour homogenates was not able to detect the heterogeneous drug distribution in tumour sections. The same group also showed that the anti-angiogenic agent bevacizumab induced changes in the tumour microenvironment (i.e. more uniform distribution of vessels and less necrosis).

Bevacizumab led to a more homogeneous distribution of paclitaxel and even though the total tumour paclitaxel concentration was lower, anti-tumour activity was greater [308]. In a comparable study, Torok et al. explored the effect of the intratumoural concentration and distribution of five receptor tyrosine kinase inhibitors on their anti-vascular and anti-tumour activities [309]. They demonstrated that limited tumour tissue drug penetration was the primary source of resistance to angiogenesis inhibitors. Both studies clearly show the impact of drug distribution on pharmacological responses and demonstrate the potential of MALDI-MSI to predict the efficacy of unlabelled small molecule drugs in malignant tissue.

Unlike whole-body autoradiography, which is the standard for quantitative assessment of drug distribution, MSI can detect the parent drug and metabolites simultaneously in a single experiment, without having to label the drug [310, 311]. For example Liu et al. imaged the time-dependent and concentration-dependent permeability and metabolism of irinotecan in tumour organoids. They discovered that the active metabolite SN-38 did not co-localize well with the parent drug irinotecan and the inactive metabolite SN-38G, which may lead to therapy heterogeneity [312]. Bruinen et al. were able to find out using MALDI and DESI that precipitation of crystal-like structures in the cortex of rabbit kidney, which were assumed to cause the renal toxicity, were mainly composed of metabolites and relatively little parent drug (figure 3B) [313].

1

Table. 1 Comparison of modalities to image spatial heterogeneity of nanomedicine

Modality		Drug	Nanoparticle	Environment	Spatial resolution
Non-invasive clinical imaging methods	PET / SPECT	Drug labelled with radioactive tracer (e.g. ^{11}C, ^{18}F and ^{123}I).	NP labelled with radioactive tracer (e.g. ^{64}Cu and ^{89}Zr).	Specific radiotracers for environmental factors such as hypoxia ([^{18}F]-FMISO), proliferation ([^{18}F]-FLT) or angiogenesis.	Clinical: ~4 mm (PET) ~10mm (SPECT) Preclinical: < 1 mm (PET/ SPECT)
	MR contrast agents as model drugs (e.g. Gd- and Mn- chelate).	- Superparamagnetic NP labelled to drugs or other NP - NP incorporating, encapsulating or labelled with MR contrast agents	Particular MRI sequences that can measure perfusion, vascular permeability, diffusion or oxygenation status.	~1 mm (clinical) ~0.1 mm (preclinical)	Slow
	CT contrast agents as model drug (e.g. iodine).	Metallic NP (e.g. gold, bismuth).	Dynamic CT with contrast injection for measuring perfusion and permeability .	50-500 µm	Fast
	US contrast agents as model drug (e.g. nanobubbles).	- Micro- and nanosized echogenic NP - NP labelled with US contrast agents.	- Specific ultrasound modes for measuring flow velocity and stiffness - Contrast-enhanced ultrasound to measure perfusion	50-500 µm	Fast
Optical Imaging	BLI/FLI	- Drug labelled with fluorescent dye - Inherently fluorescent drug - Fluorescent dyes as model drug	NP co-loaded/labelled with fluorescent dye.	- Endogenous luminescence of (tumour) cell populations (BLI) - Specific (antibody-labelled) fluorescent probes to image environmental characteristics	~5 µm
	- Drug labelled with fluorescent dye - Fluorescent dyes as model drug	NP co-loaded/labelled with fluorescent dye.	Specific dyes to image environmental characteristics.	< 1 mm	Medium
	- Drug labelled with fluorescent dye - Inherently fluorescent drug - Fluorescent dyes as model drug	NP co-loaded/labelled with fluorescent dye.	Specific dyes to image environmental characteristics.	Subcellular	Fast
	Fluorescent dye as model drug (e.g. ICG, IRDye800CW).	- Co-loading/labelling with fluorescent dye (e.g. ICG) - NP as optoacoustic contrast agent (e.g. Single-walled carbon nanotubes, gold NP)	- Endogenous contrast (e.g. Hb) - Specific (antibody-labelled) fluorescent probes to image environmental characteristics	1 µm- 1 mm	Fast
Mass Spectrometry Imaging	MSI	Label-free imaging of drugs and metabolites.	Label-free imaging of NP or NP compounds (e.g. phospholipids).	-Label-free imaging endogenous compounds (e.g. metabolites, proteins, lipids). - Imaging of tumour environmental markers (e.g. hypoxia)	1 µm (IMC) 10-20 µm (MALDI) 50-200 µm (DESI) Sub-µm (SIMS)

PET: positron emission tomography; SPECT: single photon emission computed tomography; NP: nanoparticle; F-MISO: fluoromisonidazole; FLT: fluorothymidine; CT: computed tomography; MRI: magnetic resonance imaging; US: ultrasound; BLI: bioluminescence imaging; FLI: fluorescence imaging; fDOT: fluorescence diffuse optical tomography; FMT: fluorescence-mediated

Tempor. res.	Imaging depth	Strengths	Limitations
Slow	Whole body	- Established clinical method - Non-invasive - Images biological processes and metabolic activity - Quantitative - High sensitivity (pM-nM)	- Labelling required - Low resolution - Radiation - Lacks anatomical information: combination with other modality (CT, MRI) often needed - Radiotracers can cause toxicity
	Whole body	- Established clinical method - Non-invasive - High spatial resolution - Physiological and anatomical information	- Contrast-agents can cause toxicity - Not compatible with certain pacemakers, metal implants, claustrophobia etc. - Indirect quantification
	Whole body	- Established clinical method - Non-invasive	- Radiation - Contrast-agents can cause toxicity
	~ 30 cm	- Established clinical method - Non-invasive - Possible therapeutic use in sonopermeation - Anatomical and physiological information - High spatial and temporal resolution - High sensitivity (single MB detection)	- Operator dependent - Visualization difficult behind bone and air cavities
Medium	~1 cm	- Preclinically whole-body imaging possible - Combination of tracers can be used to obtain information on more than one aspect	- Surface-weighted 2D images - Labelling often required - Limited tissue depth penetration - Invasive when used clinically (biopsy or surgery needed)
	1-2 mm	- 3D information - Possibility to combine with CT - Combination of probes can be used to obtain information on more than one aspect	- Labelling often required - Only preclinical use
	1-2 mm	- Preclinically non-invasive real-time method with high spatial and temporal resolution - Combination of probes can be used to obtain information on more than one aspect - High sensitivity (nM to μM)	- 2D information - Labelling often required - Only preclinical use
	1- 20 mm	- 3D information - Imaging at multiple scales - Penetration beyond optical diffusion limit - Combination endogenous and exogenous contrasts can be used to obtain information on more than one aspect	- Labelling often required - Operator dependent - Imaging depth is limited when the blood volume is high
Slow	Not applicable	- Label-free - Endogenous and exogenous compounds can be measured simultaneously to obtain information on more than one aspect - Quantitative measurement	- Invasive both preclinically and clinically (biopsy or surgery needed) - Susceptible to sampling error - Temporal information only with repeated sampling of tissue - Protocol has to be developed specifically for drug of interest

molecular tomography; IVM: intravital microscopy; ICG: indocyanine green; Hb: haemoglobin; MSI: mass spectrometry imaging; IMC: imaging mass cytometry; MALDI: matrix assisted laser desorption ionisation; DESI: desorption electro spray ionisation; SIMS: secondary ion mass spectrometry.

In another example, Groseclose et al. [314] reported on the nephrotoxicity of dabrafenib, an approved drug for treatment of specific tumours in adults. Pre-clinical studies showed renal pathogenesis due to obstructive nephropathy in juvenile rats. MSI allowed for spatial analysis of DAB and its metabolites and determination of the chemical composition of the renal deposits. It showed that the deposits were dabrafenib- and dabrafenib metabolite-free and they were merely composed of calcium phosphate. Hence a better risk assessment for pediatric treatment with dabrafenib was performed. So far, MALDI-MSI cannot yet match the spatial resolution of established methods for intracellular imaging such electron microscopy. However, using SIMS it is possible to map the distribution of drugs within individual cells [315]. For example, SIMS was used to localize the drug amiodarone at therapeutic dosing concentrations in four different cell types (figure 3C) [316, 317]. SIMS was also employed to study the intracellular accumulation of two drugs (p-boronophenylalanine (BPA) and sodium borocaptate (BSH)) used for boron neutron capture therapy [318]. By labelling each drug with a different boron isotope (i.e. 10BPA and 11BSH), they were able to image the subcellular distribution of both drugs independently in the same cell. In a recent paper by Vanbellingen et al. the distribution of the B-cell lymphoma 2 (Bcl-2) inhibitor ABT-737 was studied in a treated A-172 human glioblastoma cell line [319]. They were able to visualize the drug and some endogenous markers on the (sub-)surface of the cells with high spatial (~250 nm) and high mass resolution (m/Δm ~10,000), and absence in the nucleus, confirming site of action.

An alternative and novel MSI technique for imaging drug distribution at subcellular resolution, the so-called imaging mass cytometry (IMC), was introduced in the life sciences by Giessen et al. in 2014 [320]. IMC is based on laser ablation inductively coupled plasma mass spectrometry (LA-ICP-MS), and provides capability to either analyse drugs containing metal ions, like e.g. cisplatin, or use antibodies labelled with a polymer containing (rare-earth) metals (e.g. Europium, Gadolinium, Gold, Platinum). Because these metals all have distinct isotopic patterns and are absent in biological specimens, they can be quantified with high precision. Next the use of laser ablation offers the possibility to excise tissue sample of (sub-)micron size, providing an order improved spatial resolution. Using this technique Chang et al. imaged the platinum distribution at subcellular resolution (1 μm) in patient-derived pancreatic cancer xenograft-bearing mice treated with cisplatin, revealing extensive binding of platinum to collagen fibres in both tumour and normal mouse tissues (Figure 3D) [321]. Theiner and coworkers also employed LA-ICP-MS to localize platinum in the kidney in mice treated with three different Pt-containing drugs. The imaging data revealed that the drugs were mostly located outside of the malignant parts of the samples. This clearly demonstrates that determining average Pt concentrations might overestimate drug uptake and cause misleading conclusions on therapy efficacy [322].

Imaging the nanoparticle

MSI also provides the opportunity to image nanocarriers, such as lipid- and metal-based nanoparticles. Typically nanoparticles are labelled or loaded with a radioactive or fluorescent probe in order to follow the *in vivo* fate after administration. However, this requires additional chemical development and the introduction of the probe may influence the biodistribution of the nanoparticle. Recently, Zandanel et al. showed that MALDI-MSI allows for the simultaneous visualization of the polymeric nanoparticle, the encapsulated drug (doxorubicin) and its metabolite (doxorubicinol) in treated mouse liver [323]. Unfortunately, they didn't show the co-localization of the nanoparticle and the drug in the same tissue section. Fülöp et al. exploited the multiplex nature of MSI even further by determining the spatial distribution and integrity of drug-loaded liposomes in tissue with a single label-free measurement [324]. By imaging two lipids (DPPG and PEG36-DSPE) incorporated in the liposomal bi-layer they were able to visualize the liposome distribution, and in addition they could interrogate the integrity of the liposomes by looking at the co-localization of the two lipid markers (figure 3E) [324]. Furthermore, they examined the presence of remaining blood in the same tissue slice by MALDI imaging of hemoglobin, which allowed determining the localization of the liposomes with respect to the blood vessels.

Xue et al. developed an MSI method that enabled not only the visualization, but also the quantification of the in situ drug (doxorubicin) release from molybdenum disulphide (MoS2) nanosheets [325]. The quantification of the drug release was done calculating the intensity ratios for doxorubicin and MoS2 signals. In two mouse tumour models (H22 and 4T1) they observed that the accumulation of drug-loaded MoS2 nanosheets was high in the spleen and liver, but the tumour tissue accumulation was much lower. However, the highest drug release from carriers was observed in tumour tissue, which was ascribed to higher drug dissociation extent due to the acidic tumour microenvironment.

Imaging the tumour environment

As indicated earlier, mass spectrometry offers unique capabilities for untargeted exploration of biological samples and provides simultaneous information of the distribution of the drug, the nanoparticle and endogenous compounds such as metabolites, lipids and proteins. Therefore, MSI can be used to detect biomarkers associated with disease, molecular changes due to drug treatment and tumour components limiting nanomedicine distribution and effect or augmenting off-target effects.
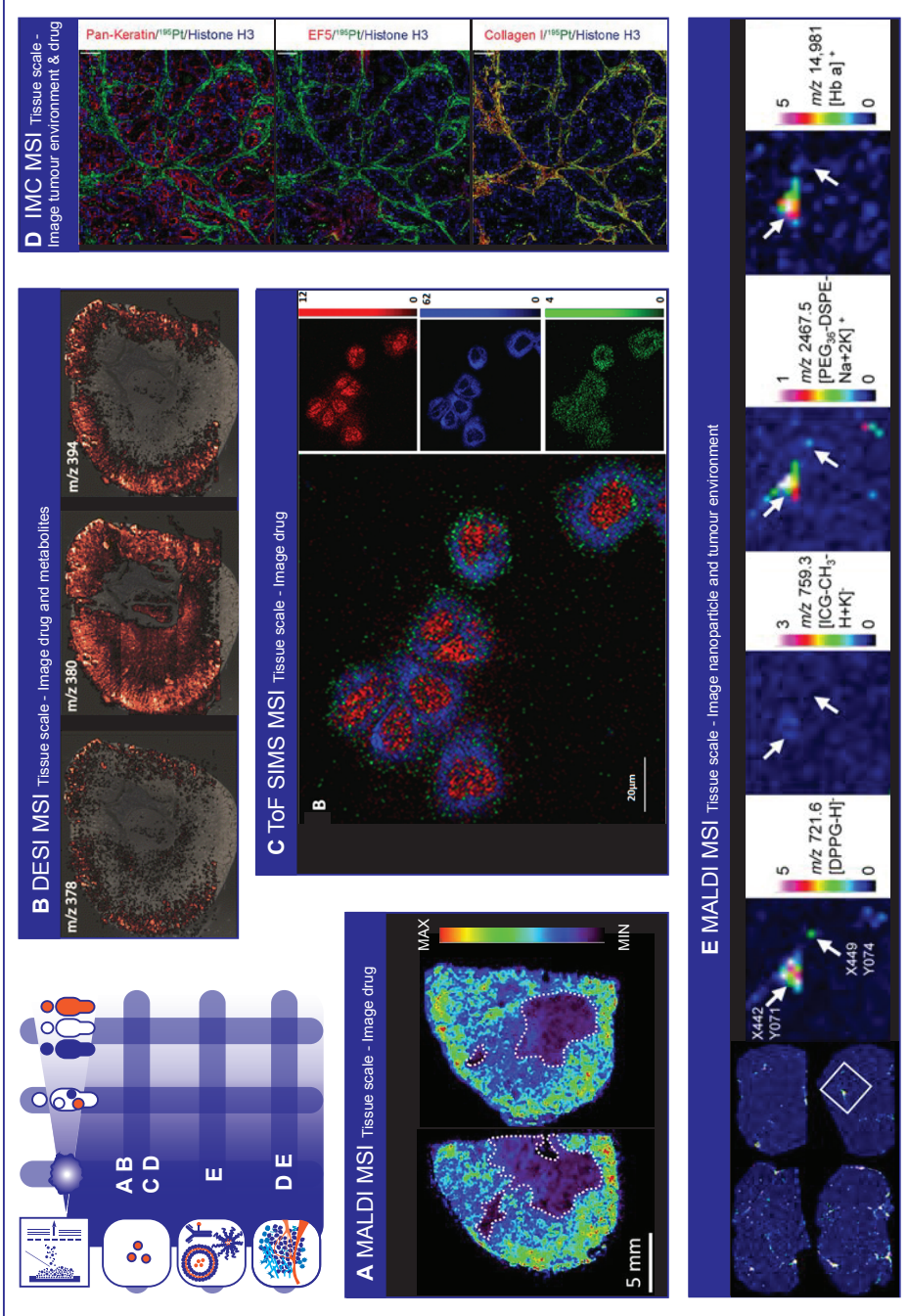
Figure 3 [Legend on the next page]

Figure 3. Mass Spectrometry Imaging to image spatial heterogeneity of nanomedicine
(A) Paclitaxel distribution by MALDI MSI. Necrotic areas, highlighted with dashed lines, are those were there is the lower drug signal. (*Adapted with permission from [307], copyright 2016 Nature Research*)
(B) DESI image overlay representing the spatial distribution of the drug compound (*m/z* 378) and its most abundant metabolites (*m/z* 380 and 394) in a tissue section of a formalin fixed frozen rabbit kidney. (*Adapted with permission from [313], copyright 2016 Springer US*)
(C) ToF SIMS 2D images of 3D data acquired in higher spatial resolution mode from HeLa cells completely consumed by the argon cluster source during analysis. The cells were incubated for 2 h with 9.7 nmol/mL amiodarone hydrochloride. Composite image where red represents ribose *m/z* 81, blue shows the signal from the phosphatidylcholine lipid fragment (m/z 184), and green shows the amiodarone signal, [M + H]+ (*m/z* 646). (*Adapted with permission from [317], copyright 2017 American Chemical Society*)
(D) Cisplatin effects on tumour proliferation, DNA damage and cisplatin distribution in the tumour. Representative Pan-Keratin, EF5, Collagen I, 195Pt, and Histone H3 images of cisplatin-treated (40mg/kg for 24h) mice with OCIP28 patient derived xenografts. Scale bar=100μm. (*Adapted with permission from [321], copyright 2016 Nature Research*)
(E) MALDI MSI images performed on brain slices of mice that were dosed with liposomes. **Four images on the left**: Half of the mice were perfused before being sacrificed (right panels) to reduce the remaining blood in the tissue. MALDI images of liposomal marker 1,2-dipalmitoyl-sn-glycero-3-phosphoglycerol (DPPG) and indocyanine green (ICG) were acquired in reflector negative ion mode, of PEG36-DSPE in reflector positive mode and of Hb α chain in linear positive mode. DPPG, ICG and 1,2-distearoyl-sn-glycero-3-phosphoethanolamine conjugated with monodisperse polyethylene glycol (PEG36-DSPE) were measured with 4-Phenyl-α-cyanocinnamic acid amide (PhCCAA) MALDI matrix. Hb was detected after delipidation and 2,5-dihydroxybenzoic acid (sDHB) deposition on the same tissue region. **Magnifications**: MALDI-MS images of the boxed parts marked in perfused brain in pixels indicated by an arrow shows the co-localisation of the liposomal components and hemoglobin at pixel X442 Y071 and the absence of HB at pixel X449 Y074. (*Adapted with permission from [324], copyright 2016 Nature Research*)

Several studies report that the heterogeneous distribution of lipids and proteins could reflect the effect of therapy and/or could be used as prognostic/predictive marker for outcome. A very nice example of identifying and using endogenous proteomic profiles for distinguishing between responders and non-responders to chemotherapy for oesophageal adenocarcinoma is given by Aichler et al. [326]. Here they selected a series of proteins in pre-therapeutic biopsies, which were identified through liquid chromatography mass spectrometry (LC-MS) analysis and investigated for functional relevance in-vitro. They identified a proteomic signature that was correlated with pre-existing defects in the mitochondrial respiratory chain complexes of cancer cells and was predictive for response to neoadjuvant cisplatin chemotherapy. Yanagisawa et al. reported for the first time in 2003 the ability of MALDI-MSI to generate proteomics patterns of tumour subsets in non-small-cell lung cancer [327]. They showed that protein profiles obtained from tumour tissue samples obtained during surgery could be used to accurately classify tumours and stratify patients into groups associated to poor or good prognosis. Bauer et al. employed MALDI-MSI to identify protein markers differentially expressed in tumour biopsies from patients displaying complete pathological response (pCR) and non-complete pathological response after neoadjuvant paclitaxel/radiation treatment for breast cancer [292]. Proteomic profiling of liver tissue using MALDI-MSI was also used to compare toxicity of hollow CuS nanoparticles and hollow gold nanospheres after intravenous administration in mice [328].

Also tumour hypoxia is investigated by many groups since it is associated with tumour aggressiveness and resistance to cancer treatment. Manscini et al. used MALDI-MSI to simultaneously detect pimonidazole, a clinically used hypoxia marker, its metabolites and associated biomolecules in a single experiment [329]. They detected several endogenous species that co-localized with the hypoxic regions. Interestingly, these identified species are known to be involved in hypoxia or metabolic reprogramming in cancer, although their specific roles remain to be elucidated. Masaki et al. studied the distribution of ^{18}F-fluoromisonidazole (FMISO), a widely used PET hypoxia imaging probe [330]. The mass spectrometry images showed that FMISO and its metabolites were nearly homogenously distributed in the tumour and did not correlate with the radioactivity distribution. However, they identified a glutathione conjugate of amino-FMISO which did co-localise with the radioactive signals and was involved in FMISO accumulation in hypoxic tumour tissues.

Interestingly, most MSI studies that investigate drug distributions do not yet exploit the multiplex capabilities of MSI. Instead of using the wealth of information on endogenous molecule distributions (lipids, proteins, hemoglobin) already available in the acquired MSI image they superimpose the drug MSI images with standard H&E stained tissue images and/or various immunohistochemistry (IHC) images. As most of these IHC images are specific to a certain protein, this can be a laborious and time consuming effort. Moreover, correlating drug distribution with the distribution of these endogenous molecules would allow for non-supervised investigations to discover new factors that impair drug transport in tumour tissue and could be used as biomarker for prognosis and therapy response prediction.

DISCUSSION/ CONCLUSION

Spatial heterogeneity in nanoparticle distribution occurs at all scales and can reduce nanotherapy efficacy. A wide range of imaging modalities help visualize nanoparticle distribution or factors contributing to heterogeneous distribution, by imaging the drug, the nanoparticle and the tumour environment.

Imaging scale

When selecting imaging modalities, researchers need to take into account the desired imaging scale. Non-invasive clinical imaging methods provide three-dimensional information of the intact body on patient, organ and tumour scale, and recent developments, such as super-resolution ultrasound, have broadened their application to provide even tissue scale information. Optical imaging modalities have a superior spatial resolution, procuring images on the tissue and cellular scale, and in the preclinical setting they can provide (sometimes non-invasive) organism and organ

scale information as well. Besides that, *in vivo* applications and intravital techniques offer the possibility to visualize dynamic processes. Clinical use of optical imaging is still hampered by the limited penetration depth and therefore requires tissue sampling or intraoperative use. MSI provides information on tissue and even cellular scale. As it requires a tissue specimen it is inherently an invasive method, regardless of preclinical or clinical use. Due to this limitation, the technique is most suitable and currently most used in the preclinical setting, where an entire tumour or even the whole animal can be analysed at once. In contrast, in the clinic MSI approaches will most likely follow a workflow similar to standard histopathology. Emerging technologies allow for more accurate tissue sampling using intra-procedural multimodality imaging during biopsies [331, 332]. Whenever biopsies are used sampling error is a disadvantage (just as it is for histopathology evaluations) and the technique is therefore less suitable for imaging on organ or tumour scale. Nonetheless, implementation of MSI in clinical research (especially when tissue samples are collected anyway) is feasible and adds a wealth of molecule distribution data on tissue scale. As such, MSI is increasingly becoming an established tool in clinical and pharmaceutical studies.

Intrinsic versus extrinsic contrast

Nuclear imaging methods and most optical imaging methods require labelling of nanoparticles, drugs or aspects of the tumour environment, which has some disadvantages. First, the stability of the link between a label and a nanoparticle determines its usefulness in tracking the nanoparticle, for one could be imaging the label on itself after disconnection from the nanoparticle. Second, attaching a label could change the pharmacokinetic and drug release properties of the nanoparticle leading to erroneous prediction of the distribution of an unlabelled equivalent. Third, administering a labelled version of a previously approved therapeutic nanoparticle or drug could cause additional toxicity and obtaining clinical approval is cumbersome and costly. Fourth, administration of radiolabelled theranostic nanoparticles may decrease the effect of subsequent therapeutic administration through the ABC phenomenon [333]. MSI provides a label-free alternative to obtain detailed tissue and cellular scale information on drugs, nanoparticles and the tumour microenvironment simultaneously.

Multimodal imaging

The integration of imaging data collected from multimodality techniques offers a unique opportunity to combine information related to drug and nanoparticle distribution and tumour environment on multiple scales and provide synergistic advantages over the use of a single modality.

Clinical imaging modalities are generally combined to merge functional (SPECT, PET) with anatomical information (CT, MR) collected on the same scale. A range of nanoparticles for multimodality imaging have been developed [169, 196, 197, 334-336]. On tissue and

cellular scale, successful examples have shown complementarity between optical imaging and MSI techniques [337]. Fluorescence and MSI have been combined to characterize local drug release and map unlabelled therapeutic drug distribution [311]. MSI enabled monitoring of the drug and related metabolites, which were impossible to differentiate with solely fluorescence. The combination of MSI and IMC with IHC and fluorescence *in situ* hybridization (FISH), creates a new dimension to molecular pathology. Now, drug levels within tumour regions can be correlated to different degrees of vascularization of the tumour – highlighted with specific vasculature staining [338]. One of the reported limitations is the impossibility to perform all analyses on the same tissue section. As a consequence and because a tumour is such an heterogeneous system, it is highly probable that two consecutive sections have different morphology / molecular content, which is then difficult to correlate accurately.

To achieve multiscale information, optical imaging and MSI have been paired with clinical imaging [59, 169, 183, 196, 197, 339]. Using dual fluorescent and MRI probes, the high sensitivity of fluorescent imaging is complemented with MRI's ability for deep-tissue penetration and high spatial and temporal resolution [340, 341].

A challenge remains the integration of molecular information provided by 2D / *ex vivo* MSI or optical imaging with 3D / *in vivo* images, such as those generated with SPECT, PET, CT or MRI. This challenge is inherent to the fact that the images are acquired at different scales, can be subjected to different deformations, and lack common fiducial markers. A first step towards combining two-dimensional MSI with three-dimensional MRI is the ability to monitor MRI contrast agents with MSI, which was demonstrated by Tata et al. [342]. They used DESI-MSI to monitor Gadoteridol, to characterize intratumoural heterogeneity and further guide delineation of tumour margins. Coregistration of MSI with other modalities is promising to bridge the gap between the different scales [343-347]. It is worth mentioning that the route towards user-friendly automated methods that are needed to integrate these methods in a routine (clinical) workflow is still long. Nonetheless, multiscale and multi-aspect (i.e. nanoparticle, drug and environment) data is believed to open new doors to improve the characterization of spatially heterogeneous distribution and heterogeneous effect and could greatly contribute in the development of new and more effective nanotherapies.

Role of imaging for clinical translation
Integration of imaging techniques in preclinical lab practice has contributed to an improved understanding of the *in vivo* behaviour of nanoparticles. Additionally, it has led to valuable information on how specific characteristics within the tumour environment can affect nanotherapy outcomes. Continued application of these imaging approaches, and especially the combination of different techniques, will further strengthen our understanding of therapy heterogeneity on organism, tissue, cellular and even subcellular scale. Meanwhile the role of imaging for monitoring PK and biodistribution

is well established in research and development stage, however in the clinical setting it is not yet adopted. Clinically, spatial heterogeneous distribution of therapeutic nanoparticles, poses the threats of under- and overtreatment. Despite the fact that many studies have shown that drug concentration does not correspond with tissue drug levels, phase I and II clinical trials mainly rely on blood samples and spatially sparse biopsies to measure PK on patient scale and biodistribution on organ scale. Imaging drugs or nanoparticles in clinical studies is still rare and often no information is acquired about spatial heterogeneity of nanomedicine on organ, tumour or tissue scale. However imaging drug/nanoparticle distribution can help predict treatment effect and therefore select which patients will benefit most and in which patients a therapy adjustment or a combination therapy that reduces heterogeneity are warranted. Combining imaging of nanoparticle and drug distribution with imaging of tumour environment characteristics or early response indicators promises to help personalize treatment further. Currently, only optical imaging is commonly used to investigate, in the preclinical setting, the interplay between environment, nanoparticle and drug. It is our hope and recommendation that non-invasive clinical imaging and MSI will play a central role in future preclinical and clinical research on the interaction of drug, nanoparticle and environment. Choosing and combining imaging modalities wisely will lay the foundation for successful future nanotherapies.

FUNDING

COMPETING INTERESTS

The authors have declared that no competing interest exists.

ABBREVIATIONS

ABC: accelerated blood clearance;

ADC: antibody-drug conjugate;

ALK5: Activin receptor-like kinase 5;

BLI: bioluminescence imaging;

BOLD: blood oxygenation level dependent;

BPA: p-boronophenylalanine;

BSH: sodium borocaptate;

CEUS: contrast-enhanced ultrasound;

CLSM: confocal laser scanning microscopy;

CT: computed tomography;

DCE: dynamic contrast enhanced;

DESI: desorption electro spray ionisation;

DPPG: 1,2-dipalmitoyl-sn-glycero-3-phosphoglycerol

DTPA: diethylenetriaminepentaacetic acid;

DWI: diffusion weighted imaging;

EGFR: epidermal growth factor receptor

EM: electron microscopy;

EPR: enhanced permeability and retention;

FDG: ^{8}F-fluorodeoxyglucose;

fDOT: fluorescence diffuse optical tomography;

FES: 18F-fluoroestradiol;

FISH: fluorescence in situ hybridization;

FLI: fluorescence imaging;

FLT: 18F-fluorothymidine;

F-MISO: 18F-fluoromisonidazole;

FMT-CT: fluorescence molecular tomography hybridized with computed tomography;

FMT: fluorescence-mediated molecular tomography;

FMX: feromoxytol;

GFP: green fluorescent protein;

Hb: haemoglobin;

HER2: human epidermal growth factor receptor 2;

HPLC: high performance liquid chromatography;

ICG: indocyanine green;

IFP: interstitial fluid pressure;

IHC: immunohistochemistry;

IVM: intravital microscopy;

LA-ICP-MS: laser ablation inductively coupled plasma mass spectrometry;

LC-MS: liquid chromatography mass spectrometry;

IMC: imaging mass cytometry;

MALDI: matrix assisted laser desorption ionisation;

MPM: multiphoton microscopy;

MPS: mononuclear phagocyte system;

MR-HIFU: magnetic resonance guided high intensity focused ultrasound;

MR-LINAC: magnetic resonance linear accelerator;

MRI: magnetic resonance imaging;

MSI: mass spectrometry imaging;

MSOT: multispectral optoacoustic tomography;

MTV: metabolic tumour volume;

NIR: near-infrared;

PDT: photodynamic therapy;

PEG: polyethylene glycol;

PEG_{36}-DSPE: 1,2-distearoyl-sn-glycero-3-phosphoethanolamine conjugated with monodisperse polyethylene glycol;

PET: positron emission tomography;

PhCCAA: 4-Phenyl-α-cyanocinnamic acid amide;

PK: pharmacokinetics;

PL: photoluminescence;

PLGA-PEG: poly(D,L-lactic-*co*-glycolic acid)-*b*-polyethylene glycol;

PSMA: prostate specific membrane antigen;

PTT: photothermal therapy;

RGD: arginylglycylaspartic acid;

sDHB: 2,5-dihydroxybenzoic acid

siRNA: small interfering ribonucleic acid;

SIMS: secondary ion mass spectrometry;

SPECT: single-photon emission computed tomography;

SPION: superparamagnetic iron oxide particles;

SUVmax: maximum standardized uptake values;

SUVpeak: peak standardized uptake values;

TMR: tetramethylrhodamine;

TOF: time of flight;

TAM: tumour associated macrophages;

T-DM1: trastuzumab-emtansine;

TLG: total lesion glycolysis;

TNF: tumour necrosis factor;

TOLD: tissue oxygenation level dependent;

US: ultrasound;

VCAM-1: vascular cell adhesion molecule 1;

VEGF: vascular endothelial growth factor;

REFERENCES

1. Global Burden of Disease Cancer Collaboration, Fitzmaurice C, Allen C, Barber RM, Barregard L, Bhutta ZA, Brenner H, Dicker DJ, Chimed-Orchir O, Dandona R, et al. (2017) Global, Regional, and National Cancer Incidence, Mortality, Years of Life Lost, Years Lived With Disability, and Disability-Adjusted Life-years for 32 Cancer Groups, 1990 to 2015: A Systematic Analysis for the Global Burden of Disease Study. JAMA Oncol 3(4):524-548. https://doi.org/10.1001/jamaoncol.2016.5688

2. Cros J, Raffenne J, Couvelard A, Pote N (2018) Tumor Heterogeneity in Pancreatic Adenocarcinoma. Pathobiology 85(1-2):64-71. https://doi.org/10.1159/000477773

3. Marusyk A, Almendro V, Polyak K (2012) Intra-tumour heterogeneity: a looking glass for cancer? Nat Rev Cancer 12(5):323-334. https://doi.org/10.1038/nrc3261

4. Andor N, Graham TA, Jansen M, Xia LC, Aktipis CA, Petritsch C, Ji HP, Maley CC (2016) Pan-cancer analysis of the extent and consequences of intratumor heterogeneity. Nat Med 22(1):105-113. https://doi.org/10.1038/nm.3984

5. Jamal-Hanjani M, Quezada SA, Larkin J, Swanton C (2015) Translational implications of tumor heterogeneity. Clin Cancer Res 21(6):1258-1266. https://doi.org/10.1158/1078-0432.CCR-14-1429

6. Nassar A, Radhakrishnan A, Cabrero IA, Cotsonis GA, Cohen C (2010) Intratumoral Heterogeneity of Immunohistochemical Marker Expression in Breast Carcinoma A Tissue Microarray-based Study. Appl Immunohistochem Mol Morphol 18(5):433-441.

7. Zhang J, Fujimoto J, Zhang J, Wedge DC, Song X, Zhang J, Seth S, Chow CW, Cao Y, Gumbs C, et al. (2014) Intratumor heterogeneity in localized lung adenocarcinomas delineated by multiregion sequencing. Science 346(6206):256-259. https://doi.org/10.1126/science.1256930

8. Gerlinger M, Catto JW, Orntoft TF, Real FX, Zwarthoff EC, Swanton C (2015) Intratumour heterogeneity in urologic cancers: from molecular evidence to clinical implications. Eur Urol 67(4):729-737. https://doi.org/10.1016/j.eururo.2014.04.014

9. Grzywa TM, Paskal W, Wlodarski PK (2017) Intratumor and Intertumor Heterogeneity in Melanoma. Transl Oncol 10(6):956-975. https://doi.org/10.1016/j.tranon.2017.09.007

10. Liu J, Dang H, Wang XW (2018) The significance of intertumor and intratumor heterogeneity in liver cancer. Exp Mol Med 50(1):e416. https://doi.org/10.1038/emm.2017.165

11. Rybinski B, Yun K (2016) Addressing intra-tumoral heterogeneity and therapy resistance. Oncotarget 7(44):72322- 72342.

12. Dzobo K, Senthebane DA, Thomford NE, Rowe A, Dandara C, Parker MI (2018) Not Everyone Fits the Mold: Intratumor and Intertumor Heterogeneity and Innovative Cancer Drug Design and Development. OMICS 22(1):17-34. https://doi.org/10.1089/omi.2017.0174

13. Saunders NA, Simpson F, Thompson EW, Hill MM, Endo-Munoz L, Leggatt G, Minchin RF, Guminski A (2012) Role of intratumoural heterogeneity in cancer drug resistance: molecular and clinical perspectives. EMBO Mol Med 4(8):675-684. https://doi.org/10.1002/emmm.201101131

14. Dagogo-Jack I, Shaw AT (2018) Tumour heterogeneity and resistance to cancer therapies. Nat Rev Clin Oncol 15(2):81-94. https://doi.org/10.1038/nrclinonc.2017.166

15. Maley CC, Galipeau PC, Finley JC, Wongsurawat VJ, Li X, Sanchez CA, Paulson TG, Blount PL, Risques RA, Rabinovitch PS, et al. (2006) Genetic clonal diversity predicts progression to esophageal adenocarcinoma. Nat Genet 38(4):468-473. https://doi.org/10.1038/ng1768

16. Park SY, Gonen M, Kim HJ, Michor F, Polyak K (2010) Cellular and genetic diversity in the progression of in situ human breast carcinomas to an invasive phenotype. J Clin Invest 120(2):636-644. https://doi.org/10.1172/JCI40724

17. Jamal-Hanjani M, Wilson GA, McGranahan N, Birkbak NJ, Watkins TBK, Veeriah S, Shafi S, Johnson DH, Mitter R, Rosenthal R, et al. (2017) Tracking the Evolution of Non-Small-Cell Lung Cancer. N Engl J Med 376(22):2109-2121. https://doi.org/10.1056/NEJMoa1616288

18. Garattini S, Fuso Nerini I, D'Incalci M (2018) Not only tumor but also therapy heterogeneity. Ann Oncol 29(1):13-18. https://doi.org/10.1093/annonc/mdx751

19. Tredan O, Galmarini CM, Patel K, Tannock IF (2007) Drug resistance and the solid tumor microenvironment. J Natl Cancer Inst 99(19):1441-1454. https://doi.org/10.1093/jnci/djm135

20. Minchinton AI, Tannock IF (2006) Drug penetration in solid tumours. Nat Rev Cancer 6(8):583-592. https://doi.org/10.1038/nrc1893

21. Allen TM, Cullis PR (2004) Drug delivery systems: entering the mainstream. Science 303:1818-1822.

22. Lammers T, Hennink WE, Storm G (2008) Tumour-targeted nanomedicines: principles and practice. Br J Cancer 99(3):392-397. https://doi.org/10.1038/sj.bjc.6604483

23. Matsumura Y, Maeda H (1986) A new concept for macromolecular therapeutics in cancer chemotherapy: mechanism of tumoritropic accumulation of proteins and the antitumor agent smancs. Cancer Research 46:6387-6392.

24. Maeda H (2012) Macromolecular therapeutics in cancer treatment: the EPR effect and beyond. J Control

Release 164(2):138-144. https://doi.org/10.1016/j.jconrel.2012.04.038

25. Arranja AG, Pathak V, Lammers T, Shi Y (2017) Tumor-targeted nanomedicines for cancer theranostics. Pharmacol Res 115:87-95. https://doi.org/10.1016/j.phrs.2016.11.014

26. Rosenblum D, Joshi N, Tao W, Karp JM, Peer D (2018) Progress and challenges towards targeted delivery of cancer therapeutics. Nat Commun 9(1):1410. https://doi.org/10.1038/s41467-018-03705-y

27. Caron WP, Song G, Kumar P, Rawal S, Zamboni WC (2012) Interpatient pharmacokinetic and pharmacodynamic variability of carrier-mediated anticancer agents. Clin Pharmacol Ther 91(5):802-812. https://doi.org/10.1038/clpt.2012.12

28. Schell RF, Sidone BJ, Caron WP, Walsh MD, White TF, Zamboni BA, Ramanathan RK, Zamboni WC (2014) Meta-analysis of inter-patient pharmacokinetic variability of liposomal and non-liposomal anticancer agents. Nanomedicine 10(1):109-117. https://doi.org/10.1016/j.nano.2013.07.005

29. Dobrovolskaia MA, Aggarwal P, Hall JB, McNeil SE (2008) Preclinical studies to understand nanoparticle interaction with the immune system and its potential effects on nanoparticle biodistribution. Mol Pharm 5(4):487-495. https://doi.org/10.1021/mp800032f

30. Yuan D, He H, Wu Y, Fan J, Cao Y (2019) Physiologically Based Pharmacokinetic Modeling of Nanoparticles. J Pharm Sci 108(1):58-72. https://doi.org/10.1016/j.xphs.2018.10.037

31. Wu H, Ramanathan RK, Zamboni BA, Strychor S, Ramalingam S, Edwards RP, Friedland DM, Stoller RG, Belani CP, Maruca LJ, et al. (2012) Population pharmacokinetics of pegylated liposomal CKD-602 (S-CKD602) in patients with advanced malignancies. J Clin Pharmacol 52(2):180-194. https://doi.org/10.1177/0091270010394851

32. Abu Lila AS, Kiwada H, Ishida T (2013) The accelerated blood clearance (ABC) phenomenon: clinical challenge and approaches to manage. J Control Release 172(1):38-47. https://doi.org/10.1016/j.jconrel.2013.07.026

33. Yokoi K, Tanei T, Godin B, van de Ven AL, Hanibuchi M, Matsunoki A, Alexander J, Ferrari M (2014) Serum biomarkers for personalization of nanotherapeutics-based therapy in different tumor and organ microenvironments. Cancer Lett 345(1):48-55. https://doi.org/10.1016/j.canlet.2013.11.015

34. Parodi A, Rudzinska M, Deviatkin AA, Soond SM, Baldin AV, Zamyatnin AA, Jr. (2019) Established and Emerging Strategies for Drug Delivery Across the Blood-Brain Barrier in Brain Cancer. Pharmaceutics 11(5). https://doi.org/10.3390/pharmaceutics11050245

35. Lafond M, Aptel F, Mestas JL, Lafon C (2017) Ultrasound-mediated ocular delivery of therapeutic agents: a review. Expert Opin Drug Deliv 14(4):539-550. https://doi.org/10.1080/17425247.2016.1198766

36. Natfji AA, Ravishankar D, Osborn HMI, Greco F (2017) Parameters Affecting the Enhanced Permeability and Retention Effect: The Need for Patient Selection. J Pharm Sci 106(11):3179-3187. https://doi.org/10.1016/j.xphs.2017.06.019

37. Nichols JW, Bae YH (2014) EPR: Evidence and fallacy. J Control Release 190:451-464. https://doi.org/10.1016/j.jconrel.2014.03.057

38. Jain RK, Stylianopoulos T (2010) Delivering nanomedicine to solid tumors. Nat Rev Clin Oncol 7(11):653-664. https://doi.org/10.1038/nrclinonc.2010.139

39. Danhier F (2016) To exploit the tumor microenvironment: Since the EPR effect fails in the clinic, what is the future of nanomedicine? J Control Release 244(Pt A):108-121. https://doi.org/10.1016/j.jconrel.2016.11.015

40. Dou YN, Chaudary N, Chang MC, Dunne M, Huang H, Jaffray DA, Milosevic M, Allen C (2017) Tumor microenvironment determines response to a heat-activated thermosensitive liposome formulation of cisplatin in cervical carcinoma. J Control Release 262:182-191. https://doi.org/10.1016/j.jconrel.2017.07.039

41. Lee H, Hoang B, Fonge H, Reilly RM, Allen C (2010) In vivo distribution of polymeric nanoparticles at the whole-body, tumor, and cellular levels. Pharm Res 27(11):2343-2355. https://doi.org/10.1007/s11095-010-0068-z

42. Bobo D, Robinson KJ, Islam J, Thurecht KJ, Corrie SR (2016) Nanoparticle-Based Medicines: A Review of FDA-Approved Materials and Clinical Trials to Date. Pharm Res 33(10):2373-2387. https://doi.org/10.1007/s11095-016-1958-5

43. Giodini L, Re FL, Campagnol D, Marangon E, Posocco B, Dreussi E, Toffoli G (2017) Nanocarriers in cancer clinical practice: a pharmacokinetic issue. Nanomedicine 13(2):583-599. https://doi.org/10.1016/j.nano.2016.07.012

44. Park K (2013) Facing the truth about nanotechnology in drug delivery. ACS Nano 7(9):7442-7447.

45. Maeda H, Khatami M (2018) Analyses of repeated failures in cancer therapy for solid tumors: poor tumor-selective drug delivery, low therapeutic efficacy and unsustainable costs. Clin Transl Med 7(1):11. https://doi.org/10.1186/s40169-018-0185-6

46. Hare JI, Lammers T, Ashford MB, Puri S, Storm G, Barry ST (2017) Challenges and strategies in anti-cancer nanomedicine development: An industry perspective. Adv Drug Deliv Rev 108:25-38. https://doi.org/10.1016/j.addr.2016.04.025

47. Blocker SJ, Shields AF (2018) Imaging of Nanoparticle Distribution to Assess Treatments That Alter Delivery. Mol Imaging Biol 20(3):340-351. https://doi.org/10.1007/s11307-017-1142-2

48. Golombek SK, May JN, Theek B, Appold L, Drude N, Kiessling F, Lammers T (2018) Tumor targeting via EPR: Strategies to enhance patient responses. Adv Drug Deliv Rev 130:17-38. https://doi.org/10.1016/j.addr.2018.07.007

49. Arms L, Smith DW, Flynn J, Palmer W, Martin A, Woldu A, Hua S (2018) Advantages and Limitations of Current Techniques for Analyzing the Biodistribution of Nanoparticles. Front Pharmacol 9:802. https://doi.org/10.3389/

fphar.2018.00802

50. Dearling JLJ, Packard AB (2017) Molecular imaging in nanomedicine - A developmental tool and a clinical necessity. J Control Release 261:23-30. https://doi.org/10.1016/j.jconrel.2017.06.011

51. Chakravarty R, Goel S, Dash A, Cai W (2017) Radiolabeled inorganic nanoparticles for positron emission tomography imaging of cancer: an overview. Q J Nucl Med Mol Imaging 61(2):181-204. https://doi.org/10.23736/S1824-4785.17.02969-7

52. Chakravarty R, Hong H, Cai W (2015) Image-Guided Drug Delivery with Single-Photon Emission Computed Tomography: A Review of Literature. Curr Drug Targets 16(6):592-609.

53. Miller MA, Arlauckas S, Weissleder R (2017) Prediction of Anti-cancer Nanotherapy Efficacy by Imaging. Nanotheranostics 1(3):296-312. https://doi.org/10.7150/ntno.20564

54. Ehlerding EB, Grodzinski P, Cai W, Liu CH (2018) Big Potential from Small Agents: Nanoparticles for Imaging-Based Companion Diagnostics. ACS Nano 12(3):2106-2121. https://doi.org/10.1021/acsnano.7b07252

55. Spence T, De Souza R, Dou Y, Stapleton S, Reilly RM, Allen C (2015) Integration of imaging into clinical practice to assess the delivery and performance of macromolecular and nanotechnology-based oncology therapies. J Control Release 219:295-312. https://doi.org/10.1016/j.jconrel.2015.09.036

56. Kunjachan S, Ehling J, Storm G, Kiessling F, Lammers T (2015) Noninvasive Imaging of Nanomedicines and Nanotheranostics: Principles, Progress, and Prospects. Chem Rev 115(19):10907-10937. https://doi.org/10.1021/cr500314d

57. Man F, Lammers T, R TMdR (2018) Imaging Nanomedicine-Based Drug Delivery: a Review of Clinical Studies. Mol Imaging Biol 20(5):683-695. https://doi.org/10.1007/s11307-018-1255-2

58. Deleye S, Van Holen R, Verhaeghe J, Vandenberghe S, Stroobants S, Staelens S (2013) Performance evaluation of small-animal multipinhole muSPECT scanners for mouse imaging. Eur J Nucl Med Mol Imaging 40(5):744-758. https://doi.org/10.1007/s00259-012-2326-2

59. Wang JT, Rubio N, Kafa H, Venturelli E, Fabbro C, Menard-Moyon C, Da Ros T, Sosabowski JK, Lawson AD, Robinson MK, et al. (2016) Kinetics of functionalised carbon nanotube distribution in mouse brain after systemic injection: Spatial to ultra-structural analyses. J Control Release 224:22-32. https://doi.org/10.1016/j.jconrel.2015.12.039

60. Molina-Garcia D, Garcia-Vicente AM, Perez-Beteta J, Amo-Salas M, Martinez-Gonzalez A, Tello-Galan MJ, Soriano-Castrejon A, Perez-Garcia VM (2018) Intratumoral heterogeneity in (18)F-FDG PET/CT by textural analysis in breast cancer as a predictive and prognostic subrogate. Ann Nucl Med 32(6):379-388. https://doi.org/10.1007/s12149-018-1253-0

61. Song H, Jiao Y, Wei W, Ren X, Shen C, Qiu Z, Yang Q, Wang Q, Luo QY (2019) Can pretreatment (18)F-FDG PET tumor texture features predict the outcomes of osteosarcoma treated by neoadjuvant chemotherapy? Eur Radiol 29(7):3945-3954. https://doi.org/10.1007/s00330-019-06074-2

62. Yoon HJ, Kim Y, Chung J, Kim BS (2019) Predicting neo-adjuvant chemotherapy response and progression-free survival of locally advanced breast cancer using textural features of intratumoral heterogeneity on F-18 FDG PET/CT and diffusion-weighted MR imaging. Breast J 25(3):373-380. https://doi.org/10.1111/tbj.13032

63. Yoon SH, Kim YH, Lee YJ, Park J, Kim JW, Lee HS, Kim B (2016) Tumor Heterogeneity in Human Epidermal Growth Factor Receptor 2 (HER2)-Positive Advanced Gastric Cancer Assessed by CT Texture Analysis: Association with Survival after Trastuzumab Treatment. PLoS One 11(8):e0161278. https://doi.org/10.1371/journal.pone.0161278

64. Lopez-Berestein G, Kasi L, Rosenblum MG, Haynie T, Jahns M, Glenn H, Mehta R, Mavligit GM, Hersh EM (1984) Clinical pharmacology of 99mTc-labeled liposomes in patients with cancer. Cancer Res 44:375-378.

65. Koukourakis M, Koukouraki S, Giatromanolaki A, Kakolyris S, Georgoulias V, Velidaki A, Archimandritis S, Karkavitsas NN (2000) High intratumoral accumulation of stealth liposomal doxorubicin in sarcomas--rationale for combination with radiotherapy. Acta Oncol 39(2):2017-2011.

66. Seymour LW, Ferry DR, Anderson D, Hesslewood S, Julyan PJ, Doran RP, Young AM, Burtles S, Kerr DJ (2002) Hepatic Drug Targeting: Phase I Evaluation of Polymer-Bound Doxorubicin J Clin Oncol 20(6):1668-1676.

67. Geretti E, Leonard SC, Dumont N, Lee H, Zheng J, De Souza R, Gaddy DF, Espelin CW, Jaffray DA, Moyo V, et al. (2015) Cyclophosphamide-Mediated Tumor Priming for Enhanced Delivery and Antitumor Activity of HER2-Targeted Liposomal Doxorubicin (MM-302). Mol Cancer Ther 14(9):2060-2071. https://doi.org/10.1158/1535-7163.MCT-15-0314

68. Head HW, Dodd III GD, Bao A, Garcia-Rojas X, Prihoda TJ, McManus LM, Goins BA, Santoyo CA, Phillips WT (2010) Combination Radiofrequency Ablation and Intravenous Radiolabeled Liposomal Doxorubicin: Imaging and Quantifi cation of Increased Drug Delivery to Tumors Radiology 255(2):405-414. https://doi.org/10.1148/radiol.10090714/-/DC1

69. Lee H, Shields AF, Siegel BA, Miller KD, Krop I, Ma CX, LoRusso PM, Munster PN, Campbell K, Gaddy DF, et al. (2017) (64)Cu-MM-302 Positron Emission Tomography Quantifies Variability of Enhanced Permeability and Retention of Nanoparticles in Relation to Treatment Response in Patients with Metastatic Breast Cancer. Clin Cancer Res 23(15):4190-4202. https://doi.org/10.1158/1078-0432.CCR-16-3193

70. Miedema IHC, Zwezerijnen GJC, Oprea-Lager DE, Verheul HMW, Vugts DJ, Huisman MC, Mathijssen RHJ, Hu Q, Rijcken CJF, van Dongen GAMS, et al. (2019) First-in-human imaging of nanoparticle entrapped docetaxel (CPC634) in patients with advanced solid tumors using 89Zr-Df-CPC634 PET/CT. J Clin Oncol 37:suppl; abstr

3093.

71. Wong PK, Lee ST, Murone C, Eng J, Lawrentschuk N, Berlangieri SU, Pathmaraj K, O'Keefe GJ, Sachinidis J, Byrne AJ, et al. (2014) In vivo imaging of cellular proliferation in renal cell carcinoma using 18F-fluorothymidine PET. Asia Oceania J Nucl Med Biol 2(1):3-11.

72. Shen G, Ma H, Pang F, Ren P, Kuang A (2017) Correlations of 18F-FDG and 18F-FLT uptake on PET with Ki-67 expression in patients with lung cancer: a meta-analysis Acta Radiologica 59(2):188-195.

73. Wieder H, Beer AJ, Siveke J, Schuster T, Buck AK, Herrmann K, Stollfuss JC (2018) 18F-fluorothymidine PET for predicting survival in patients with resectable pancreatic cancer. Oncotarget 9(11):10128-10134.

74. Rajendran JG, Krohn KA (2015) F-18 fluoromisonidazole for imaging tumor hypoxia: imaging the microenvironment for personalized cancer therapy. Semin Nucl Med 45(2):151-162. https://doi.org/10.1053/j.semnuclmed.2014.10.006

75. Andrzejewski P, Wengert G, Helbich TH, Magometschnigg H, Georg D, Hacker M, Baltzer P, Clauser P, Kapetas P, Georg P, et al. (2019) Sequential [(18)F]FDG-[(18)F]FMISO PET and Multiparametric MRI at 3T for Insights into Breast Cancer Heterogeneity and Correlation with Patient Outcomes: First Clinical Experience. Contrast Media Mol Imaging 2019:1307247. https://doi.org/10.1155/2019/1307247

76. Cheng G (2018) Non-Small-Cell Lung Cancer PET Imaging Beyond F18 Fluorodeoxyglucose. PET Clin 13(1):73-81. https://doi.org/10.1016/j.cpet.2017.09.006

77. Nagengast WB, Hooge MN, van Straten EM, Kruijff S, Brouwers AH, den Dunnen WF, de Jong JR, Hollema H, Dierckx RA, Mulder NH, et al. (2011) VEGF-SPECT with (1)(1)(1)In-bevacizumab in stage III/IV melanoma patients. Eur J Cancer 47(10):1595-1602. https://doi.org/10.1016/j.ejca.2011.02.009

78. Kurland BF, Peterson LM, Lee JH, Schubert EK, Currin ER, Link JM, Krohn KA, Mankoff DA, Linden HM (2017) Estrogen Receptor Binding (18F-FES PET) and Glycolytic Activity (18F-FDG PET) Predict Progression-Free Survival on Endocrine Therapy in Patients with ER+ Breast Cancer. Clin Cancer Res 23(2):407-415. https://doi.org/10.1158/1078-0432.CCR-16-0362

79. Yang Z, Sun Y, Xu X, Zhang Y, Zhang J, Xue J, Wang M, Yuan H, Hu S, Shi W, et al. (2017) The Assessment of Estrogen Receptor Status and Its Intratumoral Heterogeneity in Patients With Breast Cancer by Using 18F-Fluoroestradiol PET/CT. Clin Nucl Med 42(6):421-427. https://doi.org/10.1097/RLU.0000000000001587

80. Henry KE, Ulaner GA, Lewis JS (2017) Human Epidermal Growth Factor Receptor 2-Targeted PET/Single- Photon Emission Computed Tomography Imaging of Breast Cancer: Noninvasive Measurement of a Biomarker Integral to Tumor Treatment and Prognosis. PET Clin 12(3):269-288. https://doi.org/10.1016/j.cpet.2017.02.001

81. Xiao Z, Song Y, Kai W, Sun X, Shen B (2017) Evaluation of 99mTc-HYNIC-MPG as a novel SPECT radiotracer to detect EGFR-activating mutations in NSCLC. Oncotarget 8(25):40732-40740.

82. Schwarzenboeck SM, Rauscher I, Bluemel C, Fendler WP, Rowe SP, Pomper MG, Afshar-Oromieh A, Herrmann K, Eiber M (2017) PSMA Ligands for PET Imaging of Prostate Cancer. J Nucl Med 58(10):1545-1552. https://doi.org/10.2967/jnumed.117.191031

83. Pozzo L, Monteiro LR, Cerci JJ, Fanti S, Negro A, Trindade E (2019) HTA in nuclear medicine: [68Ga]PSMA PET/CT for patients with prostate cancer. ClinTransl Imaging 7(1):7-20. https://doi.org/10.1007/s40336-019-00313-8

84. Cuccurullo V, Prisco MR, Di Stasio GD, Mansi L (2017) Nuclear Medicine in Patients with NET: Radiolabeled Somatostatin Analogues and their Brothers. Curr Radiopharm 10(2):74-84.

85. Werner RA, Bluemel C, Lassmann M, Kudlich T, Higuchi T, Lopci E, Allen-Auerbach M, Colletti PM, Rubello D, Zatelli MC, et al. (2015) SPECT- and PET-Based Patient-Tailored Treatment in Neuroendocrine Tumors. Clinical Nuclear Medicine 40(5):e271-e277.

86. Gebhart G, Lamberts LE, Wimana Z, Garcia C, Emonts P, Ameye L, Stroobants S, Huizing M, Aftimos P, Tol J, et al. (2016) Molecular imaging as a tool to investigate heterogeneity of advanced HER2-positive breast cancer and to predict patient outcome under trastuzumab emtansine (T-DM1): the ZEPHIR trial. Ann Oncol 27(4):619-624. https://doi.org/10.1093/annonc/mdv577

87. Baker JHE, Lindquist KE, Huxham LA, Kyle AH, Sy JT, Minchinton AI (2008) Direct Visualization of Heterogeneous Extravascular Distribution of Trastuzumab in Human Epidermal Growth Factor Receptor Type 2 Overexpressing Xenografts. Clin Cancer Res 14(7):2171-2179. https://doi.org/10.1158/1078-0432.CCR-07-4465

88. Zhang F, Ni Q, Jacobson O, Cheng S, Liao A, Wang Z, He Z, Yu G, Song J, Ma Y, et al. (2018) Polymeric Nanoparticles with a Glutathione-Sensitive Heterodimeric Multifunctional Prodrug for In Vivo Drug Monitoring and Synergistic Cancer Therapy. Angew Chem Int Ed Engl 57(24):7066-7070. https://doi.org/10.1002/anie.201801984

89. Lamichhane N, Dewkar GK, Sundaresan G, Mahon RN, Zweit J (2017) [(18)F]-Fluorinated Carboplatin and [(111)In]-Liposome for Image-Guided Drug Delivery. Int J Mol Sci 18(5):1079. https://doi.org/10.3390/ijms18051079

90. Lagendijk JJ, Raaymakers BW, Raaijmakers AJ, Overweg J, Brown KJ, Kerkhof EM, van der Put RW, Hardemark B, van Vulpen M, van der Heide UA (2008) MRI/linac integration. Radiother Oncol 86(1):25-29. https://doi.org/10.1016/j.radonc.2007.10.034

91. Hectors SJ, Jacobs I, Moonen CT, Strijkers GJ, Nicolay K (2016) MRI methods for the evaluation of high intensity focused ultrasound tumor treatment: Current status and future needs. Magn Reson Med 75(1):302-317. https://doi.org/10.1002/mrm.25758

92. Jolesz FA (2009) MRI-guided focused ultrasound surgery. Annu Rev Med 60:417-430. https://doi.org/10.1146/annurev.med.60.041707.170303

93. Reeßing F, Szymanski W (2018) Following nanomedicine activation with magnetic resonance imaging: why, how, and what's next? Curr Opin Biotechnol 58:9-18. https://doi.org/10.1016/j.copbio.2018.10.008

94. O'Connor JP, Jackson A, Parker GJ, Roberts C, Jayson GC (2012) Dynamic contrast-enhanced MRI in clinical trials of antivascular therapies. Nat Rev Clin Oncol 9(3):167-177. https://doi.org/10.1038/nrclinonc.2012.2

95. Li W, Quan YY, Li Y, Lu L, Cui M (2018) Monitoring of tumor vascular normalization: the key points from basic research to clinical application. Cancer Manag Res 10:4163-4172. https://doi.org/10.2147/CMAR.S174712

96. Baker JHE, Kyle AH, Reinsberg SA, Moosvi F, Patrick HM, Cran J, Saatchi K, Hafeli U, Minchinton AI (2018) Heterogeneous distribution of trastuzumab in HER2-positive xenografts and metastases: role of the tumor microenvironment. Clin Exp Metastasis 35(7):691-705. https://doi.org/10.1007/s10585-018-9929-3

97. Minowa T, Kawano K, Kuribayashi H, Shiraishi K, Sugino T, Hattori Y, Yokoyama M, Maitani Y (2009) Increase in tumour permeability following TGF-beta type I receptor-inhibitor treatment observed by dynamic contrast-enhanced MRI. Br J Cancer 101(11):1884-1890. https://doi.org/10.1038/sj.bjc.6605367

98. Guo Y, Cai YQ, Cai ZL, Gao YG, An NY, Ma L, Mahankali S, Gao JH (2002) Differentiation of clinically benign and malignant breast lesions using diffusion-weighted imaging. J Magn Reson Imaging 16(2):172-178. https://doi.org/10.1002/jmri.10140

99. Yin Y, Sedlaczek O, Muller B, Warth A, Gonzalez-Vallinas M, Lahrmann B, Grabe N, Kauczor HU, Breuhahn K, Vignon-Clementel IE, et al. (2018) Tumor Cell Load and Heterogeneity Estimation From Diffusion-Weighted MRI Calibrated With Histological Data: an Example From Lung Cancer. IEEE Trans Med Imaging 37(1):35-46. https://doi.org/10.1109/TMI.2017.2698525

100. Jiang L, Weatherall PT, McColl RW, Tripathy D, Mason RP (2013) Blood oxygenation level-dependent (BOLD) contrast magnetic resonance imaging (MRI) for prediction of breast cancer chemotherapy response: a pilot study. J Magn Reson Imaging 37(5):1083-1092. https://doi.org/10.1002/jmri.23891

101. Bane O, Besa C, Wagner M, Oesingmann N, Zhu H, Fiel MI, Taouli B (2016) Feasibility and reproducibility of BOLD and TOLD measurements in the liver with oxygen and carbogen gas challenge in healthy volunteers and patients with hepatocellular carcinoma. J Magn Reson Imaging 43(4):866-876. https://doi.org/10.1002/jmri.25051

102. Brownlee WJ, Seib FP (2018) Impact of the hypoxic phenotype on the uptake and efflux of nanoparticles by human breast cancer cells. Sci Rep 8(1):12318. https://doi.org/10.1038/s41598-018-30517-3

103. Wu M, Huang S (2017) Magnetic nanoparticles in cancer diagnosis, drug delivery and treatment. Mol Clin Oncol 7(5):738-746. https://doi.org/10.3892/mco.2017.1399

104. Ramanathan RK, Korn RL, Raghunand N, Sachdev JC, Newbold RG, Jameson G, Fetterly GJ, Prey J, Klinz SG, Kim J, et al. (2017) Correlation between Ferumoxytol Uptake in Tumor Lesions by MRI and Response to Nanoliposomal Irinotecan in Patients with Advanced Solid Tumors: A Pilot Study. Clin Cancer Res 23(14):3638-3648. https://doi.org/10.1158/1078-0432.CCR-16-1990

105. Hsu FT, Liu HS, Ali AAA, Tsai PH, Kao YC, Lu CF, Huang HS, Chen CY (2018) Assessing the selective therapeutic efficacy of superparamagnetic erlotinib nanoparticles in lung cancer by using quantitative magnetic resonance imaging and a nuclear factor kappa-B reporter gene system. Nanomedicine 14(3):1019-1031. https://doi.org/10.1016/j.nano.2018.01.010

106. Langereis S, Geelen T, Grull H, Strijkers GJ, Nicolay K (2013) Paramagnetic liposomes for molecular MRI and MRI-guided drug delivery. NMR Biomed 26(7):728-744. https://doi.org/10.1002/nbm.2971

107. Zeng L, Wu D, Zou R, Chen T, Zhang J, Wu A (2018) Paramagnetic and Superparamagnetic Inorganic Nanoparticles for T1-Weighted Magnetic Resonance Imaging. Curr Med Chem 25(25):2970-2986. https://doi.org/10.2174/0929867324666170314124616

108. Nitta N, Takakusagi Y, Kokuryo D, Shibata S, Tomita A, Higashi T, Aoki I, Harada M (2018) Intratumoral evaluation of 3D microvasculature and nanoparticle distribution using a gadolinium-dendron modified nano-liposomal contrast agent with magnetic resonance micro-imaging. Nanomedicine 14(4):1315-1324. https://doi.org/10.1016/j.nano.2018.03.006

109. Manzoor AA, Lindner LH, Landon CD, Park JY, Simnick AJ, Dreher MR, Das S, Hanna G, Park W, Chilkoti A, et al. (2012) Overcoming limitations in nanoparticle drug delivery: triggered, intravascular release to improve drug penetration into tumors. Cancer Res 72(21):5566-5575. https://doi.org/10.1158/0008-5472.CAN-12-1683

110. Onuki Y, Jacobs I, Artemov D, Kato Y (2010) Noninvasive visualization of in vivo release and intratumoral distribution of surrogate MR contrast agent using the dual MR contrast technique. Biomaterials 31(27):7132-7138. https://doi.org/10.1016/j.biomaterials.2010.06.008

111. Yeo SY, de Smet M, Langereis S, Vander Elst L, Muller RN, Grull H (2014) Temperature-sensitive paramagnetic liposomes for image-guided drug delivery: Mn(2+) versus [Gd(HPDO3A)(H2O)]. Biochim Biophys Acta 1838(11):2807-2816. https://doi.org/10.1016/j.bbamem.2014.07.019

112. Koay EJ, Truty MJ, Cristini V, Thomas RM, Chen R, Chatterjee D, Kang Y, Bhosale PR, Tamm EP, Crane CH, et al. (2014) Transport properties of pancreatic cancer describe gemcitabine delivery and response. J Clin Invest 124(4):1525-1536. https://doi.org/10.1172/JCI73455

113. Lee N, Choi SH, Hyeon T (2013) Nano-sized CT contrast agents. Adv Mater 25(19):2641-2660. https://doi.org/10.1002/adma.201300081

114. Cormode DP, Naha PC, Fayad ZA (2014) Nanoparticle contrast agents for computed tomography: a focus on micelles. Contrast Media Mol Imaging 9(1):37-52. https://doi.org/10.1002/cmmi.1551

115. Ekdawi SN, Stewart JM, Dunne M, Stapleton S, Mitsakakis N, Dou YN, Jaffray DA, Allen C (2015) Spatial and temporal mapping of heterogeneity in liposome uptake and microvascular distribution in an orthotopic tumor xenograft model. J Control Release 207:101-111. https://doi.org/10.1016/j.jconrel.2015.04.006

116. Badea CT, Clark DP, Holbrook M, Srivastava M, Mowery Y, Ghaghada KB (2019) Functional imaging of tumor vasculature using iodine and gadolinium-based nanoparticle contrast agents: a comparison of spectral micro-CT using energy integrating and photon counting detectors. Phys Med Biol 64(6):065007. https://doi.org/10.1088/1361-6560/ab03e2

117. Stapleton S, Allen C, Pintilie M, Jaffray DA (2013) Tumor perfusion imaging predicts the intra-tumoral accumulation of liposomes. J Control Release 172(1):351-357. https://doi.org/10.1016/j.jconrel.2013.08.296

118. Stapleton S, Milosevic M, Tannock IF, Allen C, Jaffray DA (2015) The intra-tumoral relationship between microcirculation, interstitial fluid pressure and liposome accumulation. J Control Release 211:163-170. https://doi.org/10.1016/j.jconrel.2015.06.008

119. Anderson NG, Butler AP (2014) Clinical applications of spectral molecular imaging: potential and challenges. Contrast Media Mol Imaging 9(1):3-12. https://doi.org/10.1002/cmmi.1550

120. Lv P, Liu J, Yan X, Chai Y, Chen Y, Gao J, Pan Y, Li S, Guo H, Zhou Y (2017) CT spectral imaging for monitoring the therapeutic efficacy of VEGF receptor kinase inhibitor AG-013736 in rabbit VX2 liver tumours. Eur Radiol 27(3):918-926. https://doi.org/10.1007/s00330-016-4458-4

121. Chen XH, Ren K, Liang P, Chai YR, Chen KS, Gao JB (2017) Spectral computed tomography in advanced gastric cancer: Can iodine concentration non-invasively assess angiogenesis? World J Gastroenterol 23(9):1666-1675. https://doi.org/10.3748/wjg.v23.i9.1666

122. Guo J, Rahme K, He Y, Li LL, Holmes JD, O'Driscoll CM (2017) Gold nanoparticles enlighten the future of cancer theranostics. Int J Nanomedicine 12:6131-6152. https://doi.org/10.2147/IJN.S140772

123. Mao W, Kim HS, Son YJ, Kim SR, Yoo HS (2018) Doxorubicin encapsulated clicked gold nanoparticle clusters exhibiting tumor-specific disassembly for enhanced tumor localization and computerized tomographic imaging. J Control Release 269:52-62. https://doi.org/10.1016/j.jconrel.2017.11.003

124. Hu X, Sun J, Li F, Li R, Wu J, He J, Wang N, Liu J, Wang S, Zhou F, et al. (2018) Renal-Clearable Hollow Bismuth Subcarbonate Nanotubes for Tumor Targeted Computed Tomography Imaging and Chemoradiotherapy. Nano Lett 18(2):1196-1204. https://doi.org/10.1021/acs.nanolett.7b04741

125. Leen E, Averkiou M, Arditi M, Burns P, Bokor D, Gauthier T, Kono Y, Lucidarme O (2012) Dynamic contrast enhanced ultrasound assessment of the vascular effects of novel therapeutics in early stage trials. Eur Radiol 22(7):1442-1450. https://doi.org/10.1007/s00330-011-2373-2

126. Schinkel AF, Kaspar M, Staub D (2016) Contrast-enhanced ultrasound: clinical applications in patients with atherosclerosis. Int J Cardiovasc Imaging 32(1):35-48. https://doi.org/10.1007/s10554-015-0713-z

127. Hoyt K, Umphrey H, Lockhart M, Robbin M, Forero-Torres A (2015) Ultrasound imaging of breast tumor perfusion and neovascular morphology. Ultrasound Med Biol 41(9):2292-2302. https://doi.org/10.1016/j.ultrasmedbio.2015.04.016

128. Chen M, Wang WP, Jia WR, Tang L, Wang Y, Zhan WW, Fei XC (2014) Three-dimensional contrast-enhanced sonography in the assessment of breast tumor angiogenesis: correlation with microvessel density and vascular endothelial growth factor expression. J Ultrasound Med 33(5):835-846. https://doi.org/10.7863/ultra.33.5.835

129. Lassau N, Bonastre J, Kind M, Vilgrain V, Lacroix J, Cuinet M, Taieb S, Aziza R, Sarran A, Labbe-Devilliers C, et al. (2014) Validation of dynamic contrast-enhanced ultrasound in predicting outcomes of antiangiogenic therapy for solid tumors. Invest Radiol 49:794-800.

130. Panfilova A, Shelton SE, Caresio C, van Sloun RJG, Molinari F, Wijkstra H, Dayton PA, Mischi M (2019) On the Relationship between Dynamic Contrast-Enhanced Ultrasound Parameters and the Underlying Vascular Architecture Extracted from Acoustic Angiography. Ultrasound Med Biol 45(2):539-548. https://doi.org/10.1016/j.ultrasmedbio.2018.08.018

131. Hudson JM, Williams R, Karshafian R, Milot L, Atri M, Burns PN, Bjarnason GA (2014) Quantifying vascular heterogeneity using microbubble disruption-replenishment kinetics in patients with renal cell cancer. Invest Radiol 49:116-123.

132. Theek B, Gremse F, Kunjachan S, Fokong S, Pola R, Pechar M, Deckers R, Storm G, Ehling J, Kiessling F, et al. (2014) Characterizing EPR-mediated passive drug targeting using contrast-enhanced functional ultrasound imaging. J Control Release 182:83-89. https://doi.org/10.1016/j.jconrel.2014.03.007

133. Rojas JD, Dayton PA (2019) In Vivo Molecular Imaging Using Low-Boiling-Point Phase-Change Contrast Agents: A Proof of Concept Study. Ultrasound Med Biol 45(1):177-191. https://doi.org/10.1016/j.ultrasmedbio.2018.08.004

134. Zheng X, Goins BA, Cameron IL, Santoyo C, Bao A, Frohlich VC, Fullerton GD (2011) Ultrasound-guided intratumoral administration of collagenase-2 improved liposome drug accumulation in solid tumor xenografts. Cancer Chemother Pharmacol 67(1):173-182. https://doi.org/10.1007/s00280-010-1305-1

135. Kirtane AR, Sadhukha T, Kim H, Khanna V, Koniar B, Panyam J (2017) Fibrinolytic Enzyme Cotherapy Improves Tumor Perfusion and Therapeutic Efficacy of Anticancer Nanomedicine. Cancer Res 77(6):1465-1475. https://doi.org/10.1158/0008-5472.CAN-16-1646

136. Wang H, Mislati R, Ahmed R, Vincent P, Nwabunwanne SF, Gunn JR, Pogue BW, Doyley MM (2019) Elastography

Can Map the Local Inverse Relationship between Shear Modulus and Drug Delivery within the Pancreatic Ductal Adenocarcinoma Microenvironment. Clin Cancer Res 25(7):2136-2143. https://doi.org/10.1158/1078-0432. CCR-18-2684

137. Couture O, Hingot V, Heiles B, Muleki-Seya P, Tanter M (2018) Ultrasound Localization Microscopy and Super-Resolution: A State of the Art. IEEE Trans Ultrason Ferroelectr Freq Control 65(8):1304-1320. https://doi.org/10.1109/TUFFC.2018.2850811

138. Provost J, Papadacci C, Demene C, Gennisson J-L, Tanter M, Pernot M (2015) 3-D Ultrafast Doppler Imaging Applied to the Noninvasive and Quantitative Imaging of Blood Vessels in Vivo. IEEE Trans Ultrason Ferroelectr Freq Control 62(8):1467–1472. https://doi.org/doi:10.1109/TUFFC.2015.007032

139. Demené C, Payen T, Dizeux A, Barrois G, Gennisson JL, Bridal L, Tanter M (2019) 3-D Longitudinal Imaging of Tumor Angiogenesis in Mice in Vivo Using Ultrafast Doppler Tomography. Ultrasound Med Biol 45(5):1284-1296. https://doi.org/10.1016/j.ultrasmedbio.2018.12.010

140. Errico C, Pierre J, Pezet S, Desailly Y, Lenkei Z, Couture O, Tanter M (2015) Ultrafast ultrasound localization microscopy for deep super-resolution vascular imaging. Nature 527(7579):499-502. https://doi.org/10.1038/nature16066

141. Lin F, Shelton SE, Espindola D, Rojas JD, Pinton G, Dayton PA (2017) 3-D Ultrasound Localization Microscopy for Identifying Microvascular Morphology Features of Tumor Angiogenesis at a Resolution Beyond the Diffraction Limit of Conventional Ultrasound. Theranostics 7(1):196-204. https://doi.org/10.7150/thno.16899

142. Opacic T, Dencks S, Theek B, Piepenbrock M, Ackermann D, Rix A, Lammers T, Stickeler E, Delorme S, Schmitz G, et al. (2018) Motion model ultrasound localization microscopy for preclinical and clinical multiparametric tumor characterization. Nat Commun 9(1):1527. https://doi.org/10.1038/s41467-018-03973-8

143. Ghosh D, Xiong F, Mattrey R, Sirsi S, Hoyt K. Monitoring early tumor response to vascular targeted therapy using super-resolution ultrasound imaging. 2017 IEEE IUS2017. p. 1-1.

144. Guvener N, Appold L, de Lorenzi F, Golombek SK, Rizzo LY, Lammers T, Kiessling F (2017) Recent advances in ultrasound-based diagnosis and therapy with micro- and nanometer-sized formulations. Methods 130:4-13. https://doi.org/10.1016/j.ymeth.2017.05.018

145. Zhang X, Zheng Y, Wang Z, Huang S, Chen Y, Jiang W, Zhang H, Ding M, Li Q, Xiao X, et al. (2014) Methotrexate-loaded PLGA nanobubbles for ultrasound imaging and Synergistic Targeted therapy of residual tumor during HIFU ablation. Biomaterials 35(19):5148-5161. https://doi.org/10.1016/j.biomaterials.2014.02.036

146. Nittayacharn P, Yuan HX, Hernandez C, Bielecki P, Zhou H, Exner AA (2019) Enhancing Tumor Drug Distribution With Ultrasound-Triggered Nanobubbles. J Pharm Sci 108(9):3091-3098. https://doi.org/10.1016/j.xphs.2019.05.004

147. Ektate K, Kapoor A, Maples D, Tuysuzoglu A, VanOsdol J, Ramasami S, Ranjan A (2016) Motion Compensated Ultrasound Imaging Allows Thermometry and Image Guided Drug Delivery Monitoring from Echogenic Liposomes. Theranostics 6(11):1963-1974. https://doi.org/10.7150/thno.15922

148. Min HS, You DG, Son S, Jeon S, Park JH, Lee S, Kwon IC, Kim K (2015) Echogenic Glycol Chitosan Nanoparticles for Ultrasound-Triggered Cancer Theranostics. Theranostics 5(12):1402-1418. https://doi.org/10.7150/thno.13099

149. Li X, Sui Z, Li X, Xu W, Guo Q, Sun J, Jing F (2018) Perfluorooctylbromide nanoparticles for ultrasound imaging and drug delivery. Int J Nanomedicine 13:3053-3067. https://doi.org/10.2147/IJN.S164905

150. Kulkarni P, Haldar MK, Karandish F, Confeld M, Hossain R, Borowicz P, Gange K, Xia L, Sarkar K, Mallik S (2018) Tissue-Penetrating, Hypoxia-Responsive Echogenic Polymersomes For Drug Delivery To Solid Tumors. Chemistry 24(48):12490-12494. https://doi.org/10.1002/chem.201802229

151. Jamburidze A, Huerre A, Baresch D, Poulichet V, De Corato M, Garbin V (2019) Nanoparticle-Coated Microbubbles for Combined Ultrasound Imaging and Drug Delivery. Langmuir 35(31):10087-10096. https://doi.org/10.1021/acs.langmuir.8b04008

152. Lentacker I, Geers B, Demeester J, De Smedt SC, Sanders NN (2010) Design and evaluation of doxorubicin-containing microbubbles for ultrasound-triggered doxorubicin delivery: cytotoxicity and mechanisms involved. Mol Ther 18(1):101-108. https://doi.org/10.1038/mt.2009.160

153. Tay LM, Xu C (2016) Coating microbubbles with nanoparticles for medical imaging and drug delivery. Nanomedicine 12(2):91-94.

154. Snipstad S, Sulheim E, de Lange Davies C, Moonen C, Storm G, Kiessling F, Schmid R, Lammers T (2018) Sonopermeation to improve drug delivery to tumors: from fundamental understanding to clinical translation. Expert Opin Drug Deliv 15(12):1249-1261. https://doi.org/10.1080/17425247.2018.1547279

155. Min KH, Min HS, Lee HJ, Park DJ, Yhee JY, Kim K, Kwon IC, Jeong SY, Silvestre OF, Chen X, et al. (2015) pH-controlled gas-generating mineralized nanoparticles: a theranostic agent for ultrasound imaging and therapy of cancers. ACS Nano 9(1):134-145.

156. Ntziachristos V (2010) Going deeper than microscopy: the optical imaging frontier in biology. Nature Methods 7(8):603-614. https://doi.org/10.1038/nmeth.1483

157. Weissleder R, Pittet MJ (2008) Imaging in the era of molecular oncology. Nature 452(7187):580-589. https://doi.org/10.1038/nature06917

158. Ntziachristos V, Ripoll J, Wang LV, Weissleder R (2005) Looking and listening to light: the evolution of whole-body photonic imaging. Nature Biotechnology 23(3):313-320. https://doi.org/10.1038/nbt1074

159. Weissleder R, Ntziachristos V (2003) Shedding light onto live molecular targets. Nature Medicine 9(1):123-128.

160. Rudin M, Weissleder R (2003) Molecular imaging in drug discovery and development. Nature Reviews Drug Discovery 2(2):123-131. https://doi.org/10.1038/nrd1007

161. Pittet MJ, Weissleder R (2011) Intravital imaging. Cell 147(5):983-991. https://doi.org/10.1016/j.cell.2011.11.004

162. Amornphimoltham P, Masedunskas A, Weigert R (2011) Intravital microscopy as a tool to study drug delivery in preclinical studies. Advanced Drug Delivery Reviews 63(1-2):119-128. https://doi.org/10.1016/J.ADDR.2010.09.009

163. Baker M (2010) Whole-animal imaging: The whole picture. Nature 463(7283):977-980. https://doi.org/10.1038/463977a

164. Miller MA, Weissleder R (2017) Imaging the pharmacology of nanomaterials by intravital microscopy: Toward understanding their biological behavior. Adv Drug Deliv Rev 113:61-86. https://doi.org/10.1016/J.ADDR.2016.05.023

165. Hak S, Reitan NK, Haraldseth O, de Lange Davies C (2010) Intravital microscopy in window chambers: a unique tool to study tumor angiogenesis and delivery of nanoparticles. Angiogenesis 13(2):113-130. https://doi.org/10.1007/s10456-010-9176-y

166. Mulder WJM, Strijkers GJ, Nicolay K, Griffioen AW (2010) Quantum dots for multimodal molecular imaging of angiogenesis. Angiogenesis 13(2):131-134. https://doi.org/10.1007/s10456-010-9177-x

167. Mulder WJM, Griffioen AW, Strijkers GJ, Cormode DP, Nicolay K, Fayad ZA (2007) Magnetic and fluorescent nanoparticles for multimodality imaging. Nanomedicine 2(3):307-324. https://doi.org/10.2217/17435889.2.3.307

168. Cui L, Lin Q, Jin CS, Jiang W, Huang H, Ding L, Muhanna N, Irish JC, Wang F, Chen J, et al. (2015) A PEGylation-Free Biomimetic Porphyrin Nanoplatform for Personalized Cancer Theranostics. ACS Nano 9(4):4484-4495. https://doi.org/10.1021/acsnano.5b01077

169. Hsu JC, Naha PC, Lau KC, Chhour P, Hastings R, Moon BF, Stein JM, Witschey WRT, McDonald ES, Maidment ADA, et al. (2018) An all-in-one nanoparticle (AION) contrast agent for breast cancer screening with DEM-CT-MRI-NIRF imaging. Nanoscale 10(36):17236-17248. https://doi.org/10.1039/c8nr03741h

170. Liu T, Zhang M, Liu W, Zeng X, Song X, Yang X, Zhang X, Feng J (2018) Metal Ion/Tannic Acid Assembly as a Versatile Photothermal Platform in Engineering Multimodal Nanotheranostics for Advanced Applications. ACS Nano 12(4):3917-3927. https://doi.org/10.1021/acsnano.8b01456

171. Dean KM, Palmer AE (2014) Advances in fluorescence labeling strategies for dynamic cellular imaging. Nat Chem Biol 10(7):512-523. https://doi.org/10.1038/nchembio.1556

172. Pittet MJ, Swirski FK, Reynolds F, Josephson L, Weissleder R (2006) Labeling of immune cells for in vivo imaging using magnetofluorescent nanoparticles. Nat Protoc 1(1):73-79. https://doi.org/10.1038/nprot.2006.11

173. Fortin P-Y, Genevois C, Koenig A, Heinrich E, Texier I, Couillaud F (2012) Detection of brain tumors using fluorescence diffuse optical tomography and nanoparticles as contrast agents. J Biomed Opt 17(12):126004. https://doi.org/10.1117/1.JBO.17.12.126004

174. Ma X, Hui H, Jin Y, Dong D, Liang X, Yang X, Tan K, Dai Z, Cheng Z, Tian J (2016) Enhanced immunotherapy of SM5-1 in hepatocellular carcinoma by conjugating with gold nanoparticles and its in vivo bioluminescence tomographic evaluation. Biomaterials 87:46-56. https://doi.org/10.1016/J.BIOMATERIALS.2016.02.007

175. Huang X, Chisholm J, Zhuang J, Xiao Y, Duncan G, Chen X, Suk JS, Hanes J (2017) Protein nanocages that penetrate airway mucus and tumor tissue. Proc Natl Acad Sci U S A 114(32):E6595-E6602. https://doi.org/10.1073/pnas.1705407114

176. Nam J, Son S, Ochyl LJ, Kuai R, Schwendeman A, Moon JJ (2018) Chemo-photothermal therapy combination elicits anti-tumor immunity against advanced metastatic cancer. Nature Communications 9(1):1074-1074. https://doi.org/10.1038/s41467-018-03473-9

177. Muthu MS, Kutty RV, Luo Z, Xie J, Feng S-S (2015) Theranostic vitamin E TPGS micelles of transferrin conjugation for targeted co-delivery of docetaxel and ultra bright gold nanoclusters. Biomaterials 39:234-248. https://doi.org/10.1016/J.BIOMATERIALS.2014.11.008

178. Yeh C-Y, Hsiao J-K, Wang Y-P, Lan C-H, Wu H-C (2016) Peptide-conjugated nanoparticles for targeted imaging and therapy of prostate cancer. Biomaterials 99:1-15. https://doi.org/10.1016/J.BIOMATERIALS.2016.05.015

179. Devulapally R, Sekar NM, Sekar TV, Foygel K, Massoud TF, Willmann JK, Paulmurugan R (2015) Polymer Nanoparticles Mediated Codelivery of AntimiR-10b and AntimiR-21 for Achieving Triple Negative Breast Cancer Therapy. ACS Nano 9(3):2290-2302. https://doi.org/10.1021/nn507465d

180. Yamamoto Y, Lin PJC, Beraldi E, Zhang F, Kawai Y, Leong J, Katsumi H, Fazli L, Fraser R, Cullis PR, et al. (2015) siRNA Lipid Nanoparticle Potently Silences Clusterin and Delays Progression When Combined with Androgen Receptor Cotargeting in Enzalutamide-Resistant Prostate Cancer. Clin Cancer Res 21(21):4845-4855. https://doi.org/10.1158/1078-0432.CCR-15-0866

181. Singh A, Kim W, Kim Y, Jeong K, Kang CS, Kim Y, Koh J, Mahajan SD, Prasad PN, Kim S (2016) Multifunctional Photonics Nanoparticles for Crossing the Blood-Brain Barrier and Effecting Optically Trackable Brain Theranostics. Adv Funct Mater 26(39):7057-7066. https://doi.org/10.1002/adfm.201602808

182. Pu K, Chattopadhyay N, Rao J (2016) Recent advances of semiconducting polymer nanoparticles in in vivo molecular imaging. J Control Release 240:312-322. https://doi.org/10.1016/J.JCONREL.2016.01.004

183. Cheng S-H, Yu D, Tsai H-M, Morshed RA, Kanojia D, Lo L-W, Leoni L, Govind Y, Zhang L, Aboody KS, et al. (2016) Dynamic In Vivo SPECT Imaging of Neural Stem Cells Functionalized with Radiolabeled Nanoparticles for Tracking of Glioblastoma. J Nucl Med 57(2):279-284. https://doi.org/10.2967/jnumed.115.163006

184. Appel EA, Tibbitt MW, Webber MJ, Mattix BA, Veiseh O, Langer R (2015) Self-assembled hydrogels utilizing polymer−nanoparticle interactions. Nature Communications 6(1):6295. https://doi.org/10.1038/ncomms7295

185. Jiang W, Huang Y, An Y, Kim BY (2015) Remodeling Tumor Vasculature to Enhance Delivery of Intermediate-Sized Nanoparticles. ACS Nano 9(9):8689-8696. https://doi.org/10.1021/acsnano.5b02028

186. Guo P, Liu D, Subramanyam K, Wang B, Yang J, Huang J, Auguste DT, Moses MA (2018) Nanoparticle elasticity directs tumor uptake. Nature Commun 9(1):130. https://doi.org/10.1038/s41467-017-02588-9

187. Yang T, Tang Ya, Liu L, Lv X, Wang Q, Ke H, Deng Y, Yang H, Yang X, Liu G, et al. (2017) Size-Dependent Ag 2 S Nanodots for Second Near-Infrared Fluorescence/Photoacoustics Imaging and Simultaneous Photothermal Therapy. ACS Nano 11(2):1848-1857. https://doi.org/10.1021/acsnano.6b07866

188. Gao S, Wang G, Qin Z, Wang X, Zhao G, Ma Q, Zhu L (2017) Oxygen-generating hybrid nanoparticles to enhance fluorescent/photoacoustic/ultrasound imaging guided tumor photodynamic therapy. Biomaterials 112:324-335. https://doi.org/10.1016/J.BIOMATERIALS.2016.10.030

189. Zhu H, Li J, Qi X, Chen P, Pu K (2018) Oxygenic Hybrid Semiconducting Nanoparticles for Enhanced Photodynamic Therapy. Nano Letters 18(1):586-594. https://doi.org/10.1021/acs.nanolett.7b04759

190. Chen Q, Liang C, Wang C, Liu Z (2015) An Imagable and Photothermal "Abraxane-Like" Nanodrug for Combination Cancer Therapy to Treat Subcutaneous and Metastatic Breast Tumors. Advanced Materials 27(5):903-910. https://doi.org/10.1002/ADMA.201404308

191. Taratula O, Schumann C, Duong T, Taylor KL, Taratula O (2015) Dendrimer-encapsulated naphthalocyanine as a single agent-based theranostic nanoplatform for near-infrared fluorescence imaging and combinatorial anticancer phototherapy. Nanoscale 7(9):3888-3902. https://doi.org/10.1039/C4NR06050D

192. Chen Q, Liang C, Sun X, Chen J, Yang Z, Zhao H, Feng L, Liu Z (2017) H2O2-responsive liposomal nanoprobe for photoacoustic inflammation imaging and tumor theranostics via in vivo chromogenic assay. Proc Natl Acad Sci U S A 114(21):5343-5348. https://doi.org/10.1073/pnas.1701976114

193. Li Z, Zhang Y, Wu X, Huang L, Li D, Fan W, Han G (2015) Direct Aqueous-Phase Synthesis of Sub-10 nm "Luminous Pearls" with Enhanced in Vivo Renewable Near-Infrared Persistent Luminescence. J Am Chem Soc 137(16):5304-5307. https://doi.org/10.1021/jacs.5b00872

194. Miao Q, Xie C, Zhen X, Lyu Y, Duan H, Liu X, Jokerst JV, Pu K (2017) Molecular afterglow imaging with bright, biodegradable polymer nanoparticles. Nat Biotechnol 35(11):1102-1110. https://doi.org/10.1038/nbt.3987

195. Zebibula A, Alifu N, Xia L, Sun C, Yu X, Xue D, Liu L, Li G, Qian J (2018) Ultrastable and Biocompatible NIR-II Quantum Dots for Functional Bioimaging. Adv Funct Mater 28(9):1703451. https://doi.org/10.1002/adfm.201703451

196. Rieffel J, Chen F, Kim J, Chen G, Shao W, Shao S, Chitgupi U, Hernandez R, Graves SA, Nickles RJ, et al. (2015) Hexamodal Imaging with Porphyrin-Phospholipid-Coated Upconversion Nanoparticles. Advanced Materials 27(10):1785-1790. https://doi.org/10.1002/adma.201404739

197. Zhang J, Li C, Zhang X, Huo S, Jin S, An F-F, Wang X, Xue X, Okeke CI, Duan G, et al. (2015) In vivo tumor-targeted dual-modal fluorescence/CT imaging using a nanoprobe co-loaded with an aggregation-induced emission dye and gold nanoparticles. Biomaterials 42:103-111. https://doi.org/10.1016/J.BIOMATERIALS.2014.11.053

198. Nahrendorf M, Waterman P, Thurber G, Groves K, Rajopadhye M, Panizzi P, Marinelli B, Aikawa E, Pittet MJ, Swirski FK, et al. (2009) Hybrid In Vivo FMT-CT Imaging of Protease Activity in Atherosclerosis With Customized Nanosensors. Arterioscler Thromb Vasc Biol 29(10):1444-1451. https://doi.org/10.1161/ATVBAHA.109.193086

199. Gremse F, Doleschel D, Zafarnia S, Babler A, Jahnen-Dechent W, Lammers T, Lederle W, Kiessling F (2015) Hybrid µCT-FMT imaging and image analysis. J Vis Exp (100):52770. https://doi.org/10.3791/52770

200. Hyde D, de Kleine R, MacLaurin SA, Miller E, Brooks DH, Krucker T, Ntziachristos V (2009) Hybrid FMT–CT imaging of amyloid-β plaques in a murine Alzheimer's disease model. NeuroImage 44(4):1304-1311. https://doi.org/10.1016/J.NEUROIMAGE.2008.10.038

201. Dai Q, Wilhelm S, Ding D, Syed AM, Sindhwani S, Zhang Y, Chen YY, MacMillan P, Chan WCW (2018) Quantifying the Ligand-Coated Nanoparticle Delivery to Cancer Cells in Solid Tumors. ACS Nano 12(8):8423-8435. https://doi.org/10.1021/acsnano.8b03900

202. Peng F, Setyawati MI, Tee JK, Ding X, Wang J, Nga ME, Ho HK, Leong DT (2019) Nanoparticles promote in vivo breast cancer cell intravasation and extravasation by inducing endothelial leakiness. Nature Nanotechnology 14(3):279-286. https://doi.org/10.1038/s41565-018-0356-z

203. Shen J, Kim H-C, Su H, Wang F, Wolfram J, Kirui D, Mai J, Mu C, Ji L-N, Mao Z-W, et al. (2014) Cyclodextrin and Polyethylenimine Functionalized Mesoporous Silica Nanoparticles for Delivery of siRNA Cancer Therapeutics. Theranostics 4(5):487-497. https://doi.org/10.7150/thno.8263

204. Seynhaeve ALB, Hoving S, Schipper D, Vermeulen CE, Wiel-Ambagtsheer Gad, Tiel STv, Eggermont AMM, Hagen TLMt (2007) Tumor Necrosis Factor A Mediates Homogeneous Distribution of Liposomes in Murine Melanoma that Contributes to a Better Tumor Response. Cancer Res 53(16):3765-3770. https://doi.org/10.1158/0008-5472.can-07-1599

205. Murphy EA, Majeti BK, Barnes LA, Makale M, Weis SM, Lutu-Fuga K, Wrasidlo W, Cheresh DA (2008) Nanoparticle-

mediated drug delivery to tumor vasculature suppresses metastasis. Proc Natl Acad Sci U S A 105(27):9343-9348. https://doi.org/10.1073/pnas.0803728105

206. Popović Z, Liu W, Chauhan VP, Lee J, Wong C, Greytak AB, Insin N, Nocera DG, Fukumura D, Jain RK, et al. (2010) A Nanoparticle Size Series for In Vivo Fluorescence Imaging. Angew Chem Int Ed Engl 49(46):8649-8652. https://doi.org/10.1002/anie.201003142

207. Cabral H, Makino J, Matsumoto Y, Mi P, Wu H, Nomoto T, Toh K, Yamada N, Higuchi Y, Konishi S, et al. (2015) Systemic Targeting of Lymph Node Metastasis through the Blood Vascular System by Using Size-Controlled Nanocarriers. ACS Nano 9(5):4957-4967. https://doi.org/10.1021/nn5070259

208. Hak S, Helgesen E, Hektoen HH, Huuse EM, Jarzyna PA, Mulder WJM, Haraldseth O, Davies CdL (2012) The Effect of Nanoparticle Polyethylene Glycol Surface Density on Ligand-Directed Tumor Targeting Studied in Vivo by Dual Modality Imaging. ACS Nano 6(6):5648-5658. https://doi.org/10.1021/nn301630n

209. Smith BR, Kempen P, Bouley D, Xu A, Liu Z, Melosh N, Dai H, Sinclair R, Gambhir SS (2012) Shape Matters: Intravital Microscopy Reveals Surprising Geometrical Dependence for Nanoparticles in Tumor Models of Extravasation. Nano Letters 12(7):3369-3377. https://doi.org/10.1021/nl204175t

210. Smith BR, Cheng Z, De A, Rosenberg J, Gambhir SS (2010) Dynamic Visualization of RGD-Quantum Dot Binding to Tumor Neovasculature and Extravasation in Multiple Living Mouse Models Using Intravital Microscopy. Small 6(20):2222-2229. https://doi.org/10.1002/smll.201001022

211. van de Ven AL, Kim P, Haley OH, Fakhoury JR, Adriani G, Schmulen J, Moloney P, Hussain F, Ferrari M, Liu X, et al. (2012) Rapid tumoritropic accumulation of systemically injected plateloid particles and their biodistribution. J Control Release 158(1):148-155. https://doi.org/10.1016/J.JCONREL.2011.10.021

212. Leimgruber A, Berger C, Cortez-Retamozo V, Etzrodt M, Newton AP, Waterman P, Figueiredo JL, Kohler RH, Elpek N, Mempel TR, et al. (2009) Behavior of Endogenous Tumor-Associated Macrophages Assessed In Vivo Using a Functionalized Nanoparticle. Neoplasia 11(5):459-468. https://doi.org/10.1593/NEO.09356

213. Miller MA, Chandra R, Cuccarese MF, Pfirschke C, Engblom C, Stapleton S, Adhikary U, Kohler RH, Mohan JF, Pittet MJ, et al. (2017) Radiation therapy primes tumors for nanotherapeutic delivery via macrophage-mediated vascular bursts. Sci Transl Med 9:1-12.

214. Matsumoto Y, Nichols JW, Toh K, Nomoto T, Cabral H, Miura Y, Christie RJ, Yamada N, Ogura T, Kano MR, et al. (2016) Vascular bursts enhance permeability of tumour blood vessels and improve nanoparticle delivery. Nat Nanotechnol 11(6):533-538. https://doi.org/10.1038/nnano.2015.342

215. Jones SW, Roberts RA, Robbins GR, Perry JL, Kai MP, Chen K, Bo T, Napier ME, Ting JP, Desimone JM, et al. (2013) Nanoparticle clearance is governed by Th1/Th2 immunity and strain background. J Clin Invest 123(7):3061-3073. https://doi.org/10.1172/JCI66895

216. Tsourkas A, Shinde-Patil VR, Kelly KA, Patel P, Wolley A, Allport JR, Weissleder R (2005) In Vivo Imaging of Activated Endothelium Using an Anti-VCAM-1 Magnetooptical Probe. Bioconjug Chem 16(3):576-581. https://doi.org/10.1021/BC050002E

217. Mulder WJM, Castermans K, van Beijnum JR, oude Egbrink MGA, Chin PTK, Fayad ZA, Löwik CWGM, Kaijzel EL, Que I, Storm G, et al. (2009) Molecular imaging of tumor angiogenesis using αvβ3-integrin targeted multimodal quantum dots. Angiogenesis 12(1):17-24. https://doi.org/10.1007/s10456-008-9124-2

218. Patsialou A, Bravo-Cordero JJ, Wang Y, Entenberg D, Liu H, Clarke M, Condeelis JS (2013) Intravital multiphoton imaging reveals multicellular streaming as a crucial component of in vivo cell migration in human breast tumors. IntraVital 2(2):e25294. https://doi.org/10.4161/intv.25294

219. Pantel K, Alix-Panabières C (2019) Liquid biopsy and minimal residual disease — latest advances and implications for cure. Nat Rev Clin Oncol 16(7):409-424. https://doi.org/10.1038/s41571-019-0187-3

220. Tellez-Gabriel M, Heymann M-F, Heymann D (2019) Circulating Tumor Cells as a Tool for Assessing Tumor Heterogeneity. Theranostics 9(16):4580-4594. https://doi.org/10.7150/thno.34337

221. Xiang J, Cai X, Lou X, Feng G, Min X, Luo W, He B, Goh CC, Ng LG, Zhou J, et al. (2015) Biocompatible Green and Red Fluorescent Organic Dots with Remarkably Large Two-Photon Action Cross Sections for Targeted Cellular Imaging and Real-Time Intravital Blood Vascular Visualization. ACS Applied Materials & Interfaces 7(27):14965-14974. https://doi.org/10.1021/acsami.5b03766

222. Fu A, Wilson RJ, Smith BR, Mullenix J, Earhart C, Akin D, Guccione S, Wang SX, Gambhir SS (2012) Fluorescent magnetic nanoparticles for magnetically enhanced cancer imaging and targeting in living subjects. ACS Nano 6(8):6862-6869. https://doi.org/10.1021/nn301670a

223. Sandanaraj BS, Gremlich H-U, Kneuer R, Dawson J, Wacha S (2010) Fluorescent Nanoprobes as a Biomarker for Increased Vascular Permeability: Implications in Diagnosis and Treatment of Cancer and Inflammation. Bioconjugate Chemistry 21(1):93-101. https://doi.org/10.1021/bc900311h

224. Gaber MH, Wu NZ, Hong K, Huang SK, Dewhirst MW, Papahadjopoulos D (1996) Thermosensitive liposomes: Extravasation and release of contents in tumor microvascular networks. Int J Radiat Oncol Biol Phys 36(5):1177-1187. https://doi.org/10.1016/S0360-3016(96)00389-6

225. Ziemys A, Yokoi K, Kai M, Liu YT, Kojic M, Simic V, Milosevic M, Holder A, Ferrari M (2018) Progression-dependent transport heterogeneity of breast cancer liver metastases as a factor in therapeutic resistance. J Control Release 291:99-105. https://doi.org/10.1016/j.jconrel.2018.10.014

226. Wiench B, Eichhorn T, Korn B, Paulsen M, Efferth T (2012) Utilizing inherent fluorescence of therapeutics

1

to analyze real-time uptake and multi-parametric effector kinetics. Methods 57(3):376-382. https://doi.org/10.1016/J.YMETH.2012.01.007

227. Besse HC, Barten-van Rijbroek AD, van der Wurff-Jacobs KMG, Bos C, Moonen CTW, Deckers R (2019) Tumor drug distribution after local drug delivery by hyperthermia, in vivo. Cancers 11(10):1512. https://doi.org/https://doi.org/10.3390/cancers11101512

228. Lee SS-Y, Bindokas VP, Kron SJ (2019) Multiplex Three-Dimensional Mapping of Macromolecular Drug Distribution in the Tumor Microenvironment. Molecular cancer therapeutics 18(1):213-226. https://doi.org/10.1158/1535-7163.MCT-18-0554

229. Lamberts LE, Koch M, de Jong JS, Adams ALL, Glatz J, Kranendonk MEG, Terwisscha van Scheltinga AGT, Jansen L, de Vries J, Lub-de Hooge MN, et al. (2017) Tumor-Specific Uptake of Fluorescent Bevacizumab-IRDye800CW Microdosing in Patients with Primary Breast Cancer: A Phase I Feasibility Study. Clin Cancer Res 23(11):2730-2741. https://doi.org/10.1158/1078-0432.CCR-16-0437

230. van Keulen S, van den Berg NS, Nishio N, Birkeland A, Zhou Q, Lu G, Wang HW, Middendorf L, Forouzanfar T, Martin BA, et al. (2019) Rapid, non-invasive fluorescence margin assessment: Optical specimen mapping in oral squamous cell carcinoma. Oral Oncol 88:58-65. https://doi.org/10.1016/j.oraloncology.2018.11.012

231. Rosenthal EL, Moore LS, Tipirneni K, de Boer E, Stevens TM, Hartman YE, Carroll WR, Zinn KR, Warram JM (2017) Sensitivity and Specificity of Cetuximab-IRDye800CW to Identify Regional Metastatic Disease in Head and Neck Cancer. Clin Cancer Res 23(16):4744-4752. https://doi.org/10.1158/1078-0432.CCR-16-2968

232. Tainaka K, Kuno A, Kubota SI, Murakami T, Ueda HR (2016) Chemical Principles in Tissue Clearing and Staining Protocols for Whole-Body Cell Profiling. Annu Rev Cell Dev Biol 32:713-741. https://doi.org/10.1146/annurev-cellbio-111315-125001

233. Liu YA, Chen Y, Chiang AS, Peng SJ, Pasricha PJ, Tang SC (2011) Optical clearing improves the imaging depth and signal-to-noise ratio for digital analysis and three-dimensional projection of the human enteric nervous system. Neurogastroenterol Motil 23(10):e446-457. https://doi.org/10.1111/j.1365-2982.2011.01773.x

234. Ariel P (2017) A beginner's guide to tissue clearing. Int J Biochem Cell Biol 84:35-39. https://doi.org/10.1016/j.biocel.2016.12.009

235. Boutin ME, Hoffman-Kim D (2015) Application and assessment of optical clearing methods for imaging of tissue-engineered neural stem cell spheres. Tissue Eng Part C Methods 21(3):292-302. https://doi.org/10.1089/ten.TEC.2014.0296

236. Moy AJ, Wiersma MP, Choi B (2013) Optical histology: a method to visualize microvasculature in thick tissue sections of mouse brain. PLoS One 8(1):e53753. https://doi.org/10.1371/journal.pone.0053753

237. Chen YY, Silva PN, Syed AM, Sindhwani S, Rocheleau JV, Chan WC (2016) Clarifying intact 3D tissues on a microfluidic chip for high-throughput structural analysis. Proc Natl Acad Sci U S A 113(52):14915-14920. https://doi.org/10.1073/pnas.1609569114

238. Chung K, Wallace J, Kim SY, Kalyanasundaram S, Andalman AS, Davidson TJ, Mirzabekov JJ, Zalocusky KA, Mattis J, Denisin AK, et al. (2013) Structural and molecular interrogation of intact biological systems. Nature 497(7449):332-337. https://doi.org/10.1038/nature12107

239. Carrillo M, Chuecos M, Gandhi K, Bednov A, Moore DL, Maher J, Ventolini G, Ji G, Schlabritz-Loutsevitch N (2018) Optical tissue clearing in combination with perfusion and immunofluorescence for placental vascular imaging. Medicine (Baltimore) 97(39):e12392. https://doi.org/10.1097/MD.0000000000012392

240. Pan C, Cai R, Quacquarelli FP, Ghasemigharagoz A, Lourbopoulos A, Matryba P, Plesnila N, Dichgans M, Hellal F, Erturk A (2016) Shrinkage-mediated imaging of entire organs and organisms using uDISCO. Nat Methods 13(10):859-867. https://doi.org/10.1038/nmeth.3964

241. Neu CP, Novak T, Gilliland KF, Marshall P, Calve S (2015) Optical clearing in collagen- and proteoglycan-rich osteochondral tissues. Osteoarthritis Cartilage 23(3):405-413. https://doi.org/10.1016/j.joca.2014.11.021

242. Sindhwani S, Syed AM, Wilhelm S, Glancy DR, Chen YY, Dobosz M, Chan WC (2016) Three-Dimensional Optical Mapping of Nanoparticle Distribution in Intact Tissues. ACS Nano 10(5):5468-5478. https://doi.org/10.1021/acsnano.6b01879

243. Sindhwani S, Syed AM, Wilhelm S, Chan WC (2017) Exploring Passive Clearing for 3D Optical Imaging of Nanoparticles in Intact Tissues. Bioconjug Chem 28(1):253-259. https://doi.org/10.1021/acs.bioconjchem.6b00500

244. Togami K, Daisho T, Yumita Y, Kitayama A, Tada H, Chono S (2019) Evaluation of various tissue-clearing techniques for the three-dimensional visualization of liposome distribution in mouse lungs at the alveolar scale. Int J Pharm 562:218-227. https://doi.org/10.1016/j.ijpharm.2019.03.032

245. Cuccarese MF, Dubach JM, Pfirschke C, Engblom C, Garris C, Miller MA, Pittet MJ, Weissleder R (2017) Heterogeneity of macrophage infiltration and therapeutic response in lung carcinoma revealed by 3D organ imaging. Nat Commun 8:14293. https://doi.org/10.1038/ncomms14293

246. van Royen ME, Verhoef EI, Kweldam CF, van Cappellen WA, Kremers GJ, Houtsmuller AB, van Leenders GJ (2016) Three-dimensional microscopic analysis of clinical prostate specimens. Histopathology 69(6):985-992. https://doi.org/10.1111/his.13022

247. Wang M, Kimbrell HZ, Sholl AB, Tulman DB, Elfer KN, Schlichenmeyer TC, Lee BR, Lacey M, Brown JQ (2015) High-Resolution Rapid Diagnostic Imaging of Whole Prostate Biopsies Using Video-Rate Fluorescence Structured

Illumination Microscopy. Cancer Res 75(19):4032-4041. https://doi.org/10.1158/0008-5472.CAN-14-3806

248. Joshi BP, Wang TD (2018) Targeted Optical Imaging Agents in Cancer: Focus on Clinical Applications. Contrast Media Mol Imaging 2018:2015237. https://doi.org/10.1155/2018/2015237

249. Phillips E, Penate-Medina O, Zanzonico PB, Carvajal RD, Mohan P, Ye Y, Humm J, Gonen M, Kalaigian H, Schoder H, et al. (2014) Clinical translation of an ultrasmall inorganic optical-PET imaging nanoparticle probe. Sci Transl Med 6(260):260ra149. https://doi.org/10.1126/scitranslmed.3009524

250. Bradbury MS, Phillips E, Montero PH, Cheal SM, Stambuk H, Durack JC, Sofocleous CT, Meester RJ, Wiesner U, Patel S (2013) Clinically-translated silica nanoparticles as dual-modality cancer-targeted probes for image-guided surgery and interventions. Integr Biol (Camb) 5(1):74-86. https://doi.org/10.1039/c2ib20174g

251. Tummers WS, Warram JM, van den Berg NS, Miller SE, Swijnenburg R-J, Vahrmeijer AL, Rosenthal EL (2018) Recommendations for reporting on emerging optical imaging agents to promote clinical approval. Theranostics 8(19):5336-5347. https://doi.org/10.7150/thno.27384

252. DeLong JC, Hoffman RM, Bouvet M (2016) Current status and future perspectives of fluorescence-guided surgery for cancer. Expert Rev Anticancer Ther 16(1):71-81. https://doi.org/10.1586/14737140.2016.1121109

253. Hernot S, van Manen L, Debie P, Mieog JSD, Vahrmeijer AL (2019) Latest developments in molecular tracers for fluorescence image-guided cancer surgery. The Lancet Oncology 20(7):e354-e367. https://doi.org/10.1016/S1470-2045(19)30317-1

254. Sieroń A, Sieroń-Stołtny K, Kawczyk-Krupka A, Latos W, Kwiatek S, Straszak D, Bugaj AM (2013) The role of fluorescence diagnosis in clinical practice. Onco Targets Ther 6:977-982. https://doi.org/10.2147/OTT.S42074

255. Wang LV, Yao J (2016) A practical guide to photoacoustic tomography in the life sciences. Nat Methods 13(8):627-638. https://doi.org/10.1038/nmeth.3925

256. Manohar S, Razansky D (2016) Photoacoustics: a historical review. Adv Opt Photon 8(4):586-617. https://doi.org/10.1364/aop.8.000586

257. Wang LV, Hu S (2012) Photoacoustic Tomography In Vivo Imaging from Organelles to Organs. Science 335:1458-1462.

258. Weber J, Beard PC, Bohndiek SE (2016) Contrast agents for molecular photoacoustic imaging. Nature Methods 13(8):639-650. https://doi.org/10.1038/nmeth.3929

259. Gujrati V, Mishra A, Ntziachristos V (2017) Molecular imaging probes for multi-spectral optoacoustic tomography. Chem Commun (Camb) 53(34):4653-4672. https://doi.org/10.1039/c6cc09421j

260. Laufer J, Johnson P, Zhang E, Treeby B, Cox B, Pedley B, Beard P (2012) In vivo preclinical photoacoustic imaging of tumor vasculature development and therapy. J Biomed Opt 17(5):056016.

261. Heijblom M, Klaase JM, van den Engh FM, van Leeuwen TG, Steenbergen W, Manohar S (2011) Imaging tumor vascularization for detection and diagnosis of breast cancer. Technol Cancer Res Treat 10:607-623.

262. Tomaszewski MR, Gehrung M, Joseph J, Quiros-Gonzalez I, Disselhorst JA, Bohndiek SE (2018) Oxygen-Enhanced and Dynamic Contrast-Enhanced Optoacoustic Tomography Provide Surrogate Biomarkers of Tumor Vascular Function, Hypoxia, and Necrosis. Cancer Res 78(20):5980-5991. https://doi.org/10.1158/0008-5472.CAN-18-1033

263. May JP, Hysi E, Wirtzfeld LA, Undzys E, Li SD, Kolios MC (2016) Photoacoustic Imaging of Cancer Treatment Response: Early Detection of Therapeutic Effect from Thermosensitive Liposomes. PLoS One 11(10):e0165345. https://doi.org/10.1371/journal.pone.0165345

264. Hu S, Wang LV (2010) Photoacoustic imaging and characterization of the microvasculature. J Biomed Opt 15(1):011101. https://doi.org/10.1117/1.3281673

265. Fehm TF, Deán-Ben XL, Ford SJ, Razansky D (2016) In vivo whole-body optoacoustic scanner with real-time volumetric imaging capacity. Optica 3(11):1153-1159. https://doi.org/10.1364/optica.3.001153

266. Mallidi S, Kim S, Karpiouk A, Joshi PP, Sokolov K, Emelianov S (2015) Visualization of molecular composition and functionality of cancer cells using nanoparticle-augmented ultrasound-guided photoacoustics. Photoacoustics 3(1):26-34. https://doi.org/10.1016/j.pacs.2014.12.003

267. Levi J, Kothapalli SR, Bohndiek S, Yoon JK, Dragulescu-Andrasi A, Nielsen C, Tisma A, Bodapati S, Gowrishankar G, Yan X, et al. (2013) Molecular photoacoustic imaging of follicular thyroid carcinoma. Clin Cancer Res 19(6):1494-1502. https://doi.org/10.1158/1078-0432.CCR-12-3061

268. Okumura K, Yoshida K, Yoshioka K, Aki S, Yoneda N, Inoue D, Kitao A, Ogi T, Kozaka K, Minami T, et al. (2018) Photoacoustic imaging of tumour vascular permeability with indocyanine green in a mouse model. Eur Radiol Exp 2(1):5. https://doi.org/10.1186/s41747-018-0036-7

269. Li L, Zemp RJ, Lungu G, Stoica G, Wang LV (2007) Photoacoustic imaging of lacZ gene expression in vivo. J Biomed Opt 12(2):020504. https://doi.org/10.1117/1.2717531

270. Paproski RJ, Forbrich AE, Wachowicz K, Hitt MM, Zemp RJ (2011) Tyrosinase as a dual reporter gene for both photoacoustic and magnetic resonance imaging. Biomed Opt Express 2(4):771-780. https://doi.org/10.1364/BOE.2.000771

271. Krumholz A, Vanvickle-Chavez SJ, Yao J, Fleming TP, Gillanders WE, Wang LV (2011) Photoacoustic microscopy of tyrosinase reporter gene in vivo. J Biomed Opt 16(8):080503. https://doi.org/10.1117/1.3606568

272. Filonov GS, Krumholz A, Xia J, Yao J, Wang LV, Verkhusha VV (2012) Deep-tissue photoacoustic tomography of a genetically encoded near-infrared fluorescent probe. Angew Chem Int Ed Engl 51(6):1448-1451. https://doi.

org/10.1002/anie.201107026

273. Peters L, Weidenfeld I, Klemm U, Loeschcke A, Weihmann R, Jaeger KE, Drepper T, Ntziachristos V, Stiel AC (2019) Phototrophic purple bacteria as optoacoustic in vivo reporters of macrophage activity. Nat Commun 10(1):1191. https://doi.org/10.1038/s41467-019-09081-5

274. Binnemars-Postma K, Storm G, Prakash J (2017) Nanomedicine Strategies to Target Tumor-Associated Macrophages. Int J Mol Sci 18(5):979. https://doi.org/10.3390/ijms18050979

275. Manivasagan P, Bharathiraja S, Bui NQ, Jang B, Oh YO, Lim IG, Oh J (2016) Doxorubicin-loaded fucoidan capped gold nanoparticles for drug delivery and photoacoustic imaging. Int J Biol Macromol 91:578-588. https://doi.org/10.1016/j.ijbiomac.2016.06.007

276. Cong Z, Yang F, Cao L, Wen H, Fu T, Ma S, Liu C, Quan L, Liao Y (2018) Multispectral optoacoustic tomography (MSOT) for imaging the particle size-dependent intratumoral distribution of polymeric micelles. Int J Nanomedicine 13:8549-8560. https://doi.org/10.2147/IJN.S185726

277. Herzog E, Taruttis A, Beziere N, Lutich AA, Razansky D, Ntziachristos V (2012) Optical imaging of cancer heterogeneity with multispectral optoacoustic tomography. Radiology 263(2):461-468. https://doi.org/10.1148/radiol.11111646/-/DC1

278. Song W, Tang Z, Zhang D, Yu H, Chen X (2015) Coadministration of Vascular Disrupting Agents and Nanomedicines to Eradicate Tumors from Peripheral and Central Regions. Small 11(31):3755-3761. https://doi.org/10.1002/smll.201500324

279. Kim C, Cho EC, Chen J, Song KH, Au L, Favazza C, Zhang Q, Cobley CM, Gao F, Xia Y, et al. (2010) In vivo molecular photoacoustic tomography of melanomas targeted by bioconjugated gold nanocages. ACS Nano 4(8):4559-4564. https://doi.org/10.1021/nn100736c

280. Wang Z, Chen Z, Liu Z, Shi P, Dong K, Ju E, Ren J, Qu X (2014) A multi-stimuli responsive gold nanocage-hyaluronic platform for targeted photothermal and chemotherapy. Biomaterials 35(36):9678-9688. https://doi.org/10.1016/j.biomaterials.2014.08.013

281. Zhong J, Yang S, Wen L, Xing D (2016) Imaging-guided photoacoustic drug release and synergistic chemo-photoacoustic therapy with paclitaxel-containing nanoparticles. J Control Release 226:77-87. https://doi.org/10.1016/j.jconrel.2016.02.010

282. Hannah A, Luke G, Wilson K, Homan K, Emelianov S (2014) Indocyanine green-loaded photoacoustic nanodroplets: dual contrast nanoconstructs for enhanced photoacoustic and ultrasound imaging. ACS Nano 8(1):250-259. https://doi.org/10.1021/nn403527r

283. Yang Z, Song J, Tang W, Fan W, Dai Y, Shen Z, Lin L, Cheng S, Liu Y, Niu G, et al. (2019) Stimuli-Responsive Nanotheranostics for Real-Time Monitoring Drug Release by Photoacoustic Imaging. Theranostics 9(2):526-536. https://doi.org/10.7150/thno.30779

284. Li Y, Jiang C, Zhang D, Wang Y, Ren X, Ai K, Chen X, Lu L (2017) Targeted polydopamine nanoparticles enable photoacoustic imaging guided chemo-photothermal synergistic therapy of tumor. Acta Biomater 47:124-134. https://doi.org/10.1016/j.actbio.2016.10.010

285. Nam J, Son S, Ochyl LJ, Kuai R, Schwendeman A, Moon JJ (2018) Chemo-photothermal therapy combination elicits anti-tumor immunity against advanced metastatic cancer. Nat Commun 9(1):1074. https://doi.org/10.1038/s41467-018-03473-9

286. Zhu H, Cheng P, Chen P, Pu K (2018) Recent progress in the development of near-infrared organic photothermal and photodynamic nanotherapeutics. Biomater Sci 6(4):746-765. https://doi.org/10.1039/c7bm01210a

287. Kim HS, Lee DY (2018) Near-Infrared-Responsive Cancer Photothermal and Photodynamic Therapy Using Gold Nanoparticles. Polymers (Basel) 10(9). https://doi.org/10.3390/polym10090961

288. Pinto A, Pocard M (2018) Photodynamic therapy and photothermal therapy for the treatment of peritoneal metastasis: a systematic review. Pleura Peritoneum 3(4):20180124. https://doi.org/10.1515/pp-2018-0124

289. Swales JG, Dexter A, Hamm G, Nilsson A, Strittmatter N, Michopoulos F, Hardy C, Morentin-Gutierrez P, Mellor M, Andren PE, et al. (2018) Quantitation of Endogenous Metabolites in Mouse Tumors Using Mass-Spectrometry Imaging. Anal Chem 90(10):6051-6058. https://doi.org/10.1021/acs.analchem.7b05239

290. Paine MRL, Liu J, Huang D, Ellis SR, Trede D, Kobarg JH, Heeren RMA, Fernandez FM, MacDonald TJ (2019) Three-Dimensional Mass Spectrometry Imaging Identifies Lipid Markers of Medulloblastoma Metastasis. Sci Rep 9(1):2205. https://doi.org/10.1038/s41598-018-38257-0

291. Mirnezami R, Veselkov K, Strittmatter N, Goldin RD, Kinross JM, Stebbing J, Holmes E, Darzi AW, Nicholson JK, Takats Z (2016) Spatially resolved profiling of colorectal cancer lipid biochemistry via DESI imaging mass spectrometry to reveal morphology-dependent alterations in fatty acid metabolism. J Clin Oncol 34(15_suppl):e15104. https://doi.org/10.1200/JCO.2016.34.15_suppl.e15104

292. Bauer JA, Chakravarthy AB, Rosenbluth JM, Mi D, Seeley EH, De Matos Granja-Ingram N, Olivares MG, Kelley MC, Mayer IA, Meszoely IM, et al. (2010) Identification of markers of taxane sensitivity using proteomic and genomic analyses of breast tumors from patients receiving neoadjuvant paclitaxel and radiation. Clin Cancer Res 16(2):681-690. https://doi.org/10.1158/1078-0432.CCR-09-1091

293. Reyzer ML, Caldwell RL, Dugger TC, Forbes JT, Ritter CA, Guix M, Arteaga CL, Caprioli RM (2004) Early changes in protein expression detected by mass spectrometry predict tumor response to molecular therapeutics. Cancer Res 64(24):9093-9100. https://doi.org/10.1158/0008-5472.CAN-04-2231

294. Cole LM, Djidja MC, Bluff J, Claude E, Carolan VA, Paley M, Tozer GM, Clench MR (2011) Investigation of protein induction in tumour vascular targeted strategies by MALDI MSI. Methods 54(4):442-453. https://doi.org/10.1016/j.ymeth.2011.03.007

295. Swales JG, Hamm G, Clench MR, Goodwin RJA (2019) Mass spectrometry imaging and its application in pharmaceutical research and development: A concise review. Int J Mass Spectrom 437:99-112. https://doi.org/10.1016/j.ijms.2018.02.007

296. Schulz S, Becker M, Groseclose MR, Schadt S, Hopf C (2019) Advanced MALDI mass spectrometry imaging in pharmaceutical research and drug development. Curr Opin Biotechnol 55:51-59. https://doi.org/10.1016/j.copbio.2018.08.003

297. Ashton S, Song YH, Nolan J, Cadogan E, Murray J, Odedra R, Foster J, Hall PA, Low S, Taylor P, et al. (2016) Aurora kinase inhibitor nanoparticles target tumors with favorable therapeutic index in vivo. Sci Transl Med 8(325):325ra317. https://doi.org/10.1126/scitranslmed.aad2355

298. Nilsson A, Goodwin RJ, Swales JG, Gallagher R, Shankaran H, Sathe A, Pradeepan S, Xue A, Keirstead N, Sasaki JC, et al. (2015) Investigating nephrotoxicity of polymyxin derivatives by mapping renal distribution using mass spectrometry imaging. Chem Res Toxicol 28(9):1823-1830. https://doi.org/10.1021/acs.chemrestox.5b00262

299. Karlsson O, Hanrieder J (2017) Imaging mass spectrometry in drug development and toxicology. Arch Toxicol 91(6):2283-2294. https://doi.org/10.1007/s00204-016-1905-6

300. Munteanu B, Meyer B, von Reitzenstein C, Burgermeister E, Bog S, Pahl A, Ebert MP, Hopf C (2014) Label-free in situ monitoring of histone deacetylase drug target engagement by matrix-assisted laser desorption ionization-mass spectrometry biotyping and imaging. Anal Chem 86(10):4642-4647. https://doi.org/10.1021/ac500038j

301. Giordano S, Zucchetti M, Decio A, Cesca M, Fuso Nerini I, Maiezza M, Ferrari M, Licandro SA, Frapolli R, Giavazzi R, et al. (2016) Heterogeneity of paclitaxel distribution in different tumor models assessed by MALDI mass spectrometry imaging. Sci Rep 6:39284. https://doi.org/10.1038/srep39284

302. Connell JJ, Sugihara Y, Torok S, Dome B, Tovari J, Fehniger TE, Marko-Varga G, Vegvari A (2015) Localization of sunitinib in in vivo animal and in vitro experimental models by MALDI mass spectrometry imaging. Anal Bioanal Chem 407(8):2245-2253. https://doi.org/10.1007/s00216-014-8350-2

303. Lukowski JK, Weaver EM, Hummon AB (2017) Analyzing Liposomal Drug Delivery Systems in Three-Dimensional Cell Culture Models Using MALDI Imaging Mass Spectrometry. Anal Chem 89(16):8453-8458. https://doi.org/10.1021/acs.analchem.7b02006

304. Prideaux B, Dartois V, Staab D, Weiner DM, Goh A, Via LE, Barry CE, 3rd, Stoeckli M (2011) High-sensitivity MALDI-MRM-MS imaging of moxifloxacin distribution in tuberculosis-infected rabbit lungs and granulomatous lesions. Anal Chem 83(6):2112-2118. https://doi.org/10.1021/ac1029049

305. Kertesz V, Van Berkel GJ, Vavrek M, Koeplinger KA, Schneider BB, Covey TR (2008) Comparison of drug distribution images from whole-body thin tissue sections obtained using desorption electrospray ionization tandem mass spectrometry and autoradiography. Anal Chem 80(13):5168-5177. https://doi.org/10.1021/ac800546a

306. Khatib-Shahidi S, Andersson M, Herman JL, Gillespie TA, Caprioli RM (2006) Direct molecular analysis of whole-body animal tissue sections by imaging MALDI mass spectrometry. Anal Chem 78(18):6448-6456. https://doi.org/10.1021/ac060788p

307. Giordano S, Morosi L, Veglianese P, Licandro SA, Frapolli R, Zucchetti M, Cappelletti G, Falciola L, Pifferi V, Visentin S, et al. (2016) 3D Mass Spectrometry Imaging Reveals a Very Heterogeneous Drug Distribution in Tumors. Sci Rep 6:37027. https://doi.org/10.1038/srep37027

308. Cesca M, Morosi L, Berndt A, Fuso Nerini I, Frapolli R, Richter P, Decio A, Dirsch O, Micotti E, Giordano S, et al. (2016) Bevacizumab-Induced Inhibition of Angiogenesis Promotes a More Homogeneous Intratumoral Distribution of Paclitaxel, Improving the Antitumor Response. Mol Cancer Ther 15(1):125-135. https://doi.org/10.1158/1535-7163.MCT-15-0063

309. Torok S, Rezeli M, Kelemen O, Vegvari A, Watanabe K, Sugihara Y, Tisza A, Marton T, Kovacs I, Tovari J, et al. (2017) Limited Tumor Tissue Drug Penetration Contributes to Primary Resistance against Angiogenesis Inhibitors. Theranostics 7(2):400-412. https://doi.org/10.7150/thno.16767

310. Goodwin RJ, Nilsson A, Mackay CL, Swales JG, Johansson MK, Billger M, Andren PE, Iverson SL (2016) Exemplifying the Screening Power of Mass Spectrometry Imaging over Label-Based Technologies for Simultaneous Monitoring of Drug and Metabolite Distributions in Tissue Sections. J Biomol Screen 21(2):187-193. https://doi.org/10.1177/1087057115623740

311. Fuchs K, Kiss A, Bize PE, Duran R, Denys A, Hopfgartner G, Borchard G, Jordan O (2018) Mapping of drug distribution in the rabbit liver tumor model by complementary fluorescence and mass spectrometry imaging. J Control Release 269:128-135. https://doi.org/10.1016/j.jconrel.2017.10.042

312. Liu X, Flinders C, Mumenthaler SM, Hummon AB (2018) MALDI Mass Spectrometry Imaging for Evaluation of Therapeutics in Colorectal Tumor Organoids. J Am Soc Mass Spectrom 29(3):516-526. https://doi.org/10.1007/s13361-017-1851-4

313. Bruinen AL, van Oevelen C, Eijkel GB, Van Heerden M, Cuyckens F, Heeren RM (2016) Mass Spectrometry Imaging of Drug Related Crystal-Like Structures in Formalin-Fixed Frozen and Paraffin-Embedded Rabbit Kidney Tissue Sections. J Am Soc Mass Spectrom 27(1):117-123. https://doi.org/10.1007/s13361-015-1254-3

314. Groseclose MR, Castellino S (2019) An Investigation into Retigabine (Ezogabine) Associated Dyspigmentation in

1

Rat Eyes by MALDI Imaging Mass Spectrometry. Chem Res Toxicol 32(2):294-303. https://doi.org/10.1021/acs.chemrestox.8b00313

315. Gamble LJ, Anderton CR (2016) Secondary Ion Mass Spectrometry Imaging of Tissues, Cells, and Microbial Systems. Micros Today 24(2):24-31. https://doi.org/10.1017/S1551929516000018

316. Passarelli MK, Newman CF, Marshall PS, West A, Gilmore IS, Bunch J, Alexander MR, Dollery CT (2015) Single-Cell Analysis: Visualizing Pharmaceutical and Metabolite Uptake in Cells with Label-Free 3D Mass Spectrometry Imaging. Anal Chem 87(13):6696-6702. https://doi.org/10.1021/acs.analchem.5b00842

317. Newman CF, Havelund R, Passarelli MK, Marshall PS, Francis I, West A, Alexander MR, Gilmore IS, Dollery CT (2017) Intracellular Drug Uptake-A Comparison of Single Cell Measurements Using ToF-SIMS Imaging and Quantification from Cell Populations with LC/MS/MS. Anal Chem 89(22):11944-11953. https://doi.org/10.1021/acs.analchem.7b01436

318. Chandra S, Lorey ID, Smith DR (2002) Quantitative subcellular secondary ion mass spectrometry (SIMS) imaging of boron-10 and boron-11 isotopes in the same cell delivered by two combined BNCT drugs: in vitro studies on human glioblastoma T98G cells. Radiat Res 157(6):700-710. https://www.ncbi.nlm.nih.gov/pubmed/12005550

319. Vanbellingen QP, Castellanos A, Rodriguez-Silva M, Paudel I, Chambers JW, Fernandez-Lima FA (2016) Analysis of Chemotherapeutic Drug Delivery at the Single Cell Level Using 3D-MSI-TOF-SIMS. J Am Soc Mass Spectrom 27(12):2033-2040. https://doi.org/10.1007/s13361-016-1485-y

320. Giesen C, Wang HA, Schapiro D, Zivanovic N, Jacobs A, Hattendorf B, Schuffler PJ, Grolimund D, Buhmann JM, Brandt S, et al. (2014) Highly multiplexed imaging of tumor tissues with subcellular resolution by mass cytometry. Nat Methods 11(4):417-422. https://doi.org/10.1038/nmeth.2869

321. Chang Q, Ornatsky OI, Siddiqui I, Straus R, Baranov VI, Hedley DW (2016) Biodistribution of cisplatin revealed by imaging mass cytometry identifies extensive collagen binding in tumor and normal tissues. Sci Rep 6:36641. https://doi.org/10.1038/srep36641

322. Theiner S, Kornauth C, Varbanov HP, Galanski M, Van Schoonhoven S, Heffeter P, Berger W, Egger AE, Keppler BK (2015) Tumor microenvironment in focus: LA-ICP-MS bioimaging of a preclinical tumor model upon treatment with platinum(IV)-based anticancer agents. Metallomics 7(8):1256-1264. https://doi.org/10.1039/c5mt00028a

323. Zandanel C, Legouffe R, Trochon-Joseph V, Tomezyk A, Gaudin M, Bonnel D, Stauber J, Vasseur B, Bromet N (2018) Biodistribution of polycyanoacrylate nanoparticles encapsulating doxorubicin by Matrix-Assisted Laser Desorption Ionization (MALDI) Mass Spectrometry Imaging (MSI). J Drug Deliv Sci Technol 47:55-61. https://doi.org/10.1016/j.jddst.2018.06.023

324. Fulop A, Sammour DA, Erich K, von Gerichten J, van Hoogevest P, Sandhoff R, Hopf C (2016) Molecular imaging of brain localization of liposomes in mice using MALDI mass spectrometry. Sci Rep 6:33791. https://doi.org/10.1038/srep33791

325. Xue J, Liu H, Chen S, Xiong C, Zhan L, Sun J, Nie Z (2018) Mass spectrometry imaging of the in situ drug release from nanocarriers. Sci Adv 4(10):eaat9039. https://doi.org/10.1126/sciadv.aat9039

326. Aichler M, Elsner M, Ludyga N, Feuchtinger A, Zangen V, Maier SK, Balluff B, Schone C, Hierber L, Braselmann H, et al. (2013) Clinical response to chemotherapy in oesophageal adenocarcinoma patients is linked to defects in mitochondria. J Pathol 230(4):410-419. https://doi.org/10.1002/path.4199

327. Yanagisawa K, Shyr Y, Xu BJ, Massion PP, Larsen PH, White BC, Roberts JR, Edgerton M, Gonzalez A, Nadaf S, et al. (2003) Proteomic patterns of tumour subsets in non-small-cell lung cancer. The Lancet 362(9382):433-439. https://doi.org/10.1016/s0140-6736(03)14068-8

328. Guo L, Panderi I, Yan DD, Szulak K, Li Y, Chen YT, Ma H, Niesen DB, Seeram N, Ahmed A, et al. (2013) A comparative study of hollow copper sulfide nanoparticles and hollow gold nanospheres on degradability and toxicity. ACS Nano 7(10):8780-8793. https://doi.org/10.1021/nn403202w

329. Mascini NE, Cheng M, Jiang L, Rizwan A, Podmore H, Bhandari DR, Rompp A, Glunde K, Heeren RM (2016) Mass Spectrometry Imaging of the Hypoxia Marker Pimonidazole in a Breast Tumor Model. Anal Chem 88(6):3107-3114. https://doi.org/10.1021/acs.analchem.5b04032

330. Masaki Y, Shimizu Y, Yoshioka T, Tanaka Y, Nishijima K, Zhao S, Higashino K, Sakamoto S, Numata Y, Yamaguchi Y, et al. (2015) The accumulation mechanism of the hypoxia imaging probe "FMISO" by imaging mass spectrometry: possible involvement of low-molecular metabolites. Sci Rep 5:16802. https://doi.org/10.1038/srep16802

331. Venkatesan AM, Kadoury S, Abi-Jaoudeh N, Levy EB, Maass-Moreno R, Krücker J, Dalal S, Xu S, Glossop N, Wood BJ (2011) Real-time FDG PET guidance during biopsies and radiofrequency ablation using multimodality fusion with electromagnetic navigation. Radiology 260(3):848-856. https://doi.org/10.1148/radiol.11101985/-/DC1

332. Sheth RA, Heidari P, Esfahani SA, Wood BJ, Mahmood U (2014) Interventional optical molecular imaging guidance during percutaneous biopsy. Radiology 271(3):770-777.

333. Borresen B, Henriksen JR, Clergeaud G, Jorgensen JS, Melander F, Elema DR, Szebeni J, Engelholm SA, Kristensen AT, Kjaer A, et al. (2018) Theranostic Imaging May Vaccinate against the Therapeutic Benefit of Long Circulating PEGylated Liposomes and Change Cargo Pharmacokinetics. ACS Nano 12(11):11386-11398. https://doi.org/10.1021/acsnano.8b06266

334. Yang CT, Ghosh KK, Padmanabhan P, Langer O, Liu J, Eng DNC, Halldin C, Gulyas B (2018) PET-MR and SPECT-MR multimodality probes: Development and challenges. Theranostics 8(22):6210-6232. https://doi.org/10.7150/thno.26610

335. Lahooti A, Sarkar S, Laurent S, Shanehsazzadeh S (2016) Dual nano-sized contrast agents in PET/MRI: a systematic review. Contrast Media Mol Imaging 11(6):428-447. https://doi.org/10.1002/cmmi.1719

336. Key J, Leary JF (2014) Nanoparticles for multimodal in vivo imaging in nanomedicine. Int J Nanomedicine 9:711-726. https://doi.org/10.2147/IJN.S53717

337. Porta Siegel T, Hamm G, Bunch J, Cappell J, Fletcher JS, Schwamborn K (2018) Mass Spectrometry Imaging and Integration with Other Imaging Modalities for Greater Molecular Understanding of Biological Tissues. Mol Imaging Biol 20(6):888-901. https://doi.org/10.1007/s11307-018-1267-y

338. Huber K, Feuchtinger A, Borgmann DM, Li Z, Aichler M, Hauck SM, Zitzelsberger H, Schwaiger M, Keller U, Walch A (2014) Novel approach of MALDI drug imaging, immunohistochemistry, and digital image analysis for drug distribution studies in tissues. Anal Chem 86(21):10568-10575. https://doi.org/10.1021/ac502177y

339. Zhu Y, Wang X, Chen J, Zhang J, Meng F, Deng C, Cheng R, Feijen J, Zhong Z (2016) Bioresponsive and fluorescent hyaluronic acid-iodixanol nanogels for targeted X-ray computed tomography imaging and chemotherapy of breast tumors. J Control Release 244(Pt B):229-239. https://doi.org/10.1016/j.jconrel.2016.08.027

340. Park J, Pei Y, Hyun H, Castanares MA, Collins DS, Yeo Y (2017) Small molecule delivery to solid tumors with chitosan-coated PLGA particles: A lesson learned from comparative imaging. J Control Release 268:407-415. https://doi.org/10.1016/j.jconrel.2017.10.037

341. Sun Q, You Q, Wang J, Liu L, Wang Y, Song Y, Cheng Y, Wang S, Tan F, Li N (2018) Theranostic Nanoplatform: Triple-Modal Imaging-Guided Synergistic Cancer Therapy Based on Liposome-Conjugated Mesoporous Silica Nanoparticles. ACS Appl Mater Interfaces 10(2):1963-1975. https://doi.org/10.1021/acsami.7b13651

342. Tata A, Zheng J, Ginsberg HJ, Jaffray DA, Ifa DR, Zarrine-Afsar A (2015) Contrast Agent Mass Spectrometry Imaging Reveals Tumor Heterogeneity. Anal Chem 87(15):7683-7689. https://doi.org/10.1021/acs.analchem.5b01992

343. Abdelmoula WM, Regan MS, Lopez BGC, Randall EC, Lawler S, Mladek AC, Nowicki MO, Marin BM, Agar JN, Swanson KR, et al. (2019) Automatic 3D Nonlinear Registration of Mass Spectrometry Imaging and Magnetic Resonance Imaging Data. Anal Chem 91(9):6206-6216. https://doi.org/10.1021/acs.analchem.9b00854

344. Thiele H, Heldmann S, Trede D, Strehlow J, Wirtz S, Dreher W, Berger J, Oetjen J, Kobarg JH, Fischer B, et al. (2014) 2D and 3D MALDI-imaging: conceptual strategies for visualization and data mining. Biochim Biophys Acta 1844(1 Pt A):117-137. https://doi.org/10.1016/j.bbapap.2013.01.040

345. Oetjen J, Aichler M, Trede D, Strehlow J, Berger J, Heldmann S, Becker M, Gottschalk M, Kobarg JH, Wirtz S, et al. (2013) MRI-compatible pipeline for three-dimensional MALDI imaging mass spectrometry using PAXgene fixation. J Proteomics 90:52-60. https://doi.org/10.1016/j.jprot.2013.03.013

346. Sinha TK, Khatib-Shahidi S, Yankeelov TE, Mapara K, Ehtesham M, Cornett DS, Dawant BM, Caprioli RM, Gore JC (2008) Integrating spatially resolved three-dimensional MALDI IMS with in vivo magnetic resonance imaging. Nat Methods 5(1):57-59. https://doi.org/10.1038/nmeth1147

347. Van de Plas R, Yang J, Spraggins J, Caprioli RM (2015) Image fusion of mass spectrometry and microscopy: a multimodality paradigm for molecular tissue mapping. Nat Methods 12(4):366-372. https://doi.org/10.1038/nmeth.3296

1

PART II
MR-HIFU hyperthermia and temperature sensitive liposomes in *de novo* metastatic breast cancer

2
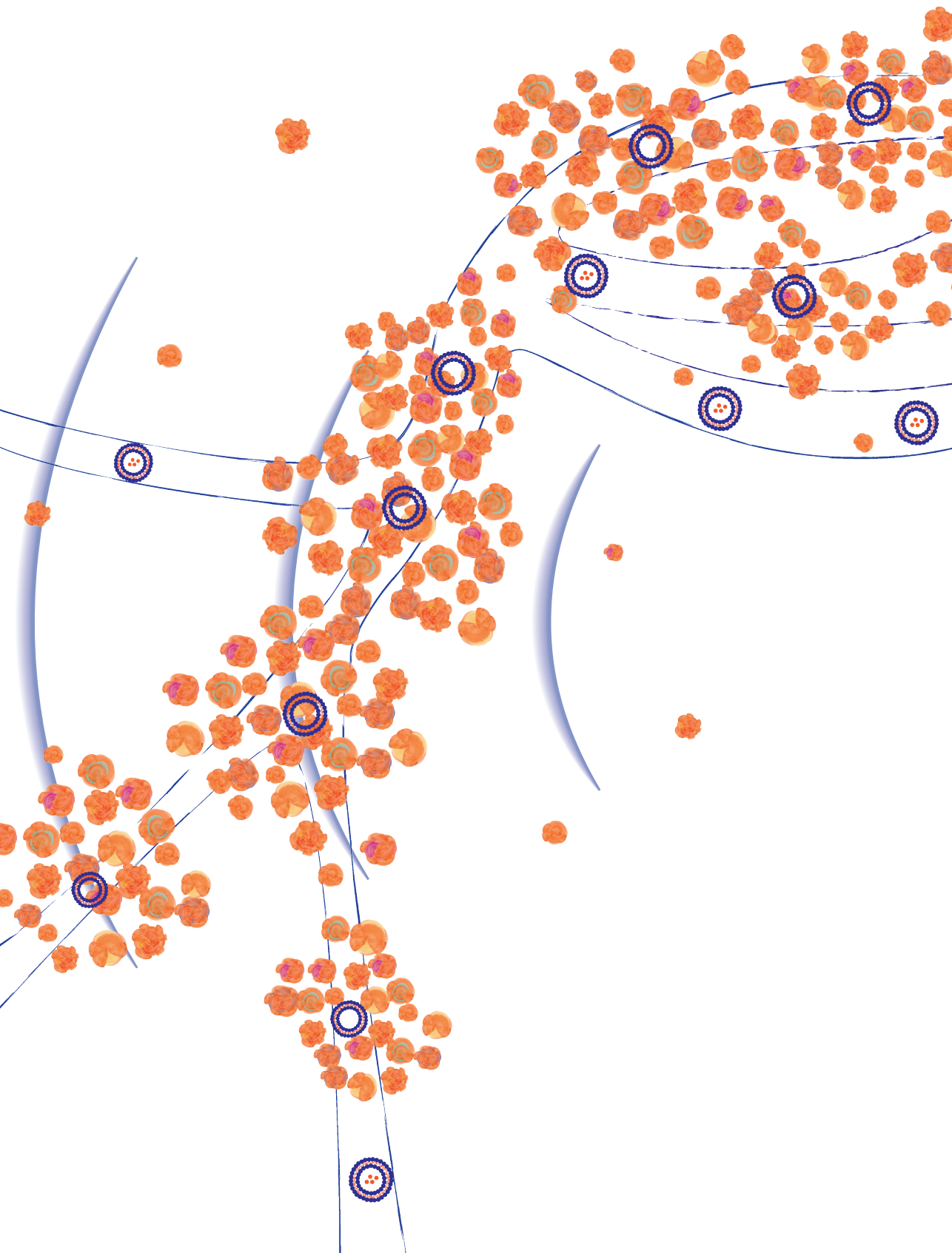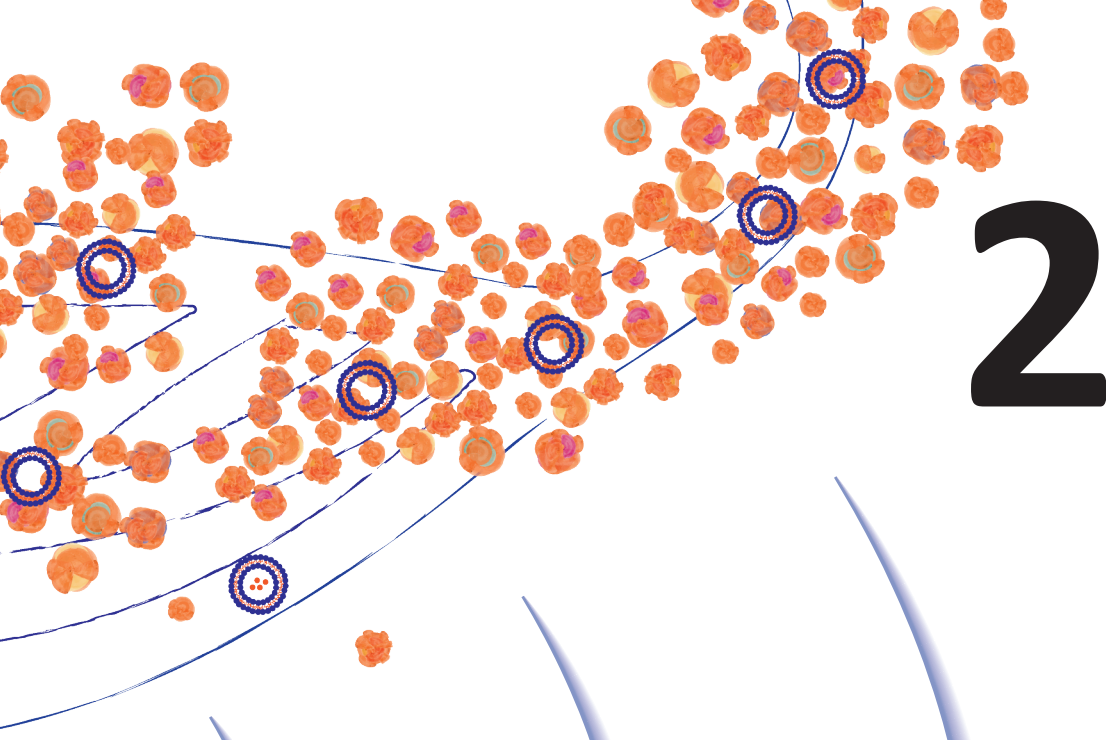
COMPARISON BETWEEN *DE NOVO* AND METACHRONOUS METASTATIC BREAST CANCER: THE PRESENCE OF A PRIMARY TUMOUR IS NOT THE ONLY DIFFERENCE - *A DUTCH POPULATION BASED STUDY FROM 2008-2018.*

Josanne S. de Maar* [1], Marianne Luyendijk* [2,3], Britt B.M. Suelmann[4],

Dave E.W. van der Kruijssen[4], Sjoerd G. Elias[5], Sabine Siesling[2, 6], Elsken van der Wall[4]

*both authors contributed equally

1. Division of Imaging and Oncology, University Medical Center Utrecht, the Netherlands.
2. Department of Research and Development, Netherlands Comprehensive Cancer Centre (IKNL), Utrecht, the Netherlands
3. Erasmus School of Health Policy and Management, Erasmus University, Rotterdam, the Netherlands.
4. Department of Medical Oncology, Division of Imaging and Oncology, University Medical Center Utrecht, the Netherlands.
5. Julius Center for Health Sciences and Primary Care, University Medical Center Utrecht, the Netherlands
6. Department of Health Technology and Services Research, Technical Medical Centre, University of Twente, Enschede, the Netherlands

ABSTRACT

Purpose

The aim of this study was to compare characteristics and survival of patients with *de novo* and metachronous metastatic breast cancer.

Methods

Data of patients with metastatic breast cancer were obtained from the Netherlands Cancer Registry. Patients were categorized as having *de novo* metastatic breast cancer (n=8,656) if they had distant metastases at initial presentation, or metachronous metastatic disease (n= 2,374) in case they developed metastases within 5 or 10 years after initial breast cancer diagnosis. Clinicopathological characteristics and treatments of these two groups were compared, after which multiple imputation was performed to account for missing data. Overall survival was compared for patients treated with systemic therapy in the metastatic setting, using Kaplan Meier curves and multivariable Cox proportional hazards models. The hazard ratio for overall survival of *de novo* versus metachronous metastases was assessed accounting for time-varying effects.

Results

Compared to metachronous patients, patients with de *novo* metastatic breast cancer were more likely to be ≥70 years, to have invasive lobular carcinoma, clinical T3 or T4 tumours, loco-regional lymphnode metastases, HER2 positivity, bone only disease and to have received systemic therapy in the metastatic setting. They were less likely to have triple negative tumours and liver or brain metastases. Patients with *de novo* metastases survived longer (median 34.7 months) than patients with metachronous metastases (median 24.3 months) and the hazard ratio (0.75) varied over time.

Conclusions

Differences in clinicopathological characteristics and survival between *de novo* and metachronous metastatic breast cancer highlight that these are distinct patients groups.

Keywords

metastatic breast cancer
de novo stage IV
metachronous metastatic breast cancer
overall survival
prognosis

INTRODUCTION

In the Netherlands, around 14,500 patients annually are diagnosed with invasive breast cancer [1]. Around 5% of these patients present with *de novo* distant metastases at the time of initial diagnosis [2]. Moreover, in 15-20% distant metastases are diagnosed in the years following their initial breast cancer diagnosis (metachronous metastases)[3, 4]. While systemic treatment, with a palliative intent, is the standard of care for both *de novo* and metachronous metastatic breast cancer (MBC) [5, 6], there are specific therapeutic considerations for each group. For instance, in *de novo* MBC the best approach regarding the primary tumour is still unclear. Many studies suggested an overall survival (OS) benefit of local treatment [7-9], but recent randomized studies have refuted this [10, 11]. Unlike patients with *de novo* MBC, many patients with metachronous MBC have already received (neoadjuvant or adjuvant) systemic treatment in addition to loco-regional treatment following diagnosis of the primary tumour. Recurrence following these previous systemic therapies could reflect resistance to these drugs or mean that the maximum tolerated cumulative dose of these drugs was already reached. Moreover, patients can suffer from lasting side effects and therefore be less fit for further systemic treatment. These specific considerations illustrate the importance of understanding differences between patients with *de novo* and metachronous MBC.

So far, characteristics and OS of patients with *de novo* MBC have been analysed in several cohorts [12-27] and in some studies have been compared to patients with metachronous MBC [4, 21, 28-36]. Typically, patients with *de novo* MBC have more favourable disease characteristics and longer OS compared to metachronous patients [4, 21, 28-35]. However, in younger patients (≤40 years) the opposite appears to be true (i.e. larger tumours, more widespread metastatic disease and more brain metastasis in *de novo* MBC) [21]. Differences in gene expression profiles between *de novo* and metachronous MBC have been found, which lead to believe that these tumours possess biologically different behaviour [36]. Moreover, whereas studies consistently reported improvements in OS over time for *de novo* MBC [2, 37-39], little evidence supports such a positive trend in metachronous MBC [39], which again emphasizes the difference between these groups. While literature on *de novo* MBC is often based on nationwide registry data, data on metachronous MBC is usually based on regional cohorts [39]. Our study demonstrates nationwide data of patients with *de novo* MBC and a large cohort of patients with metachronous MBC diagnosed in 2008-2018 in the Netherlands, to compare clinicopathological characteristics, treatment and survival.

PATIENTS AND METHODS

Data source

The Netherlands Cancer Registry (NCR) is a nation-wide cancer registry hosted by the Netherlands Comprehensive Cancer Organisation (IKNL) and includes all patients with newly diagnosed cancer, with an estimated coverage of 96%[40]. Cancer diagnoses are notified through the nationwide Pathology Archive (PALGA) and the National Registry of Hospital Discharge Diagnoses. Trained data managers register data on diagnosis, clinicopathological characteristics and primary treatment directly from the patient files. Tumour location and morphology are coded according to the International Classification of Diseases for Oncology (ICD-O, third edition) and tumour stage is coded following the Tumor Node Metastasis (TNM) classification. Estrogen receptor (ER) and Progesterone receptor (PR) positivity of the primary tumour are set at ≥10% according to Dutch nationwide guidelines. Additional data on recurrences (including local, regional recurrences and distant metastases) were collected by the NCR retrospectively. Specifically, for patients with a primary diagnosis in 2003 and 2005 all recurrences up to 10 years after initial breast cancer diagnosis were identified. In addition, for half of the patients diagnosed in 2008, the first recurrence up to 5 years afterwards was identified and for patients diagnosed in the first quartile of 2012 (Q1 2012), all recurrences up to 5 years after diagnosis were recorded (**Fig. 1**). Recurrence locations were also registered following the ICD-O third edition. After diagnosis of metastases, the first systemic and/ or local treatment is registered. Information on vital status was derived from the official municipal population database.

Patient selection

All patients diagnosed with *de novo* MBC between 2008 and 2018, as well as registered patients diagnosed with distant metachronous metastases between 2008-2018 were selected from the NCR. Patients with distant metastasis within 3 months of the primary diagnosis were excluded, because they are often considered as *de novo* MBC. For the survival analyses we excluded a small group of patients (n = 333, 3.0%) with tumour morphologies other than ductal carcinoma NOS or invasive lobular carcinoma (ILC). Moreover, we excluded patients from the survival analyses who had not received systemic therapy in the metastatic setting, because untreated patients likely have severe comorbidities and inherently have a different prognosis. Moreover, knowledge about patients eligible for systemic treatment can support medical oncologists' clinical decision making.

Data definition

Patient characteristics (age at diagnosis of metastasis, sex, performance status), primary tumour characteristics (morphology, multifocality, tumour grade, clinical T stage, receptor

and HER2 status), clinical N stage at primary diagnosis and location of metastases and treatment (local and systemic therapy after diagnosis of primary tumour and metastases) were analysed. Receptor and HER2 status of the metachronous metastases were not available. Period of metastasis diagnosis was categorized in 2008-2011, 2012-2015 and 2016-2018. Within metachronous MBC, metastasis free interval (MFI), defined as time between primary diagnosis and distant recurrence, was categorized in 3-12 months, 12-24 months, 24-60 months and MFI > 60 months. OS was analysed using time between diagnosis of distant metastasis and death or end of follow-up. If patients were alive at the end of follow-up (January 31st 2022), they were censored.

Statistical analysis

Descriptive statistics were used to depict clinicopathological and treatment characteristics and to describe missing data. Chi-squared tests or Fisher's exact tests were used to test difference in characteristics between *de novo* and metachronous MBC. To describe OS of the groups, Kaplan Meier curves were plotted and multivariable Cox proportional hazards (PH) analyses were performed including important confounders. Because some confounders included missing data, we used multiple imputation by chained equations (MICE)[41]. Data were incomplete for any of the chosen variables in 19% of patients, therefore we considered 19 simulated datasets to have a sufficiently reliable estimation of missing values[42, 43]. The imputation model included MFI, which was used to categorize *de novo* versus metachronous MBC, and the following confounders: year of metastasis diagnosis; sex; age at metastasis diagnosis; tumour morphology; tumour multifocality; clinical T stage; clinical N stage; receptor status; metastasis location; tumour grade; performance status (assessed at primary diagnosis) and therapy variables, plus the outcome variables (vital status and the Nelson-Aalen estimator) as was recommended in literature[44-47].

The multivariable Cox PH model comparing survival of patients with *de novo* and metachronous MBC included the same variables included in the imputation model, except for tumour grade and performance status, which were considered confounders but contained too many missings. For the variable 'age at metastasis diagnosis' we used a restricted cubic spline with four knots. We also excluded therapy variables for several reasons. First, therapy choices are partly determined by the variable of interest (*de novo* versus metachronous MBC influences therapy choices) and are therefore not a confounder but an intermediary variable. Second, specifically in *de novo* MBC a RCT reported that local therapy of the primary tumour did not improve OS [10, 11], so local therapy is not a confounder either. Likelihood ratio tests of Cox PH models were used to compare OS between the groups. The PH assumption is the most important assumption underlying the Cox model [48]. The assumption was tested for each variable included in the Cox model using Schoenfeld residuals plots [49]). Confounding variables that did not meet the PH assumption were added as strata to the model. For the variable

of interest (*de novo* versus metachronous MBC), we visualised the time-varying effect of the hazards by plotting the hazard ratio (HR) against time. For this purpose, we generated a time dependent Cox model with an interaction between the variable (*de novo* vs metachronous) and a restricted cubic spline of survival time with five knots [50]. This time dependent model was based on one imputation dataset.

In addition to the described analyses we performed supplementary analyses to study patients with *de novo* and metachronous MBC separately in more detail, to test the robustness of our results and to explore hypotheses behind the differences in OS (Supplementary methods 1).

A p-value <0.05 was considered significant.

Statistical analyses were performed in Stata/SE 17.0 and R version 4.0.3.

RESULTS

Clinicopathological characteristics

Between 2008-2018, 8,656 patients were diagnosed with *de novo* MBC in the Netherlands. In addition, 2,374 patients were identified with metachronous MBC, of those, 639 had a primary tumour diagnosed in 2003, 1,006 in 2005, 524 in 2008 and 205 in Q1 of 2012.

Table 1 lists patient, tumour and treatment characteristics in patients with *de novo* and metachronous MBC. Most notable differences were those in T and N stages, metastasis locations and receptor status. Patients with *de novo* MBC were more likely than metachronous to have T3 or T4 tumours and positive loco-regional lymph nodes, while the majority (68%) of metachronous MBC had N0 at time of primary diagnosis. Notably, *de novo* metastases were more commonly limited to the bone with less frequent involvement of the liver or central nervous system (CNS) than in metachronous disease. However, in young *de novo* patients (≤ 40 years, n=489) we saw more liver metastases (39%, versus 25% in *de novo* patients of all ages and 38% in young metachronous patients). CNS involvement was the same (3%) in *de novo* patients above or below 40 years of age. ER-negative/HER2-negative tumours were observed less in *de novo* MBC. Although ER positivity did not differ between *de novo* patients and the entire group of metachronous MBC, supplementary analyses showed that ER-positive (HER2 negative/ unknown) tumours were more common in patients with metachronous MBC with a MFI > 60 months (83%), while patients with shorter MFI's had less ER positive tumours (39 to 65%) than patients with *de novo* MBC (67%) (supplementary table 1). Supplementary table 2 shows changes in patients with *de novo* MBC over time.

Table 1 Descriptive statistics *de novo* versus metachronous MBC, without multiple imputation

Characteristic	*De novo* or metachronous MBC patients				Statistics
	De novo MBC (N= 8,656)		Metachronous MBC (N=2,374)		
	N	(%)	N	(%)	P
Patient characteristics					
Sex					
Female	8,564	(99)	2,351	(99)	Pearson Chi² p = 0.690
Male	92	(1)	23	(1)	
Age at diagnosis of metastasis					
<50	1,774	(20)	457	(19)	Pearson Chi² **p<0.001**
50-69	3,658	(42)	1,135	(48)	
70+	3,224	(37)	782	(33)	
Age at diagnosis of metastasis	Mean age 63.7 (22-102)		Mean age: 63.2 yrs (24.6-97.7)		T-test p = 0.1296
Metastasis free interval (MFI)					
MFI 0 (*de novo*)	8,656		-		Not applicable
MFI 3-12 months	-		87	(3.7)	
MFI 12-24 months	-		204	(8.6)	
MFI 24-60 months	-		1,061	(44.7)	
MFI > 60 months	-		1,022	(43.0)	
Tumour characteristics					
Clinical T stage					
T0 or Tis	167	(2)	6	(0.3)	Pearson Chi² **p<0.001**
T1	1,226	(15)	1,022	(46)	
T2	2,889	(36)	917	(41)	
T3	1,130	(14)	151	(7)	
T4	2,675	(33)	115	(5)	
T unknown	569	-	163	-	
Multifocality					
No	5,679	(74)	1,842	(80)	Pearson Chi² **p<0.001**
Yes	2,037	(26)	447	(20)	
Unknown	940	-	85	-	
Clinical N stage					
N0	1,771	(22)	1,529	(68)	Pearson Chi² **p<0.001**
N1	4,389	(54)	689	(31)	
N2	337	(4)	14	(1)	
N3	1,594	(20)	21	(1)	
N unknown	565	-	121	-	
Tumour morphology					
Ductal carcinoma NOS	7,030	(81)	1,997	(84)	Pearson Chi² **p<0.001**
Ductal carcinoma in situ	33	(0.4)	31	(1)	
Invasive lobular carcinoma	1,361	(16)	309	(13)	
Low grade special types	105	(1)	29	(1)	
Other	127	(1)	8	(0.3)	
Tumour grade					
Low grade	287	(8)	206	(10)	Too many missings, no test performed
Intermediate grade	1,865	(51)	939	(45)	
High grade	1,514	(41)	963	(46)	
Undifferentiated/anaplastic	9	(0.2)	0	(0)	
Unknown	4,981	-	266	-	
ER status					
ER negative (<10%)	1,807	(21)	512	(22)	Pearson Chi2 p = 0.643
ER positive (≥10%)	6,641	(79)	1,833	(78)	
ER unknown/not determined	208	-	29	-	

2

Table 1 Continued

Characteristic	De novo or metachronous MBC patients				Statistics
	De novo MBC (N= 8,656)		Metachronous MBC (N=2,374)		
	N	(%)	N	(%)	P
Tumour characteristics					
PR status					
PR negative (<10%)	3,494	(43)	928	(42)	Pearson Chi^2 p = 0.468
PR positive (≥10%)	4,700	(57)	1,293	(58)	
PR unknown/not determined	462	-	153	-	
Her2 status					
Her2 negative	5,934	(77)	1,471	(80)	Pearson Chi^2 **p = 0.002**
Her2 positive	1,767	(23)	358	(20)	
Her2 unclear	955	-	545	-	
Receptor status					
ER pos HER2 neg/unknown	5,629	(67)	1,622	(69)	Pearson Chi^2 **p<0.001**
Her2 pos	1,767	(21)	358	(15)	
ER neg Her2 neg/unknown	1,072	(13)	368	(16)	
Insufficient information	188	-	26	-	
Localization of metastasis					
Lymph nodes only	468	(5)	60	(3)	Pearson Chi^2 **p<0.001**
Bone only	2,949	(34)	510	(22)	
Liver (no CNS)	2,177	(25)	727	(31)	
CNS (with/without liver)	274	(3)	290	(12)	
All other locations	2,760	(32)	774	(33)	
Metastasis location unknown	28	-	13	-	
Treatment characteristics					
Local treatment primary tumour					
No local treatment primary	6,383	(74)	1	(0)	Fisher's exact **p<0.001**
Surgery and radiotherapy	975	(11)	1,624	(68)	
Surgery without radiotherapy	996	(12)	749	(32)	
Radiotherapy without surgery	302	(3)	0	(0)	
Any systemic therapy after previous primary tumour diagnosis					
No	Not applicable		617	(26)	Not applicable
Yes			1,757	(74)	
Unknown			0	-	
Any systemic therapy in metastatic setting					
No	937	(11)	478	(21)	Pearson Chi^2 **p<0.001**
Yes	7,719	(89)	1,816	(79)	
Unknown	0	-	80	-	
Systemic therapy in metastatic setting contains chemotherapy					
No	5,239	(61)	1,383	(60)	Fisher's exact **p<0.001**
Yes	3,417	(39)	824	(36)	
Systemic therapy of unknown type	0	(0)	87	(4)	
Unknown	0	-	80	-	
Systemic therapy in metastatic setting contains endocrine treatment					
No	4,385	(51)	1,312	(57)	Fisher's exact **p<0.001**
Yes	4,271	(49)	895	(39)	
Systemic therapy of unknown type	0	(0)	87	(4)	
Unknown	0	-	80	-	

Table 1 Continued

Characteristic	*De novo* or metachronous MBC patients				Statistics
	De novo MBC (N= 8,656)		Metachronous MBC (N=2,374)		
	N	(%)	N	(%)	P
Treatment characteristics					
Systemic therapy in metastatic setting contains targeted therapy					
No	6,924	(80)	1,903	(83)	Fisher's exact **p<0.001**
Yes	1,732	(20)	304	(13)	
Systemic therapy of unknown type	0	(0)	87	(4)	
Unknown	0	-	80	-	
Systemic therapy in metastatic setting					
No systemic therapy	937	(11)	478	(21)	Pearson Chi^2 **p<0.001**
Endocrine treatment	4,119	(48)	875	(38)	
Chemotherapy (without HER2 targeted therapy)	2,116	(24)	661	(29)	
HER2 targeted therapy	1,484	(17)	191	(8)	
Systemic therapy of unknown type	0	(0)	89	(4)	
Unknown	0	-	80	-	
Any local treatment of metastasis					
No	6,497	(75)	1,803	(76)	Pearson Chi^2 p = 0.309
Yes	2,159	(25)	567	(24)	
Unknown	0		4	-	
Surgery of metastasis					
No	8,337	(96)	2,059	(87)	Pearson Chi^2 **p<0.001**
Yes	319	(4)	311	(13)	
Unknown	0	-	4	-	
Radiotherapy of metastasis					
No	6,728	(78)	2,071	(87)	Pearson Chi^2 **p<0.001**
Yes	1,928	(22)	299	(13)	
Unknown	0	-	4		

Treatment characteristics

Local treatment of the primary breast tumour was performed in 26% of patients with *de novo* MBC, in 43% consisting of surgery combined with radiotherapy, and in all patients with metachronous MBC at initial diagnosis. 74% of patients with metachronous metastases had received systemic treatment after primary tumour diagnosis.

Systemic therapy for metastatic disease was administered in 89% of *de novo* and in 79% of metachronous stage IV patients. Chemotherapy (without HER2 targeting agents) was administered less often to patients with *de novo* MBC (24% vs 29%) (**Table 1**). Meanwhile, *de novo* ER positive patients received endocrine treatment more often (67% vs 48%) and *de novo* HER2 positive patients received HER2 targeted therapy more often (75% vs 41%). Radiotherapy was the preferred locoregional treatment in *de novo* patients while surgery was more common in metachronous patients.

Supplementary table 2 shows changes in treatment of patients with de novo MBC over time, these changes could not reliably be compared between de novo and metachronous MBC due to the method of registration for patients with metachronous metastases (from just four primary tumour years, **Fig. 1**.).
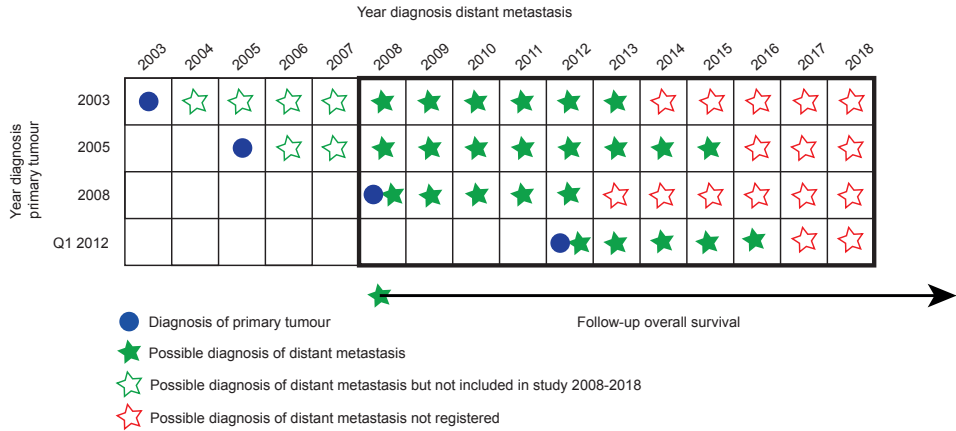
Fig. 1 Selection of patients with metachronous metastatic breast cancer. Patients diagnosed with metachronous distant metastases in 2008-2018 were identified among patients diagnosed with primary tumours in 2003, 2005, 2008 and the first quartile of 2012 (Q1 2012). For patients with a primary diagnosis in 2003 and 2005 all recurrences up to 10 years after initial breast cancer diagnosis were identified. For half of the patients with a primary diagnosis in 2008 the first recurrence up to 5 years after initial diagnosis was identified. For patients diagnosed in the first quartile of 2012, all recurrences up to 5 years post diagnosis were identified. Blue circles indicate primary tumour diagnosis, green filled stars indicate a possible diagnosis of distant metastasis included in our study. Empty stars indicate a possible diagnosis of distant metastasis that was not included in our study because it was outside the study period (green) or because it was not registered (red).

Survival in de novo versus metachronous MBC

Among patients treated with systemic therapy in the metastatic setting, median OS in patients with metachronous MBC was 24.3 months (95% CI 22.5 − 25.5 months), compared to 34.7 months (95% CI 33.7-35.8 months) in those with *de novo* MBC (Log-rank test p<0.001) (**Fig. 2**). In the multivariable Cox PH analysis a difference in OS between *de novo* and metachronous MBC persisted (HR *de novo* MBC versus metachronous MBC 0.75, 95% CI 0.70-0.80, Likelihood ratio test p<0.001) (**Table 2**). Sensitivity analysis supported these findings when analysing complete cases and showed that within patients with metachronous MBC, patients with a longer MFI survived longer, although still not similar to patients with *de novo* MBC (Supplementary: fig 1, table 3, and table 4). **Figure 3** shows the changes in HR of patients with *de novo* versus metachronous MBC over time, while keeping all other variables constant. Although the HR varied over time, *de novo* MBC appeared to have a lower risk of death than metachronous MBC over the

entire period of follow-up. The difference is most pronounced two years after diagnosis of metastatic disease. Beyond approximately eight years the HR estimate becomes increasingly imprecise.

Further exploratory analysis showed that d*e novo* MBC is not always associated with longer survival. In fact, patients with metachronous MBC who had not received previous (neoadjuvant or adjuvant) systemic treatment following their primary tumour diagnosis (n=461) survived longer than patients with *de novo* MBC (median OS 37.2 months, multivariable HR de novo MBC 1.13, 95% CI 1.01- 1.27) (Supplementary fig. 3 and table 6). Note that these were patients with favourable characteristics at primary tumour diagnosis, nearly all (97%) had T1 (75%) or T2 (22%) and 74% was ER positive and HER2 negative or unknown.
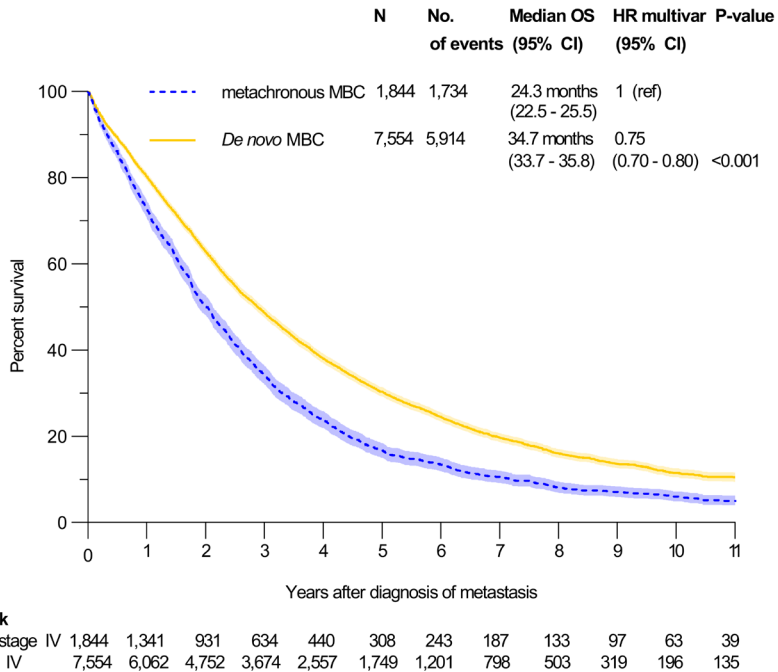
Fig. 2 Overall survival in patients with *de novo* versus patients metachronous metastatic breast cancer (treated with systemic therapy in the metastatic setting). The 95% confidence interval is indicated by colour around the line, number of patients at risk is noted below each year of follow-up. Overall survival is significantly longer in *de novo* MBC patients compared to metachronous MBC patients

Table 2 Multivariable Cox proportional hazards analysis *de novo* versus metachronous MBC patients (treated with systemic therapy in metastatic setting). Multiple imputation was used before multivariable analysis. Stratification was performed for receptor status and localization of metastasis.

Characteristic	Category	HR (95% CI)	Likelihood ratio test P Value
De novo versus metachronous MBC	Metachronous MBC	1 (ref)	
	De novo MBC	0.75 (0.70-0.80)	**<0.001**
Patient characteristics			
Period of metastasis diagnosis	2008-2011	1 (ref)	
	2012-2015	0.81 (0.77-0.85)	**<0.001**
	2016-2018	0.71 (0.66-0.76)	**<0.001**
Sexe	Male	1 (ref)	
	Female	0.86 (0.69-1.07)	0.173
Age at diagnosis of metastasis, restricted cubic spline (rcs))	Restricted cubic spline with four knots.		p-value omitted
Tumour characteristics			
Morphology	Ductal carcinoma NOS	1 (ref)	
	Invasive lobular carcinoma	1.12 (1.05-1.19)	**<0.001**
Multifocality	Unifocal primary tumour	1 (ref)	
	Multifocal primary tumour	0.96 (0.91-1.01)	0.149
Clinical T stage	T0 or Tis	1.11 (0.92-1.35)	0.269
	T1	1 (ref)	
	T2	1.09 (1.02-1.16)	**0.013**
	T3	1.13 (1.04-1.24)	**0.006**
	T4	1.31 (1.22-1.42)	**<0.001**
Clinical N stage	N0	1 (ref)	
	N1	1.13 (1.06-1.20)	**<0.001**
	N2	1.20 (1.05-1.38)	**0.008**
	N3	1.20 (1.10-1.30)	**<0.001**
Receptor status	ER + HER2- /unknown	Stratification factor	
	Her2 + (regardless of ER)		
	ER- HER2- / unknown		
Localization of metastasis	Lymph nodes only	Stratification factor	
	Bone only		
	Liver (no CNS)		
	CNS (with/without liver)		
	All other locations		

Fig. 3 Overall survival in patients with *de novo* versus metachronous metastatic breast cancer (treated with systemic therapy in the metastatic setting), hazard ratio over time in multivariable analysis performed on the first multiple imputed dataset. The 95% confidence interval is indicated by colour around each line. The difference in overall survival was not proportional over time, with a lower HR in favour of *de novo* MBC in the first years of follow-up in the multivariable model, while the HR starts to rise towards 1.0 after about 5 years. Note that the confidence interval widens after about eight years

DISCUSSION

In this large population-based study, we compared clinicopathological features, treatment and OS between all patients with *de novo* MBC diagnosed in the Netherlands between 2008 and 2018 to a group of patients with metachronous MBC diagnosed in that same period. Our study shows that these are not only two very distinct groups but also that patients with *de novo* MBC survive longer.

A number of differences in characteristics between the groups are notable. Our data corroborate earlier reports of frequent bone and lymph node metastases and less involvement of viscera and brain in patients with *de novo* MBC [4, 30, 31]. However, in our comparison of both groups, we did not observe more ER positive tumours in *de novo* patients [28], most likely caused by the 43% of metachronous patients with a MFI >60 months, who are more often ER positive. Stage T3 and T4 and multifocal tumours were more often encountered in patients with *de novo* MBC, possibly reflecting delay in time to diagnosis. In *de novo* MBC, metastases limited to the bone were more common than in metachronous MBC resulting in increased use of endocrine treatment in this group, as was local radiotherapy on painful bone metastases [5]. The higher prevalence of triple

negative tumours, liver and CNS metastases reflect unfavourable tumour characteristics and biology in metachronous patients. For example, triple negative tumours are known to metastasize hematogenously more often.

Regarding outcome, our data support a better OS in *de novo* MBC compared to patients with metachronous MBC, partly explained by differences in disease characteristics. Even after correction for known confounding characteristics, improved survival persists in patients with *de novo* MBC. This finding is consistent with previous literature [4, 21, 28, 30, 33-35] showing that absolute differences in median OS range from 1.5 months (when comparing *de novo* to MFI > 24 months) to 20.3 months (comparing to MFI < 24 months) [31]. Without selection for MFI the reported median OS differences are similar to the 10.4 months found in our study [28, 30, 32, 33]. In our sensitivity analysis we found a similar effect of MFI on OS compared to the literature: longer MFI was associated with longer OS after diagnosis of metastases. However, even MFI>60 months did not have better survival than *de novo* MBC, which is not a consistent observation [21, 31, 34].

There are a number of possible explanations for the longer survival observed in *de novo* MBC. The most likely hypothesis is that shorter survival of patients with metachronous MBC is related to previous (neo)adjuvant systemic therapies. Recurrence despite previous therapy could reflect 1) disadvantageous tumour-characteristics, 2) patient comorbidity / fitness and 3) primary or acquired therapy resistance. In our study, we could not quantify to what extent these factors played a role because we did not have data on the exact regimens and duration of systemic therapy nor could we account for fitness because data on performance score was only assessed at primary breast cancer diagnosis and contained too many missing values to include in the model. Nevertheless, the difference in use of systemic therapy in the metastatic setting (any systemic therapy in 89% of *de novo* and 79% of metachronous MBC and specifically targeted therapy in 75% of *de novo* and 41% of metachronous HER2 positive patients) may indicate that metachronous patients were less fit or had less treatment options for other reasons. As mentioned before, previous therapy can decrease treatment options in the metastatic setting due to acquired resistance to a drug, reaching a maximum tolerated cumulative dose or lasting side effects such as peripheral neuropathy or cardiotoxicity. Of note, due to the method of registration our data on systemic therapy could be an underestimation, as therapies administered not directly after metastasis diagnosis, but for example when symptoms did arise, may have been missed. In addition, the difference in targeted therapy among HER2 positive patients could be an overestimation because HER2 status was determined on the primary tumour and (a small percentage of) metachronous patients may have converted to HER2 negative. The same might be true for endocrine treatment, as metastases of an ER positive primary may be ER negative.

Still, we did find some evidence to corroborate the hypothesis that previous systemic therapy plays a role in the survival difference between *de novo* and metachronous MBC. In a supplementary exploratory analysis we observed a longer OS among patients with

metachronous MBC who were not systemically treated for their primary tumour. While this metachronous group had favourable characteristics at primary tumour diagnosis, the difference remained after correcting for baseline characteristics.

We also hypothesize that differences in metastatic burden could contribute to the observed differences in survival. Possibly, clinicians are inclined to perform more (and perhaps more sensitive) diagnostic imaging in a patient presenting with *de novo* MBC than in those diagnosed with recurrent disease. This would lead to detection of smaller, asymptomatic or oligo metastases in *de novo* MBC, associated with longer survival and possibly even curative treatment options. Although we have no data on number or volume of metastases, our data do support this hypothesis (Supplementary table 2) as we saw an increase in patients with *de novo* distant metastases limited to lymph nodes and increased use of anthracycline and taxane treatment (first choice in the neoadjuvant curative setting [5] and used for curative treatment of oligometastases).

In this study we extensively studied OS of patients with *de novo* and metachronous MBC using Kaplan Meier curves and Cox PH analysis. In the literature it is seldom reported whether the PH assumption was met and time-varying effects are often overlooked[51]. In our study, the variable of interest (*de novo* versus metachronous MBC) did not meet the PH assumption and therefore we additionally estimated the time-varying effects on OS. Overall, it appeared that the OS difference between de novo and metachronous MBC persisted over the years. The relatively small difference in OS between *de novo* and metachronous MBC in the first year could mean that a group of patients progress and die quickly despite any beneficial characteristic. Apparently, differences between *de novo* and metachronous MBC start to count after surviving longer than a year.

This study is unique as it presents a complete overview of patients with *de novo* MBC diagnosed in 2008 - 2018 in the Netherlands and the comparison to patients with metachronous MBC. The data convincingly shows that patients with *de novo* and metachronous MBC are distinct patient groups.

However, there are some limitations of our data. It would be relevant to also study metachronous patients in more detail using nationwide data. The MFI of our patients was probably not an accurate representation of all patients with metachronous MBC in 2008-2018 because the majority of metachronous patients in our cohort had their initial diagnosis in 2003 or 2005 (thus MFI at least 5 or 3 years respectively) (**Fig. 1**). Another limitation is that for patients with an initial diagnosis in 2008, distant metastases were only registered if they did not have a local or regional recurrence preceding the occurrence of metastases. Due to this registration difference, we probably missed approximately 20% of patients with metachronous MBC and an initial diagnosis in 2008 (i.e. of patients with a primary tumour in 2003/2005/Q1 2012, about 20% had a local or regional preceding their distant metastases). Additional patients were missed because recurrences from 2008 had only been registered in half of the hospitals. Nationwide data including all patients with metachronous metastases in a given period would

2

have allowed a more accurate comparison of the two groups. Ideally, such data would also include information on metastatic burden (e.g. oligometastases), receptor and HER2 status of the metastases and information about treatment administered in the metastatic setting in more detail and beyond those given as initial therapy.

CONCLUSION

Dutch patients with *de novo* MBC survive longer compared to patients with metachronous metastases, also following correction for different clinicopathological characteristics. Our data show that *de novo* and metachronous MBC represent two distinct groups, the presence of a primary tumour being not the only difference.

ETHICS AND DISSEMINATION

The datasets generated and/or analysed during the current study are not publicly available due to privacy reasons but are available from the Netherlands Cancer Registry on reasonable request.
This study was approved by the Netherlands Cancer Registry's Supervisory Committee (reference number K19.155).

AUTHOR CONTRIBUTIONS

All authors contributed to the study conception and design. Josanne de Maar and Marianne Luyendijk contributed equally. Material preparation, data collection and analysis were performed by Josanne de Maar and Marianne Luyendijk. The first draft of the manuscript was written by Josanne de Maar and revised by Marianne Luyendijk and all authors commented on previous versions of the manuscript. All authors read and approved the final manuscript.

FUNDING

ACKNOWLEDGEMENTS

CONFLICTS OF INTEREST

The authors declare that they have no relevant financial or non-financial interests to disclose.

2

ABBREVIATIONS

CNS	central nervous system
ER	estrogen receptor
HER2	human epidermal growth factor receptor 2
HR	hazard ratio
ICD-O	international classification of diseases for oncology
ILC	invasive lobular carcinoma
MFI	metastasis-free interval
MICE	multiple imputation by chained equations
NCR	Netherlands cancer registry
IKNL	Netherlands comprehensive cancer organisation (Dutch: integraal kankercentrum Nederland)
(ductal carcinoma) NOS	not otherwise specified
OS	overall survival
PALGA	Dutch nationwide pathology archive
PH	proportional hazards
PR	progesterone receptor
TNM	tumour, node, metastasis classification of the Union for International Cancer Control

REFERENCES

1.   IKNL (2021) Breast cancer in the Netherlands, trends 1989 - 2020 based on data from the Netherlands Cancer Registry (Flyer IKNL, title translated from Dutch). https://iknl.nl/getmedia/fe459c3a-c561-40de-b740-fff15997f020/IKNL-Folder-Borstkanker-2020.pdf. Accessed 15 February 2022

2.   Ruiterkamp J, Ernst MF, de Munck L, van der Heiden-van der Loo M, Bastiaannet E, van de Poll-Franse LV, Bosscha K, Tjan-Heijnen VC, Voogd AC (2011) Improved survival of patients with primary distant metastatic breast cancer in the period of 1995-2008. A nationwide population-based study in the Netherlands. Breast Cancer Res Treat 128(2):495-503. https://doi.org/10.1007/s10549-011-1349-x

3.   van den Hurk CJ, Eckel R, van de Poll-Franse LV, Coebergh JW, Nortier JW, Holzel D, Breed WP, Engel J (2011) Unfavourable pattern of metastases in M0 breast cancer patients during 1978-2008: a population-based analysis of the Munich Cancer Registry. Breast Cancer Res Treat 128(3):795-805. https://doi.org/10.1007/s10549-011-1372-y

4.   Malmgren JA, Mayer M, Atwood MK, Kaplan HG (2018) Differential presentation and survival of de novo and recurrent metastatic breast cancer over time: 1990-2010. Breast Cancer Res Treat 167(2):579-590. https://doi.org/10.1007/s10549-017-4529-5

5.   Federatie Medisch Specialisten (Last authorised 2020) Borstkanker (Dutch guideline breast cancer). https://richtlijnendatabase.nl/richtlijn/borstkanker/algemeen.html Accessed 17 February 2022

6.   Gennari A, Andre F, Barrios CH, Cortes J, de Azambuja E, DeMichele A, Dent R, Fenlon D, Gligorov J, Hurvitz SA, et al. (2021) ESMO Clinical Practice Guideline for the diagnosis, staging and treatment of patients with metastatic breast cancer. Ann Oncol 32(12):1475-1495. https://doi.org/10.1016/j.annonc.2021.09.019

7.   Khan SA (2016) Surgical Management of de novo Stage IV Breast Cancer. Semin Radiat Oncol 26(1):79-86. https://doi.org/10.1016/j.semradonc.2015.08.004

8.   Headon H, Wazir U, Kasem A, Mokbel K (2016) Surgical treatment of the primary tumour improves the overall survival in patients with metastatic breast cancer: A systematic review and meta-analysis. Mol Clin Oncol 4(5):863-867. https://doi.org/10.3892/mco.2016.778

9.   Soran A, Ozmen V, Ozbas S, Karanlik H, Muslumanoglu M, Igci A, Canturk Z, Utkan Z, Ozaslan C, Evrensel T, et al. (2018) Randomized Trial Comparing Resection of Primary Tumor with No Surgery in Stage IV Breast Cancer at Presentation: Protocol MF07-01. Ann Surg Oncol 25(11):3141-3149. https://doi.org/10.1245/s10434-018-6494-6

10. Tsukioki T, Shien T, Doihara H (2020) Effect of local surgery on outcomes of stage IV breast cancer. Translational Cancer Research 9(8):5102-5107. https://doi.org/10.21037/tcr.2020.01.60

11. Khan SA, Zhao F, Goldstein LJ, Cella D, Basik M, Golshan M, Julian TB, Pockaj BA, Lee CA, Razaq W, et al. (2022) Early local therapy for the primary site in de novo stage IV breast cancer: results of a randomized clinical trial (EA2108). Journal of Clinical Oncology 40(9):978-987. https://doi.org/https://doi.org/10.1200/JCO.21.02006

12. Miao H, Hartman M, Bhoo-Pathy N, Lee SC, Taib NA, Tan EY, Chan P, Moons KG, Wong HS, Goh J, et al. (2014) Predicting survival of de novo metastatic breast cancer in Asian women: systematic review and validation study. PLoS One 9(4):e93755. https://doi.org/10.1371/journal.pone.0093755

13. Zeichner SB, Herna S, Mani A, Ambros T, Montero AJ, Mahtani RL, Ahn ER, Vogel CL (2015) Survival of patients with de-novo metastatic breast cancer: analysis of data from a large breast cancer-specific private practice, a university-based cancer center and review of the literature. Breast Cancer Res Treat 153(3):617-624. https://doi.org/10.1007/s10549-015-3564-3

14. Bertaut A, Mounier M, Desmoulins I, Guiu S, Beltjens F, Darut-Jouve A, Ponnelle T, Arnould L, Arveux P (2015) Stage IV breast cancer: a population-based study about prognostic factors according to HER2 and HR status. Eur J Cancer Care (Engl) 24(6):920-928. https://doi.org/10.1111/ecc.12306

15. Eng LG, Dawood S, Sopik V, Haaland B, Tan PS, Bhoo-Pathy N, Warner E, Iqbal J, Narod SA, Dent R (2016) Ten-year survival in women with primary stage IV breast cancer. Breast Cancer Res Treat 160(1):145-152. https://doi.org/10.1007/s10549-016-3974-x

16. Tao L, Chu L, Wang LI, Moy L, Brammer M, Song C, Green M, Kurian AW, Gomez SL, Clarke CA (2016) Occurrence and outcome of de novo metastatic breast cancer by subtype in a large, diverse population. Cancer Causes Control 27(9):1127-1138. https://doi.org/10.1007/s10552-016-0791-9

17. Leone BA, Vallejo CT, Romero AO, Machiavelli MR, Perez JE, Leone J, Leone JP (2017) Prognostic impact of metastatic pattern in stage IV breast cancer at initial diagnosis. Breast Cancer Res Treat 161(3):537-548. https://doi.org/10.1007/s10549-016-4066-7

18. Press DJ, Miller ME, Liederbach E, Yao K, Huo D (2017) De novo metastasis in breast cancer: occurrence and overall survival stratified by molecular subtype. Clin Exp Metastasis 34(8):457-465. https://doi.org/10.1007/s10585-017-9871-9

19. Vaz-Luis I, Lin NU, Keating NL, Barry WT, Winer EP, Freedman RA (2017) Factors Associated with Early Mortality Among Patients with De Novo Metastatic Breast Cancer: A Population-Based Study. Oncologist 22(4):386-393. https://doi.org/10.1634/theoncologist.2016-0369

20. Ogiya R, Sagara Y, Niikura N, Freedman RA (2019) Impact of Subtype on Survival of Young Patients With Stage IV Breast Cancer. Clin Breast Cancer 19(3):200-207.e. https://doi.org/10.1016/j.clbc.2019.01.005

21. McKenzie HS, Maishman T, Simmonds P, Durcan L, Group PS, Eccles D, Copson E (2020) Survival and disease characteristics of de novo versus recurrent metastatic breast cancer in a cohort of young patients. Br J Cancer 122(11):1618-1629. https://doi.org/10.1038/s41416-020-0784-z

22. He ZY, Lian CL, Wang J, Lei J, Hua L, Zhou J, Wu SG (2020) Incorporation of biologic factors for the staging of de novo stage IV breast cancer. NPJ Breast Cancer 6:43. https://doi.org/10.1038/s41523-020-00186-5

23. Plichta JK, Thomas SM, Sergesketter AR, Greenup RA, Rosenberger LH, Fayanju OM, Kimmick G, Force J, Hyslop

T, Hwang ES (2020) A Novel Staging System for De Novo Metastatic Breast Cancer Refines Prognostic Estimates. Ann Surg 275(4). https://doi.org/10.1097/SLA.0000000000004231

24. Gu Y, Wu G, Zou X, Huang P, Yi L (2020) Prognostic Value of Site-Specific Metastases and Surgery in De Novo Stage IV Triple-Negative Breast Cancer: A Population-Based Analysis. Med Sci Monit 26:e920432. https://doi.org/10.12659/MSM.920432

25. Li Y, Wang S, Yang W, Liu H (2021) Prognostic significance of molecular subtype, metastatic site and primary tumor surgery for survival in primary metastatic breast cancer: A SEER-based study. Medicine (Baltimore) 100(27):e26619. https://doi.org/10.1097/MD.0000000000026619

26. Zheng A, Guo BL, Zhang JG, Jin F, Chinese Society of Breast Surgery (2021) Clinical information and management status of de novo stage IV breast cancer patients: a Chinese multicenter investigation (CSBrS-002). Chin Med J (Engl) 134(13):1569-1575. https://doi.org/10.1097/CM9.0000000000001415

27. Leone JP, Leone BA, Zwenger AO, Vallejo CT, Romero AO, Machiavelli MR, Perez JE, Leone J (2021) The prognostic significance of metastatic pattern in stage IV male breast cancer at initial diagnosis: a population-based study. Breast Cancer Res Treat 187(1):237-244. https://doi.org/10.1007/s10549-020-06052-z

28. Dawood S, Broglio K, Ensor J, Hortobagyi GN, Giordano SH (2010) Survival differences among women with de novo stage IV and relapsed breast cancer. Ann Oncol 21(11):2169-2174. https://doi.org/10.1093/annonc/mdq220

29. Rossi V, Nole F, Redana S, Adamoli L, Martinello R, Aurilio G, Verri E, Sapino A, Viale G, Aglietta M, et al. (2014) Clinical outcome in women with HER2-positive de novo or recurring stage IV breast cancer receiving trastuzumab-based therapy. Breast 23(1):44-49. https://doi.org/10.1016/j.breast.2013.10.005

30. Yardley DA, Kaufman PA, Brufsky A, Yood MU, Rugo H, Mayer M, Quah C, Yoo B, Tripathy D (2014) Treatment patterns and clinical outcomes for patients with de novo versus recurrent HER2-positive metastatic breast cancer. Breast Cancer Res Treat 145(3):725-734. https://doi.org/10.1007/s10549-014-2916-8

31. Lobbezoo DJ, van Kampen RJ, Voogd AC, Dercksen MW, van den Berkmortel F, Smilde TJ, van de Wouw AJ, Peters FP, van Riel JM, Peters NA, et al. (2015) Prognosis of metastatic breast cancer: are there differences between patients with de novo and recurrent metastatic breast cancer? Br J Cancer 112(9):1445-1451. https://doi.org/10.1038/bjc.2015.127

32. Lambertini M, Ferreira AR, Di Meglio A, Poggio F, Puglisi F, Sottotetti F, Montemurro F, Poletto E, Bernardo A, Risi E, et al. (2017) Patterns of Care and Clinical Outcomes of HER2-positive Metastatic Breast Cancer Patients With Newly Diagnosed Stage IV or Recurrent Disease Undergoing First-line Trastuzumab-based Therapy: A Multicenter Retrospective Cohort Study. Clin Breast Cancer 17(8):601-610. https://doi.org/10.1016/j.clbc.2017.04.002

33. den Brok WD, Speers CH, Gondara L, Baxter E, Tyldesley SK, Lohrisch CA (2017) Survival with metastatic breast cancer based on initial presentation, de novo versus relapsed. Breast Cancer Res Treat 161(3):549-556. https://doi.org/10.1007/s10549-016-4080-9

34. Yamamura J, Kamigaki S, Fujita J, Osato H, Komoike Y (2018) The Difference in Prognostic Outcomes Between De Novo Stage IV and Recurrent Metastatic Patients with Hormone Receptor-positive, HER2-negative Breast Cancer. In Vivo 32(2):353-358. https://doi.org/10.21873/invivo.11245

35. Hassett MJ, Uno H, Cronin AM, Carroll NM, Hornbrook MC, Ritzwoller DP (2018) Comparing Survival After Recurrent vs De Novo Stage IV Advanced Breast, Lung, and Colorectal Cancer. JNCI Cancer Spectr 2(2):pky024. https://doi.org/10.1093/jncics/pky024

36. Seltzer S, Corrigan M, O'Reilly S (2020) The clinicomolecular landscape of de novo versus relapsed stage IV metastatic breast cancer. Exp Mol Pathol 114:104404. https://doi.org/10.1016/j.yexmp.2020.104404

37. Ernst MF, van de Poll-Franse LV, Roukema JA, Coebergh JW, van Gestel CM, Vreugdenhil G, Louwman MJ, Voogd AC (2007) Trends in the prognosis of patients with primary metastatic breast cancer diagnosed between 1975 and 2002. Breast 16(4):344-351. https://doi.org/10.1016/j.breast.2007.01.001

38. van der Meer DJ, Kramer I, van Maaren MC, van Diest PJ, S CL, Maduro JH, L JAS, Siesling S, Schmidt MK, Voogd AC (2021) Comprehensive trends in incidence, treatment, survival and mortality of first primary invasive breast cancer stratified by age, stage and receptor subtype in the Netherlands between 1989 and 2017. Int J Cancer 148(9):2289-2303. https://doi.org/10.1002/ijc.33417

39. Lord SJ, Bahlmann K, O'Connell DL, Kiely BE, Daniels B, Pearson SA, Beith J, Bulsara MK, Houssami N (2022) De novo and recurrent metastatic breast cancer – A systematic review of population-level changes in survival since 1995. eClinicalMedicine 44. https://doi.org/10.1016/j.eclinm.2022.101282

40. Schouten Lj, Höppener P, van den Brandt PA, Knottnerus JA, Jager JJ (1993) Completeness of cancer registration in Limburg, the Netherlands. International journal of epidemiology 22(3):369-376. https://doi.org/10.1093/ije/22.3.369

41. Rubin DB. Multiple imputation for nonresponse in surveys: John Wiley & Sons Inc., New York.; 1987.

42. Bodner TE (2008) What improves with increased missing data imputations? Structural equation modeling: a multidisciplinary journal 15:651-675.

43. White IR, Royston PW, A. M. (2011) Multiple imputation using chained equations: issues and guidance for practice. Statistics in medicine 30:377-399.

44. White IR, Royston P (2009) Imputing missing covariate values for the Cox model. Stat Med 28(15):1982-1998. https://doi.org/10.1002/sim.3618

45. Nelson W (1969) Hazard plotting for incomplete failure data. Journal of quality technology 1:27-52.

46. Nelson W (1972) Theory and applications of hazard plotting for censored failure data. Technometrics 14.

47. Aalen OO (1978) Nonparameteric inference for a family of counting processes. Annals of Statistics 6:701-726.

48. Cox DR (1972) Regression models and life-tables. Journal of the royal statistical society Series B (methodological) 34(2):187-220.

49. Schoenfeld D (1982) Partial residuals for the proportional hazards regression model. Biometrika 69(1):239-241. http://links.jstor.org/sici?sici=0006-3444%28198204%2969%3A1%3C239%3APRFTPH%3E2.0.CO%3B2-3

2

50.   Heinzl H, Kaider A (1997) Gaining more flexibility in Cox proportional hazards regression models with cubic spline functions. Computer methods and programs in biomedicine 54:201-208.
51.   Rulli E, Ghilotti F, Biagioli E, Porcu L, Marabese M, D'Incalci M, Bellocco R, Torri V (2018) Assessment of proportional hazard assumption in aggregate data: a systematic review on statistical methodology in clinical trials using time-to-event endpoint. Br J Cancer 119(12):1456-1463. https://doi.org/10.1038/s41416-018-0302-8

2

SUPPLEMENTARY MATERIALS

Supplementary methods 1 Methods used for supplementary analyses
In addition to the above described analyses we performed supplementary analyses in order to study patients with *de novo* and metachronous MBC separately in more detail, to test the robustness of our results and to explore hypotheses behind the differences in OS.

First, differences in clinicopathological characteristics were described between patients with *de novo* MBC diagnosed in different periods, and between patients with metachronous MBC with different MFIs. Next, to study whether OS of patients with *de novo* MBC has improved over time, a multivariable Cox PH analysis among patients with *de novo* MBC was performed to compare OS in different periods of diagnosis. In this Cox model, the same variables were included, but additionally therapy variables (local treatment of the primary tumour; type of first systemic therapy in the metastatic setting; surgery of metastases and radiotherapy of metastases) were included and additional strata were added for local therapy of the primary tumour and type of first systemic therapy in the metastatic setting.

As sensitivity analysis, the multivariable Cox PH analysis comparing *de novo* and metachronous MBC was repeated on the complete cases (n= 7774), to see what the effect of multiple imputation had been. Moreover, an additional multivariable Cox PH analysis was performed to compare OS between patients with *de novo* MBC and patients with metachronous MBC with different MFIs.

In an exploratory analysis we evaluated the OS of patients with *de novo* MBC compared to patients with metachonous MBC who had not received systemic treatment for their primary breast cancer diagnosis. Objective of this analysis was to explore whether the survival difference between *de novo* and metachronous MBC might be related to previous systemic treatment in metachronous MBC.
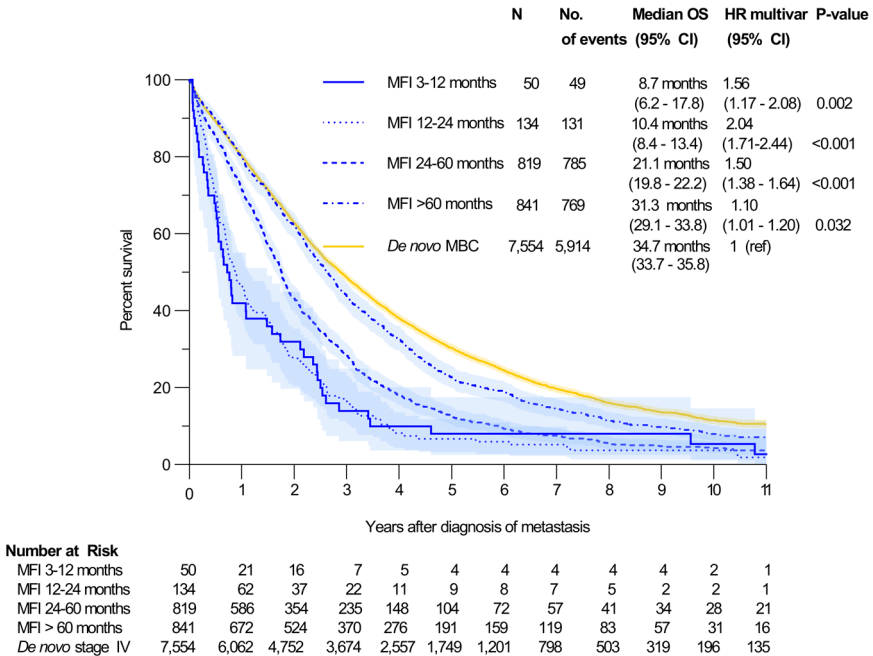
Supplementary fig. 1 Overall survival in patients with metastatic breast cancer (treated with systemic therapy in the metastatic setting), according to metastasis-free interval.

	N	No. of events	Median OS (95% CI)	HR multivar (95% CI)	P-value
2008-2011	2,347	2,184	29.3 months (27.5 - 30.7)	1 (ref)	
2012-2015	2,877	2,337	36.1 months (34.2 - 37.8)	0.82 (0.77 - 0.87)	<0.001
2016-2018	2,330	1,393	40.7 months (38.5 - 43.3)	0.73 (0.68 - 0.79)	<0.001

Number at Risk

	0	1	2	3	4	5	6	7	8	9	10	11
2008-2011	2,347	1,794	1,358	976	725	548	427	337	269	229	192	135
2012-2015	2,877	2,321	1,809	1,439	1,130	923	753	461	234	90	4	-
2016-2018	2,330	1,947	1,585	1,259	702	286	21	-	-	-	-	-

Supplementary fig. 2 Overall survival in patients with *de novo* metastatic breast cancer (treated with systemic therapy), according to period of diagnosis

	N	No. of events	Median OS (95% CI)	HR multivar (95% CI)	P-value
metachronous stage IV	461	411	37.2 months (32.3 - 41.0)	1 (ref)	
De novo MBC	7,554	5,914	34.7 months (33.7 - 35.8)	1.13 (1.01 - 1.27)	0.038

Number at Risk

	0	1	2	3	4	5	6	7	8	9	10	11
Metachronous stage IV	461	363	295	236	188	144	124	97	68	49	31	19
De novo stage IV	7,554	6,062	4,752	3,674	2,557	1,749	1,201	798	503	319	196	135
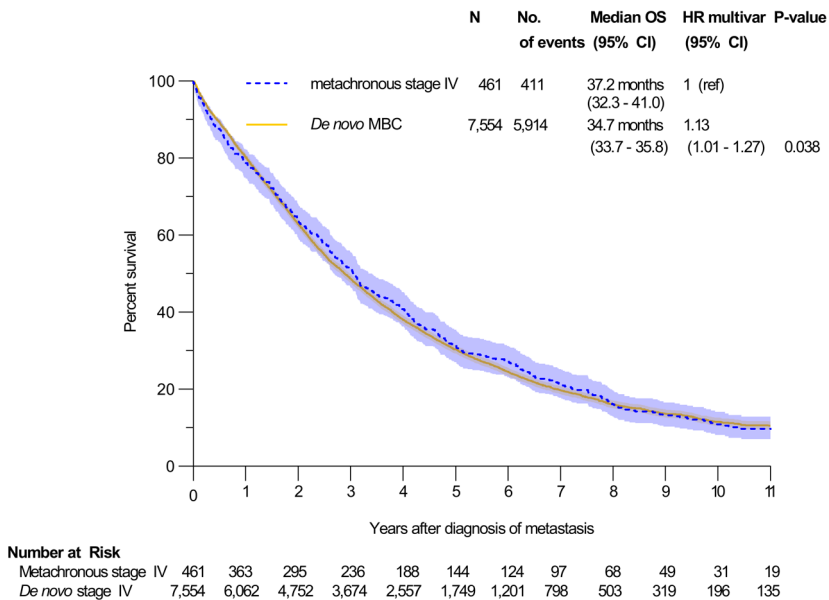
Supplementary fig. 3 Overall survival in patients with *de novo* versus metachronous metastatic breast cancer (treated with systemic therapy in the metastatic setting), these metachronous patients were not treated with systemic therapy at the time of their primary tumour

Supplementary table 1 Descriptive statistics patients with metachronous metastatic breast cancer: comparison by metastasis-free interval

Characteristic	Patients with metachronous MBC								Statistics
	MFI 3-12 months (N=87)		MFI 12-24 months (N=204)		MFI 24-60 months (N=1,061)		MFI > 60 months (N=1,022)		
	N	(%)	N	(%)	N	(%)	N	(%)	P
Patient characteristics									
Sex									
Female	87	(100)	198	(97)	1,054	(99)	1,012	(99)	Pearson Chi^2 **p = 0.017**
Male	0	(0)	6	(3)	7	(3)	10	(1)	
Age at diagnosis of metastasis									
<50	13	(15)	59	(29)	233	(22)	152	(15)	Pearson Chi^2 **p = 0.000**
50-69	26	(30)	77	(38)	502	(47)	530	(52)	
70+	48	(55)	68	(33)	326	(31)	340	(33)	
Age at diagnosis of metastasis	Mean age: 68.6 yrs (39.8-94)		Mean age 60.8 yrs (24.6-93.6)		Mean age 62.1 yrs (26.3-97.7)		Mean age 64.3 yrs (29.2-96.1)		
Performance status									
WHO-PS 0	5	(100)	14	(78)	46	(81)	1	(100)	Too many missings, no test performed
WHO-PS 1	0	(0)	2	(11)	9	(16)	0	(0)	
WHO-PS 2	0	(0)	2	(11)	2	(4)	0	(0)	
WHO-PS 3	0	(0)	0	(0)	0	(0)	0	(0)	
WHO-PS 4	0	(0)	0	(0)	0	(0)	0	(0)	
Unknown	82	-	186	-	1,004	-	1,022	-	
Tumour characteristics									
Clinical T stage									
T0 or Tis	1	(1)	0	(0)	1	(0)	4	(0)	Pearson Chi^2 **p = 0.000**
T1	22	(25)	60	(30)	443	(45)	497	(54)	
T2	33	(38)	99	(49)	433	(44)	352	(38)	
T3	15	(17)	27	(13)	66	(7)	43	(5)	
T4	16	(18)	17	(8)	51	(5)	31	(3)	
T unknown	0	-	1	-	67	-	95	-	
Multifocality									
No	71	(85)	155	(77)	804	(78)	812	(84)	Pearson Chi^2 **p = 0.003**
Yes	13	(15)	47	(23)	229	(22)	158	(16)	
Unknown	3	-	2	-	28	-	52	-	

Supplementary table 1 Continued

Characteristic	Patients with metachronous MBC								Statistics
	MFI 3-12 months (N=87)		MFI 12-24 months (N=204)		MFI 24-60 months (N=1,061)		MFI > 60 months (N=1,022)		
	N	(%)	N	(%)	N	(%)	N	(%)	P
Tumour characteristics									
Clinical N stage									
N0	44	(52)	104	(52)	656	(65)	725	(76)	Pearson Chi[2] **p = 0.000**
N1	38	(45)	90	(45)	340	(34)	221	(23)	
N2	1	(1)	1	(1)	5	(0.5)	7	(1)	
N3	2	(2)	4	(1)	13	(1)	2	(0.2)	
N unknown	2	-	5	-	47	-	67	-	
Tumour morphology									
Ductal carcinoma NOS	78	(90)	187	(92)	895	(84)	837	(82)	Pearson Chi[2] **p = 0.001**
Ductal carcinoma in situ	1	(1)	3	(1)	16	(2)	11	(1)	
Invasive lobular carcinoma	5	(6)	12	(6)	132	(12)	160	(16)	
Low grade special types	1	(1)	1	(0.5)	15	(1)	12	(1)	
Other	2	(2)	1	(0.5)	3	(0.3)	2	(0.2)	
Tumour grade									
Low grade	7	(9)	8	(5)	72	(8)	119	(13)	Too many missings, no test performed
Intermediate grade	19	(25)	39	(24)	409	(43)	472	(51)	
High grade	50	(66)	117	(71)	469	(49)	327	(36)	
Undifferentiated/anaplastic	0	(0)	0	(0)	0	(0)	0	(0)	
Unknown	11	-	40	-	111	-	104	-	
ER status									
ER negative (<10%)	50	(57)	105	(51)	263	(25)	94	(9)	Pearson Chi[2] **p = 0.000**
ER positive (≥10%)	37	(43)	99	(49)	789	(75)	908	(91)	
ER unknown/not determined	0	-	0	-	9	-	20	-	
PR status									
PR negative (<10%)	59	(70)	140	(71)	466	(47)	263	(28)	Pearson Chi[2] **p = 0.000**
PR positive (≥10%)	25	(30)	57	(29)	534	(53)	677	(72)	
PR unknown/not determined	3	-	7	-	61	-	82	-	
Her2 status									
Her2 negative	71	(85)	154	(76)	717	(79)	529	(84)	Pearson Chi[2] **p = 0.021**
Her2 positive	13	(15)	48	(24)	195	(21)	102	(16)	
Her2 unclear	3	-	2	-	149	-	391	-	

Supplementary table 1 Continued

Characteristic	Patients with metachronous MBC								Statistics
	MFI 3-12 months (N=87)		MFI 12-24 months (N=204)		MFI 24-60 months (N=1,061)		MFI > 60 months (N=1,022)		
	N	(%)	N	(%)	N	(%)	N	(%)	P
Tumour characteristics									
Receptor status									
ER pos HER2 neg/unknown	34	(39)	78	(38)	679	(65)	831	(83)	Pearson Chi[2]
Her2 pos	13	(15)	48	(24)	195	(19)	102	(10)	**p = 0.000**
ER neg Her2 neg/unknown	40	(46)	78	(38)	178	(17)	72	(7)	
Insufficient information	0	-	0	-	9	-	17	-	
Localization of metastasis									
Lymph nodes only	3	(3)	4	(2)	29	(3)	24	(2)	Pearson Chi[2]
Bone only	17	(20)	45	(22)	245	(23)	203	(20)	**p = 0.023**
Liver (no CNS)	26	(30)	65	(32)	341	(32)	295	(29)	
CNS (with/without liver)	15	(17)	37	(18)	108	(10)	130	(13)	
All other locations	26	(30)	53	(26)	330	(31)	365	(36)	
Metastasis location unknown	0	-	0	-	8	-	5	-	
Treatment characteristics									
Local treatment primary tumour									
No local treatment primary	0	(0)	0	(0)	1	(0.1)	0	(0)	Fisher's exact
Surgery and radiotherapy	56	(64)	143	(70)	738	(70)	687	(67)	p = 0.573
Surgery without radiotherapy	31	(36)	61	(30)	322	(30)	335	(33)	
Radiotherapy without surgery	0	-	0	-	0	-		-	
Any systemic therapy in metastatic setting									
No	34	(40)	67	(33)	214	(21)	163	(17)	Pearson Chi[2]
Yes	50	(60)	134	(67)	818	(79)	814	(83)	**p = 0.000**
Unknown	3	-	3	-	29	-	45	-	
Systemic therapy in metastatic setting contains chemotherapy									
No	54	(64)	123	(61)	592	(57)	614	(63)	Pearson Chi[2]
Yes	30	(36)	78	(39)	427	(41)	289	(30)	**p = 0.000**
Systemic therapy of unknown type	0	(0)	0	(0)	13	(1)	74	(8)	
Unknown	3	-	3	-	29	-	45	-	

Supplementary table 1 Continued

Characteristic	Patients with metachronous MBC								Statistics	
	MFI 3-12 months (N=87)		MFI 12-24 months (N=204)		MFI 24-60 months (N=1,061)		MFI > 60 months (N=1,022)			
	N	(%)	N	(%)	N	(%)	N	(%)		P
Treatment characteristics										
Systemic therapy in metastatic setting contains endocrine treatment										
No	64	(76)	145	(72)	646	(63)	457	(47)	Pearson Chi[2]	**p=0.000**
Yes	20	(24)	56	(28)	373	(36)	446	(46)		
Systemic therapy of unknown type	0	(0)	0	(0)	13	(1)	74	(8)		
Unknown	3	-	3	-	29	-	45	-		
Systemic therapy in metastatic setting contains targeted therapy										
No	77	(92)	180	(90)	845	(82)	801	(82)	Pearson Chi[2]	**p = 0.000**
Yes	7	(8)	21	(10)	174	(17)	102	(10)		
Systemic therapy of unknown type	0	(0)	0	(0)	13	(1)	74	(8)		
Unknown	3	-	3	-	29	-	45	-		
Systemic therapy at time of metastasis										
No systemic therapy as first line	34	(40)	67	(33)	214	(21)	163	(17)	Pearson Chi[2]	**p = 0.000**
Endocrine treatment as first line	20	(24)	53	(26)	362	(35)	440	(45)		
Chemotherapy (without HER2 targeted therapy) as first line	25	(30)	71	(35)	333	(32)	232	(24)		
HER2 targeted therapy as first line	5	(6)	10	(5)	110	(11)	66	(7)		
Systemic therapy of unknown type	0	(0)	0	(0)	13	(1)	76	(8)		
Unknown	3	-	3	-	29	-	45	-		
Any local treatment of metastasis										
No	71	(82)	161	(79)	797	(75)	774	(76)	Pearson Chi[2]	p= 0.440
Yes	16	(18)	43	(21)	260	(25)	248	(25)		
Unknown	0	-	0	-	4	-	0	-		
Surgery of metastasis										
No	78	(90)	181	(89)	922	(89)	878	(87)	Pearson Chi[2]	p = 0.541
Yes	9	(10)	23	(11)	135	(11)	144	(13)		
Unknown	0	-	0	-	4	-	0	-		
Radiotherapy of metastasis										
No	80	(92)	181	(89)	909	(89)	901	(86)	Pearson Chi[2]	p = 0.223
Yes	7	(8)	23	(11)	148	(11)	121	(14)		
Unknown	0	-	0	-	4	-	0	-		

Supplementary table 2 Descriptive statistics patients with *de novo* metastatic breast cancer: changes over time

Characteristic	Patients with *de novo* MBC						Statistics
	2008-2011 N=2,676 (31%)		2012-2015 N=3,291 (38%)		2016-2018 N=2,689 (31%)		
	N	(%)	N	(%)	N	(%)	P
Patient characteristics							
Sex							
Female	2,648	(99)	3,262	(99)	2,654	(99)	Pearson Chi^2 p = 0.287
Male	28	(1)	29	(1)	35	(1)	
Age at diagnosis of metastasis							
< 50 years	577	(22)	654	(20)	543	(20)	Pearson Chi^2 p = 0.185
50-69 years	1,085	(41)	1,434	(44)	1,139	(42)	
70+ years	1,014	(38)	1,203	(37)	1,007	(37)	
Age at diagnosis of metastasis	Mean age: 63.7 yrs (22-101)		Mean age 63.8 yrs (22-102)		Mean age 63.6 yrs (22-98)		
WHO-PS							
WHO-PS 0	101	(54)	676	(53)	776	(51)	Too many missings, no test performed
WHO-PS 1	60	(32)	405	(32)	475	(32)	
WHO-PS 2	18	(10)	115	(9)	165	(11)	
WHO-PS 3	4	(2)	53	(4)	77	(5)	
WHO-PS 4	3	(2)	23	(2)	14	(1)	
Unknown	2,490	-	2,019	-	1,182	-	
Tumour characteristics							
Clinical T stage							
T0 or Tis	43	(2)	68	(2)	56	(2)	Pearson Chi^2 **p = 0.000**
T1	426	(17)	462	(15)	338	(13)	
T2	861	(35)	1,107	(36)	921	(36)	
T3	282	(12)	438	(14)	410	(16)	
T4	833	(34)	1,017	(33)	825	(32)	
T unknown	231	-	199	-	139	-	
Multifocality							
No	1,759	(77)	2,220	(74)	1,700	(70)	Pearson Chi^2 **p = 0.000**
Yes	529	(23)	762	(26)	746	(31)	
Unknown	388	-	309	-	243	-	

Supplementary table 2 Continued

Characteristic	Patients with *de novo* MBC						Statistics
	2008-2011 N=2,676 (31%)		2012-2015 N=3,291 (38%)		2016-2018 N=2,689 (31%)		
	N	(%)	N	(%)	N	(%)	P
Tumour characteristics							
Clinical N stage							Pearson Chi² **p = 0.000**
N0	627	(26)	689	(22)	455	(18)	
N1	1,416	(58)	1,687	(54)	1,286	(50)	
N2	81	(3)	124	(4)	132	(5)	
N3	305	(13)	598	(19)	691	(27)	
N unknown	247	-	193	-	125	-	
Tumour morphology							Pearson Chi² **p = 0.043**
Ductal carcinoma NOS	2,213	(83)	2,651	(81)	2,166	(81)	
Ductal carcinoma in situ	10	(0.4)	12	(0.4)	11	(0.4)	
Invasive lobular carcinoma	403	(15)	523	(16)	435	(16)	
Low grade special types	28	(1)	48	(1)	29	(1)	
Other	22	(1)	57	(2)	48	(2)	
Tumour grade							Too many missings, no test performed
Low grade	62	(7)	87	(8)	138	(8)	
Intermediate grade	354	(41)	554	(49)	957	(57)	
High grade	447	(52)	485	(43)	582	(35)	
Undifferentiated/anaplastic	3	(0.4)	4	(0.4)	2	(0.1)	
Unknown	1,810	-	2,161	-	1,010	-	
Receptor status							Pearson Chi² p=0.212
ER pos HER2 neg/unknown	1,673	(65)	2,195	(68)	1,761	(66)	
HER2 pos	563	(22)	644	(20)	560	(21)	
ER neg Her2 neg/unknown	342	(13)	395	(12)	335	(13)	
Insufficient information	98	-	57	-	33	-	
Localization of metastasis							Pearson Chi² **p = 0.000**
Lymph nodes only	93	(4)	202	(6)	173	(6)	
Bone only	964	(36)	1,082	(33)	903	(34)	
Liver (no CNS)	732	(28)	800	(24)	645	(24)	
CNS (with/without liver)	86	(3)	105	(3)	83	(3)	
All other locations	780	(29)	1,095	(33)	885	(33)	
Metastasis location unknown	21	-	7	-	0	-	

Supplementary table 2 Continued

Characteristic	Patients with *de novo* MBC						Statistics
	2008-2011 N=2,676 (31%)		2012-2015 N=3,291 (38%)		2016-2018 N=2,689 (31%)		
	N	(%)	N	(%)	N	(%)	P
Treatment characteristics							
Local treatment primary tumour							
No local treatment primary	1,925	(72)	2,415	(73)	2,043	(76)	Pearson Chi^2 **p = 0.000**
Surgery and radiotherapy	231	(9)	355	(11)	389	(14)	
Surgery without radiotherapy	414	(15)	411	(12)	171	(6)	
Radiotherapy without surgery	106	(4)	110	(3)	86	(3)	
Any systemic therapy in metastatic setting							
No	285	(11)	344	(10)	308	(11)	Pearson Chi^2 p = 0.436
Yes	2,391	(89)	2,947	(90)	2,381	(89)	
Systemic therapy in metastatic setting contains chemotherapy							
No	1,604	(60)	1,998	(61)	1,637	(61)	Pearson Chi^2 p = 0.752
Yes	1,072	(40)	1,293	(39)	1,052	(39)	
Type of first chemotherapy in *de novo* stage IV							
No chemotherapy	1,604	-	1,998	-	1,637	-	Pearson Chi^2 **p = 0.000**
Anthracycline containing chemotherapy	130	(24)	314	(28)	260	(26)	
Taxane containing chemotherapy	347	(63)	472	(42)	449	(45)	
Anthracycline and taxane containing chemotherapy	55	(10)	314	(28)	188	(19)	
Platinum containing chemotherapy	16	(3)	12	(1)	66	(7)	
Capecitabine monotherapy	2	(0.4)	6	(1)	39	(4)	
Other type of chemotherapy	2	(0.4)	2	(0.2)	3	(0.3)	
Chemotherapy not otherwise specified	520	-	173	-	47	-	

Supplementary table 2 Continued

Characteristic	Patients with *de novo* MBC						Statistics
	2008-2011 N=2,676 (31%)		2012-2015 N=3,291 (38%)		2016-2018 N=2,689 (31%)		
	N	(%)	N	(%)	N	(%)	P
Treatment characteristics							
Systemic therapy in metastatic setting contains endocrine treatment							
No	1,367	(51)	1,653	(50)	1,365	(51)	Pearson Chi² p=0.799
Yes	1,309	(49)	1,638	(50)	1,324	(49)	
Systemic therapy in metastatic setting contains targeted therapy							
No	2,228	(83)	2,670	(81)	2,026	(75)	Pearson Chi² **p = 0.000**
Yes	448	(17)	621	(19)	663	(25)	
Systemic therapy in metastatic setting							
No systemic therapy as first line	285	(11)	344	(10)	308	(11)	Pearson Chi² p = 0.598
Endocrine treatment as first line	1,276	(48)	1,566	(48)	1,277	(47)	
Chemotherapy (without HER2 targeted therapy) as first line	671	(25)	818	(25)	627	(23)	
HER2 targeted therapy as first line	444	(17)	563	(17)	477	(18)	
Any local treatment of metastasis							
No	2,047	(76)	2,454	(75)	1,996	(74)	Pearson Chi² p = 0.113
Yes	629	(24)	837	(25)	693	(26)	
Surgery of metastasis							
No	2,579	(96)	3,168	(96)	2,590	(96)	Pearson Chi² p = 0.974
Yes	97	(4)	123	(4)	99	(4)	
Radiotherapy of metastasis							
No	2,121	(79)	2,544	(77)	2,063	(77)	Pearson Chi² p = 0.062
Yes	555	(21)	747	(23)	626	(23)	

2

CHAPTER 2

Supplementary table 3 Sensitivity analysis in complete cases: Multivariable Cox proportional hazards analysis patients with *de novo* versus metachronous metastatic breast cancer (treated with systemic therapy in metastatic setting).

Characteristic	Category	Hazard Ratio (95% Confidence interval)	Likelihood ratio test P Value
De novo versus metachronous MBC			
	Metachronous MBC	1 (ref)	
	De novo MBC	0.71 (0.66-0.76)	**<0.001**
Patient characteristics			
Period of metastasis diagnosis			
	2008-2011	1 (ref)	
	2012-2015	0.81 (0.76-0.86)	**<0.001**
	2016-2018	0.71 (0.66-0.76)	**<0.001**
Sexe			
	Male	1 (ref)	
	Female	0.88 (0.67-1.12)	0.308
Age at diagnosis of metastasis, restricted cubic spline (rcs))	Restricted cubic spline with four knots.		p-value omitted
Tumour characteristics			
Morphology			
	Ductal carcinoma NOS	1 (ref)	
	Invasive lobular carcinoma	1.12 (1.05-1.20)	**0.001**
Multifocality			
	Unifocal primary tumour	1 (ref)	
	Multifocal primary tumour	0.96 (0.90-1.01)	**0.135**
Clinical T stage			
	T0 or Tis	1.11 (0.86 – 1.45))	**0.424**
	T1	1 (ref)	
	T2	1.08 (1.01-1.16)	**0.023**
	T3	1.13 (1.03-1.24)	**0.013**
	T4	1.32 (1.21-1.43)	**<0.001**
Clinical N stage			
	N0	1 (ref)	
	N1	1.15 (1.08-1.23)	**<0.001**
	N2	1.25 (1.07-1.45)	**0.004**
	N3	1.21 (1.11-1.33)	**<0.001**
Receptor status			
	ER + HER2- /unknown	Stratification factor	
	Her2 + (regardless of ER)		
	ER- HER2- / unknown		
Localization of metastasis			
	Lymph nodes only	Stratification factor	
	Bone only		
	Liver (no CNS)		
	CNS (with/without liver)		
	All other locations		

Supplementary table 4 Multivariable Cox proportional hazards analysis on multiple imputed data by metastasis-free interval in patients with metastatic breast cancer (treated with systemic therapy in metastatic setting).

Characteristic	Category	HR (95% CI)	Likelihood ratio test P Value
De novo versus metachronous MBC, divided by metastasis free interval	*De novo* MBC	1 (ref)	
	MFI 3-12 months	1.56 (1.17-2.08)	**0.002**
	MFI 12-24 months	2.04 (1.71-2.44)	**<0.001**
	MFI 24-60 months	1.50 (1.38-1.64)	**<0.001**
	MFI > 60 months	1.10 (1.01-1.20)	**0.032**
Patient characteristics			
Period of metastasis diagnosis	2008-2011	1 (ref)	
	2012-2015	0.82 (0.78-0.87)	**<0.001**
	2016-2018	0.71 (0.67-0.76)	**<0.001**
Sexe	Male	1 (ref)	
	Female	0.86 (0.69-1.07)	0.182
Age at diagnosis of metastasis, restricted cubic spline (rcs))	Restricted cubic spline with four knots.		p-value omitted
Tumour characteristics			
Morphology	Ductal carcinoma NOS	1 (ref)	
	Invasive lobular carcinoma	1.11 (1.04-1.18)	**0.001**
Multifocality	Unifocal primary tumour	1 (ref)	
	Multifocal primary tumour	0.95 (0.90-1.01)	0.091
Clinical T stage	T0 or Tis	1.10 (0.91-1.33)	0.314
	T1	1 (ref)	
	T2	1.07 (1.00-1.15)	**0.044**
	T3	1.11 (1.02-1.22)	**0.020**
	T4	1.30 (1.20-1.40)	**<0.001**
Clinical N stage	N0	1 (ref)	
	N1	1.11 (1.04-1.18)	**<0.001**
	N2	1.19 (1.04-1.37)	**0.013**
	N3	1.19 (1.09-1.29)	**<0.001**
Receptor status	ER + HER2- /unknown	Stratification factor	
	Her2 + (regardless of ER)		
	ER- HER2- / unknown		
Localization of metastasis	Lymph nodes only	Stratification factor	
	Bone only		
	Liver (no CNS)		
	CNS (with/without liver)		
	All other locations		

Supplementary Table 5 Multivariable Cox proportional hazards analysis in patients with *de novo* metastatic breast cancer (treated with systemic therapy in metastatic setting).

Characteristic	Category	Multivariable analysis HR (95% CI)	Likelihood ratio test P Value
Period of metastasis diagnosis			
	2008-2011	1 (ref)	
	2012-2015	0.82 (0.77-0.87)	**<0.001**
	2016-2018	0.73 (0.68-0.79)	**<0.001**
Sexe			
	Male	1 (ref)	
	Female	0.97 (0.75-1.25)	0.809
Age at diagnosis of metastasis, restricted cubic spline (rcs))	Restricted cubic spline with four knots.		p-value omitted
Tumour characteristics			
Tumour morphology			
	Ductal carcinoma NOS	1 (ref)	
	Invasive lobular carcinoma	1.08 (1.01-1.16)	**0.030**
Multifocality			
	Unifocal primary tumour	1 (ref)	
	Multifocal primary tumour	0.95 (0.89-1.01)	0.130
Clinical T stage			
	T0 or Tis	1.02 (0.83-1.24)	0.883
	T1	1 (ref)	
	T2	1.06 (0.98-1.16)	0.150
	T3	1.08 (0.97-1.20)	0.141
	T4	1.22 (1.12-1.33)	**<0.001**
Clinical N stage			
	N0	1 (ref)	
	N1	1.06 (0.99-1.14)	0.109
	N2	1.14 (0.98-1.32)	0.085
	N3	1.13 (1.03-1.24)	**0.008**
Receptor status			
	ER + HER2- /unknown	Stratification factor	
	Her2 + (regardless of ER)		
	ER- HER2- / unknown		
Localization of metastasis			
	Lymph nodes only	Stratification factor	
	Bone only		
	Liver (no CNS)		
	CNS (with/without liver)		
	All other locations		
Treatment characteristics			
Local treatment primary tumor			
	No local treatment primary	Stratification factor	
	Surgery and radiotherapy		
	Surgery without radiotherapy		
	Radiotherapy without surgery		
Type of systemic therapy in metastatic setting	Endocrine treatment	Stratification factor	
	Chemotherapy (without HER2 targeted therapy)		
	HER2 targeted therapy		

Supplementary Table 5 Continued

Characteristic	Category	**Multivariable analysis** HR (95% CI)	Likelihood ratio test P Value
Treatment characteristics			
Surgery of metastasis			
	No	1 (ref)	
	Yes	0.81 (0.69-0.96)	**0.013**
Radiotherapy of metastasis			
	No	1 (ref)	
	Yes	1.18 (1.03-1.26)	**<0.001**

2

Supplementary table 6 Multivariable Cox proportional hazards analysis in patients with *de novo* MBC versus patients with metachronous MBC (treated with systemic therapy in the metastatic setting), these metachronous patients were not treated with systemic therapy at the time of their primary tumour.

Characteristic	Category	HR (95% CI)	Likelihood ratio test P Value
De novo versus metachronous MBC	Metachronous MBC	1 (ref)	
	De novo MBC	1.13 (1.01-1.27)	**0.038**
Patient characteristics			
Period of metastasis diagnosis	2008-2011	1 (ref)	
	2012-2015	0.81 (0.76-0.86)	**<0.001**
	2016-2018	0.71 (0.66-0.76)	**<0.001**
Sexe	Male	1 (ref)	
	Female	0.92 (0.72-1.17)	0.495
Age at diagnosis of metastasis, restricted cubic spline (rcs))	Restricted cubic spline with four knots.		p-value omitted
Tumour characteristics			
Morphology	Ductal carcinoma NOS	1 (ref)	
	Invasive lobular carcinoma	1.11 (1.04-1.19)	**0.002**
Multifocality	Unifocal primary tumour	1 (ref)	
	Multifocal primary tumour	0.95 (0.90-1.01)	0.121
Clinical T stage	T0 or Tis	1.05 (0.87-1.26)	0.627
	T1	1 (ref)	
	T2	1.04 (0.96-1.12)	0.334
	T3	1.09 (0.99-1.20)	0.069
	T4	1.26 (1.16-1.37)	**<0.001**
Clinical N stage	N0	1 (ref)	
	N1	1.09 (1.02-1.16)	**0.012**
	N2	1.17 (1.01-1.35)	**0.034**
	N3	1.16 (1.06-1.26)	**<0.001**
Receptor status	ER + HER2- /unknown	Stratification factor	
	Her2 + (regardless of ER)		
	ER- HER2- / unknown		
Localization of metastasis	Lymph nodes only	Stratification factor	
	Bone only		
	Liver (no CNS)		
	CNS (with/without liver)		
	All other locations		

2

3

STUDY PROTOCOL OF THE I-GO STUDY, A
PHASE I FEASIBILITY STUDY OF MAGNETIC
RESONANCE GUIDED HIGH-INTENSITY FOCUSED
ULTRASOUND-INDUCED HYPERTHERMIA, LYSO-
THERMOSENSITIVE LIPOSOMAL DOXORUBICIN
AND CYCLOPHOSPHAMIDE IN *DE NOVO* STAGE IV
BREAST CANCER PATIENTS.

J.S. de Maar1, B.B.M. Suelmann[1], M.N.G.J.A. Braat[1], P.J. van Diest[1], H.H.B. Vaessen[1],
A. J. Witkamp[1], S. Linn[1, 2] , C.T.W. Moonen[1], E. van der Wall[1], R. Deckers[1]

1. University Medical Center Utrecht, Utrecht University, Utrecht, The Netherlands
2. Netherlands Cancer Institute - Antoni van Leeuwenhoek hospital, Amsterdam, The Netherlands

ABSTRACT

Introduction

In breast cancer, local tumour control is thought to be optimized by administering higher local levels of cytotoxic chemotherapy, in particular doxorubicin. However, systemic administration of higher dosages of doxorubicin is hampered by its toxic side effects. In this study, we aim to increase doxorubicin deposition in the primary breast tumour without changing systemic doxorubicin concentration and thus without interfering with systemic efficacy and toxicity. This is to be achieved by combining lyso-thermosensitive liposomal doxorubicin (LTLD, ThermoDox®, Celsion Corporation, Lawrenceville, NJ, USA) with mild local hyperthermia, induced by Magnetic Resonance guided High Intensity Focused Ultrasound (MR-HIFU). When heated above 39.5 °C, LTLD releases a high concentration of doxorubicin intravascularly within seconds. In absence of hyperthermia, LTLD leads to a similar biodistribution and antitumour efficacy compared to conventional doxorubicin.

Methods and analysis

This is a single-arm phase I study in 12 chemotherapy-naïve patients with *de novo* stage IV HER2-negative breast cancer. Previous endocrine treatment is allowed. Study treatment consists of up to 6 cycles of LTLD at 21-day intervals, administered during MR-HIFU induced hyperthermia to the primary tumour. We will aim for 60 minutes of hyperthermia at 40-42 °C using a dedicated MR-HIFU breast system (Profound Medical, Mississauga, Canada). Afterwards, intravenous cyclophosphamide will be administered. Primary endpoints are safety, tolerability and feasibility. The secondary endpoint is efficacy, assessed by radiological response.

This approach could lead to optimal loco-regional control with less extensive or even no surgery, in *de novo* stage IV patients and in stage II/III patients allocated to receive neo-adjuvant chemotherapy.

Ethics and dissemination

This study has obtained ethical approval by the Medical Research Ethics Committee Utrecht (Protocol NL67422.041.18, METC number 18-702). Informed consent will be obtained from all patients before study participation. Results will be published in an academic peer-reviewed journal.

Trial registration number

NCT03749850, EudraCT 2015-005582-23.

Keywords

High Intensity Focused Ultrasound,
MR-HIFU

ThermoDox
Lyso-thermosensitive liposomal doxorubicin (LTLD)
Temperature sensitive liposome
Targeted drug delivery
Hyperthermia
Image-guided therapy
De novo stage IV breast cancer
Synchronous stage IV breast cancer
Metastatic breast cancer

Strengths and limitations
- This first in human clinical trial investigates the combination of Lyso-Thermosensitive Liposomal Doxorubicin and Magnetic Resonance guided High Intensity Focused Ultrasound induced hyperthermia in breast cancer patients.
- A dedicated MR-HIFU breast system with real-time MR temperature feedback will be used for safe non-invasive local hyperthermia treatment of breast tumours.
- Because the study population consists of patients with *de novo* stage IV breast cancer, both local and systemic response to the treatment can be monitored.
- A survival benefit of treating the primary tumour in patients with metastatic breast cancer has not been proven, therefore study participants will participate altruistically in the interest of future patients.
- This approach could lead to improved local control during palliative chemotherapy in *de novo* stage IV breast cancer or neoadjuvant chemotherapy in stage II/III disease, with less extensive or even no surgery.

3

INTRODUCTION

Both neo-adjuvant and adjuvant chemotherapy of breast cancer aim to improve survival by eradicating microscopic distant metastases. In addition, neo-adjuvant treatment offers the opportunity to observe the biological behaviour of the primary tumour and increase the likelihood of less extensive radical (breast conserving) surgery. Given the fact that pathological complete response (pCR) is achieved at best in 68% of patients [1], efforts should be focused on improving primary tumour response. This may be achieved by increasing the dose of chemotherapy at the site of the tumour. In pre-clinical data, a higher concentration of chemotherapy in the tumour is correlated with increased tumour response, in particular for doxorubicin, one of the most frequently applied cytostatics in breast cancer treatment [2-4]. Clinically this was confirmed by studies using other chemotherapeutics, i.e. 5-fluorouracil and docetaxel. Higher tumour uptake of radio-active labelled 5-fluorouracil or docetaxel chemotherapy on PET was shown to correlate respectively with longer survival in patients with liver metastasis of colorectal carcinoma [5] and with better tumour response in lung cancer patients [6]. In a study comparing different dose schedules of the adjuvant AC regimen, the highest dosages (60mg/m^2 doxorubicin and 600mg/m^2 cyclophosphamide) were most effective, and this is currently the standard of care [7]. However, the administration of higher doses of doxorubicin is hampered by its systemic side effects. A randomized study evaluating even higher doxorubicin dosages (60mg/m^2 versus 75mg/m^2 and 90 mg/m^2) did not find a difference in disease-free or overall survival. However, the higher dose levels did lead to significantly more dose reductions and delays, which could explain why the efficacy did not increase further [8]. In the i-GO study we aim to increase doxorubicin levels in the primary tumour, without interfering with systemic efficacy and toxicity, by combining lyso-thermosensitive liposomal doxorubicin (LTLD, ThermoDox®; Celsion Corporation, Lawrenceville, NJ, USA) with mild local hyperthermia, induced by Magnetic Resonance guided High Intensity Focused Ultrasound (MR-HIFU). This will be followed by the intravenous administration of a second cytostatic agent, cyclophosphamide. The combined administration of doxorubicin and cyclophosphamide (AC) is a well-known regimen in the standard of care treatment in both the (neo-) adjuvant setting as in the treatment of metastatic breast cancer.

The i-GO study will be a phase I feasibility study in stage IV breast cancer patients who present with distant metastases and a primary tumour in situ (*de novo* stage IV patients). Several studies have suggested that by obtaining loco-regional control in metastatic breast cancer, overall survival in advanced disease would be improved [9-11] However, randomized controlled trials have contradicted this [12, 13] A recent presentation at ASCO 2020 [14] confirmed that local treatment in addition to systemic therapy did not improve survival. As such, besides a personal preference of the patient and the possibility of preventing local morbidity, study participation will not have a benefit compared to the standard of care. However, based on pharmacokinetic studies (details outlined in Supplementary materials

1) we do expect at least an equally effective treatment. Study participants will participate altruistically in the interest of future patients in the neoadjuvant setting. In the future, the combination of LTLD, MR-HIFU hyperthermia, and cyclophosphamide may lead to improved local control during neoadjuvant chemotherapy in stage II/III disease, with less extensive or even no surgery.

Lyso-thermosensitive liposomal doxorubicin

LTLD is a temperature-sensitive liposomal encapsulation of doxorubicin. Doxorubicin is a cytotoxic (chemotherapy) agent that is approved and frequently used for the treatment of a wide range of cancers, including breast cancer. When heated to 40-42 °C, LTLD releases the encapsulated doxorubicin intravascularly within seconds [15-17]. (Figure 1.) In small animal tumour models, LTLD combined with hyperthermia results in a 3-25 fold higher tumour concentration than conventional doxorubicin [2, 18-22] and increased antitumour efficacy [2, 16, 18]. In the absence of hyperthermia, doxorubicin leaks slowly from the liposome, and after two hours all of the doxorubicin is released [15]. Furthermore, LTLD without hyperthermia leads to a similar biodistribution [19, 20] and antitumour efficacy [16, 18] compared to conventional doxorubicin.
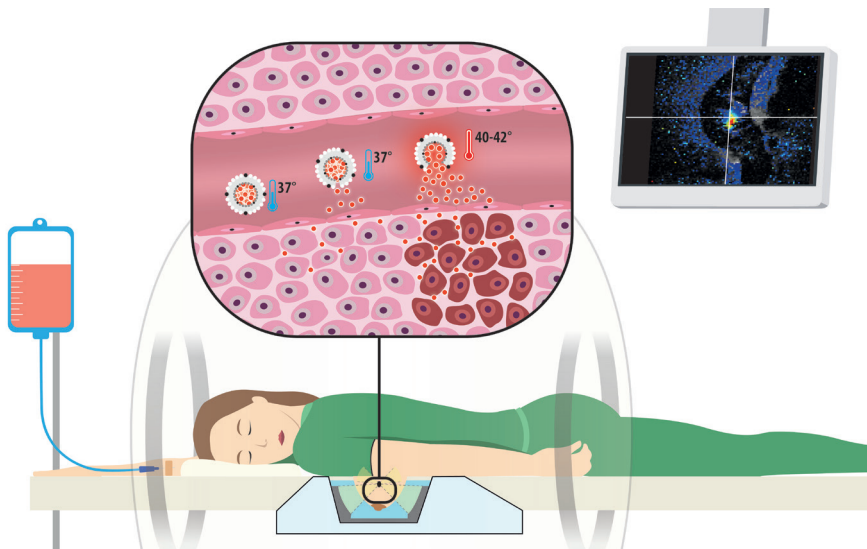
Figure 1 The concept of LTLD combined with MR-HIFU hyperthermia for local drug delivery in the primary breast tumour. The patient is lying in prone position on the dedicated MR-HIFU breast system under procedural sedation and analgesia, with the breast hanging in the water-filled cup. HIFU-induced hyperthermia is administered to the tumour for 60 minutes. Real-time MR thermometry (screen on the right) allows for precise control of the target temperature of 40-42 °C in the tumour. After intravenous infusion, LTLD circulates through the vasculature and releases a small amount of doxorubicin at 37°C. However, when LTLD reaches the heated tumour it releases a high amount of doxorubicin intravascularly within seconds. We hypothesize that the combination of LTLD and MR-HIFU hyperthermia will increase the tumour concentration of doxorubicin without interfering with systemic treatment efficacy and toxicity.

Magnetic resonance-guided high intensity focused ultrasound

MR-HIFU is a truly non-invasive treatment modality, that combines magnetic resonance imaging (MRI) and high intensity focused ultrasound to perform image-guided thermal tissue ablation (55-70 °C) [23-25] or mild local hyperthermia (40-43 °C) [26-28]. Unlike other heating methods, using microwaves, radiofrequency or non-focused ultrasound, HIFU allows for non-invasive localized heating of deep-seated tumours [29]. In addition to treatment planning based on anatomical MRI, MR-guidance can provide temperature feedback and control during hyperthermia treatment, through real-time MR thermometry. For this study we will use a dedicated MR-HIFU breast system: the Sonalleve MR-HIFU breast tumour therapy system (hereafter referred to as 'MR-HIFU breast system', Profound Medical, Mississauga, Canada), integrated with a clinical 1.5 Tesla MR scanner (Achieva, Philips Healthcare, Best, The Netherlands). This system has a lateral sonication approach, which enables specific heating of the breast tumour, while reducing the risk of heating the skin or other organs to a minimum [30]. A phase I study in our hospital with MR-HIFU ablation of breast tumours showed that the MR-HIFU breast system allows for safe, accurate and precise thermal ablation [31, 32].

Previous clinical studies

This will be the first-in-human study to evaluate LTLD with MR-HIFU hyperthermia in breast cancer patients. LTLD has been studied previously in combination with superficial hyperthermia in patients with chest wall recurrences of breast cancer [33]. This phase I/II study showed that LTLD at 40 mg/m^2 with superficial hyperthermia was safe and the 48% overall response (14/29, 95% CI:30–66%) was promising in this heavily pre-treated population. A large randomized phase III study in 701 patients with hepatocellular carcinoma compared LTLD at 50 mg/m^2 with radiofrequency ablation (RFA) to RFA alone (the HEAT study) [34, 35]. In that study the primary endpoint of 33% improvement in progression free survival was not met. However, a post-hoc analysis in the subgroup of 285 patients with solitary lesions that were treated with ≥45 min of RFA showed a significant overall survival benefit for the combination treatment (Hazard Ratio for Overall Survival 0.63 (95% CI, 0.41–0.96; P < 0.05), in favour of RFA+LTLD with ≥45 minutes heating). Systemic adverse events increased in the RFA+LTLD arm (83% vs 35% with RFA alone) as expected, with a similar profile to that of conventional doxorubicin [35].

Furthermore, the combination of LTLD and ultrasound guided HIFU hyperthermia has been evaluated in a phase I proof-of-concept study in ten patients with incurable primary or metastatic liver tumours (the TARDOX study) [36, 37]. Adverse events did not differ from those associated with doxorubicin alone and in the group of patients that underwent invasive thermometry sufficient mean tumour temperatures were measured. In seven out of ten patients, the intratumoural doxorubicin concentration doubled after HIFU, although a within-patient comparison was not possible for all patients. We aim to take advantage of the same principle to treat the primary tumour in patients presenting with metastatic

breast cancer. Monitoring the treatment by MR thermometry may further enhance safety, efficacy and feasibility. Using multiple cycles of LTLD + MR-HIFU hyperthermia is expected to increase treatment efficacy and mimics the standard of care treatment.

METHODS AND ANALYSIS

This single-arm phase I feasibility study aims to determine the safety, tolerability and feasibility of the combination of LTLD, MR-HIFU induced mild local hyperthermia, and cyclophosphamide, for the enhanced local treatment of the primary tumour in patients presenting with metastatic breast cancer. All eligible participants will receive up to 6 cycles of LTLD at 21-day intervals, administered during MR-HIFU induced hyperthermia to the primary tumour and cyclophosphamide administered afterwards.

Patient population

We will include 6 or 12 adult female patients with *de novo* stage IV (distant metastases at the time of diagnosis, with the primary tumour in situ) HER2-negative breast cancer, who have not received previous chemotherapy for their disease. Previous endocrine treatment in those with hormone-receptor positive disease is allowed. The small samples size was chosen because this is the first study evaluating the combination of MR-HIFU hyperthermia, LTLD and cyclophosphamide. No formal sample size calculation was performed. Potentially eligible patients will be referred to the department of Medical Oncology at the University Medical Center Utrecht, The Netherlands. In order to achieving adequate participant enrolment, medical oncologists in hospitals in the Netherlands will be asked to refer potentially eligible and interested patients.

Inclusion criteria

Patients must meet all of the following inclusion criteria:

- Histologically confirmed adenocarcinoma of the breast and planned for palliative chemotherapy with doxorubicin and cyclophosphamide.
- Biopsy-proven stage T1-2AnyNM1 at diagnosis of breast cancer.
- Measurable disease according to either RECIST 1.1 or PERCIST 1.0 at baseline.
- Non-pregnant, non-lactating female at least 18 years of age. If the patient is of child-bearing age, she must have a negative serum pregnancy test prior to enrolment and must agree to practice an acceptable form of birth control while on study.
- The tumour is located within the reach of the HIFU beam (based on pre-treatment dynamic contrast-enhanced (DCE-) MRI findings).
- The distance of the tumour from the skin, nipple, and pectoral wall is at least 1.0

cm (based on pre-treatment DCE-MRI findings).

- The target breast is expected to fit in the cup of the MR-HIFU breast system (based on pre-treatment MRI findings).
- The patient is able to provide written informed consent and willing to comply with protocol requirements.

Exclusion criteria

Patients will be excluded if any of the following conditions are observed:

- HER2-positive disease or classic invasive lobular carcinoma (ILC).
- A treatment plan with curative intent is available.
- Any prior chemotherapy treatment for invasive breast cancer (previous anti-hormonal therapy is allowed).
- Any prior therapy with anthracyclines.
- The patient weighs ≥90 kg (restriction of the HIFU table top).
- Any concomitant malignancy or previous malignancy in the last 5 years, except basal cell or squamous cell cancer of the skin or in situ carcinoma of the cervix. Subjects with a prior contralateral breast malignancy more than 5 years ago can be included if they did not receive any chemotherapy.
- Any previous malignancy in the unilateral breast (even if more than 5 years ago)
- Prior sensitivity (including rash, dyspnoea, wheezing, urticarial, or other symptoms) attributed to any liposomal-encapsulated drug.
- Baseline laboratory values:

Absolute Neutrophil Count (ANC)	< 1.5 x 10^9/L
Platelets	< 75 x 10^9/L
Haemoglobin	< 5.6 mmol/L (transfusion is allowed)
Total Bilirubin	> 1.5 times upper limit of normal

  Alanine Transaminase (ALAT) and Aspartate Transaminase (ASAT)

  > 2.5 times upper limit of normal

  >5 times upper limit of normal in case of liver metastases

  Estimated Glomerular Filtration Rate < 30 ml/min/1.73m^2
- World Health Organization Performance Status (WHO-PS) >2.
- Left Ventricular Ejection Fraction <50% (validated by baseline scan).
- History of: acute coronary syndrome in the last year, cerebral vascular accident in the last year, abnormal cardiac stress testing within the last six months, symptomatic coronary artery disease, uncontrolled hypertension or cardiomyopathy, cardiac valvular surgery or open-heart surgery in the last year or known structural heart disease.
- Any condition which may interfere with the hyperthermia portion of the trial such as: functioning cardiac pacemaker; metal plates, rods or prosthesis of the chest

wall, breast prosthesis in the treated breast, severe numbness and/or tingling of the chest wall or breast, skin grafts and/or flaps on the breast or chest wall, scar tissue or surgical clips in the HIFU beam path.

- Active infection.
- Body temperature > 38.0 degrees Celsius on the day of a MR-HIFU treatment.
- Concurrent use of any of the following prohibited medications within a reasonable wash-out time: protease inhibitors, cyclosporine, carbamazepine, phenytoin, valproic acid, paclitaxel, trastuzumab and other liposomal drugs (AbelectTM, Ambisome™, NyotranTM, etc.) or lipid-complexed drugs. Caution will be exercised with medications, dietary components and herbal supplements that affect CYP2A4, CYP2D6 or P-gp or have been described to interact with doxorubicin in other ways.
- Contraindications to MR imaging (e.g., pacemaker in situ, severe claustrophobia, metal implants incompatible with the MRI-scan, body size incompatible with MR bore).
- Contraindications to gadolinium-based contrast agents and the tumour is not sufficiently visible on MRI without contrast (including prior allergic reaction to gadolinium-based contrast agent, and/or renal failure).
- Contraindications to sedation and analgesia with Propofol and Remifentanil, including history of Chronic Obstructive Pulmonary Disease (COPD) that results in the inability to perform a physical activity corresponding with a Metabolic Equivalent (MET(57)) of 4; dependence on artificial ventilation at home; sleep apnoea or an American Society of Anaesthesiologists (ASA) classification ≥4.
- Inability to lie in prone position.
- A medical or psychiatric condition or other circumstances which would significantly decrease the chances of understanding the informed consent process, obtaining reliable data, achieving study objectives, or completing the study treatment and/ or examinations.

Endpoints

Primary endpoints are safety, tolerability and feasibility. These will be evaluated by the following assessments.

Safety and tolerability:
- Incidence and severity of Adverse Events and Severe Adverse Events
- Incidence of Dose Limiting Toxicity (DLT, systemic and loco-regional)
- Necessity for dose adjustments, delay and early cessation
- Incidence and severity of post-procedural pain
- Patient reported tolerability (questionnaires)
- Cardiotoxicity: Left Ventricular Ejection Fraction measurement and

electrocardiogram abnormalities.

Feasibility:
- The number of cycles in which hyperthermia treatment was sufficient: at least 30 minutes at the target temperature of 40-42 °C.
- The number of completed cycles with MR-HIFU induced hyperthermia, LTLD and cyclophosphamide
- Quality of MR thermometry data acquired during the MR-HIFU treatment
- Spatiotemporal temperature distribution in the tumour
- Total duration of the study procedures on a treatment day.

Secondary endpoints consist of efficacy parameters:
- Assessment of distant radiological objective response rates
- Assessment of local radiological objective response rates

Study procedures

The study design (Figure 2) was based on the AC regimen, a well-known chemotherapeutic regimen that consists of doxorubicin and cyclophosphamide. This regimen is used in the (neo-)adjuvant setting as well as in the first-line chemotherapy treatment of metastatic breast cancer. Standard of care for our study population consists of 6 cycles at 21-days intervals. In this study we will replace doxorubicin in this regimen with the combination of LTLD and MR-HIFU induced hyperthermia.

All participants will receive procedural sedation and analgesia with propofol and remifentanil to limit patient movement during the treatment and to establish a regular breathing pattern that will facilitate respiratory gated MR thermometry [38]. To prevent any hypersensitivity reactions to LTLD, the participants will also receive a premedication regimen of steroids, H1- and H2- histamine antagonists. Anti-emetics will be administered according to standard-of-care hospital guidelines for the AC regimen.

MR-HIFU hyperthermia will be performed on the MR-HIFU breast system, with the patient in prone position. We will aim for 60 minutes of hyperthermia at 40-42 °C to the breast tumour, in four blocks of 15 minutes. After each block the MR thermometry is restarted to minimize the possible influence of magnetic field drift or patient displacement. When MR thermometry indicates that the target temperature is reached, 50 mg/m^2 of LTLD will be administered intravenously over 30 minutes, via a peripherally inserted central catheter (PICC), while the patient is on the MR-HIFU breast system. Temperature will be monitored by respiratory navigator-gated MR thermometry, using the proton resonance frequency shift method [39, 40]. In case the target temperature is not reached, conventional doxorubicin (60 mg/m^2) will be administered instead of LTLD. Shortly after MR-HIFU, 600 mg/m^2 of cyclophosphamide will be administered intravenously according to standard of care in the AC regimen.
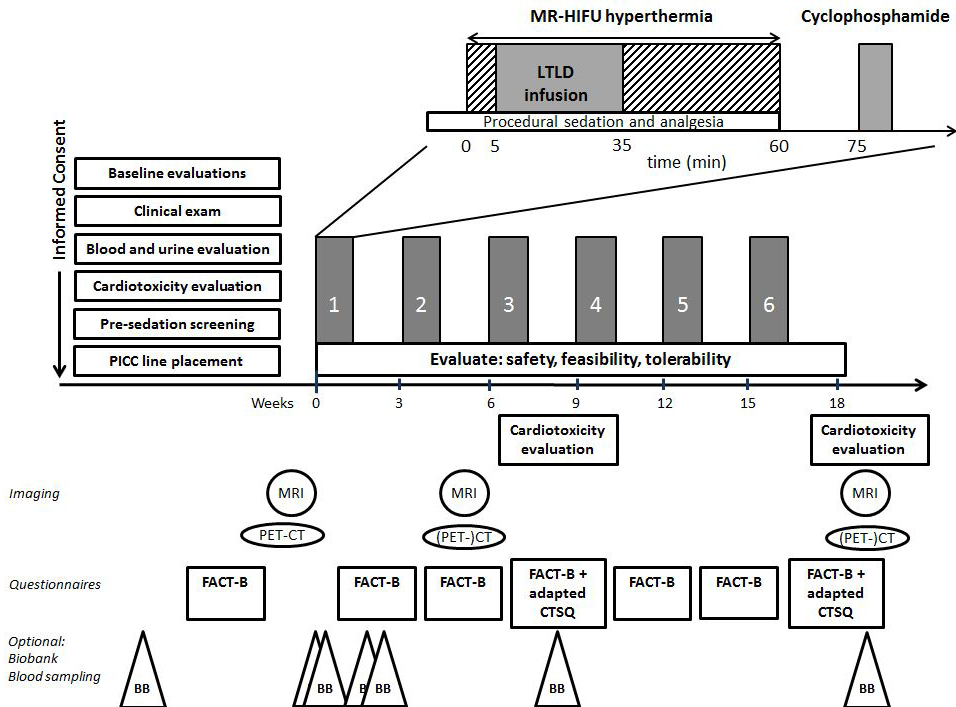
Figure 2 Study procedures. The standard of care palliative AC regimen consists of 6 cycles of doxorubicin and cyclophosphamide at 21-days intervals. In this study we will replace doxorubicin with the combination of LTLD and MR-HIFU induced hyperthermia, in up to six cycles. After informed consent, the baseline procedures will be performed as mentioned. During the cycles, the primary endpoints of safety (adverse events), feasibility and tolerability will be monitored, including cardiotoxicity evaluation and questionnaires on specified time points as indicated in the bottom of the figure. Imaging to determine local (MRI) and systemic ((PET/)CT) response will be performed at baseline, after cycle two and after cycle six. Optionally, the patient can consent to additional blood sampling for future research, which will be stored in the Biobank.

Participants will receive up to six treatment cycles. Feasibility will be evaluated after each MR-HIFU treatment and during the course of the cycles. Safety and tolerability will be assessed three hours after MR-HIFU treatment, during telephone contact on day +1 and +7 and during a hospital visit on day +14 and +21 of each cycle, by monitoring of adverse events, laboratory measurements and evaluation of pain. Cardiotoxicity evaluations (LVEF and ECG) will be performed at baseline, after cycle 3 and after cycle 6. The participants will be asked to fill out the Dutch version of the Functional Assessment of Cancer Therapy – Breast (FACT-B, version 4, FACIT)[41] at baseline and after each treatment cycle, combined with a selection of questions adapted from the Dutch version of the Cancer Therapy Satisfaction Questionnaire (CTSQ, Pfizer 2007, modified with permission from Pfizer)[42, 43] in cycles 3 and 6. Before starting the next cycle, any toxicities will be evaluated and if necessary, dose reductions will be made. DLT will be categorized in systemic or loco-regional toxicity (Table 1). Thus, we aim to distinguish systemic chemotherapy effects from

local effects of MR-HIFU hyperthermia and/or the high local doxorubicin concentration. Planned dose adjustments for these categories have been established (Supplementary materials 2). In case of a systemic DLT the LTLD dosage will be decreased, while for loco-regional DLT the duration of hyperthermia will be decreased. Cyclophosphamide dose will not be reduced. No dose increases will be performed. Depending on the severity and nature of the toxicity, study treatment can be delayed or even ceased. In case of solely loco-regional DLT, technical issues or other feasibility issues that restrict the use of MR-HIFU treatment, the participant will receive the standard of care AC regimen. If hyperthermia is insufficient (i.e. the target temperature of 40-42 °C is not reached or was only maintained for less than 30 minutes) in two separate cycles, the treatment is not considered feasible for that patient and study participation will end.

Table 1 Definitions of Dose Limiting Toxicity

Dose limiting systemic toxicity	
A	*Hematologic DLT* defined as Grade 3 anaemia, Grade 4 thrombocytopenia, febrile neutropenia, or Grade 4 neutropenia ≥ 7 days in duration.
B	*Non-hematologic DLT (non-loco-regional)* defined as Grade 3 or greater toxicity with the exceptions of alopecia, fatigue, nausea or vomiting and loco-regional effects. Including Cardiotoxicity DLT, defined as: • Grade 3 or greater cardiac disorders OR • a decline in LVEF of > 15% while the LVEF remains > 40% OR • a decline to an LVEF of ≤ 40%.
Dose limiting loco-regional toxicity	
C	*Loco-regional DLT* defined as post-procedural effects (e.g. pain or skin effects) on the treated breast warranting dose adjustment or delay.

For the secondary endpoint of efficacy, MRI of the breast will be performed using a 3 Tesla MRI scanner with a dedicated breast coil, at baseline and after cycle 2 and 6 to determine local radiological objective response. In addition, MRI of the breast will be performed during each MR-HIFU treatment. However, the receiver coil in the MR-HIFU breast system is not suited for clinical imaging. In case a complete radiological response of the breast tumour is obtained after less than 6 cycles, the patient will continue with the conventional AC regimen. ^{18}F-fluorodeoxyglucose (FDG-) Positron Emission Tomography combined with Computed Tomography (PET/CT) of the thorax and abdomen will be performed at baseline and CT or PET/CT after cycle 2 and cycle 6, to determine the distant objective response according to RECIST 1.1 [44] or PERCIST 1.0 [45]. PET/CT will be performed for response evaluation in patients with only PERCIST-measurable disease, such as patients with only bone metastases. If a patient shows distant progression of disease, study participation will end and the patient will be treated according to the standard of care. Additional specific

reasons for study withdrawal are dose limiting toxicity that warrants a delay in treatment administration for longer than 14 days or a recurrence of dose limiting toxicity after dose reduction of LTLD (Supplementary materials 2).

The participants will be followed for adverse events from the time of signing informed consent until the end of study visit after six cycles of chemotherapy. Afterwards patients will receive standard of care treatment.

If the patient consents to the biobank study, additional blood samples will be taken from the PICC-line at seven time points (Figure 2) when the patient is already at the hospital. These blood samples will be collected in the UMC Utrecht Biobank for future research. Moreover, in case tissue samples of the breast tumour and/or metastases were obtained in standard care before inclusion or following study participation, we will ask for consent to perform additional analyses on these samples.

Concomitant care and prohibited interventions

All supportive measures consistent with optimal medical care will be employed, including transfusion of blood and blood products, and treatment with antibiotics, antiemetics, antidiarrheals, and analgesics, as appropriate.

Certain concomitant medications, a number of herbal supplements, food stuffs and nutritions are restricted during the study (Supplementary materials 3). Patients cannot use creams, ointments or lotions on the breast on the MR-HIFU treatment day, to avoid additional risks during the procedure. Patients cannot use methods or treatments that increase the body temperature or skin temperature during the study period (e.g. sauna, hot-water baths, warmth massages), because this could result in increased release of doxorubicin in the warmed areas, possibly causing extra adverse events.

Interim analysis

An interim analysis of safety and efficacy will determine whether accrual will continue after six participants (Supplementary materials 4). Safety will be evaluated once the first six patients complete two treatment cycles. If safety is sufficiently proven or is deemed inadequate, the trial will end after six participants. Otherwise accrual will continue until twelve patients have been treated, if necessary after dose adjustments. All patients who have signed informed consent will be evaluated for the primary endpoints of safety, feasibility and tolerability. Patients who have been withdrawn from the study because MR-HIFU induced hyperthermia was insufficient in two separate treatment cycles and who did not experience a DLT, will be replaced by another participant for in the interim safety evaluation. If this happens to four patients, the study will be terminated, because of insufficient feasibility.

Systemic efficacy will be evaluated once the first six patients have received the CT scan after cycle 2. If four or more of the first six participants show distant disease progression at that time the trial will be stopped, as this suggests that efficacy against disease outside the

heated treatment field is inadequate. This early stopping rule was based on a phase III trial with liposomal doxorubicin in metastatic breast cancer [46] where 77.5% of the subjects were free of disease progression at two months post-randomization (the 95% confidence interval of 2/6 patients does not contain 0.775).

An independent, qualified monitor will monitor the study procedures. An external Data Safety Monitoring Board (DSMB) will review accumulating safety data at regular intervals throughout the study, perform the interim safety and efficacy analyses and monitor trial data integrity (DSMB charter in Supplementary materials 5).

Data analysis

Descriptive statistics will be used to describe the incidence and severity of adverse events (National Cancer Institute Common Terminology Criteria for Adverse Events version 5.0), the patient reported outcomes in the questionnaires and feasibility parameters including the number of completed study treatment cycles, duration of study procedures and spatiotemporal temperature distribution during MR-HIFU treatment. For the secondary endpoint of efficacy, distant and local radiological objective response rates (RECIST 1.1) will be described.

DISCUSSION

This is the first clinical trial that investigates the combination of LTLD and MR-HIFU induced hyperthermia in breast cancer. In a small number of patients we will focus primarily on safety, tolerability and feasibility of this procedure. We hypothesize that the combination of LTLD and MR-HIFU hyperthermia leads to improved treatment of the primary tumour, without changing the systemic doxorubicin concentration and thus without interfering with systemic efficacy and toxicity. A future randomized study with a control group receiving the standard of care AC regimen would be needed to prove this. Including patients with *de novo* stage IV breast cancer provides the unique possibility to monitor both local and systemic disease simultaneously. While in this setting a survival benefit of treating the primary tumour has not been proven, the study treatment (if proven safe and feasible) could in the future improve outcomes in the neoadjuvant setting.

We aim to replace doxorubicin by LTLD plus MR-HIFU hyperthermia in all six cycles of the AC regimen, because we expect this to maximize the local treatment effect. In each cycle, the feasibility to achieve tumour hyperthermia at 40-42 °C for 30 minutes will be verified with MR thermometry. If hyperthermia treatment is repeatedly insufficient, or if (after any number of cycles) radiological complete response is already obtained, patients will continue on the standard-of-care AC regimen. The number of MR-HIFU hyperthermia plus LTLD cycles that our patients are willing and able to complete could be less than six, which would be an important feasibility finding.

Our goal is to maintain an equivalent systemic efficacy compared to the standard-of-care AC regimen using 60 mg/m^2 conventional doxorubicin. Pharmacokinetic studies showed that the area-under the curve (AUC0-∞) of free/unencapsulated doxorubicin in plasma of patients receiving LTLD 50 mg/m^2 with local hyperthermia or RFA [33, 47, 48] was higher than the AUC0-∞ of conventional doxorubicin 60 mg/m^2 [49-51]. To be able to compare the AUCs we converted the AUC0-∞ of the metabolite doxorubicinol that was measured in the LTLD studies to the AUC0-∞ of doxorubicin [52-54] (Additional explanation in Supplementary materials 1). The 50 mg/m^2 LTLD dose was also recommended for and well-tolerated in the phase III trial in combination with RFA [35]. Due to local toxicity, the recommended dose for LTLD combined with local superficial hyperthermia for chest wall recurrences was decreased to 40 mg/m^2 [47]. In our study local (skin) toxicity is not expected because a margin of at least 1.0 cm is preserved from the tumour to the skin, therefore the LTLD dose of 50 mg/m^2 was chosen. Real time MR thermometry and the lateral configuration of the MR-HIFU breast system will help mitigate this risk. If however local DLT do occur, the duration of hyperthermia will be decreased while maintaining the LTLD dosage to avoid decreasing systemic efficacy. We will only decrease LTLD dosage in case of systemic DLT. If despite these measures, systemic efficacy seems inadequate, the trial will be halted prematurely based on the interim analysis for efficacy.

Because this is a small phase I feasibility study, the results will only provide a rough indication of local efficacy based on radiological response. To diminish the burden on participants, we will not perform tissue biopsies or breast surgery and therefore cannot describe the number of pathological complete responses or measure the concentration of doxorubicin in the tumour. Proof-of-concept that hyperthermia increases the tumour doxorubicin concentration has already been established in the Tardox study, although doxorubicin concentrations were not compared between heated and unheated tumours.

With this phase I clinical trial, we aim to show that LTLD combined with MR-HIFU induced hyperthermia on a dedicated MR-HIFU breast system can safely replace doxorubicin in the AC regimen. We hypothesize that this combination will result in improved response of the primary tumour without compromising the systemic efficacy on metastatic sites or increasing systemic toxicity. If feasibility and tolerability are adequate, this approach could in the future lead to optimal loco-regional control with less extensive or even no surgery, in stage II or III breast cancer patients allocated to receive neo-adjuvant chemotherapy. Finally, it could also be suitable for other doxorubicin sensitive tumour types that benefit from enhanced local treatment, such as soft tissue sarcoma.

Ethics and dissemination

This study has obtained ethical approval by the Medical Research Ethics Committee of the UMC Utrecht (METC Utrecht) on May 29th 2019 (Protocol NL67422.041.18, METC number 18-702). This paper is based on protocol version 6, dated August 28th 2020. Substantial

protocol amendments will also be evaluated by METC Utrecht and communicated to relevant parties by the investigators. Informed consent will be obtained from all patients by an authorized representative of the Principal Investigator before study participation (Informed consent form in Supplementary materials 6). The results of this study will be disseminated by publication in an academic peer-reviewed journal.

Roles and responsibilities

This is an investigator-driven single-centre clinical trial, with the UMC Utrecht as sponsor and trial site. The UMC Utrecht is responsible for the study design, data collection, data management, analysis, interpretation of data, writing and submission of the report for publication. The Principal Investigator will rapport (serious) adverse (device) events to the METC Utrecht, to the Central Committee on Research Involving Human Subjects (CCMO), and to Celsion Corporation and Profound Medical according to national guidelines. UMC Utrecht has liability insurance which provides cover for damage to research subjects through injury or death caused by the study. Celsion Corporation (manufacturer of the investigational medicinal product) and Profound Medical (manufacturer of the investigational medical device) will provide technical support during the trial and have provided input on the study protocol. Both manufacturers will be allowed to review and comment on draft publications prior to submission. The investigators at the UMC Utrecht will have ultimate authority over the publication. An external Data Safety Monitoring Board (two clinicians and one statistician) has been established and an independent qualified monitor (Julius Clinical) has been appointed to perform intensive monitoring.

Data management

The handling of personal data will comply with the General Data Protection Regulation (GDPR, in Dutch known as AVG). After informed consent is signed, each patient receives a unique subject number. A subject identification code list will be used to link the data to the subject. The key to this pseudonymization code will be available only to the investigators and employees of the research team.

Research data that are relevant for the study will be collected by the investigators on electronical Case Report Forms (eCRFs) in Research Online, in compliance with the Good Clinical Practice (GCP) guidelines for electronic data collection. An audit trail will be available. The completed eCRFs will be reviewed, signed and dated by the Principal Investigator or Co-investigator. Scans, results and registrations of medical imaging will be collected on the Research Imaging Architecture (RIA), which is secured by password-protection and stores pseudonymized images. Data from the MR-HIFU device such as log files and MR images obtained during the MR-HIFU treatment that cannot be stored on the Research Imaging Architecture will be stored in a secured UMC Utrecht bulk-storage folder. Celsion and Profound will not receive any patient's identifiable (personal) information. UMC Utrecht shall provide pseudonymized data regarding the occurrence and severity of adverse

device effects to Profound Medical and regarding the occurrence and severity of adverse events to Celsion Corporation. This cannot be refused by the patient and is obligatory for study participation. If the patient consents (optional), additional pseudonymized data on the study treatment, will also be provided to Profound Medical and Celsion Corporation. Research data will be stored for 15 years after the end of study. Biomaterial is stored in the Central biobank (blood) or at the UMC Utrecht pathology department (tissue samples).

Patient and public involvement

Patient experiences have been the starting point for the grant proposal to the Dutch Cancer Foundation and patients were involved in the design of the study and the choice of outcome measures. Patients will not be actively involved in recruitment or dissemination of study results, however information regarding the study can be found by individual patients on the UMC Utrecht website and clinicaltrials.gov.

Trial status

Patient recruitment was initiated on March 10th 2020. Due to the COVID-19 outbreak, the study has been temporarily discontinued, but the study is now open for enrollment.

Authors' contributions

JdM, BS, MB, SL, CM, EW and RD were all involved in the design of the study and in writing the manuscript.
PvD, HV and AW critically reviewed the design of the study providing additional comments and suggestions.

ACKNOWLEDGEMENTS

Finally, we thank Profound Medical for their support relating the use and safety of the MR-HIFU breast system in their role as legal manufacturer of this investigational medical device.

COMPETING INTERESTS STATEMENT

The authors have no competing interest to declare.

LIST OF ABBREVIATIONS

AC	Doxorubicin (A) and cyclophosphamide (C)
AF	Alkaline Phosphatase
ALAT	Alanine Transaminase
ANC	Absolute Neutrophil Count
ASAT	Aspartate Transaminase
AUC0-∞	Area Under the Curve 0-infinity
CCMO	Central Committee on Research Involving Human Subjects
CTSQ	Cancer Therapy Satisfaction Questionnaire
DCE	Dynamic contrast-enhanced
DLT	Dose Limiting Toxicity
DSMB	Data Safety Monitoring Board
eCRF	electronical Case Report Forms
FACT-B	Functional Assessment of Cancer Therapy – Breast
GCP	Good Clinical Practice
GDPR	General Data Protection Regulation
LTLD	Lyso-Thermosensitive Liposomal Doxorubicin
MR-HIFU	Magnetic Resonance guided High Intensity Focused Ultrasound
MRI	Magnetic Resonance Imaging
(FDG-) PET/CT	^{18}F-Fluorodeoxyglucose Positron Emission Tomography combined with Computed Tomography
PICC	Peripherally inserted central catheter
RFA	Radiofrequency ablation
RIA	Research Imaging Architecture

REFERENCES

1.   van Ramshorst MS, van der Voort A, van Werkhoven ED, Mandjes IA, Kemper I, Dezentjé VO, Oving IM, Honkoop AH, Tick LW, van de Wouw AJ, et al. (2018) Neoadjuvant chemotherapy with or without anthracyclines in the presence of dual HER2 blockade for HER2-positive breast cancer (TRAIN-2): a multicentre, open-label, randomised, phase 3 trial. The Lancet Oncology 19(12):1630-1640. https://doi.org/10.1016/s1470-2045(18)30570-9

2.   Ponce AM, Viglianti BL, Yu D, Yarmolenko PS, Michelich CR, Woo J, Bally MB, Dewhirst MW (2007) Magnetic resonance imaging of temperature-sensitive liposome release: drug dose painting and antitumor effects. J Natl Cancer Inst 99(1):53-63. https://doi.org/10.1093/jnci/djk005

3.   Koechli OR, Sevin B, Perras JP, Angioli R, Untch M, Steren A, Ramachandran C, Averette HE (1995) Comparative chemosensitivity profiles in three human breast cancer cell lines with the ATP-cell viability assay. Oncology 51:552-558.

4.   Besse HC, Barten-van Rijbroek AD, van der Wurff-Jacobs KMG, Bos C, Moonen CTW, Deckers R (2019) Tumor drug distribution after local drug delivery by hyperthermia, in vivo. Cancers (Basel) 11(10). https://doi.org/10.3390/cancers11101512

5.   Moehler M, Dimitrakopoulou-Strauss A, Gutzler F, Raeth U, Strauss LG, Stremmel W (1998) 18F-Labeled fluorouracil Positron Emission Tomography and the prognoses of colorectal carcinoma patients with metastases to the liver treated with 5-fluorouracil. Cancer 83(2):245-253.

6.   van der Veldt AA, Lubberink M, Mathijssen RH, Loos WJ, Herder GJ, Greuter HN, Comans EF, Rutten HB, Eriksson J, Windhorst AD, et al. (2013) Toward prediction of efficacy of chemotherapy: a proof of concept study in lung cancer patients using [(1)(1)C]docetaxel and positron emission tomography. Clin Cancer Res 19(15):4163-4173. https://doi.org/10.1158/1078-0432.CCR-12-3779

7.   Budman DR, Berry DA, Cirrincione CT, Henderson IC, Wood WC, Weiss RB, Ferree CR, Muss HB, Green MR, Norton L, et al. (1998) Dose and dose intensity as determinants of outcome in the adjuvant treatment of breast cancer. Journal of the National Cancer Institute, 90(16):1205-1211.

8.   Henderson IC, Berry DA, Demetri GD, Cirrincione CT, Goldstein LJ, Martino S, Ingle JN, Cooper MR, Hayes DF, Tkaczuk KH, et al. (2003) Improved outcomes from adding sequential Paclitaxel but not from escalating Doxorubicin dose in an adjuvant chemotherapy regimen for patients with node-positive primary breast cancer. J Clin Oncol 21(6):976-983. https://doi.org/10.1200/JCO.2003.02.063

9.   Khan SA (2016) Surgical Management of de novo Stage IV Breast Cancer. Semin Radiat Oncol 26(1):79-86. https://doi.org/10.1016/j.semradonc.2015.08.004

10.   Headon H, Wazir U, Kasem A, Mokbel K (2016) Surgical treatment of the primary tumour improves the overall survival in patients with metastatic breast cancer: A systematic review and meta-analysis. Mol Clin Oncol 4(5):863-867. https://doi.org/10.3892/mco.2016.778

11.   Soran A, Ozmen V, Ozbas S, Karanlık H, Muslumanoglu M, Igci A, Canturk Z, Utkan Z, Ozaslan C, Evrensel T, et al. (2019) The importance of primary surgery in patients with de novo stage IV breast cancer; finalizing the protocol MF07-01 randomized clinical trial. Poster P1-20-01 at San Antonio Breast Cancer Symposium 2019.

12.   Badwe R, Hawaldar R, Nair N, Kaushik R, Parmar V, Siddique S, Budrukkar A, Mittra I, Gupta S (2015) Locoregional treatment versus no treatment of the primary tumour in metastatic breast cancer: an open-label randomised controlled trial. Lancet Oncol 16(13):1380-1388. https://doi.org/10.1016/s1470-2045(15)00135-7

13.   Tsukioki T, Shien T, Doihara H (2020) Effect of local surgery on outcomes of stage IV breast cancer. Translational Cancer Research 9(8):5102-5107. https://doi.org/10.21037/tcr.2020.01.60

14.   Khan SA, Zhao F, Solin LJ, Goldstein LJ, Cella D, Basik M, Golshan M, Julian TB, Pockaj BA, Lee CA, et al. (2020) A randomized phase III trial of systemic therapy plus early local therapy versus systemic therapy alone in women with de novo stage IV breast cancer: A trial of the ECOG-ACRIN Research Group (E2108). Journal of Clinical Oncology 38(18_suppl; abstr LBA2). https://doi.org/10.1200/JCO.2020.38.18_suppl.LBA2

15.   Al-Jamal WT, Al-Ahmady ZS, Kostarelos K (2012) Pharmacokinetics & tissue distribution of temperature-sensitive liposomal doxorubicin in tumor-bearing mice triggered with mild hyperthermia. Biomaterials 33(18):4608-4617. https://doi.org/10.1016/j.biomaterials.2012.03.018

16.   Needham D, Anyarambhatla G, Kong G, Dewhirst MW (2000) A new temperature-sensitive liposome for use with mild hyperthermia: characterization and testing in a human tumor xenograft model. Cancer Res 60:1197-1201.

17.   Needham D, Dewhirst MW (2001) The development and testing of a new temperature-sensitive drug delivery system for the treatment of solid tumors. Adv Drug Deliv Rev 53:285-305.

18.   Kong G, Anyarambhatla G, Petros WP, Braun RD, Colvin M, Needham D, Dewhirst MW (2000) Efficacy of Liposomes and Hyperthermia in a Human Tumor Xenograft Model: Importance of Triggered Drug Release. Cancer Res 60:6950-6957.

19.   Ranjan A, Jacobs GC, Woods DL, Negussie AH, Partanen A, Yarmolenko PS, Gacchina CE, Sharma KV, Frenkel V, Wood BJ, et al. (2012) Image-guided drug delivery with magnetic resonance guided high intensity focused ultrasound and temperature sensitive liposomes in a rabbit Vx2 tumor model. J Control Release 158(3):487-494. https://doi.org/10.1016/j.jconrel.2011.12.011

3

20. Staruch RM, Ganguly M, Tannock IF, Hynynen K, Chopra R (2012) Enhanced drug delivery in rabbit VX2 tumours using thermosensitive liposomes and MRI-controlled focused ultrasound hyperthermia. Int J Hyperthermia 28(8):776-787. https://doi.org/10.3109/02656736.2012.736670

21. de Smet M, Hijnen NM, Langereis S, Elevelt A, Heijman E, Dubois L, Lambin P, Grüll H (2013) Magnetic Resonance Guided High-Intensity Focused Ultrasound Mediated Hyperthermia Improves the Intratumoral Distribution of Temperature-Sensitive Liposomal Doxorubicin. Invest Radiol 48:395-405.

22. Li L, ten Hagen TL, Hossann M, Suss R, van Rhoon GC, Eggermont AM, Haemmerich D, Koning GA (2013) Mild hyperthermia triggered doxorubicin release from optimized stealth thermosensitive liposomes improves intratumoral drug delivery and efficacy. J Control Release 168(2):142-150. https://doi.org/10.1016/j.jconrel.2013.03.011

23. Kim YS, Keserci B, Partanen A, Rhim H, Lim HK, Park MJ, Kohler MO (2012) Volumetric MR-HIFU ablation of uterine fibroids: role of treatment cell size in the improvement of energy efficiency. Eur J Radiol 81(11):3652-3659. https://doi.org/10.1016/j.ejrad.2011.09.005

24. Hurwitz MD, Ghanouni P, Kanaev SV, Iozeffi D, Gianfelice D, Fennessy FM, Kuten A, Meyer JE, LeBlang SD, Roberts A, et al. (2014) Magnetic resonance-guided focused ultrasound for patients with painful bone metastases: phase III trial results. J Natl Cancer Inst 106(5). https://doi.org/10.1093/jnci/dju082

25. Hsiao YH, Kuo SJ, Tsai HD, Chou MC, Yeh GP (2016) Clinical Application of High-intensity Focused Ultrasound in Cancer Therapy. J Cancer 7(3):225-231. https://doi.org/10.7150/jca.13906

26. Chu W, Staruch RM, Pichardo S, Tillander M, Kohler MO, Huang Y, Ylihautala M, McGuffin M, Czarnota G, Hynynen K (2016) Magnetic Resonance-Guided High-Intensity Focused Ultrasound Hyperthermia for Recurrent Rectal Cancer: MR Thermometry Evaluation and Preclinical Validation. Int J Radiat Oncol Biol Phys 95(4):1259-1267. https://doi.org/10.1016/j.ijrobp.2016.03.019

27. Bing C, Patel P, Staruch RM, Shaikh S, Nofiele J, Wodzak Staruch M, Szczepanski D, Williams NS, Laetsch T, Chopra R (2019) Longer heating duration increases localized doxorubicin deposition and therapeutic index in Vx2 tumors using MR-HIFU mild hyperthermia and thermosensitive liposomal doxorubicin. Int J Hyperthermia 36(1):196-203. https://doi.org/10.1080/02656736.2018.1550815

28. Zhu L, Partanen A, Talcott MR, Gach HM, Greco SC, Henke LE, Contreras JA, Zoberi I, Hallahan DE, Chen H, et al. (2019) Feasibility and safety assessment of magnetic resonance-guided high-intensity focused ultrasound (MRgHIFU)-mediated mild hyperthermia in pelvic targets evaluated using an in vivo porcine model. Int J Hyperthermia 36(1):1147-1159. https://doi.org/10.1080/02656736.2019.1685684

29. Deckers R, Rome C, Moonen CT (2008) The role of ultrasound and magnetic resonance in local drug delivery. J Magn Reson Imaging 27(2):400-409. https://doi.org/10.1002/jmri.21272

30. Merckel LG, Bartels LW, Kohler MO, van den Bongard HJ, Deckers R, Mali WP, Binkert CA, Moonen CT, Gilhuijs KG, van den Bosch MA (2013) MR-guided high-intensity focused ultrasound ablation of breast cancer with a dedicated breast platform. Cardiovasc Intervent Radiol 36(2):292-301. https://doi.org/10.1007/s00270-012-0526-6

31. Deckers R, Merckel LG, Denis de Senneville B, Schubert G, Kohler M, Knuttel FM, Mali WP, Moonen CT, van den Bosch MA, Bartels LW (2015) Performance analysis of a dedicated breast MR-HIFU system for tumor ablation in breast cancer patients. Phys Med Biol 60(14):5527-5542. https://doi.org/10.1088/0031-9155/60/14/5527

32. Merckel LG, Knuttel FM, Deckers R, van Dalen T, Schubert G, Peters NH, Weits T, van Diest PJ, Mali WP, Vaessen PH, et al. (2016) First clinical experience with a dedicated MRI-guided high-intensity focused ultrasound system for breast cancer ablation. Eur Radiol 26(11):4037-4046. https://doi.org/10.1007/s00330-016-4222-9

33. Zagar TM, Vujaskovic Z, Formenti S, Rugo H, Muggia F, O'Connor B, Myerson R, Stauffer P, Hsu IC, Diederich C, et al. (2014) Two phase I dose-escalation/pharmacokinetics studies of low temperature liposomal doxorubicin (LTLD) and mild local hyperthermia in heavily pretreated patients with local regionally recurrent breast cancer. Int J Hyperthermia 30(5):285-294. https://doi.org/10.3109/02656736.2014.936049

34. Poon RT, Borys N (2011) Lyso-thermosensitive liposomal doxorubicin: an adjuvant to increase the cure rate of radiofrequency ablation in liver cancer. Future Oncol 7(8):937-945.

35. Tak WY, Lin SM, Wang Y, Zheng J, Vecchione A, Park SY, Chen MH, Wong S, Xu R, Peng CY, et al. (2018) Phase III HEAT Study Adding Lyso-Thermosensitive Liposomal Doxorubicin to Radiofrequency Ablation in Patients with Unresectable Hepatocellular Carcinoma Lesions. Clin Cancer Res 24(1):73-83. https://doi.org/10.1158/1078-0432.CCR-16-2433

36. Lyon PC, Gray MD, Mannaris C, Folkes LK, Stratford M, Campo L, Chung DYF, Scott S, Anderson M, Goldin R, et al. (2018) Safety and feasibility of ultrasound-triggered targeted drug delivery of doxorubicin from thermosensitive liposomes in liver tumours (TARDOX): a single-centre, open-label, phase 1 trial. Lancet Oncol 19(8):1027-1039. https://doi.org/10.1016/s1470-2045(18)30332-2

37. Gray MD, Lyon PC, Mannaris C, Folkes LK, Stratford M, Campo L, Chung DYF, Scott S, Anderson M, Goldin R, et al. (2019) Focused Ultrasound Hyperthermia for Targeted Drug Release from Thermosensitive Liposomes: Results from a Phase I Trial. Radiology 291(1):232-238. https://doi.org/10.1148/radiol.2018181445

38. van Breugel JM, Wijlemans JW, Vaessen HH, de Greef M, Moonen CT, van den Bosch MA, Ries MG (2016) Procedural sedation and analgesia for respiratory-gated MR-HIFU in the liver: a feasibility study. J Ther Ultrasound 4:19. https://doi.org/10.1186/s40349-016-0063-x

39. Ishihara Y, Calderon A, Watanabe H, Okamoto K, Suzuki Y, Kuroda K, Suzuki Y (1995) A precise and fast temperature

mapping using water proton chemical shift. MRM 34:814-823.

40. de Poorter J (1995) Noninvasive MRI thermometry with the proton resonance frequency method: study of susceptibility effects. MRM 34:359-367.

41. Brady MJ, Cella DF, Mo F, Bonomi AE, Tulsky DS, Lloyd SR, Deasy S, Cobleigh M, Shiomoto G (1997) Reliability and Validity of the Functional Assessment of Cancer Therapy-Breast Quality-of-Life Instrument. J Clin Oncol 15:974-986.

42. Abetz L, Coombs JH, Keininger DL, Earle CC, Wade C, Bury-Maynard D, Copley-Merriman K, Hsu MA (2005) Development of the cancer therapy satisfaction questionnaire: item generation and content validity testing. Value Health 8 Suppl 1:S41-53. https://doi.org/10.1111/j.1524-4733.2005.00073.x

43. Cheung K, de Mol M, Visser S, Den Oudsten BL, Stricker BH, Aerts JG (2016) Reliability and validity of the Cancer Therapy Satisfaction Questionnaire in lung cancer. Qual Life Res 25(1):71-80. https://doi.org/10.1007/s11136-015-1062-z

44. Eisenhauer EA, Therasse P, Bogaerts J, Schwartz LH, Sargent D, Ford R, Dancey J, Arbuck S, Gwyther S, Mooney M, et al. (2009) New response evaluation criteria in solid tumours: revised RECIST guideline (version 1.1). Eur J Cancer 45(2):228-247. https://doi.org/10.1016/j.ejca.2008.10.026

45. Wahl RL, Jacene H, Kasamon Y, Lodge MA (2009) From RECIST to PERCIST: Evolving Considerations for PET response criteria in solid tumors. J Nucl Med 50 Suppl 1:122S-150S. https://doi.org/10.2967/jnumed.108.057307

46. Chan S, Davidson N, Juozaityte E, Erdkamp F, Pluzanska A, Azarnia N, Lee LW (2004) Phase III trial of liposomal doxorubicin and cyclophosphamide compared with epirubicin and cyclophosphamide as first-line therapy for metastatic breast cancer. Ann Oncol 15(10):1527-1534. https://doi.org/10.1093/annonc/mdh393

47. Celsion Corporation (2019) ThermoDox®, Lyso-Thermosensitive Liposomal Doxorubicin (LTLD), Investigator's Brochure.

48. Wood BJ, Poon RT, Locklin JK, Dreher MR, Ng KK, Eugeni M, Seidel G, Dromi S, Neeman Z, Kolf M, et al. (2012) Phase I study of heat-deployed liposomal doxorubicin during radiofrequency ablation for hepatic malignancies. J Vasc Interv Radiol 23(2):248-255 e247. https://doi.org/10.1016/j.jvir.2011.10.018

49. Gabizon A, Catane R, Uziely B, Kaufman B, Safra T, Cohen R, Martin F, Huang A, Barenholz Y (1994) Prolonged circulation time and enhanced accumulation in malignant exudates of doxorubicin encapsulated in polyethylene-glycol coated liposomes. Cancer Res 54(4):987-992.

50. Swenson CE, Bolcsak LE, Batist G, Guthrie TH, Jr., Tkaczuk KH, Boxenbaum H, Welles L, Chow SC, Bhamra R, Chaikin P (2003) Pharmacokinetics of doxorubicin administered i.v. as Myocet (TLC D-99; liposome-encapsulated doxorubicin citrate) compared with conventional doxorubicin when given in combination with cyclophosphamide in patients with metastatic breast cancer. Anticancer Drugs 14(3):239-246. https://doi.org/10.1097/01.cad.0000060626.61556.da

51. Joerger M, Huitema ADR, Richel DJ, Dittrich C, Pavlidis N, Briasoulis E, Vermorken JB, Strocchi E, Martoni A, Sorio R, et al. (2007) Population pharmacokinetics and pharmacodynamics of doxorubicin and cyclophosphamide in breast cancer patients. Clin Pharmacokinet 46(12):1051-1068.

52. Jacquet JM, Bressolle F, Galtier M, Bourrier M, Donadio D, Jourdan J, Rossi JF (1990) Doxorubicin and doxorubicinol: intra- and inter-individual variations of pharmacokinetic parameters. Cancer Chemother Pharmacol 27(3):219-225.

53. Callies S, de Alwis DP, Wright JG, Sandler A, Burgess M, Aarons L (2003) A population pharmacokinetic model for doxorubicin and doxorubicinol in the presence of a novel MDR modulator, zosuquidar trihydrochloride (LY335979). Cancer Chemother Pharmacol 51(2):107-118.

54. Joerger M, Huitema AD, Meenhorst PL, Schellens JH, Beijnen JH (2005) Pharmacokinetics of low-dose doxorubicin and metabolites in patients with AIDS-related Kaposi sarcoma. Cancer Chemother Pharmacol 55(5):488-496. https://doi.org/10.1007/s00280-004-0900-4

3

SUPPLEMENTARY MATERIAL

The Supplementary Material for this article can be found online at: https://bmjopen.bmj.com/content/10/11/e040162.long#supplementary-materials

Supplement 1 Comparison of $AUC_{0-\infty}$ of free doxorubicin for LTLD and conventional doxorubicin.
Supplement 2 Dose adjustments in the i-GO study.
Supplement 3 Restrictions to concomitant medications and products
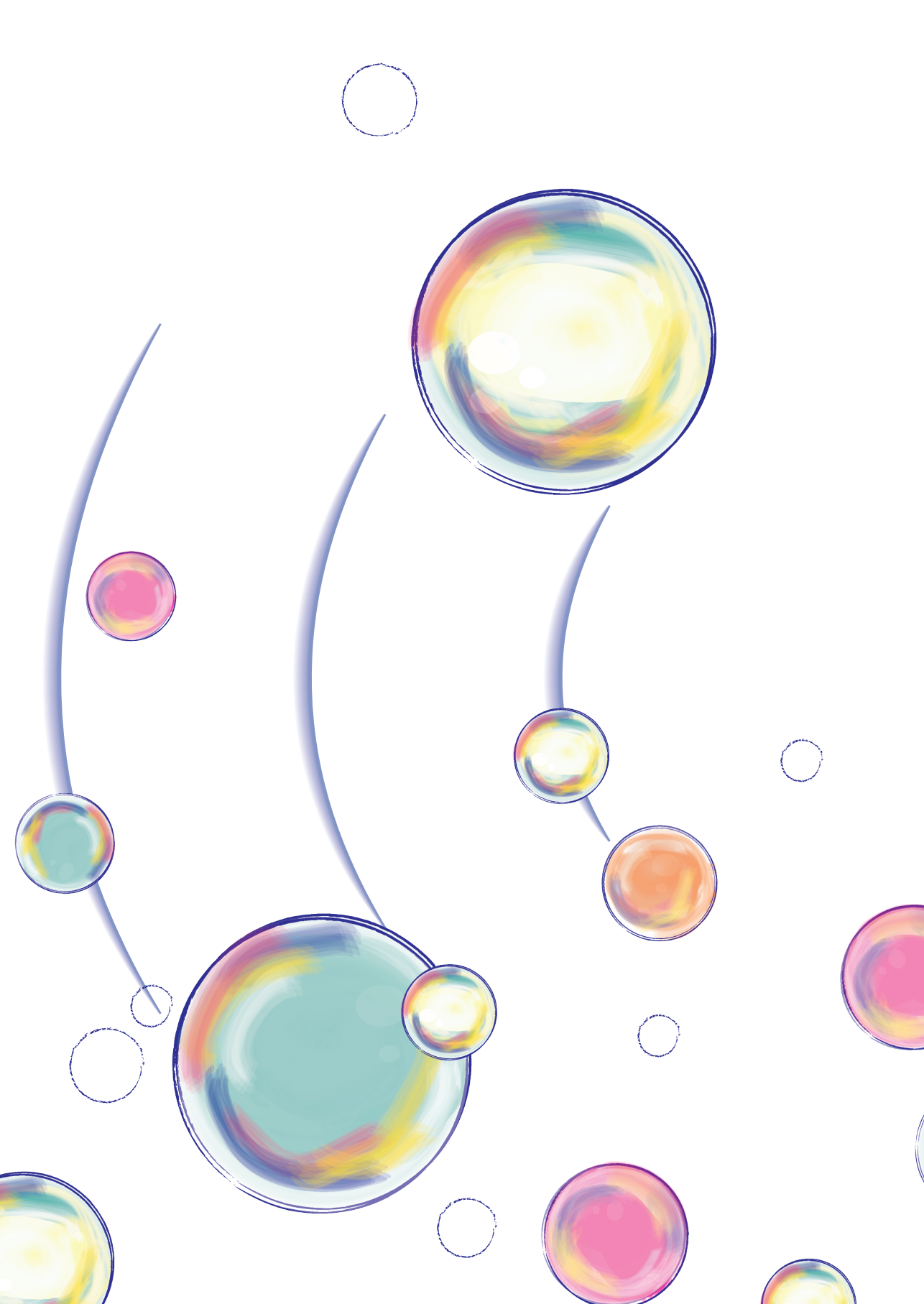**Supplement 4** Flow-chart interim analysis
Supplement 5 Data Safety Monitoring Board Charter
Supplement 6 Patient informed consent form in English

3

3

PART III

Ultrasound and microbubbles: therapy and diagnostics in head and neck cancer

ULTRASOUND-MEDIATED DRUG DELIVERY WITH A CLINICAL ULTRASOUND SYSTEM: *IN VITRO* EVALUATION

Josanne S de Maar[1], Charis Rousou[2], Benjamin van Elburg[3], Hendrik J Vos[4], Guillaume PR Lajoinie[3], Clemens Bos[1], Chrit TW Moonen[1], Roel Deckers[1*]

[1]Imaging & Oncology Division, University Medical Center Utrecht, Utrecht University, Utrecht, The Netherlands
[2]Department of Pharmaceutical Sciences, Utrecht Institute for Pharmaceutical Sciences (UIPS), Utrecht University, Utrecht, The Netherlands
[3]Physics of Fluids Group, MIRA Institute of Biomedical Technology and Technical Medicine, University of Twente, Enschede, The Netherlands
[4]Laboratory of Acoustical Wavefield Imaging, Faculty of Applied Sciences, Delft University of Technology, Delft, The Netherlands

ABSTRACT

Chemotherapy efficacy is often reduced by insufficient drug uptake in tumor cells. The combination of ultrasound and microbubbles (USMB) has been shown to improve drug delivery and to enhance the efficacy of several drugs *in vitro* and *in vivo*, through effects collectively known as sonopermeation. However, clinical translation of USMB therapy is hampered by the large variety of (non-clinical) US set-ups and US parameters that are used in these studies, which are not easily translated to clinical practice. In order to facilitate clinical translation, the aim of this study was to prove that USMB therapy using a clinical ultrasound system (Philips iU22) in combination with clinically approved microbubbles (SonoVue) leads to efficient *in vitro* sonopermeation. To this end, we measured the efficacy of USMB therapy for different US probes (S5-1, C5-1 and C9-4) and US parameters in FaDu cells. The US probe with the lowest central frequency (i.e. 1.6 MHz for S5-1) showed the highest USMB-induced intracellular uptake of the fluorescent dye SYTOX™ Green (SG). These SG uptake levels were comparable to or even higher than those obtained with a custom-built US system with optimized US parameters. Moreover, USMB therapy with both the clinical and the custom-built US system increased the cytotoxicity of the hydrophilic drug bleomycin. Our results demonstrate that a clinical US system can be used to perform USMB therapy as efficiently as a single-element transducer set-up with optimized US parameters. Therefore, future trials could be based on these clinical US systems, including validated US parameters, in order to accelerate successful translation of USMB therapy.

Keywords
USMB, sonoporation, sonopermeation, ultrasound, microbubbles, chemotherapy, drug delivery, imaging

INTRODUCTION

Chemotherapy is typically used as systemic treatment to destroy metastatic cancer cells that have spread away from the primary tumor. However, local action of chemotherapy is also of importance throughout the spectrum of oncological therapy. First, surgically unresectable tumors can be made operable with neoadjuvant chemotherapy [1, 2]. Secondly, neoadjuvant chemotherapy can lead to less extensive surgery and reduce the risk of local recurrences [3, 4]. Third, chemotherapy can enhance the local effect of radiotherapy during chemoradiation [5-7]. Finally, local response to palliative chemotherapy can decrease morbidity [8-10]. Unfortunately, there is substantial heterogeneity in the local response to systemic treatment within and across cancer types. A plausible explanation for suboptimal response is the heterogeneous and/or insufficient delivery of drugs to tumor cells caused by biophysical barriers of the tumor tissue [11, 12].

The combination of ultrasound and microbubbles (USMB) has been shown to overcome these biophysical barriers and increase local tumor uptake of several drugs resulting in enhanced efficacy [13-15]. Microbubbles are micron sized (1-10 μm in diameter) gas-filled particles with a biocompatible shell that are widely used as vascular contrast agents for ultrasound imaging [16, 17]. In addition, the interaction of US waves and microbubbles has the potential to enhance the delivery of drugs. Microbubbles exposed to low-intensity US fields will oscillate (i.e. stable cavitation), while microbubbles exposed to higher intensities will collapse violently (i.e. inertial cavitation). Both types of cavitation lead to a number of bio-effects collectively known as sonopermeation, such as the formation of pores in cell membranes (sonoporation), enhanced endocytosis and increased vascular permeability, that improve the deposition of drugs in tumor tissue [14, 18].

In particular, hydrophilic drugs such as bleomycin and cisplatin, that have difficulties crossing the cell membrane, may benefit from local USMB therapy, leading to increased delivery of such drugs *in vitro* [19-32] and increased anti-tumor response *in vivo* [19, 23-25, 28, 29, 31]. The first clinical trials using the combination of chemotherapy and USMB have been conducted. In a phase 1 clinical trial, USMB with clinically available microbubble SonoVue was combined with gemcitabine in ten inoperable pancreatic cancer patients. Trial participants could tolerate significantly more treatment cycles and the median overall survival was longer compared to historical controls treated with gemcitabine alone [33, 34]. Another phase 1 trial in eleven patients with hepatic metastases and one patient with pancreatic cancer concluded that treatment with physician's choice chemotherapy (most commonly FOLFIRI, i.e. folinic acid, fluorouracil and irinotecan) plus USMB with SonoVue was safe [35]. Several follow-up phase 1 / 2 studies are currently recruiting or being prepared (Clinicaltrials.gov NCT04146441, NCT04821284, NCT03477019 and NCT03458975). A phase 3 trial investigates the addition of USMB to neoadjuvant chemotherapy in breast cancer (Clinicaltrials.gov NCT03385200, current status unknown).

4

Despite these promising developments, translation of USMB therapy from *in vitro* and small animal studies to the clinic is still limited. One major obstacle for clinical translation of USMB therapy is the lack of a clinically approved US system with settings optimized to perform USMB therapy. A large variety of (non-clinical) US set-ups and US parameters have been used for *in vitro* and *in vivo* studies [36]. While these studies have provided invaluable insights on the underlying mechanisms of USMB therapy and provided *in vivo* proof of concept, their methods and results cannot be easily transferred to clinical studies because the US equipment is not, and will not likely be, approved for clinical use. In this study we take a different approach to facilitate the clinical translation of USMB therapy by investigating the potential of an existing clinical ultrasound system (Philips iU22) in combination with clinically available microbubbles (SonoVue) to perform USMB therapy. To this end, we use *in vitro* experiments to evaluate the effect of USMB therapy on the intracellular uptake of a model drug (SYTOX™ Green) and the efficacy of the hydrophilic chemotherapeutic drug bleomycin.

MATERIALS AND METHODS

Chemicals and reagents

All cells were cultured in high glucose Dulbecco's modified eagle medium (DMEM) supplemented with 10% fetal bovine serum (FBS) and 1% non-essential amino acids (NEAA).

Dulbecco's Phosphate Buffered Saline (PBS), modified, without calcium, chloride and magnesium chloride was used as solvent and for washing steps.

PBS, DMEM, FBS, NEAA and trypsin / ethylenediaminetetraacetic acid (EDTA) were purchased from Sigma-Aldrich (St. Louis, USA).

Bleomycin sulfate (Bleomedac® powder for solution for injection, GmbH, Wedel, Germany) was dissolved in sterile 0.9% NaCl to reach a final concentration of 10µg/mL, which corresponds to at least 15IU (Ph. Eur) per mL. Bleomycin is hydrophilic (LogP-7.5) and has a molecular weight of 1415.6 g/mol[1].

SYTOX™ Green is a cell-impermeant fluorescent nuclear acid stain with excitation/ emission wavelength of 504/523 nm. Its impermeability and >500-fold fluorescence enhancement after binding to nuclear acids makes it suitable to visualize USMB therapy efficacy. DRAQ5™ fluorescent probe is a cell-permeant fluorescent dye (excitation 647 nm, emission 681nm) that was used to counterstain the DNA content of all cells. AlamarBlue™ reagent was used for the cell viability assay. The eBioscience™ Annexin V Apoptosis Detection Kit APC, containing both fluorescently labelled Annexin V and Propidium Iodide (PI), was used for the apoptosis assay. SYTOX™ Green, DRAQ5™,

---

1   https://pubchem.ncbi.nlm.nih.gov/compound/Bleomycin#section=CAS [Accessed August 31st, 2021]

AlamarBlue™ and eBioscience™ Annexin V Apoptosis Detection Kit APC were purchased from ThermoFisher Scientific (Waltham, Massachusetts, USA).

Cell culture

A human pharyngeal squamous cell carcinoma cell-line (FaDu) (ATCC® HTB-43™, LGC Standards GmbH, Wedel, Germany) was cultured in high glucose DMEM supplemented with 10% FBS and 1% NEAA. FaDu cells were cultured in a humidified incubator at 37 °C and 5% CO_2. They were split 2-3 times per week at a confluency of around 80%, until a maximum passage number of 20. One day before each experiment, FaDu cells collected using trypsin/EDTA and seeded in a 35 mm diameter lumox® culture dish (Sarstedt AG& Co. KG, Nümbrecht, Germany).

Ultrasound systems and microbubbles

SonoVue (Bracco International B.V., Amsterdam, the Netherlands) was prepared according to the manufacturer's instructions, producing sulfurhexafluoride-filled phospholipid microbubbles with a mean bubble diameter of ~2.5 µm and a concentration of $1-5*10^8$ microbubbles/mL in sterile 0.9% NaCl. Microbubbles were kept at 4°C in between use, resuspended before every use and used within 2 hours after preparation.

We used a clinical ultrasound system (iU22 Ultrasound system, Philips Medical Systems Nederland B.V, Best, the Netherlands) combined with the following probes: S5-1, C5-1 and C9-4. USMB therapy was done in Pulsed Wave (PW) Doppler mode. The transmission frequency of each transducer was set by the system and cannot be changed. The Pulse Repetition Period (PRP) was set to the longest period for each transducer by setting the scale parameter to the minimum. The acoustic pressure was varied by changing the mechanical index (MI). The number of cycles per pulse was varied by changing the sample volume (SV), while the MI (pressure) was kept constant.

The acoustic field of each transducer in PW Doppler mode as well as the acoustic pressure for each setting was measured using a 0.2 mm needle hydrophone (Precision acoustics Ltd., Dorset, UK) in degassed water.

As reference, we used a custom-built US set-up that was previously used for USMB therapy [37]. This US set-up consisted of a single-element transducer operated at 1.5 MHz, 150 cycles per pulse, pulse repetition frequency of 1.0 kHz and Peak negative pressures (P_{neg}) of 0.39, 0.56 and 0.72 MPa.

Microbubble response

The acoustic bubble response to the specific acoustic pulses used in the experiment was characterized by attenuation measurements. A sample holder (acoustical path length of 8 mm) with two acoustically transparent windows was positioned such that its center coincided with the focal point of two single-element transducers. The transmit transducer (Olympus V304, f = 2.25 MHz, F = 1.88 inch, D = 1 inch) was calibrated using a

fibre-optic hydrophone (Precision Acoustics). The receiving transducer (Olympus V307, f = 5 MHz, F = 1.93 inch, D = 1 inch, was aligned such that the received signal (without microbubbles) was at a maximum.

Eight differently shaped US pulses were used, four with a rectangular envelop (as used in the single-element set-up) and four with a Gaussian envelop (to recreate the pulses of the US imager probe), with 11, 23, 46 and 150 cycles. These pulses were generated by a waveform generator (Tabor 8026) and amplified (vectawave, VBA100-200) before transmission. The receiving transducer and the waveform generator were connected to a digital oscilloscope (picoscope 5444d) such that both the transmitted and received signal were recorded. The waveform generator as well as the oscilloscope were triggered (BNC, 575) simultaneously.

Each US pulse was repeated 5 times, with a pulse repetition frequency (PRF) of 6.7 kHz, for 5 different Peak negative pressures (150 kPa to 750 kPa with 150 kPa steps), such that one measurement consisted of 200 pulses. During the measurements the sample in the holder was continuously refreshed by a gravity-driven flow. Measurements were done at the frequencies used throughout the rest of the paper, namely 1.6 MHz, 2.25 MHz and 4 MHz. All measurements were performed with diluted (1000x) SonoVue and without microbubbles for reference.

Attenuation coefficients were calculated by comparing the transmission through the SonoVue solution to that through distilled water:

where is the attenuation coefficient in dB/cm, is the acoustical path length through the sample in cm, and are the amplitudes of the frequency spectra of the SonoVue and reference signal, respectively, at the transmit frequency .

USMB therapy experimental set-up

In order to apply USMB therapy to cells cultured in lumox® dishes we used TwentiCells, which were designed and manufactured at Twente University (**Figure 1**). The TwentiCell consists of a 3D-printed lumox® dish holder and a screw-on ring to seal the lumox® dish with a polyolefin (25 μm thick), creating a water-tight compartment. The holder contains an in-let and out-let to the fill the compartment with drugs/microbubbles in solution and remove unwanted air, respectively. The parts were assembled before each experiment and UV-sterilized before inserting the lumox® dish containing the cells to avoid infection. Acoustic transparency of the TwentiCells and inserted lumox® dishes is close to 100% (data not shown).

For the USMB therapy the TwentiCell was immersed in degassed water (T = 37°C) and fixed above the transducer in a custom-built frame. The distance between the surface of the clinical ultrasound probes and the lumox® dish membrane was 3.0 cm and the PW Doppler Sample Volume was centered on this position **(Figure 1 (C))**. In the single-element transducer set-up the lumox® dish membrane was positioned in the focal zone

of the transducer, i.e. 8.0 cm above the transducer surface (**Figure 1 (D)**).
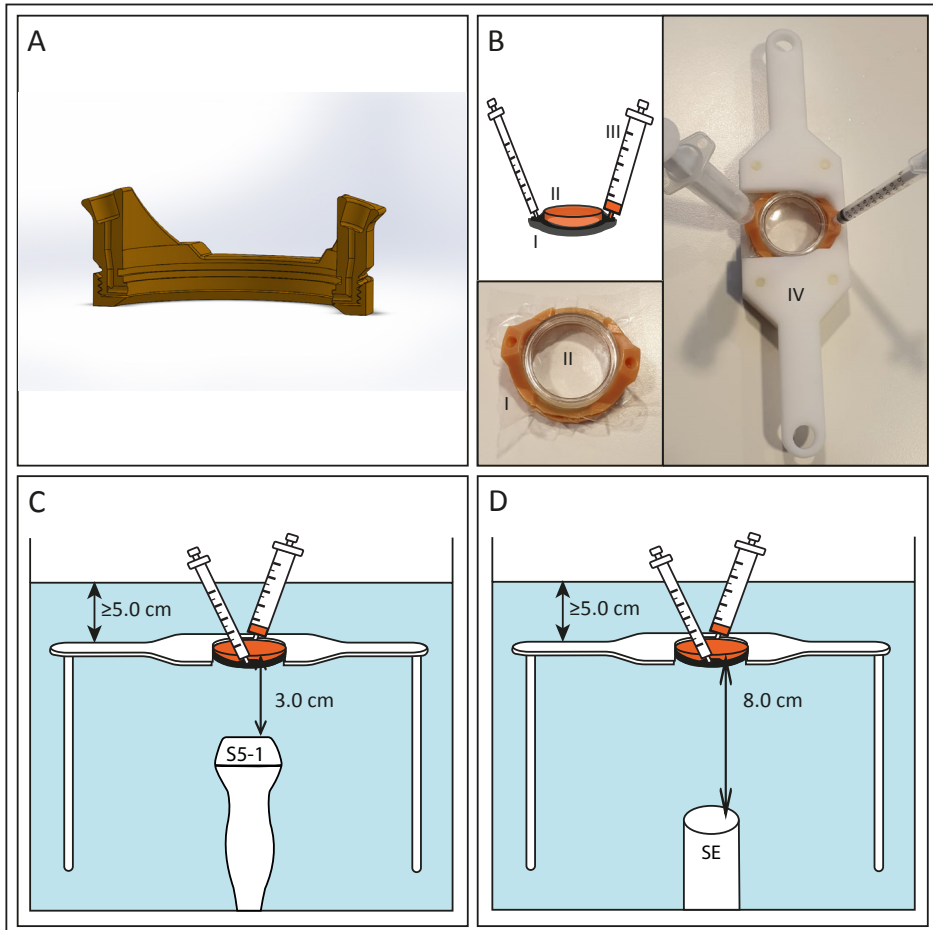
Figure 1. Experimental US set-up for *in vitro* experiments. **(A)** Cross section of 3D-printed TwentiCell **(B)** Schematic drawing and photos of TwentiCell (I) including upside-down inserted lumox® dish (II) in custom-build frame (IV). A 5 mL syringe (III) is used to insert the medium and to remove air. **(C)** TwentiCell immersed in degassed water, in a custom-build frame, with clinical US probe 3.0 cm below the cells or **(D)** with single element transducer 8.0 cm below the cells. In both set-ups at least 5 cm of water was above the cells.

SYTOX™ Green experiments

One day after seeding $3.0*10^5$ FaDu cells in lumox® dishes, the medium was removed and a mixture of 2µL SYTOX™ Green (SG, 5 mM solution in DMSO), 180µL SonoVue and 4.8 mL medium was added to the TwentiCell. For USMB-untreated samples, a lumox® dish with regular lid was used and the volumes were adjusted to 0.5 µL SG, 45µL 0.9%

NaCl and 1.2mL medium. The TwentiCells were incubated (37 °C and 5% CO_2) for 15 minutes with the cell containing surface upwards, in order for the microbubbles to float towards the cells. Next, the TwentiCell was placed in the waterbath (cell containing surface remaining upwards), exposed to ultrasound for 15 seconds and put back in the incubator. The US-untreated samples were not removed from the incubator. 30 minutes after USMB treatment, the SG-containing medium was removed and clean medium was added. Afterwards, the cells were washed with PBS, fixated with paraformaldehyde (4% in PBS) and stained with 1 mL DRAQ5 (5 µM in PBS) at 37°C for about 20 minutes. The lumox® membrane was covered with solidifying mounting medium FluorSave™ (Merck Millipore, Burlington, Massachusetts, USA) and a glass cover slip, and kept in the dark at 4°C until fluorescence imaging. These experiments were performed with the single element transducer as well as the clinical US system.

Bleomycin experiments

One day after seeding $1.5*10^5$ FaDu cells in lumox® dishes, the medium was removed and a mixture of 498 µL bleomycin solution or 0.9% NaCl, 180µL SonoVue and 4.302 mL medium was added to the TwentiCell. For US-untreated samples, a lumox® dish with regular lid was used and the volumes were adjusted to 125 µL bleomycin solution or 0.9% NaCl, 45µL 0.9% NaCl and 1.075 mL medium. The TwentiCells were incubated (37 °C and 5% CO_2) for 15 minutes with the cell containing surface upwards. Next, the TwentiCell was placed in the waterbath (cell containing surface remaining upwards), exposed to ultrasound for 15 seconds and put back in the incubator. The US-untreated samples were not removed from the incubator.

To determine the IC_{50} and IC_{25} of bleomycin with or without USMB, the final bleomycin concentrations were 0, 0.1, 0.5, 1, 5, 10, 50, 100 and 500 µg/mL and the single-element transducer set-up was used. The apoptosis assay was performed at a single bleomycin concentration (10 µg/mL) using the single-element set-up as well as the clinical US system.

Two hours after USMB therapy, the bleomycin or 0.9% NaCl containing medium was removed, the cells were washed with PBS and clean medium was added. The cells were then incubated at 37°C, 5% CO_2 until 48 hours after adding the bleomycin, microbubbles and/or 0.9% NaCl.

Fluorescence microscopy

Fluorescence imaging for the SG experiments was performed on a Confocal Zeiss LSM 700 microscope. SG was imaged with excitation 488 nm and emission >500 nm. DRAQ5 was imaged with excitation 639nm and emission > 640 nm. All microscope settings, including laser power, gain, pinhole size and digital offset, were kept constant during all experiments. Images were obtained with 10 times enlargement with a frame size of 512x512 and a square tile size of 640.17 μm^2. For each lumox® dish, a square of 10 by

10 tiles was imaged with a 10% overlap, starting in the visual center of the SG signal. The tiles were stitched immediately after acquisition. In each tile a Z-stack of 3 levels was created to compensate for height variances of the cells over the tiles.

To quantify the USMB efficacy for different US-settings we performed automated cell segmentation of SG-positive and DRAQ5-positive cells using (Fiji Is Just) ImageJ 2.0.0-rc-69. First, a standard-deviation Z-projection was created for the SG and DRAQ5 images. To segment the SG-positive cells global thresholding was applied, with a fixed threshold for all samples, whereas for segmenting the DRAQ5-positive cells a local threshold was applied (i.e. mean method with a radius of 5). Next, the noise in the binary masks after thresholding was removed with a median filter and the watershed algorithm was applied to split clustered objects. Objects with a size ≥20 pixel units were counted as cells, regardless of circularity.

The number of SG and DRAQ5-positive cells were analyzed in a region of interest (ROI) of 600x600 pixels, centered on the position with the highest SG signal after blurring the SG image with a 2-D Gaussian smoothing kernel with standard deviation of 200 in Matlab (R2019a). When there was no noteworthy SG signal, the ROI was positioned in center of the 10x10 square. Objects on the edges of the ROI were not counted.

Viability assay

The effect of bleomycin with or without USMB therapy on cell viability was determined with an AlamarBlue assay. 48 hours after adding medium with or without bleomycin and microbubbles to the Twenticell, a solution of 1mL medium and 100µ AlamarBlue reagent (500 µM solution in PBS) was added to each lumox® and incubated (37 °C and 5% CO_2). After two hours, the mixture was removed from each lumox® and pipetted into a well plate.

The fluorescence intensity in the well plate was measured using the FLUOstar OPTIMA (BMG LABTECH) plate reader, with excitation and emission wavelengths of 550-10 and 600-610 nm and a gain of 1500. The cell viability of a sample was calculated as percentage fluorescent signal relative to that of untreated control samples, after subtraction of the fluorescent signal of a negative control without cells.

To determine IC_{50}/IC_{25} in each group (with or without USMB), the cell viability percentages were calculated with reference to their own controls, i.e. no exposure to bleomycin but with or without USMB depending on the group. The IC_{50} was then defined as the concentration resulting in 50% inhibition of cell viability, likewise, the IC_{25} was the concentration resulting in 25% inhibition of cell viability. The method to determine IC_{50}/IC_{25} is described in 2.11.

Apoptosis assay

In addition to the viability assay, an apoptosis assay was performed to determine the effect of USMB on bleomycin efficacy. The apoptosis and viability assays were performed

in separate experiments. 48 hours after adding medium with or without bleomycin and with or without microbubbles to the Twenticell, the medium and detached cells were collected from each lumox® dish. The remaining cells were detached from the lumox® membrane with trypsin/EDTA and added to the rest of the medium. Residual EDTA was removed by centrifugation and washing with PBS. The cells were resuspended in binding buffer with a concentration of ~$1*10^6$ cells/mL and then stained and incubated for 15 minutes with Annexin V. The cells were washed, resuspended in binding buffer, stained with Propidium Iodide (PI) and then kept on ice protected from light.

Within 4 hours, the samples were analyzed by flow cytometry using the BD FACSCanto ™ II Cell Analyzer, for PI (488nm) and Annexin V (633nm). Compensation was performed with samples stained with only PI and only Annexin V. The FACS data was analyzed using FlowJo 10.7.1. The four quadrants (live, early apoptotic, late apoptotic, and necrotic cells) were distinguished based on a control sample containing 50% necrotic and 50% live cells.

Statistical analysis

Statistical analysis was performed in GraphPad Prism 8.3.0. For the fluorescence microscopy data and cell viability data we used the Kruskal Wallis test and a Dunn's test for multiple comparisons. The absolute IC_{50} for bleomycin with and without USMB was determined with a nonlinear least-squares regression of the bleomycin concentration versus the response (cell viability percentage) with the Hill's slope fixed at -1.0 and the top and bottom of the fitted curve restrained to 100 and 0 %, respectively. To compare the IC_{50}'s of both groups we used the extra sum of squares F-test. Because the IC_{50}'s had a very broad confidence interval we also calculated the IC_{25} for both groups with the same method. A p-value < 0.05 was considered to indicate a statistically significant difference.

RESULTS

Acoustic characterization of clinical US system

The acoustic output of the clinical ultrasound system as well as the US beam profile were characterized for the probes S5-1, C5-1 and C9-4. The acoustic output as function of different US settings is summarized in **Table 1**. With increasing SV, the number of cycles per pulse increased. The maximum MI (and therefore pressure) increased with decreasing SV. **Figure 2** shows the characteristics of the S5-1 probe. **Supplementary figures 1-3** show these characteristics for the other clinical US probes and the single-element transducer. In PW mode the S5-1 probe emits a US pulse with a Gaussian shaped envelope with a center frequency of 1.6 MHz and an increasing number of cycles when SV is increased (**Figure 2(A** and **B))**. The pressure field maps in PW mode **(Figure**

2(C)) show that the ultrasound energy is limited to a beam with dimensions of 5.0 mm by 6.3 mm (Full width at half maximum) at the middle of the sample volume. **Figure 2(D)** demonstrates the difference in signal intensity in the Twenticell (red rectangle) before and after USMB therapy (15 sec sonication at MI 0.6, SV 20mm), due to microbubble disruption.

Table 1. US parameters and corresponding measurements on clinical US system

Clinical US probe		Pulse repetition period		Pulse length		Maximum pressure at SV 20mm		Evaluated pressures at SV 20mm	
	PW freq (MHz)	Min. Scale (cm/sec)	Max. PRP (µs)	SV (mm)	Cycles per pulse	Max. MI	Max. P_{neg} (MPa)	MI evaluated	P_{neg} (MPa)
S5-1	1.6	-30 – 30	800	20	46	0.6	0.59	0.6	0.59
				10	23			0.5	0.46
				5	11			0.4	0.38
								0.3	0.30
								0.2	0.22
C5-1	2.25	-6 – 6	2500	20	64	0.8	0.59	0.8	0.59
				10	32			0.5	0.39
				5	16			0.3	0.25
C9-4	4.0	-12 – 12	800	20	117	0.3	0.44	0.3	0.44
				10	59			0.2	0.37
				5	29			0.2	0.30
								0.1	0.19

Bubble response to US

Figure 3 shows the attenuation coefficient for SonoVue for different pulse envelop shapes and lengths as a function of acoustic pressure and frequency.

The attenuation curve shows a maximum at 1.6 and 2.25 MHz indicating a maximum attenuation for the frequencies that are closest to resonance frequency of SonoVue.

The attenuation coefficient decreased, mainly at 1.6 MHz, as the excitation pressure was increased from 150 kPa to 750 kPa. This observation is not consistent with previous experimental measurements of pressure-dependent attenuation coefficients [38, 39]. As we have observed no visible trace of bubble destruction based on the repeated pulses, the refreshment rate of the bubble solution appears to be sufficient, and we ascribe this effect to radiation forces and bubble clustering. As such, this effect may be even more prominent at the higher concentrations used for the cell experiments.

When comparing rectangular versus Gaussian envelop shapes no differences were observed in attenuation coefficient. Furthermore, the number of cycles per pulse did not influence the attenuation coefficient.
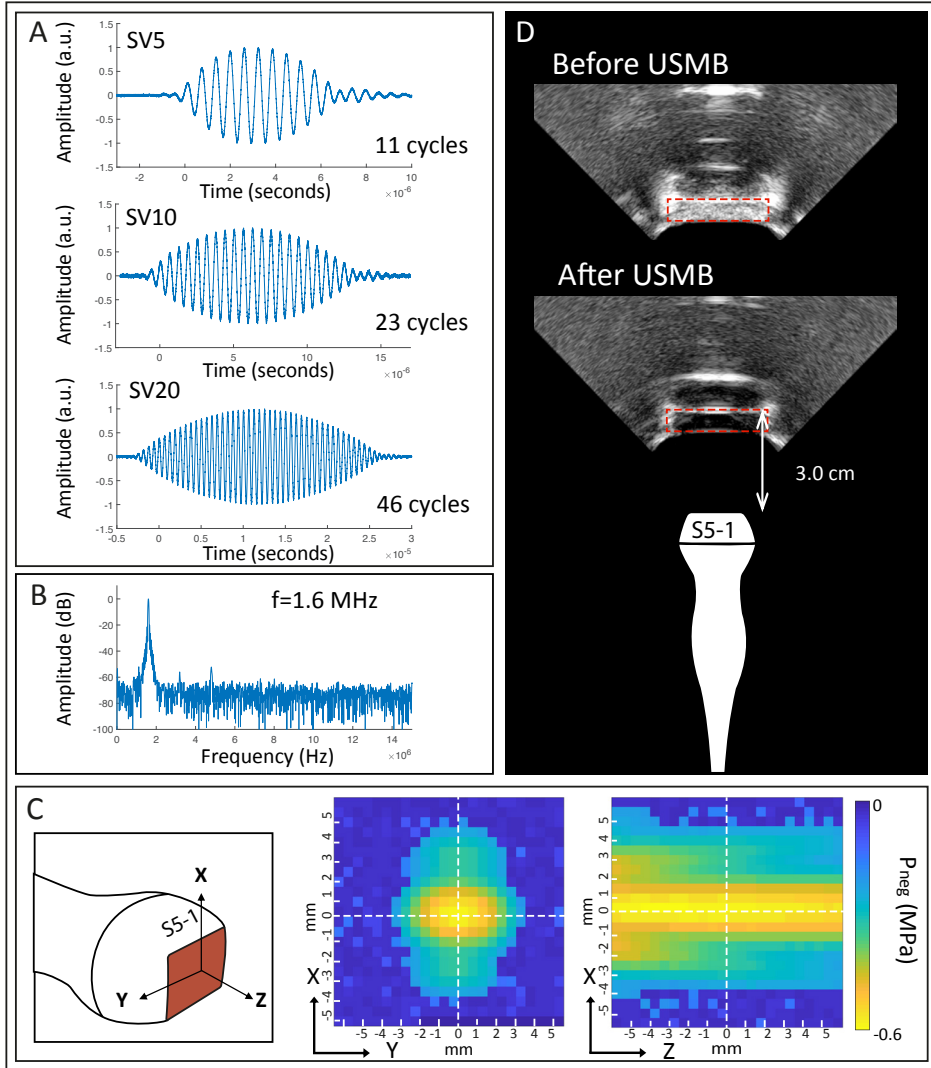
Figure 2. Characteristics of S5-1 probe **(A)** Shape of emitted ultrasound pulses in PW mode for different pulse length. **(B)** Frequency spectrum of SV 20 mm pulse. **(C)** Pressure field maps in PW mode. **(D)** B-mode images of TwentiCell (red rectangle) containing microbubbles, before and after USMB therapy (15 seconds at MI 0.6, SV 20mm). SV: sample volume; f: frequency; a.u.: arbitrary units; P_{neg}: Peak negative pressure; USMB: ultrasound and microbubbles.
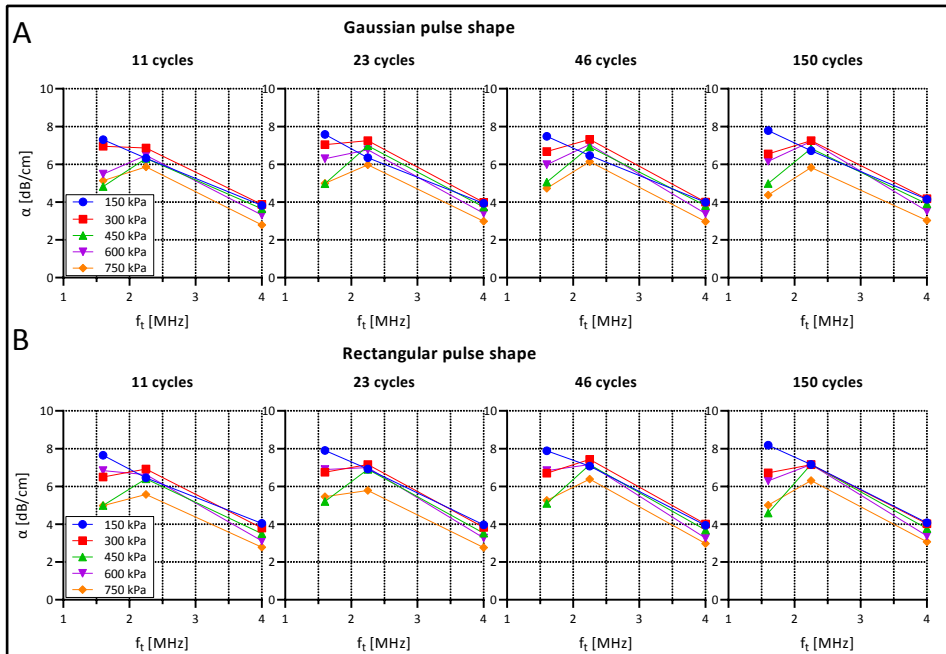
Figure 3. Attenuation coefficient α for SonoVue for different pulse shapes and lengths as a function of acoustic pressure and frequency. **(A)** Gaussian pulse envelop (as used in PW Doppler mode on clinical US system). **(B)** Rectangular pulse envelop (as used in single-element set-up). α: attenuation coefficient; f_t: transmit frequency.

4

Effect of transducer and ultrasound settings on USMB efficiency

The USMB efficacy for each transducer as function of acoustic pressure is shown in **Figure 4(A)**. The percentage of SG positive cells increased significantly with the addition of USMB treatment using the S5-1 (1.6 MHz) or C5-1 (2.25 MHz) probes and was comparable (C5-1) or even higher (S5-1) than with the single element transducer (**Figure 4(A)**). In contrast, no relevant SG uptake was observed using the C9-4 probe (4.0 MHz). For the S5-1 probe a similar percentage of SG positive cells (i.e. ~30%) was observed for all pressures above 0.30 MPa. In contrast, the C5-1 probe and the single element transducer showed a pressure-dependent increase of SG positive cells, reaching ~30% and 15% at the highest pressures, respectively.

The effect of pulse length for the S5-1 and C5-1 is shown in **Figure 4(B)**. For the S5-1 probe at maximum pressure (0.59 MPa), a similar percentage of SG positive cells (i.e. 38%) was observed independent of pulse length. For the S5-1 probe at a lower pressure (0.38 MPa) only a higher number of cycles per pulse (SV 20 and 10mm) caused a significant increase in SG positive cells compared to USMB untreated samples. For the C5-1 probe at maximum pressure (0.59 MPa), the percentage SG positive cells increased with increasing pulse length.

Figure 4(C) shows representative fluorescence images of the ROI after USMB therapy

with S5-1 probe at MI 0.6 and SV 20mm, stained with SG and DRAQ5.
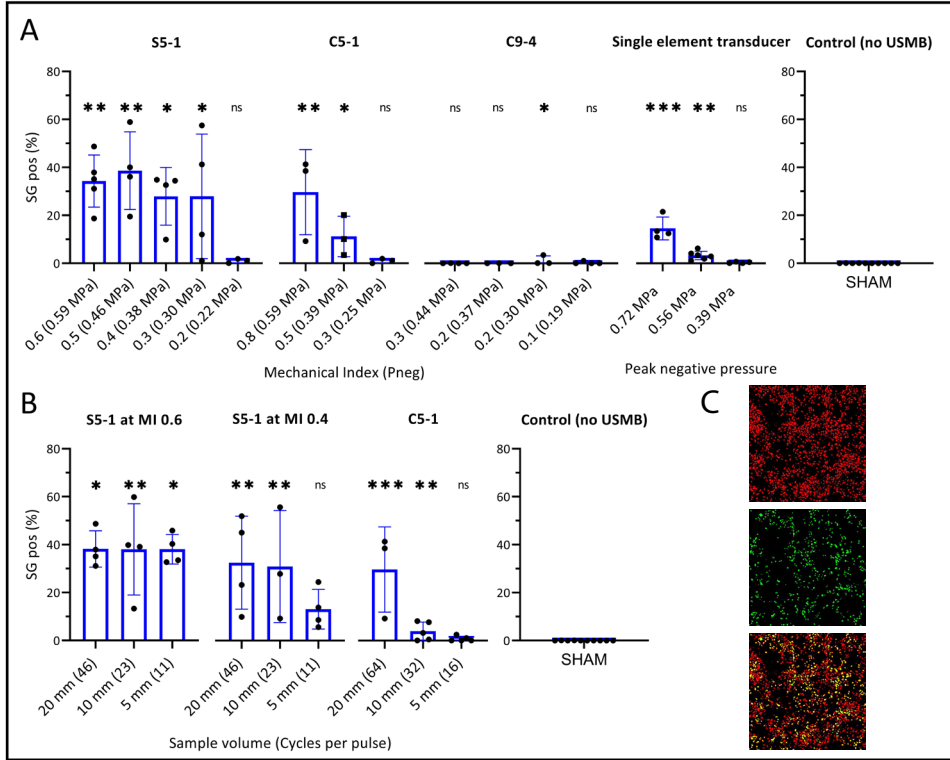
Figure 4. Effect of transducer and ultrasound settings on USMB efficiency measured by percentage SG positive cells in ROI. **(A)** Effect of pressure on USMB efficiency with (from left to right) clinical US system with S5-1, C5-1 or C9-4 probe and custom-build US set-up with single-element transducer. **(B)** Effect of pulse length on USMB efficiency of clinical US system with (from left to right) S5-1 probe at maximum pressure (MI 0.6, P_{neg} 0.59 MPa), S5-1 probe at MI 0.4 (P_{neg} 0.38 MPa) and C5-1 probe at maximum pressure (MI 0.8, P_{neg} 0.59 MPa). Symbols indicate individual measurements and bars indicate mean and SD (n ≥ 3) All values were statistically compared to USMB untreated samples (right). * p<0.05 ** p<0.01 *** p<0.001. **(C)** Representative fluorescence images of ROI after USMB with S5-1 probe at MI 0.6 (0.59 MPa) and maximum pulse length (SV 20mm). Top: DRAQ5™ staining, middle: SG staining, Bottom: composite, cells stained for DRAQ5™ (red), SG (green) or both (yellow). SG uptake in 35.1% of cells. ns: not significant; SG: SYTOX™ Green; USMB: ultrasound and microbubbles.

Effect of USMB on bleomycin efficacy

To confirm that USMB therapy improved the efficacy of bleomycin, the IC_{50} and IC_{25} of bleomycin were determined, with or without USMB with the single-element transducer **(Figure 5(A))**. The absolute IC_{50} of bleomycin decreased from 791.8µg/L (95% CI 578.8 - 1125) to 173.2µg/mL (95% CI 96.06 – 333.0) when combined with USMB (P_{neg} = 0.56 MPa). The USMB-induced difference in IC_{50} was statistically significant (p < 0.0001). The IC_{25} decreased significantly from 263.9 µg/mL (95% CI 192.9 – 374.8) to 57.73 µg/mL

(95% CI 32.02 - 111.0) (p < 0.0001). Note that both curves have their own reference of 100% cell viability without bleomycin (i.e. with or without USMB), which guarantees that the observed differences in IC_{25} and IC_{50} are not a direct cytotoxic effect of USMB alone, but due to enhanced intracellular delivery of bleomycin causing more cell death at the same concentration. The effect of USMB treatment in the absence of bleomycin is illustrated in **Figure 5(B).** Cell viability did not significantly decrease with increasing acoustic pressure.

The apoptosis assay confirmed the decreasing cell viability with addition of USMB to bleomycin. **Figure 5(C)** shows the mean distribution of cells over the quadrants after USMB with the single-element transducer. Representative dot plots of flow cytometry analysis from experiments with two or three samples per group are shown in **Figure 5(D)**. Increased apoptosis was observed 48 hours after bleomycin plus USMB (P_{neg} 0.56 MPa), compared to untreated samples or samples treated with either bleomycin alone or USMB alone.

Effect of USMB with clinical US system on bleomycin efficacy

Figure 6 demonstrates that the cytotoxicity of bleomycin could also be increased by USMB therapy using the clinical US system with the S5-1 probe. The combination of bleomycin (10 µg/mL) and USMB with significantly decreased the cell viability compared to untreated samples at the three pressures used, while either bleomycin alone or USMB alone had little effect (**Figure 6(A)**). Addition of USMB at P_{neg} 0.59 MPa (MI 0.6) to bleomycin, also significantly decreased the cell viability from 94 to 47% compared to samples treated with bleomycin alone. At the lower pressures we also observed a decrease in cell viability when USMB was added to bleomycin (from 94% to 57% at P_{neg} 0.46 MPa and to 54% at P_{neg} 0.38 MPa), however these changes were not significant.

The results of the apoptosis assay again confirmed the decrease in cell viability with the combination of bleomycin and USMB. **Figure 6(B)** shows the mean distribution of cells over the quadrants after USMB with the clinical US system and S5-1 probe. Representative dot plots of flow cytometry analysis from experiments with two or three samples per group are shown in **Figure 6(C)**. Besides increased apoptosis, similar to what was seen with the single element transducer, also increased necrosis (11.4 % versus 8% with bleomycin alone) was observed after bleomycin plus USMB with the clinical US system.
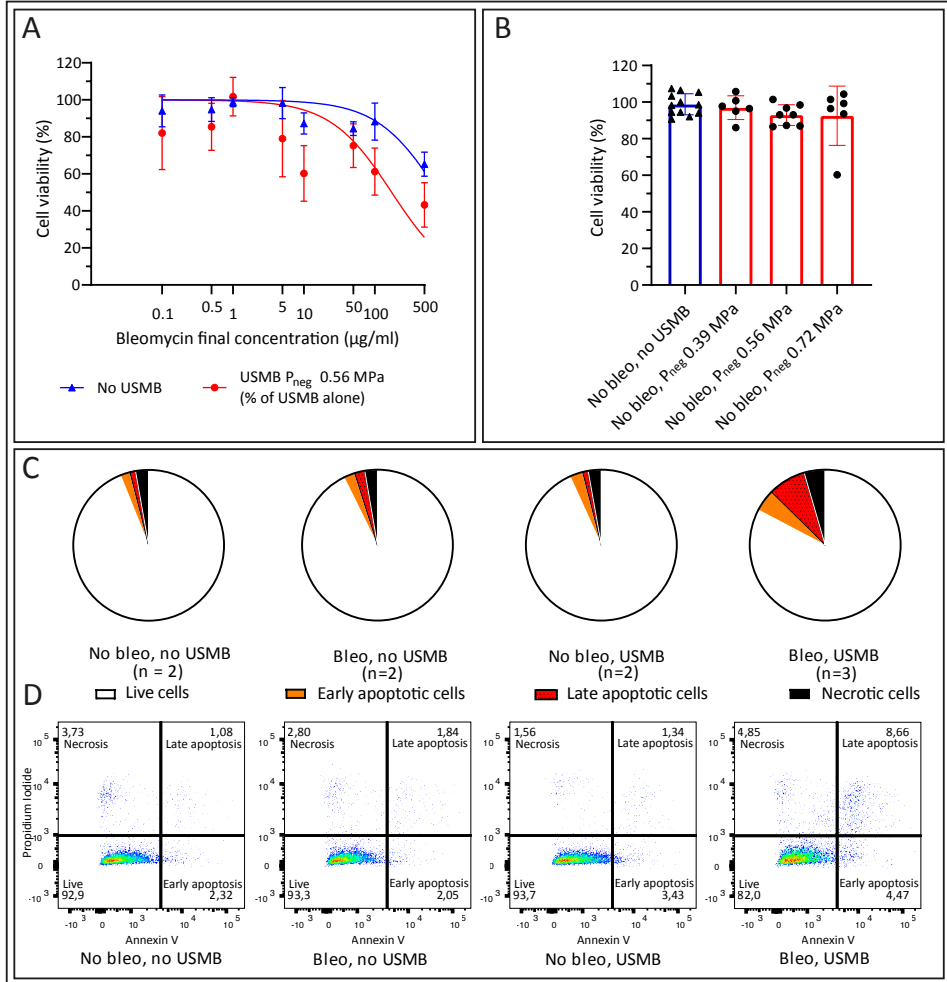
Figure 5. Cell viability after bleomycin +/- USMB using the custom-build US set-up with single element transducer. **(A)** Nonlinear least-squares regression of bleomycin concentration versus cell viability percentage (relative to samples without bleomycin), with (red circles) and without (blue triangles) USMB at P_{neg} 0.56 MPa. Symbols and bars indicate mean and SD (n ≥ 3). **(B)** Cell viability with (red, circles) or without (blue, triangles) USMB alone at three pressures, symbols indicate individual measurements and bars indicate mean and SD (n ≥ 6). **(C)** Flow cytometry analysis of Propidium Iodide and Annexin V staining 48 hours after bleomycin 10 μg/mL or NaCl 0.9% with or without USMB at P_{neg} 0.56 MPa. Pie charts represent the mean of the samples with n=2 or (for bleomycin + USMB samples) n=3. **(D)** Representative dot plots of flow cytometry analysis shown in (**C**). More apoptosis was observed after bleomycin + USMB. Bleo: bleomycin; P_{neg}: Peak negative pressure; USMB: ultrasound and microbubbles.
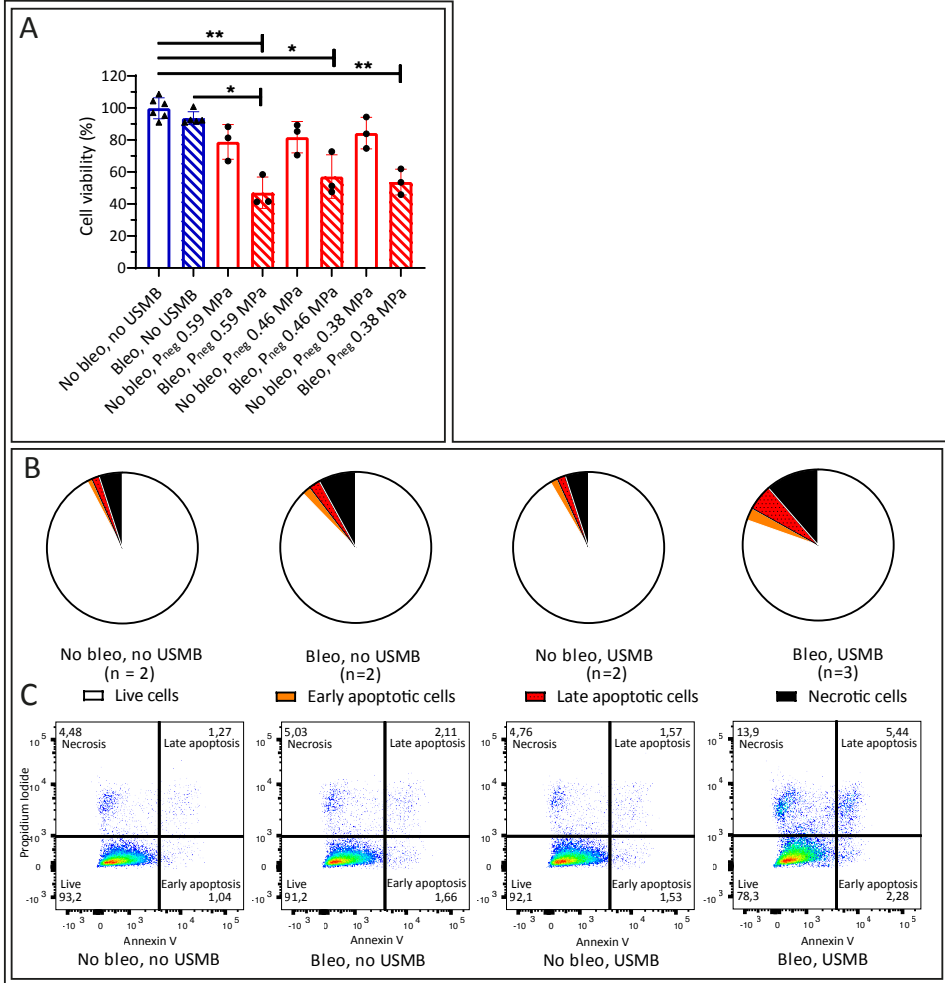
Figure 6. Cell viability after bleomycin +/- USMB using the clinical US system with S5-1 probe **(A)** Bleomycin 10 μg/mL or NaCl 0.9% with (red, circles) and without (blue, triangles) USMB at three pressures (MI 0.6, 0.5 and 0.4). Symbols indicate individual measurements and bars indicate mean and SD (n ≥ 3). * p<0.05 ** p<0.01 **(B)** Flow cytometry analysis of Propidium Iodide and Annexin V staining 48 hours after bleomycin 10μg/mL or NaCl 0.9% with or without USMB at P_{neg} 0.59 MPa (MI 0.6), pie charts represent the mean of the samples with n=2 or (for bleomycin + USMB samples) n=3. **(C)** Representative dot plots of flow cytometry analysis shown in (**B**). More apoptosis and necrosis was observed after bleomycin + USMB. Bleo: bleomycin; MI: Mechanical Index; P_{neg}: Peak negative pressure; USMB: ultrasound and microbubbles.

DISCUSSION

In preclinical studies, USMB therapy has overcome biophysical barriers that cause heterogeneous and/or insufficient drug delivery to tumor cells, thereby increasing intracellular uptake and enhancing the efficacy of several drugs. Although the first clinical studies have been published, clinical translation of USMB therapy is still limited. We hypothesize that clinically available US systems with fixed and validated parameters will accelerate clinical translation. To pave the road forwards, we characterized several clinical probes and US-parameters and showed that effective USMB therapy can be performed *in vitro* with a non-modified clinical US system and EMA/FDA approved microbubbles.

After evaluation of three clinical US probes and a set of parameters, the US probe with the lowest center frequency (i.e. 1.6 MHz for S5-1) showed the highest USMB efficiency as measured by SG uptake. This was consistent with literature showing that a frequency close to the resonance frequency of SonoVue (i.e. $1.6 - 3.1$ MHz depending on the bubble size [40]) was the most efficient [36, 41]. Moreover, at lower pressures a larger number of cycles per pulse was beneficial. This was also seen in previous studies, although some conflicting results have been reported and intermediate pulse lengths might be optimal [36, 42-45]. The SG uptake levels that we achieved with the clinical US system were comparable, or even higher depending on the transducer and US-settings, to those obtained with a custom-built US set-up with a single-element transducer and optimized US parameters [37]. A possible explanation for these higher uptake levels would be that the gradually increasing pressure in the Gaussian pulse shape of the PW Doppler mode leads to a more efficient bubble response than the block shaped pulse of the single-element transducer. However, we found no evidence in our microbubble attenuation experiments to support this. Since the experimental set-up and handling were equal for both set-ups and the frequencies of S5-1 probe (1.6 MHz) and the transducer of the custom-build set-up (1.5 MHz) were very similar we conclude that the improved USMB efficiency using the S5-1 and C5-1 probes must be due to other factors that we did not investigate (e.g. PRF, non-lineair US propagation and beam shape). Future experiments including cavitation measurements might further elude the underlying mechanisms.

In this study we used the PW Doppler mode for USMB therapy, in contrast to previous clinical studies that used B-mode and contrast mode, or color power angiography doppler (Clinicaltrials.gov NCT03385200, personal communication). The first clinical trial used B-mode, with settings optimized to achieve a linear acoustic signal, the maximum possible duty cycle (1%), center frequency of 1.9 MHz and MI 0.4 (measured pressure 0.27 MPa P_{neg}) [33, 34]. The second clinical trial did not provide details about specific ultrasound settings used, apart from the MI that varied between 0.4 and 1.0 [35]. Although not clinically applied, PW Doppler on a clinical US system has been evaluated in a mouse study for blood-brain barrier disruption using a variation of clinically available

US parameters (e.g., frequency 5.0-8.0 MHz) [46]. As demonstrated by the pressure fields (**Figure 2(B)** and **Supplementary figures 1 and 2**), PW Doppler mode creates a very small (5.0 mm by 6.3 mm for S5-1) USMB therapy focus, much smaller than the treatment area described in the previous phase 1 clinical trial (i.e. 69 * >100 * 1.0 mm^3) [33]. Therefore, PW Doppler mode is well suited for precisely targeted treatment. In addition, the use of a clinical US imager provides the opportunity to perform imaging and therapy consecutively, thus performing image-guided therapy.

This is to our best knowledge the first *in vitro* study that evaluates the effect of USMB therapy using a clinical US system and approved SonoVue microbubbles, while performing extensive evaluation of multiple transducers and US settings available in PW Doppler mode. Previously, *in vitro* studies have used Optison microbubbles for USMB therapy with clinical US systems in spectral Doppler, 2-D scan mode or harmonic imaging (Octave) mode at a frequency of 1.5 of 3.5 MHz [47, 48]. Compared to our findings, these methods resulted in a lower USMB efficacy (below 10%), which could indicate that PW Doppler mode is more effective. Other *in vitro* studies have used a diagnostic US system to evaluate microbubble response, while therapeutic USMB was omitted or administered with a non-clinical transducer [45, 49, 50]. USMB therapy would benefit from simultaneous (real-time) cavitation monitoring with a single transducer of a clinical US system. This solution would allow for monitoring of bioeffects [51-54], while using standardized US settings. Currently, simultaneous USMB therapy and cavitation monitoring is not yet available on clinical US systems, although our work and the work by Keller et al. show it is technically feasible [50]. Meanwhile, our approach leads to a standardization of US parameters used and may be immediately used in clinics.

Next to correct determination and extensive reporting of the US exposure conditions used [55], which has been performed for clinical US systems, and performing cavitation monitoring during treatment, the use of mono-disperse microbubbles will further reduce the disparity of experimental results. Currently, commercial, clinically approved microbubbles are polydisperse. However, recent papers show that monodisperse microbubbles have a more uniform acoustic response and an increased imaging sensitivity [56, 57], which will also improve the reproducibility and controllability of USMB therapy.

We hypothesized that USMB therapy with a clinical US system and approved microbubbles could improve the local efficacy of chemotherapy. Both the Alamar Blue assay and the flow cytometry analysis showed that *in vitro* USMB therapy with both the clinical and the custom-built US system clearly increased the cytotoxicity of the hydrophilic drug bleomycin. However, our absolute IC_{50} values have to be interpreted with caution. The nonlinear regression model included only one concentration above the IC_{50} for the cells treated with USMB, and none for the cells treated without USMB. This led to a large confidence interval in the IC_{50} estimations. Unfortunately, due to a worldwide shortage of bleomycin [58] it was not feasible to increase the concentration further, in order to

achieve an effect closer to 100% cell death. For this reason, we additionally calculated the IC_{25} of each group and compared those. These data confirmed the increased cytotoxicity of bleomycin with the addition of USMB therapy.

While in clinical practice bleomycin is only used in a few tumor types, these results could be extended to a wide range of treatments with other hydrophilic chemotherapeutics. For example, based on previous *in vitro* results of Lammertink et al. future patients receiving chemotherapy or chemoradiation containing cisplatin could benefit from the addition of local USMB therapy [30]. Furthermore, USMB therapy could be used to enhance the effect of therapeutic antibodies or nanoparticles [25, 59-62]. Finally, clinical studies evaluating the potential of USMB therapy in addition to radiotherapy in the absence of drugs are ongoing [63] (Clinicaltrials.gov NCT04431674, NCT04431648).

The custom-made TwentiCells used in our experiments are an attractive alternative to for example CLINIcells and provide the opportunity to perform USMB experiments with a large number of independently sonicated samples, while using small volumes of medium, drugs and microbubbles. In addition, the TwentiCells hardly interfere with the applied ultrasound field, a common limitation of *in vitro* US set-ups [64, 65]. To obtain reliable and reproducible results we standardized the procedures throughout our experiments as much as possible. This is essential, as many parameters (e.g. position of cells with respect to transducer, time between preparation and use of microbubbles, time between addition of microbubbles and sonication [45, 66]) can affect outcome of USMB therapy.

To conclude, we have shown that a non-modified clinical US system in combination with clinically approved microbubbles can be used to perform highly effective USMB therapy *in vitro*. The next step towards clinical translation is to apply these methods *in vivo*. Future trials should determine the safety and efficacy of our methods and US parameters in patients.

AUTHOR CONTRIBUTIONS

JM, CB, CM, and RD conceived and designed the analysis. JM, CR, and RD collected the data. BE, HV, GL, and RD contributed data or analysis tools. JM, BE, and RD performed the analysis. JM and RD wrote the manuscript. CR, BE, HV, GL, CB, and CM revised and approved the submitted version.

FUNDING

ACKNOWLEDGEMENTS

CONFLICTS OF INTEREST

The authors declare that the research was conducted in the absence of any commercial or financial relationships that could be construed as a potential conflict of interest.

4

REFERENCES

1. Sclafani F, Brown G, Cunningham D, Rao S, Tekkis P, Tait D, Morano F, Baratelli C, Kalaitzaki E, Rasheed S, et al. (2017) Systemic chemotherapy as salvage treatment for locally advanced rectal cancer patients who fail to respond to standard neoadjuvant chemoradiotherapy. The Oncologist 22:728-736. https://doi.org/10.1634/theoncolo-gist.2016-0396

2. Fietkau R, Grutzmann R, Wittel UA, Croner RS, Jacobasch L, Neumann UP, Reinacher-Schick A, Imhoff D, Boeck S, Keilholz L, et al. (2021) R0 resection following chemo (radio)therapy improves survival of primary inoperable pancreatic cancer patients. Interim results of the German randomized CONKO-007+/- trial. Strahlenther Onkol 197(1):8-18. https://doi.org/10.1007/s00066-020-01680-2

3. Dietz A, Wichmann G, Kuhnt T, Pfreundner L, Hagen R, Scheich M, Kolbl O, Hautmann MG, Strutz J, Schreiber F, et al. (2018) Induction chemotherapy (IC) followed by radiotherapy (RT) versus cetuximab plus IC and RT in advanced laryngeal/hypopharyngeal cancer resectable only by total laryngectomy-final results of the larynx organ preservation trial DeLOS-II. Ann Oncol 29(10):2105-2114. https://doi.org/10.1093/annonc/mdy332

4. van Ramshorst MS, van der Voort A, van Werkhoven ED, Mandjes IA, Kemper I, Dezentjé VO, Oving IM, Honkoop AH, Tick LW, van de Wouw AJ, et al. (2018) Neoadjuvant chemotherapy with or without anthracyclines in the presence of dual HER2 blockade for HER2-positive breast cancer (TRAIN-2): a multicentre, open-label, randomised, phase 3 trial. The Lancet Oncology 19(12):1630-1640. https://doi.org/10.1016/s1470-2045(18)30570-9

5. Geoffrois L, Martin L, De Raucourt D, Sun XS, Tao Y, Maingon P, Buffet J, Pointreau Y, Sire C, Tuchais C, et al. (2018) Induction chemotherapy followed by cetuximab radiotherapy is not superior to concurrent chemoradiotherapy for head and neck carcinomas: results of the GORTEC 2007-02 phase III randomized trial. J Clin Oncol 36(31):3077-3083. https://doi.org/10.1200/JCO.2017.76.2591

6. Versteijne E, Suker M, Groothuis K, Akkermans-Vogelaar JM, Besselink MG, Bonsing BA, Buijssen J, Busch OR, Creemers G-JM, van Dam RM, et al. (2020) Preoperative chemoradiotherapy versus immediate surgery for resectable and borderline resectable pancreatic cancer: results of the dutch randomized phase III PREOPANC trial J Clin Oncol 38(16):1763-1773. https://doi.org/10.1200/JCO.19.02274

7. Zhao Z, Wen Y, Liao D, Miao J, Gui Y, Cai H, Chen Y, Wei M, Jia Q, Tian H, et al. (2020) Single-Agent Versus Double-Agent Chemotherapy in Concurrent Chemoradiotherapy for Esophageal Squamous Cell Carcinoma: Prospective, Randomized, Multicenter Phase II Clinical Trial. Oncologist 25(12):e1900-e1908. https://doi.org/10.1634/theoncologist.2020-0808

8. Vermorken JB, Mesia R, Rivera F, Remenar E, Kawecki A, Rottey S, Erfan J, Zabolotnyy D, Kienzer H-R, Cupissol D, et al. (2008) Platinum-Based Chemotherapy plus Cetuximab in Head and Neck Cancer. N Engl J Med 359(11):1116-1127.

9. Loupakis F, Cremolini C, Masi G, Lonardi S, Zagonel V, Salvatore L, Cortesi E, Tomasello G, Ronzoni M, Spadi R, et al. (2014) Initial therapy with FOLFOXIRI and bevacizumab for metastatic colorectal cancer. N Engl J Med 371(17):1609-1618. https://doi.org/10.1056/NEJMoa1403108

10. Judson I, Verweij J, Gelderblom H, Hartmann JT, Schöffski P, Blay J-Y, Kerst JM, Sufliarsky J, Whelan J, Hohenberger P, et al. (2014) Doxorubicin alone versus intensified doxorubicin plus ifosfamide for first-line treatment of advanced or metastatic soft-tissue sarcoma: a randomised controlled phase 3 trial. The Lancet Oncology 15(4):415-423. https://doi.org/10.1016/s1470-2045(14)70063-4

11. Tredan O, Galmarini CM, Patel K, Tannock IF (2007) Drug resistance and the solid tumor microenvironment. J Natl Cancer Inst 99(19):1441-1454. https://doi.org/10.1093/jnci/djm135

12. de Maar JS, Sofias AM, Porta Siegel T, Vreeken RJ, Moonen C, Bos C, Deckers R (2020) Spatial heterogeneity of nanomedicine investigated by multiscale imaging of the drug, the nanoparticle and the tumour environment. Theranostics 10(4):1884-1909. https://doi.org/10.7150/thno.38625

13. Lammertink BH, Bos C, Deckers R, Storm G, Moonen CT, Escoffre JM (2015) Sonochemotherapy: from bench to bedside. Front Pharmacol 6:138. https://doi.org/10.3389/fphar.2015.00138

14. Snipstad S, Sulheim E, de Lange Davies C, Moonen C, Storm G, Kiessling F, Schmid R, Lammers T (2018) Sonopermeation to improve drug delivery to tumors: from fundamental understanding to clinical translation. Expert Opin Drug Deliv 15(12):1249-1261. https://doi.org/10.1080/17425247.2018.1547279

15. Kooiman K, Roovers S, Langeveld SAG, Kleven RT, Dewitte H, O'Reilly MA, Escoffre JM, Bouakaz A, Verweij MD, Hynynen K, et al. (2020) Ultrasound-Responsive Cavitation Nuclei for Therapy and Drug Delivery. Ultrasound Med Biol 46(6):1296-1325. https://doi.org/10.1016/j.ultrasmedbio.2020.01.002

16. Chong WK, Papadopoulou V, Dayton PA (2018) Imaging with ultrasound contrast agents: current status and future. Abdom Radiol (NY) 43(4):762-772. https://doi.org/10.1007/s00261-018-1516-1

17. Frinking P, Segers T, Luan Y, Tranquart F (2020) Three Decades of Ultrasound Contrast Agents: A Review of the Past, Present and Future Improvements. Ultrasound Med Biol 46(4):892-908. https://doi.org/10.1016/j.ultrasmedbio.2019.12.008

18. Deprez J, Lajoinie G, Engelen Y, De Smedt SC, Lentacker I (2021) Opening doors with ultrasound and

microbubbles: Beating biological barriers to promote drug delivery. Adv Drug Deliv Rev 172:9-36. https://doi.org/10.1016/j.addr.2021.02.015

19. Iwanaga K, Tominaga K, Yamamoto K, Habu M, Maeda H, Akifusa S, Tsujisawa T, Okinaga T, Fukuda J, Nishihara T (2007) Local delivery system of cytotoxic agents to tumors by focused sonoporation. Cancer Gene Ther 14(4):354-363. https://doi.org/10.1038/sj.cgt.7701026

20. Maeda H, Tominaga K, Iwanaga K, Nagao F, Habu M, Tsujisawa T, Seta Y, Toyoshima K, Fukuda J, Nishihara T (2009) Targeted drug delivery system for oral cancer therapy using sonoporation. J Oral Pathol Med 38(7):572-579. https://doi.org/10.1111/j.1600-0714.2009.00759.x

21. Lamanauskas N, Novell A, Escoffre JM, Venslauskas M, Satkauskas S, Bouakaz A (2013) Bleomycin delivery into cancer cells in vitro with ultrasound and SonoVue(R) or BR14(R) microbubbles. J Drug Target 21(4):407-414. https://doi.org/10.3109/1061186X.2012.761223

22. Tamosiunas M, Mir LM, Chen WS, Lihachev A, Venslauskas M, Satkauskas S (2016) Intracellular Delivery of Bleomycin by Combined Application of Electroporation and Sonoporation in Vitro. J Membr Biol 249(5):677-689. https://doi.org/10.1007/s00232-016-9911-4

23. Hirabayashi F, Iwanaga K, Okinaga T, Takahashi O, Ariyoshi W, Suzuki R, Sugii M, Maruyama K, Tominaga K, Nishihara T (2017) Epidermal growth factor receptor-targeted sonoporation with microbubbles enhances therapeutic efficacy in a squamous cell carcinoma model. PLoS One 12(9):e0185293. https://doi.org/10.1371/journal.pone.0185293

24. Watanabe Y, Aoi A, Horie S, Tomita N, Mori S, Morikawa H, Matsumura Y, Vassaux G, Kodama T (2008) Low-intensity ultrasound and microbubbles enhance the antitumor effect of cisplatin. Cancer Sci 99(12):2525-2531. https://doi.org/10.1111/j.1349-7006.2008.00989.x

25. Heath CH, Sorace A, Knowles J, Rosenthal E, Hoyt K (2012) Microbubble therapy enhances anti-tumor properties of cisplatin and cetuximab in vitro and in vivo. Otolaryngol Head Neck Surg 146(6):938-945. https://doi.org/10.1177/0194599812436648

26. Sasaki N, Ishi K, Kudo N, Nakayama SMM, Nakamura K, Morishita K, Ohta H, Ishizuka M, Takiguchi M (2017) Spatial and temporal profile of cisplatin delivery by ultrasound-assisted intravesical chemotherapy in a bladder cancer model. PLoS One 12(11):e0188093. https://doi.org/10.1371/journal.pone.0188093

27. Sasaki N, Kudo N, Nakamura K, Lim SY, Murakami M, Kumara WR, Tamura Y, Ohta H, Yamasaki M, Takiguchi M (2012) Activation of microbubbles by short-pulsed ultrasound enhances the cytotoxic effect of cis-diamminedichloroplatinum (II) in a canine thyroid adenocarcinoma cell line in vitro. Ultrasound Med Biol 38(1):109-118. https://doi.org/10.1016/j.ultrasmedbio.2011.09.017

28. Sato T, Mori S, Arai Y, Kodama T (2014) The combination of intralymphatic chemotherapy with ultrasound and nano-/microbubbles is efficient in the treatment of experimental tumors in mouse lymph nodes. Ultrasound Med Biol 40(6):1237-1249. https://doi.org/10.1016/j.ultrasmedbio.2013.12.012

29. Sato T, Mori S, Sakamoto M, Arai Y, Kodama T (2015) Direct delivery of a cytotoxic anticancer agent into the metastatic lymph node using nano/microbubbles and ultrasound. PLoS One 10(4):e0123619. https://doi.org/10.1371/journal.pone.0123619

30. Lammertink BH, Bos C, van der Wurff-Jacobs KM, Storm G, Moonen CT, Deckers R (2016) Increase of intracellular cisplatin levels and radiosensitization by ultrasound in combination with microbubbles. J Control Release 238:157-165. https://doi.org/10.1016/j.jconrel.2016.07.049

31. Chen HK, Zhang SM, Chang JL, Chen HC, Lin YC, Shih CP, Sytwu HK, Fang MC, Lin YY, Kuo CY, et al. (2018) Insonation of Systemically Delivered Cisplatin-Loaded Microbubbles Significantly Attenuates Nephrotoxicity of Chemotherapy in Experimental Models of Head and Neck Cancer. Cancers (Basel) 10(9). https://doi.org/10.3390/cancers10090311

32. Fekri F, Abousawan J, Bautista S, Orofiamma L, Dayam RM, Antonescu CN, Karshafian R (2019) Targeted enhancement of flotillin-dependent endocytosis augments cellular uptake and impact of cytotoxic drugs. Sci Rep 9(1):17768. https://doi.org/10.1038/s41598-019-54062-9

33. Kotopoulis S, Dimcevski G, Gilja OH, Hoem D, Postema M (2013) Treatment of human pancreatitc cancer using combined ultrasound, microbubbles and gemcitabine: a clinical case study. Medical Physics 40(7). https://doi.org/10.1118/1.4808149]

34. Dimcevski G, Kotopoulis S, Bjanes T, Hoem D, Schjott J, Gjertsen BT, Biermann M, Molven A, Sorbye H, McCormack E, et al. (2016) A human clinical trial using ultrasound and microbubbles to enhance gemcitabine treatment of inoperable pancreatic cancer. J Control Release 243:172-181. https://doi.org/10.1016/j.jconrel.2016.10.007

35. Wang Y, Li Y, Yan K, Shen L, Yang W, Gong J, Ding K (2018) Clinical study of ultrasound and microbubbles for enhancing chemotherapeutic sensitivity of malignant tumors in digestive system. Chin J Cancer Res 30(5):553-563. https://doi.org/10.21147/j.issn.1000-9604.2018.05.09

36. Roovers S, Segers T, Lajoinie G, Deprez J, Versluis M, De Smedt SC, Lentacker I (2019) The Role of Ultrasound-Driven Microbubble Dynamics in Drug Delivery: From Microbubble Fundamentals to Clinical Translation. Langmuir 35(31):10173-10191. https://doi.org/10.1021/acs.langmuir.8b03779

37. Lammertink B, Deckers R, Storm G, Moonen C, Bos C (2015) Duration of ultrasound-mediated enhanced plasma membrane permeability. Int J Pharm 482(1-2):92-98. https://doi.org/10.1016/j.ijpharm.2014.12.013

38. Tang MX, Eckersley RJ (2007) Frequency and pressure dependent attenuation and scattering by microbubbles.

4

Ultrasound Med Biol 33(1):164-168. https://doi.org/10.1016/j.ultrasmedbio.2006.07.031

39. Emmer M, Vos HJ, Goertz DE, van Wamel A, Versluis M, de Jong N (2009) Pressure-dependent attenuation and scattering of phospholipid-coated microbubbles at low acoustic pressures. Ultrasound Med Biol 35(1):102-111. https://doi.org/10.1016/j.ultrasmedbio.2008.07.005

40. van der Meer S, Versluis M, Lohse D, Chin CT, Bouakaz A, de Jong N (2004) The resonance frequency of SonoVueTM as observed by high-speed optical imaging. IEEE Ultrasonics Symposium 1:343-345. https://doi.org/10.1109/ULTSYM.2004.1417735

41. Kooiman K, Vos HJ, Versluis M, de Jong N (2014) Acoustic behavior of microbubbles and implications for drug delivery. Adv Drug Deliv Rev 72:28-48. https://doi.org/10.1016/j.addr.2014.03.003

42. Rahim A, Taylor SL, Bush NL, ter Haar GR, Bamber JC, Porter CD (2006) Physical parameters affecting ultrasound/microbubble-mediated gene delivery efficiency in vitro. Ultrasound Med Biol 32(8):1269-1279. https://doi.org/10.1016/j.ultrasmedbio.2006.04.014

43. Karshafian R, Bevan PD, Williams R, Samac S, Burns PN (2009) Sonoporation by ultrasound-activated microbubble contrast agents: effect of acoustic exposure parameters on cell membrane permeability and cell viability. Ultrasound Med Biol 35(5):847-860. https://doi.org/10.1016/j.ultrasmedbio.2008.10.013

44. Phillips LC, Klibanov AL, Wamhoff BR, Hossack JA (2010) Targeted gene transfection from microbubbles into vascular smooth muscle cells using focused, ultrasound-mediated delivery. Ultrasound Med Biol 36(9):1470-1480. https://doi.org/10.1016/j.ultrasmedbio.2010.06.010

45. Keller S, Bruce M, Averkiou MA (2019) Ultrasound Imaging of Microbubble Activity during Sonoporation Pulse Sequences. Ultrasound Med Biol 45(3):833-845. https://doi.org/10.1016/j.ultrasmedbio.2018.11.011

46. Bing KF, Howles GP, Qi Y, Palmeri ML, Nightingale KR (2009) Blood-brain barrier (BBB) disruption using a diagnostic ultrasound scanner and Definity in Mice. Ultrasound Med Biol 35(8):1298-1308. https://doi.org/10.1016/j.ultrasmedbio.2009.03.012

47. Miller DL, Dou C, Song J (2003) DNA transfer and cell killing in epidermoid cells by diagnostic ultrasound activation of contrast agent gas bodies in vitro. Ultrasound in Medicine & Biology 29(4):601-607. https://doi.org/10.1016/s0301-5629(02)00783-4

48. Miller DL, Quddus J (2000) Sonoporation of monolayer cells by diagnostic ultrasound activation of contrast-agent gas bodies. Ultrasound in Medicine & Biology 26:661-667.

49. Keravnou CP, Mannaris C, Averkiou MA (2015) Accurate measurement of microbubble response to ultrasound with a diagnostic ultrasound scanner. IEEE Trans Ultrason Ferroelectr Freq Control 62(1):176-184. https://doi.org/10.1109/TUFFC.2014.006664

50. Keller SB, Sheeran PS, Averkiou MA (2021) Cavitation therapy monitoring of commercial microbubbles with a clinical scanner. IEEE Trans Ultrason Ferroelectr Freq Control 68(4):1144-1154. https://doi.org/10.1109/TUFFC.2020.3034532

51. Chen W-S, Brayman AA, Matula TJ, Crum LA, Miller MW (2003) The pulse length-dependence of inertial cavitation dose and hemolysis. Ultrasound in Medicine & Biology 29(5):739-748. https://doi.org/10.1016/s0301-5629(03)00029-2

52. Hallow DM, Mahajan AD, McCutchen TE, Prausnitz MR (2006) Measurement and correlation of acoustic cavitation with cellular bioeffects. Ultrasound Med Biol 32(7):1111-1122. https://doi.org/10.1016/j.ultrasmedbio.2006.03.008

53. Maciulevicius M, Tamosiunas M, Jurkonis R, Venslauskas MS, Satkauskas S (2015) Analysis of Metrics for Molecular Sonotransfer in Vitro. Mol Pharm 12(10):3620-3627. https://doi.org/10.1021/acs.molpharmaceut.5b00347

54. Tamosiunas M, Jurkonis R, Mir LM, Lukosevicius A, Venslauskas M, Satkauskas S (2012) Microbubble sonodestruction rate as a metric to evaluate sonoporation efficiency. J Ultrasound Med 31(12):1993-2000. https://doi.org/10.7863/jum.2012.31.12.1993

55. ter Haar G, Shaw A, Pye S, Ward B, Bottomley F, Nolan R, Coady AM (2011) Guidance on reporting ultrasound exposure conditions for bio-effects studies. Ultrasound Med Biol 37(2):177-183. https://doi.org/10.1016/j.ultrasmedbio.2010.10.021

56. Segers T, Kruizinga P, Kok MP, Lajoinie G, de Jong N, Versluis M (2018) Monodisperse Versus Polydisperse Ultrasound Contrast Agents: Non-Linear Response, Sensitivity, and Deep Tissue Imaging Potential. Ultrasound Med Biol 44(7):1482-1492. https://doi.org/10.1016/j.ultrasmedbio.2018.03.019

57. Helbert A, Gaud E, Segers T, Botteron C, Frinking P, Jeannot V (2020) Monodisperse versus Polydisperse Ultrasound Contrast Agents: In Vivo Sensitivity and safety in Rat and Pig. Ultrasound Med Biol 46(12):3339-3352. https://doi.org/10.1016/j.ultrasmedbio.2020.07.031

58. Carrai M (2019) Shortages of generic cancer medicines are harming patients. So why can't we fix it? Cancerworld Summer 2019:12-17. https://doi.org/https://archive.cancerworld.net/spotlight-on/shortages-of-generic-cancer-medicines-are-harming-patients-so-why-cant-we-fix-it/

59. Togtema M, Pichardo S, Jackson R, Lambert PF, Curiel L, Zehbe I (2012) Sonoporation delivery of monoclonal antibodies against human papillomavirus 16 E6 restores p53 expression in transformed cervical keratinocytes. PLoS One 7(11):e50730. https://doi.org/10.1371/journal.pone.0050730

60. Bellary A, Villarreal A, Eslami R, Undseth QJ, Lec B, Defnet AM, Bagrodia N, Kandel JJ, Borden MA, Shaikh S, et al. (2020) Perfusion-guided sonopermeation of neuroblastoma: a novel strategy for monitoring and predicting

4

liposomal doxorubicin uptake in vivo. Theranostics 10(18):8143-8161. https://doi.org/10.7150/thno.45903

61. Snipstad S, Hanstad S, Bjorkoy A, Morch Y, de Lange Davies C (2021) Sonoporation Using Nanoparticle-Loaded Microbubbles Increases Cellular Uptake of Nanoparticles Compared to Co-Incubation of Nanoparticles and Microbubbles. Pharmaceutics 13(5). https://doi.org/10.3390/pharmaceutics13050640

62. Snipstad S, Morch Y, Sulheim E, Aslund A, Pedersen A, Davies CL, Hansen R, Berg S (2021) Sonopermeation Enhances Uptake and Therapeutic Effect of Free and Encapsulated Cabazitaxel. Ultrasound Med Biol 47(5):1319-1333. https://doi.org/10.1016/j.ultrasmedbio.2020.12.026

63. Shi J, Fu C, Su X, Feng S, Wang S (2021) Ultrasound-Stimulated Microbubbles Inhibit Aggressive Phenotypes and Promotes Radiosensitivity of esophageal squamous cell carcinoma. Bioengineered 12(1):3000-3013. https://doi.org/10.1080/21655979.2021.1931641

64. Hensel K, Mienkina MP, Schmitz G (2011) Analysis of ultrasound fields in cell culture wells for in vitro ultrasound therapy experiments. Ultrasound Med Biol 37(12):2105-2115. https://doi.org/10.1016/j.ultrasmedbio.2011.09.007

65. Leskinen JJ, Hynynen K (2012) Study of factors affecting the magnitude and nature of ultrasound exposure with in vitro set-ups. Ultrasound Med Biol 38(5):777-794. https://doi.org/10.1016/j.ultrasmedbio.2012.01.019

66. Beekers I, Vegter M, Lattwein KR, Mastik F, Beurskens R, van der Steen AFW, de Jong N, Verweij MD, Kooiman K (2020) Opening of endothelial cell-cell contacts due to sonoporation. J Control Release 322:426-438. https://doi.org/10.1016/j.jconrel.2020.03.038

4

SUPPLEMENTARY FIGURES

The Supplementary Material for this article can be found online at:
https://www.frontiersin.org/articles/10.3389/fphar.2021.768436/full#supplementary-material

Supplementary figure 1. Characteristics of C5-1 probe
Supplementary figure 2. Characteristics of C9-4 probe
Supplementary figure 3. Characteristics of custom-build US set-up with single element transducer.

4
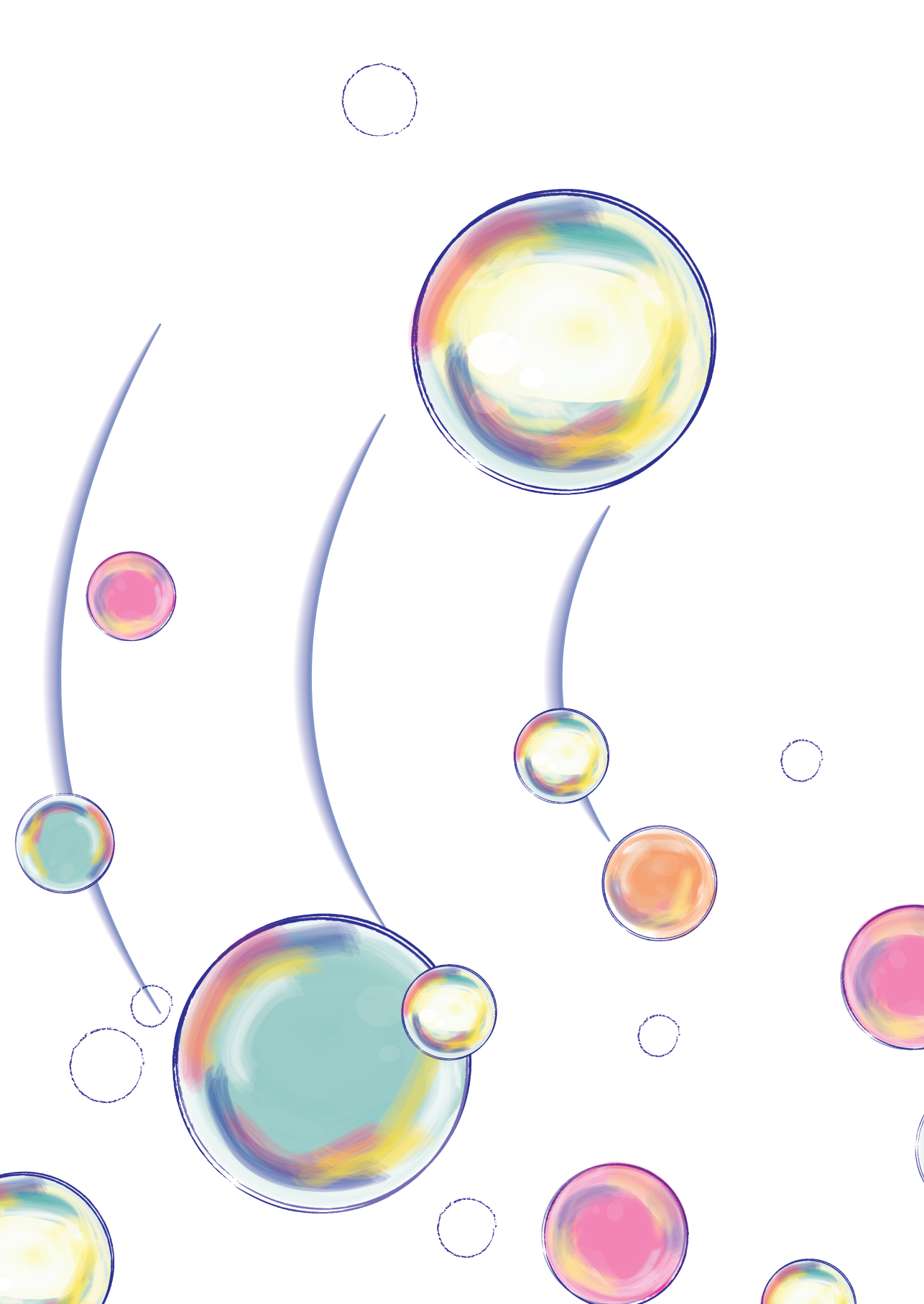
5

ULTRASOUND AND MICROBUBBLES MEDIATED BLEOMYCIN DELIVERY IN FELINE ORAL SQUAMOUS CELL CARCINOMA – A VETERINARY STUDY

Josanne S. de Maar[1], Maurice M.J.M. Zandvliet[2], Stefanie Veraa[2], Mauricio Tobón Restrepo[2], Chrit T.W. Moonen[1], Roel Deckers[1*]

[1] Imaging and Oncology Division, University Medical Center Utrecht, Utrecht University, Utrecht, The Netherlands
[2] Department of Clinical Sciences, Faculty of Veterinary Medicine, Utrecht University, Utrecht, The Netherlands

ABSTRACT

To investigate the feasibility and tolerability of ultrasound and microbubbles (USMB) enhanced chemotherapy delivery in patients with head and neck cancer, we performed a veterinary trial in feline companion animals with oral squamous cell carcinomas. Five cats without treatment options besides supportive care were treated with a combination of bleomycin and USMB therapy three times with 1 week intervals, using the Pulse Wave Doppler mode on a clinical ultrasound system and EMA/FDA approved microbubbles. They were evaluated for adverse events, quality of life, tumour response and survival. Furthermore, tumour perfusion was monitored before and after USMB therapy using contrast-enhanced ultrasound (CEUS). USMB treatments were feasible and well tolerated. Among the four cats treated with optimized US settings, three had stable disease at first, but showed disease progression 5 or 11 weeks after first treatment. One cat had progressive disease one week after the first treatment session, maintaining a stable disease thereafter. Eventually, all cats showed progressive disease, but each survived longer than the reported median overall survival time of 44 days. CEUS performed immediately before and after USMB therapy suggested an increase in tumour perfusion based on an increase in median area under the curve (AUC) in 5 out of 9 evaluated treatment sessions. In this small hypothesis-generating study USMB plus chemotherapy was feasible and well-tolerated in a feline companion animal model and showed potential for enhancing tumour perfusion in order to increase drug delivery. This could be a step forwards toward clinical translation of USMB therapy to human patients with head and neck cancer or other tumours with a clinical need for locally enhanced treatment.

Keywords

INTRODUCTION

Head and neck squamous cell carcinoma (HNSCC) is diagnosed in approximately 900.000 patients yearly worldwide, 5% of all cancer diagnoses [1]. Most patients present with locally advanced disease [2, 3], and because primary surgery is often not possible or is expected to result in unacceptable morbidity, they are often treated with combination therapies including radiotherapy, chemotherapy and targeted therapy [4]. Even so, up to half of the patients develop (often incurable) local recurrences [5, 6] and treatment is associated with acute and long-term toxicity [7-9]. Primary chemoradiotherapy with cisplatin as a radiosensitizer is often used in locally advanced HNSCC. Higher cumulative cisplatin dose is associated with better local control and to some extent longer overall survival [7, 10], but due to local and systemic toxicities 30-50% of patients cannot complete all planned cycles of cisplatin [7, 11]. This emphasizes the need for improved local tumour delivery of cisplatin, without increasing the chemotherapy dose in healthy tissues. To this end, a method to increase local drug delivery without increasing systemic toxicity could lead to improved outcomes of (chemo)radiotherapy.

We hypothesize that this goal could be achieved by means of ultrasound and microbubbles (USMB) therapy. Microbubbles are micron-sized gas-filled bubbles used for contrast-enhanced ultrasound (CEUS) imaging [12, 13]. When exposed to ultrasound, stable or inertial cavitation of microbubbles can occur, creating a number of biological effects collectively termed sonopermeation [14, 15]. USMB therapy has been shown to improve drug delivery for various molecules *in vitro* and *in vivo* [15]. In particular, addition of USMB therapy improved the effect of chemotherapy or chemoradiotherapy with cisplatin on HNSCC cells *in vitro* [16]. However, pre-clinical studies often use custom-made set-ups and a large variety of US parameters, which cannot easily be translated to the clinic. Thus far, USMB therapy has not been studied in human head and neck cancer patients. Most (ongoing) clinical studies of USMB therapy have focused on brain applications, using dedicated systems not applicable to other organs [17-19]. Meanwhile, studies outside the brain are limited to small numbers of patients with pancreatic cancer, liver metastases and breast cancer, which all used different ultrasound settings [20-23]. Using clinically available US systems and settings (preferably uniform US settings across clinical studies) combined with FDA/EMA approved microbubbles can help make this technique more accessible.

In order to bridge the gap between human HNSCC patients and *in vitro* and small animal studies, we performed a veterinary feasibility trial. Cats are a suitable model because they are big enough to use clinical ultrasound equipment, and because many pathophysiological and genetic similarities exist between humans and cats [24-26]. Furthermore, feline oral squamous cell carcinoma (FOSCC) is very common in aged cats [27]. Like human patients, cats often present with advanced stage disease [28] and often succumb to local disease progression, rather than metastatic disease [26, 29]. Standard of care treatment options are similar to the human setting: when surgery is not an option, primary radiotherapy can

be combined with chemotherapy as a radiosensitizer [30-32]. Supportive care (antibiotics and/or anti-inflammatory drugs) results in a median overall survival of approximately 44 days [33]. The platinum-based drug cisplatin, often used in human patients, creates unacceptable toxicity in cats when systemically administered [34]. Instead, bleomycin is a well-tolerated cytostatic drug in cats, but has limited efficacy because efficacy is dependent on intracellular uptake, which is complicated by the hydrophilic nature and dependence on protein receptors to enter the cell [35, 36]. To improve the efficacy of bleomycin, electroporation can be used, also known as electropermeabilization: making cell membranes reversibly permeable by application of an electrical current [37, 38]. In a feline study the combination of bleomycin plus electroporation resulted in an overall response of 89%, compared to 33% with bleomycin alone [39] but it causes unpleasant muscle contractions and possibly an increased risk for cardiac arrhythmias [39, 40]. After electroporation of large bulky tumours, patients could be more susceptible to adverse events such as tumour lysis syndrome, thromboembolism, disseminated intravascular coagulation, delayed wound healing and local necrosis [38]. These adverse effects have not been described for USMB therapy. A safety study performing USMB therapy on the livers of eight pigs with a clinical US system did not result in any clinical adverse events or histopathological damage to the liver [41]. Meanwhile, CEUS imaging has been studied in hundreds of cats, without significant adverse effects [42-47]. *In vitro*, USMB therapy was shown to enhance local bleomycin effect using a clinical US system with standard settings and clinically available microbubbles [48].

The combination of bleomycin with USMB therapy using a clinically available US system and microbubbles could provide a low-toxicity low-burden additional treatment option for these cats as well as a step towards clinical translation to human head and neck cancer patients. The primary objectives of this veterinary study were to evaluate tolerability and feasibility of bleomycin plus USMB therapy while using a clinical US system and microbubbles, while secondary objectives were to assess tumour response, survival and effect of USMB therapy on tumour perfusion.

METHODS

Subjects

Five cats with spontaneously arisen FOSCC were eligible for inclusion in our single-arm prospective study. They had at least cytologically proven squamous cell carcinoma, without other suitable treatment options except for palliative care and informed consent was provided by the pet owner. Exclusion criteria were life-threatening comorbidities leading to a life expectancy of less than 1 month, contraindications for anaesthesia and known hypersensitivity to bleomycin or any of the excipients of SonoVue (Bracco).
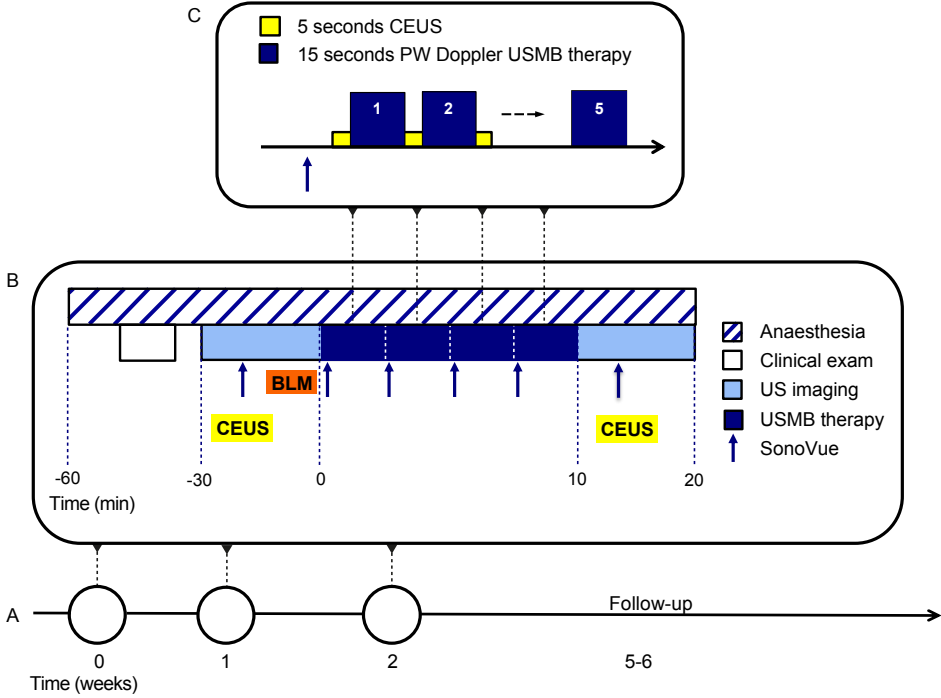
USMB treatment

Each cat was treated three times, once per week (see **Figure 1** for timeline of treatment procedures). US imaging and treatment were performed using an EPIQ5 or EPIQ7 imager with a C9-2 transducer (Philips) complemented by a L18-5 transducer solely for US imaging. A tissue mimicking gel was used to obtain enough distance between probe and cat for the region of interest to be outside the near field of the transducer. The treatment was performed under general anaesthesia, while continuously monitoring vital signs. USMB therapy was started 7 minutes after intravenous (i.v.) injection of bleomycin (10.000 IU/ m^2). Microbubbles (SonoVue, Bracco, conc. 1-5 x 10^8 bubbles/mL, dosage 0.1 mL/kg body weight per bolus injection) followed by a 1.5mL saline flush were administered through an i.v. catheter of at least 22 gauge. When the microbubbles appeared in the tumour (based on CEUS imaging), treatment of the oral tumour was started in Pulse Wave (PW) Doppler mode. PW Doppler for 15 seconds was alternated with CEUS imaging for five seconds (to allow for complete reperfusion of the tumour with fresh microbubbles) and repeated five times per MB injection, as by that time no more MBs were visible on CEUS images. This process was repeated three times to a total of four microbubble injections for therapy. During USMB therapy the probe was hand-held by a veterinary radiologist and the Sample Volume of the PW Doppler was slowly moved to treat the entire tumour. Before a new microbubble injection, transducer orientation was changed to treat a different cross-section of the tumour. Optimized PW Doppler settings for USMB therapy and CEUS parameters used in cats 2-5 are shown in **Table 1**. These procedures have been optimized during treatment of cat 1 and the first treatment session of cat 2.

Table 1 Optimized Pulsed Wave Doppler settings for USMB therapy and CEUS parameters used in cats 2-5

Parameter	Indication / setting on EPIQ5 or EPIQ7	Value
Optimized Pulse Wave (PW) Doppler settings for ultrasound and microbubble (USMB) therapy		
Frequency	C9-2 probe in PW mode	2.9 MHz
Pulse length	Sample volume: 7.5 mm (maximum)	21 cycles per pulse
Pulse Repetition Frequency	Scale:-4 – 4 cm/sec (minimum)	0.4 kHz
Mechanical index	Relative intensity:- 10 dB *	MI 0.3-0.4 at target depth
Contrast enhanced ultrasound (CEUS) settings		
Mechanical Index (MI)	MI in CEUS mode <0.1	CEUS MI = 0.06
Gain	Gain slightly above the noise floor in absence of microbubbles and kept constant	Gain = 45%
Dynamic range (compression)		Dynamic range = 50
Focus position	Focus positioned at the target or a bit deeper (2/3 of image depth)	Adjusted per treatment session and moved during USMB therapy
Time Gain compensation (TGC)	All switches in central position	All switches in central position
Persistence		Off

* In cat 4 relative intensity was increased to-7dB to account for enhanced attenuation due to extensive bone invasion and fibrous tissue formation of bone**.**

5

Figure 1 Ultrasound and microbubbles (USMB) treatment procedures. A: each cat is treated three times, once per week. B: Each treatment session is performed under general anaesthesia and starts with a clinical exam. Ultrasound imaging and contrast-enhanced ultrasound imaging (CEUS) are performed before and after USMB therapy. 7 minutes after intravenous injection (i.v.) of bleomycin (BLM), USMB therapy is started by i.v. bolus injection of SonoVue microbubbles. C: when the microbubbles appear on the CEUS image, 15 seconds of Pulsed Wave (PW) Doppler are alternated by 5 seconds of CEUS imaging. This is repeated five times per microbubble injection, for a total of four microbubble injections.

Other study procedures

Primary endpoints were tolerability and feasibility, assessed at baseline and 1, 2 and 5 weeks after the first USMB therapy. Tolerability was assessed by reporting adverse events, clinical performance score and quality of life. Adverse events were reported by VCOG Common Terminology Criteria for Adverse Events version 1.1, clinical performance (CPS, 0-5 [49]) was monitored and quality of life (QoL) was assessed using a 16-item owner-completed questionnaire, translated to Dutch with permission from Adelphi UK and Zoetis [50]. Feasibility was assessed by the amount of time needed for study procedures and the ability to complete study treatments per cat. Secondary endpoints were clinical response (including tumour response and survival) and the effect of USMB therapy on tumour perfusion. Tumour response was evaluated by calliper measurements at baseline and 1, 2 and 5 weeks after the first USMB therapy. Overall survival was registered from first USMB therapy until death. To evaluate the effect of USMB on tumour perfusion, CEUS was performed immediately before and after USMB treatment using a mechanical arm

to position the US probe and with the same volume of MBs used for USMB therapy. All equipment settings (MI = 0.06, gain = 45%, TGC at central position, dynamic range = 50, persistence set to Off, see **Table 1** for more details) were kept consistent for all cats and between CEUS measurements before and after USMB therapy.

Quantitative CEUS evaluation

Time-intensity curve analysis was performed on contrast loops before and after USMB treatment to evaluate changes in tumour perfusion using in-house developed Matlab software. Image data post-processing consisted of 5 steps. First, the DICOM images, transferred from the ultrasound imager, were loaded using the standard Matlab DICOM reader and the colour images were converted into greyscale. Second, the onset of the contrast enhancement was determined. Third, from the images obtained before the onset of contrast enhancement, an averaged image (background image) was calculated and this background image was subtracted from the original images. Fourth, the temporal data was smoothed using a moving-average filter. Finally, peak intensity (PI: maximum signal intensity, also known as peak enhancement), time-to-peak (TTP: time between first arrival of contrast and reaching maximum intensity) and area under the curve (AUC: area under the time versus signal intensity curve) maps were calculated for each pixel [51]. Using a region of interest (ROI) with the same size before and after USMB therapy, the parameters were visualized with a colour scale and plotted in histograms to compare results pre and post USMB therapy. Pixels with high signal intensity already before onset of the contrast enhancement (e.g. regions containing bone) were excluded for analysis. The percentage of pixels reaching >25% of the peak intensity in that ROI were compared between before and after USMB with a paired samples Wilcoxon test. A two-sided p-value < 0.05 was considered significant. Median values of the AUC in the ROI are compared after discarding AUC values ≤ 0.

RESULTS

Baseline characteristics

We included five feline patients with tumours located in different oral regions.

Table 2 describes relevant patient and tumour characteristics. All cats were domestic shorthairs over 10 years of age, with T2 or T3 tumours [52], two cats had known lymph node metastases and one cat had pulmonary metastases. All cats received supportive care with antibiotics and pain medication, two cats required assisted feeding (oesophageal feeding tube). Two cats received concomitant treatment for hyperthyroidism (thiamazole or carbimazole).

Table 2 Relevant patient and tumour characteristics, including survival

Patient	1	2	3	4	5
Sex	male	male	male	female	male
Age at inclusion (years)	11	11	18	15	14
Body weight at inclusion (kg)	2.8	7.2	3.4	2.8	6.7
TNM stage [52]	T2N1M0	T2bN0M1 (lungs)	T2bN0M0	T3bN0Mx	cT3N1Mx
Tumour location	tongue, frenulum, and sublingual soft tissue	right maxilla	lip and cheek extending into corner of mouth and caudal maxilla	rostrally in the mouth, infiltrated into mandibula	tongue base and floor of mouth
Supportive care measures	Antibiotics Analgesics (NSAIDs, tramadol) Tube feeding	Antibiotics Analgesics (NSAIDs)	Antibiotics Analgesics (NSAIDs, gabapentin)	Antibiotics Analgesics (NSAIDs, gabapentin)	Antibiotics Analgesics (NSAIDs, buprenorphine) Tube feeding
Concomitant drugs	Treatment for hyperthyroidism (carbimazole) initiated during study	Treatment for hyperthyroidism (carbimazole) initiated during study	-	-	-
Survival (days)	46	85	64	56	57
Death	euthanasia	euthanasia	euthanasia	euthanasia	natural death

Bleomycin plus USMB therapy was tolerable without serious adverse events

The USMB treatments were well tolerated. All cats experienced adverse events, but these were not severe, mainly grade 1 or 2 (**Table 3** lists all adverse events). In addition, adverse events were considered related to anaesthesia (e.g. constipation, fatigue, hypotension, hypothermia, lethargy and vomiting), comorbidity (untreated hyperthyroidism) or progressive tumour growth (e.g. anorexia, generalized weakness, fatigue haemorrhage from the tumour, pain, ptyalism, skin ulceration, soft tissue necrosis and weight loss). One cat had localized alopecia and erythema related to an i.v. catheter. Another cat experienced a mild sinus tachycardia during the treatment session, which could be related to USMB therapy or anaesthesia but resolved spontaneously.. Clinical performance score (CPS) did not change from 0 ("fully active") in cat 1-3. In cat 2 it temporarily decreased one point in week 1 but then recovered to "fully active" and in cat 5 it decreased from 1 ("slight tiredness/dyspnoea after severe exertion") to 3 ("Spontaneous tiredness or dyspnoea without exertion, lies often on the floor.") after 5 weeks. **Figure 2** shows QoL scores. QoL remained stable in cats 1-3, and decreased gradually in cat 5, most likely due to tumour progression. In cat 4, QoL decreased temporarily after 1 week, due to pain and inability to eat. Supportive treatment was intensified (antibiotics restarted, pain medication increased) and the next USMB treatment was postponed for 1 week. In this week the cat's condition and QoL improved. Since QoL

recovered quickly, infection at the tumour site was considered the most likely cause.
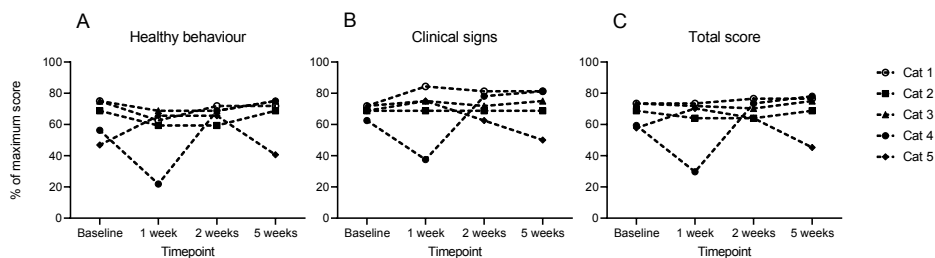
Figure 2 Quality of life per cat during the study, assessed by a 16-item owner-completed measure of feline quality of life, translated to Dutch with permission from Adelphi UK and Zoetis. Higher scores indicate better quality of life. A: healthy behaviour score, B: clinical signs score, C: total score, which is the mean of healthy behaviour and clinical signs.

Three treatment sessions of bleomycin plus USMB therapy were feasible

The study treatment was considered feasible, as all five pet owners completed all planned study visits including three USMB treatment sessions and a follow-up visit. In the four cats with optimized procedures, mean time in hospital ranged from 153 minutes in cat 4 to 207 minutes in cat 3 and mean time spent on US imaging plus therapy ranged from 44 minutes in cat 2 to 66 minutes in cat 3 (**Figure 3**).
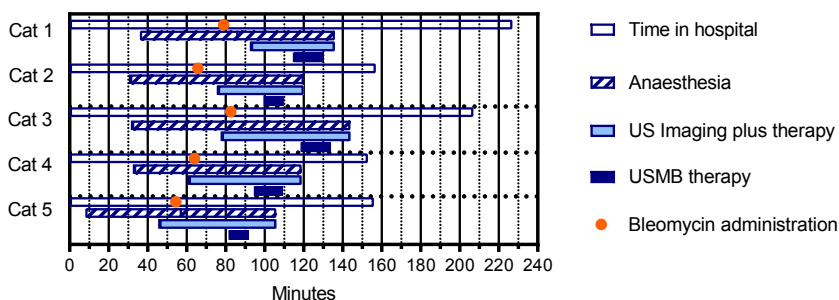

Figure 3 Feasibility of USMB treatment, assessed by duration of study procedures. For each procedure, the mean of three treatment days was calculated. In cat 1, treatment procedures had not yet been optimized.

Modest clinical response

For cat 1 USMB therapy procedures had not yet been optimized, therefore its clinical response parameters are not reported here. Upon clinical examination three cats had stable disease during the three treatment sessions, but disease progression was observed at five weeks (cats 3 and 5) or 11 weeks after the first treatment session (cat 2). Cat 4 had

progressive disease one week after the first treatment session (possibly due to tumour infection), but remained stable at follow-up. Eventually, all cats had progressive disease (**Figure 4**). Three cats were euthanized respectively 85, 64 and 56 days after their first treatment session, the fourth cat died spontaneously after 57 days (**Table 2**).
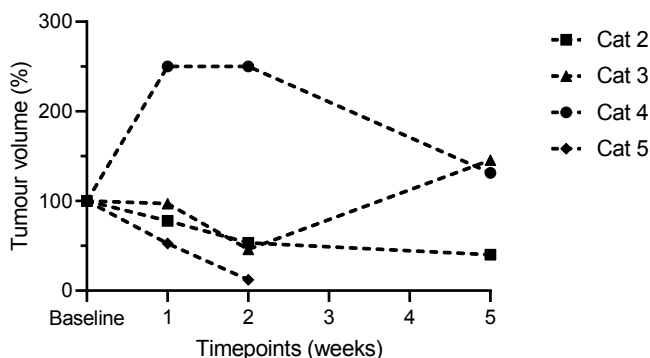
Figure 4 Estimation of tumour volumes (length * width * depth, percentage of baseline) in cats treated with optimized USMB settings, based on calliper measurements of the tumour prior to that day's study treatment. Cats 2, 3 and 5 had stable disease during the three treatment sessions, but showed disease progression five weeks (cats 3 and 5) or 11 weeks after first treatment (cat 2, not shown here). In cat 5, reliable tumour measurement was not possible five weeks after treatment due to tumour necrosis, but clear disease progression was noted. Cat 4 had progressive disease one week after the first treatment (possibly due to tumour infection), but remained stable at follow-up.

Indication of increased tumour perfusion assessed by contrast-enhanced ultrasound
CEUS imaging before and after USMB treatment was available for cat 2 (two treatment sessions), cat 3 (three treatment sessions) cat 4 (one treatment session) and cat 5 (three treatment sessions). During the first treatment session of cat 2 the US probe was unintentionally moved during CEUS acquisition and during the second and third treatment sessions of cat 4 the US system with contrast license was unavailable. **Figure 5** shows representative parametric maps in cat 3 and **Supplementary Figures** 1, 2 and 3 show an overview of all cats. Based on visual interpretation of the data, peak intensity (PI) increased in six out of nine treatment sessions, decreased in two and did not change in one (**Supplementary figure 1**), while for time-to-peak (TTP) the changes were small and there was no clear trend (**Supplementary figure 2**). The median AUC in the ROI decreased in four out of nine treatment sessions (mean decrease 23.5%, range -4 to -45%) while it increased in five out of nine treatment sessions (median increase 118%, range 10 to 1039%) (**Supplementary figure 3**). These findings were supported by the percentage of pixels in the ROI reaching >25% of the peak intensity (PI). Taking nine evaluated treatment sessions together, this percentage was significantly higher after USMB therapy compared to baseline (**Figure 6**, Wilcoxon matched-pairs signed rank test p = 0.0391).
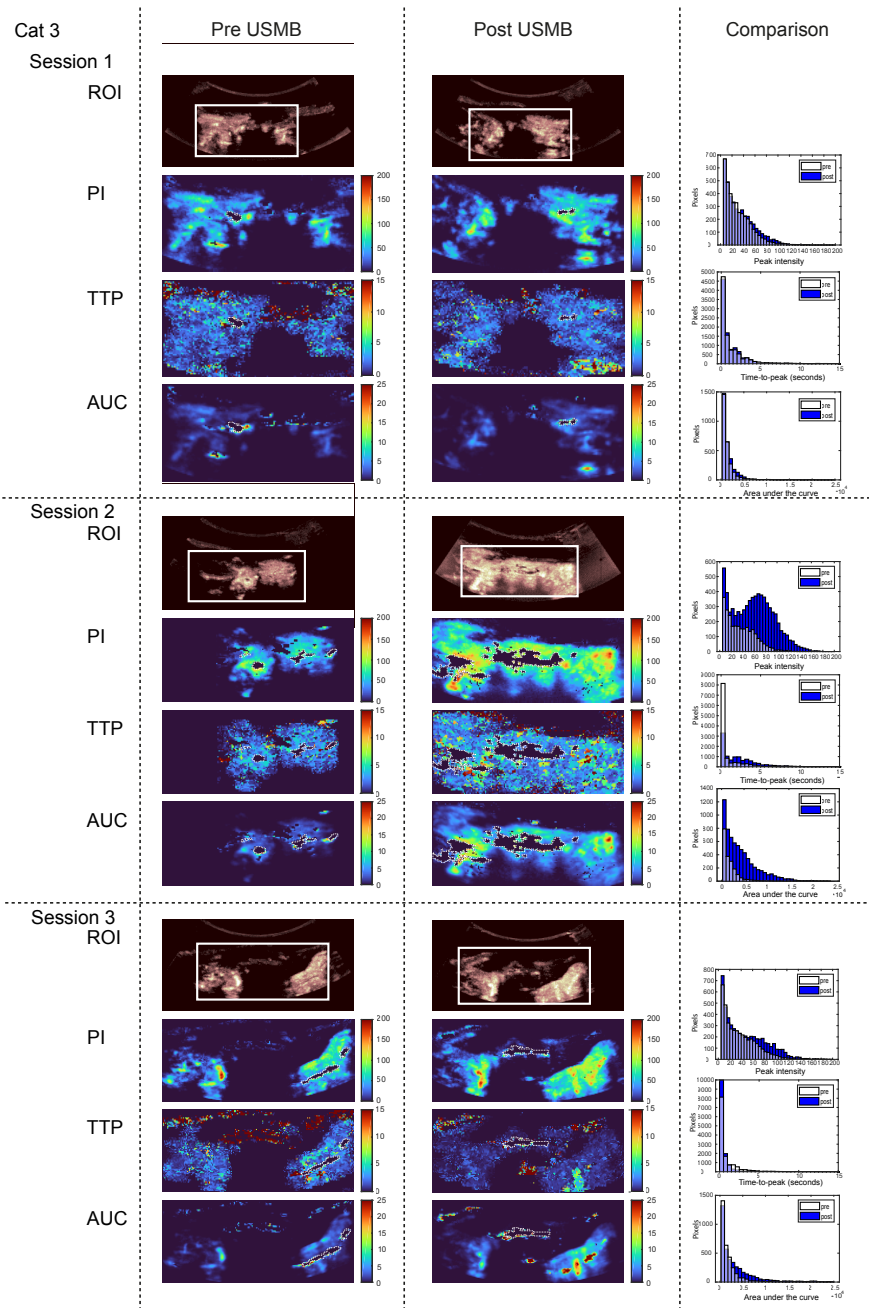
Figure 5 Contrast enhanced ultrasound (CEUS) parametric maps of cat 3 before (first column) and after (second column) USMB therapy for visual comparison. For each of the three treatment sessions from top to bottom the following parameters are depicted: selection of region of interest (ROI), peak intensity (PI), time-to-peak (TTP), area under the curve (AUC). Pixels with high signal intensity before administration of microbubbles (e.g. regions containing bone) were set to zero and delineated with white dotted lines. In the third column these parameters are compared in histograms between before (white) and after (blue) USMB. Note that the range of the y-axes differs between different treatment sessions. ROIs pre and post USMB are identical in size within one treatment

session and matched in position as much as possible. CEUS parameters were kept constant between treatment sessions, except in treatment session 2 of cat 3 when gain inadvertently changed from 45% (before USMB) to 49% (after USMB).
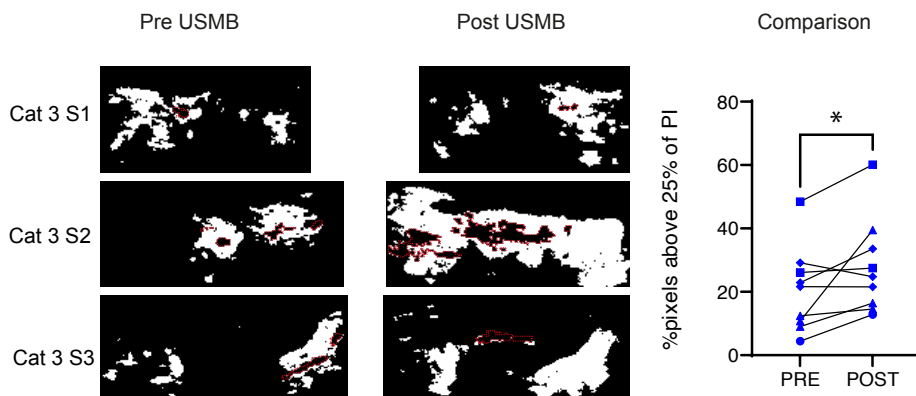
Figure 6 Peak Intensity (PI) on CEUS in the tumour before (left) and after (right) USMB therapy. Representative maps of cat 3 in three treatment sessions (S1-3). Pixels with high signal intensity before administration of microbubbles (e.g. regions containing bone) were set to zero and delineated with red dotted lines. Percentage of pixels reaching >25% of the peak intensity (white pixels) in the ROI was significantly higher after USMB therapy compared to baseline. * = Wilcoxon matched-pairs signed rank test p = 0.0391

DISCUSSION

We conducted a clinical feasibility study in a small cohort of non-laboratory cats, evaluating the combination of bleomycin chemotherapy and USMB therapy in cats with oral squamous cell carcinoma.

The USMB treatment sessions were feasible and well tolerated. Due to our patient selection process, all tumours were accessible to USMB therapy. Adverse events were considered related to anaesthesia, comorbidity or progressive tumour growth. We did not observe severe adverse events such as tumour lysis syndrome and disseminated intravascular coagulation, which have been described with electroporation [38]. Muscle contractions and arrhythmias are not expected to occur with USMB due to the difference in technique (ultrasound versus electrical pulses) and while vascular disruption caused by electroporation leads to acute tumour necrosis, USMB therapy may have a more gradual and tolerable anti-tumour effect. The relatively mild adverse effects of USMB therapy could reflect that it is a more tolerable and feasible option than electroporation and that there is room for treatment intensification (i.e. more treatment sessions or higher dosages of chemotherapy).

Unfortunately, all cats eventually had progressive disease based on clinical tumour

measurements. However, while the median overall survival is (historically) around 44 days with supportive care alone [33], survival in our study (albeit small and without a control group) was somewhat longer (46- 85 days). A number of hypotheses could explain why tumour responses and overall survival did not improve more substantially. First, the cavitation-induced permeabilization of cancer cells to enhance the intracellular uptake of bleomycin, which we previously demonstrated *in vitro* [48], may not have worked as well *in vivo* in our veterinary study. Unfortunately, we could not measure sonopermeation efficacy directly, i.e. by quantifying bleomycin uptake in tumours, nor indirectly, by monitoring microbubble cavitation activity during the procedure. Future application of simultaneous USMB therapy and cavitation detection could confirm our assumption and lead to further optimization of US settings. Based on previous literature this is feasible using a clinical US system, but it requires modifying predefined factory settings, which could lengthen the process towards clinical approval [53]. Second, USMB therapy will only cause sonopermeation in cells in the close proximity of microbubbles [54], i.e. endothelial cells and perhaps a few layers of tumour cells. Moreover, CEUS imaging showed that microbubbles did not spread throughout the entire tumour, which further diminishes the efficacy of sonopermeation. Third, the US parameters we used (which are standard settings for PW Doppler on the clinical US system) are likely to be suboptimal. Our previous *in vitro* results demonstrated that PW Doppler using an unmodified clinical ultrasound probe with the lowest centre frequency (S5-1 with a frequency of 1.6MHz), and the maximum number of cycles per pulse (46) resulted in the most efficient cell permeabilization [48]. While it was not feasible to use the exact same settings in this veterinary study (the S5-1 probe provided insufficient anatomical detail for target identification in the cat) we were able to closely mimic them. Optimization steps were performed during the first treatment sessions. In the first treatment session of cat 1, a lower MB dosage and the S5-1 probe were used. In all treatment sessions of cat 1 and the first treatment session of cat 2 a higher mechanical index was applied (relative intensity 0 dB, MI =1.0 - 1.2). However, decreased perfusion was noted on CEUS after USMB therapy in the first treatment session of cat 2 and therefore the relative intensity was decreased to -10 dB (i.e. MI = 0.3 - 0.4). With this drop of MI, we expect that we moved from an inertial cavitation to a stable cavitation regime. On the other hand, customized settings, such as used by Keller et al. in a healthy porcine model, may provide even better results [41]. Fourth, if sonopermeation did occur successfully, (part of) these tumours may have not been intrinsically sensitive to bleomycin, meaning that bleomycin could not kill the cell even after entering it [55]. Finally, it is possible that more bleomycin plus USMB treatment sessions are needed to obtain a durable clinical response. It would be interesting to continue study treatment until tumour progression or unacceptable toxicity in a future study.

Although clinical response in our small study was modest, our findings on increased tumour perfusion after USMB treatment were promising. Most notably, we saw an increase in median AUC in 5 out of 9 treatment sessions and a significant increase in percentage of

pixels with an intensity above 25% of the PI in the ROI. Increased AUC is a typical feature of increased perfusion, which indicates increased microvascular blood volume (MBV: the proportion of tissue volume existing of blood) [56, 57]. Increased perfusion should also lead to shorter TTP, but this was not observed in our study. Improving MBV will benefit the exchange of oxygen, nutrients and drugs [58]. Note that these findings have to be interpreted with caution, as the number of evaluable treatment sessions is small and the position of the transducer (i.e. anatomical location) for CEUS ROIs before and after USMB were matched to our best effort but were never identical. More so, similar transducer positions for CEUS in different treatment sessions of the same cat are even harder to obtain. Nevertheless, previous studies have also shown that USMB therapy can affect tissue perfusion and thereby reduce tumour hypoxia. Both increased and decreased perfusion have been described, and more research is needed to determine exactly which ultrasound parameters induce either effect. Decreased perfusion seems to be related to vascular damage and platelet activation, while increased perfusion is associated with vessel dilation and (on longer term) induction of angiogenesis [59]. Improving tumour perfusion is also of interest for (chemo)radiotherapy in HNSCC since clinical response to chemoradiotherapy is negatively affected by tumour hypoxia [60], caused by structural abnormalities in the tumour vasculature [61, 62]. Consequently, increased tumour perfusion could decrease hypoxia and thereby improve outcomes. Because the effect of bleomycin is mainly limited by intracellular uptake, rather than by perfusion, only a small survival benefit can be expected in our study as a result of increased tumour perfusion. In contrast, combining USMB therapy with drugs known to be perfusion-limited could lead to improved outcome in future studies.

Due to the similarities between humans and cats in size and tumour characteristics, a feline veterinary trial provides a great opportunity to study feasibility of USMB therapy using an unmodified clinical US system and clinically available microbubbles. Our optimized USMB therapy procedure can easily be translated to human patients. In the future, we expect that USMB therapy, if proven safe and feasible in human patients with head and neck cancer, could be added to standard of care chemo(radio)therapy to improve local drug delivery (e.g. of cisplatin and/or cetuximab) or to standard of care radiotherapy (to enhance tumour perfusion and consequently reduce hypoxia). Finally, adding USMB therapy to chemoradiotherapy could in the future lead to adapted treatment regimens with similar efficacy while reducing systemic toxicity. Early clinical trials using USMB in combination with chemotherapy in patients with various tumour types have already shown promising results or are still ongoing [20-23] (ClinicalTrials.gov Identifiers: NCT04146441, NCT04821284, NCT03477019 and NCT03458975, NCT03385200), as well as clinical studies on USMB therapy with radiotherapy in the absence of a drug (Clinicaltrials.gov NCT04431674, NCT04431648). Since we used a clinical US system and EMA/FDA approved microbubbles in this study, the step to a clinical trial in human head and neck cancer patients can be taken in the near future. While customized USMB therapy settings might

lead to even better results in the long term, the approval process could take longer and we expect that the use of PW Doppler without adaptations will accelerate the road to clinical benefit.

CONCLUSIONS

Our veterinary feasibility trial shows that the combination of bleomycin and ultrasound and microbubbles therapy, using an unmodified clinical ultrasound system and FDA/EMA approved microbubbles, is a feasible and well-tolerable treatment in cats with oral squamous cell carcinoma. Besides a modest clinical response, we found indications of enhanced tumour perfusion after USMB therapy. This could be a step forwards toward clinical translation of USMB therapy to human patients with head and neck cancer or other tumours with a clinical need for locally enhanced treatment.

ACKNOWLEDGEMENTS

ANIMAL RIGHTS

The research protocol was approved by the Animal Welfare Body Utrecht

CONFLICTS OF INTEREST DISCLOSURE

5

REFERENCES

1. Bray F, Ferlay J, Soerjomataram I, Siegel RL, Torre LA, Jemal A (2018) Global cancer statistics 2018: GLOBOCAN estimates of incidence and mortality worldwide for 36 cancers in 185 countries. CA Cancer J Clin 68(6):394-424. https://doi.org/10.3322/caac.21492

2. Braakhuis BJ, Leemans CR, Visser O (2014) Incidence and survival trends of head and neck squamous cell carcinoma in the Netherlands between 1989 and 2011. Oral Oncol 50(7):670-675. https://doi.org/10.1016/j.oraloncology.2014.03.008

3. van der Kamp MF, van Dijk BAC, Plaat BEC, van der Laan B, Halmos GB (2021) To what extent has the last two decades seen significant progress in the management of older patients with head and neck cancer? Eur J Surg Oncol 47(6):1398-1405. https://doi.org/10.1016/j.ejso.2021.01.014

4. Chow LQM (2020) Head and Neck Cancer. N Engl J Med 382(1):60-72. https://doi.org/10.1056/NEJMra1715715

5. Leeman JE, Li JG, Pei X, Venigalla P, Zumsteg ZS, Katsoulakis E, Lupovitch E, McBride SM, Tsai CJ, Boyle JO, et al. (2017) Patterns of Treatment Failure and Postrecurrence Outcomes Among Patients With Locally Advanced Head and Neck Squamous Cell Carcinoma After Chemoradiotherapy Using Modern Radiation Techniques. JAMA Oncol 3(11):1487-1494. https://doi.org/10.1001/jamaoncol.2017.0973

6. Rohde M, Rosenberg T, Pareek M, Nankivell P, Sharma N, Mehanna H, Godballe C (2020) Definition of locally recurrent head and neck squamous cell carcinoma: a systematic review and proposal for the Odense-Birmingham definition. Eur Arch Otorhinolaryngol 277(6):1593-1599. https://doi.org/10.1007/s00405-020-05953-5

7. Szturz P, Wouters K, Kiyota N, Tahara M, Prabhash K, Noronha V, Adelstein D, Van Gestel D, Vermorken JB (2019) Low-Dose vs. High-Dose Cisplatin: Lessons Learned From 59 Chemoradiotherapy Trials in Head and Neck Cancer. Front Oncol 9:86. https://doi.org/10.3389/fonc.2019.00086

8. Buchberger AMS, Strzelczyk EA, Wollenberg B, Combs SE, Pickhard A, Pigorsch SU (2021) Report on Late Toxicity in Head-and-Neck Tumor Patients with Long Term Survival after Radiochemotherapy. Cancers (Basel) 13(17). https://doi.org/10.3390/cancers13174292

9. Nilsen ML, Belsky MA, Scheff N, Johnson JT, Zandberg DP, Skinner H, Ferris R (2020) Late and Long-Term Treatment-Related Effects and Survivorship for Head and Neck Cancer Patients. Curr Treat Options Oncol 21(12):92. https://doi.org/10.1007/s11864-020-00797-x

10. Strojan P, Vermorken JB, Beitler JJ, Saba NF, Haigentz M, Jr., Bossi P, Worden FP, Langendijk JA, Eisbruch A, Mendenhall WM, et al. (2016) Cumulative cisplatin dose in concurrent chemoradiotherapy for head and neck cancer: A systematic review. Head Neck 38 Suppl 1:E2151-2158. https://doi.org/10.1002/hed.24026

11. Buglione M, Alterio D, Maddalo M, Greco D, Gerardi MA, Tomasini D, Pegurri L, Augugliaro M, Marvaso G, Turturici I, et al. (2021) Three weekly versus weekly concurrent cisplatin: safety propensity score analysis on 166 head and neck cancer patients. Radiat Oncol 16(1):239. https://doi.org/10.1186/s13014-021-01966-4

12. Chong WK, Papadopoulou V, Dayton PA (2018) Imaging with ultrasound contrast agents: current status and future. Abdom Radiol (NY) 43(4):762-772. https://doi.org/10.1007/s00261-018-1516-1

13. Frinking P, Segers T, Luan Y, Tranquart F (2020) Three Decades of Ultrasound Contrast Agents: A Review of the Past, Present and Future Improvements. Ultrasound Med Biol 46(4):892-908. https://doi.org/10.1016/j.ultrasmedbio.2019.12.008

14. Snipstad S, Sulheim E, de Lange Davies C, Moonen C, Storm G, Kiessling F, Schmid R, Lammers T (2018) Sonopermeation to improve drug delivery to tumors: from fundamental understanding to clinical translation. Expert Opin Drug Deliv 15(12):1249-1261. https://doi.org/10.1080/17425247.2018.1547279

15. Deprez J, Lajoinie G, Engelen Y, De Smedt SC, Lentacker I (2021) Opening doors with ultrasound and microbubbles: Beating biological barriers to promote drug delivery. Adv Drug Deliv Rev 172:9-36. https://doi.org/10.1016/j.addr.2021.02.015

16. Lammertink BH, Bos C, van der Wurff-Jacobs KM, Storm G, Moonen CT, Deckers R (2016) Increase of intracellular cisplatin levels and radiosensitization by ultrasound in combination with microbubbles. J Control Release 238:157-165. https://doi.org/10.1016/j.jconrel.2016.07.049

17. Chen KT, Wei KC, Liu HL (2019) Theranostic Strategy of Focused Ultrasound Induced Blood-Brain Barrier Opening for CNS Disease Treatment. Front Pharmacol 10:86. https://doi.org/10.3389/fphar.2019.00086

18. Wu SK, Tsai CL, Huang Y, Hynynen K (2020) Focused Ultrasound and Microbubbles-Mediated Drug Delivery to Brain Tumor. Pharmaceutics 13(1). https://doi.org/10.3390/pharmaceutics13010015

19. Schoen S, Jr., Kilinc MS, Lee H, Guo Y, Degertekin FL, Woodworth GF, Arvanitis C (2022) Towards controlled drug delivery in brain tumors with microbubble-enhanced focused ultrasound. Adv Drug Deliv Rev 180:114043. https://doi.org/10.1016/j.addr.2021.114043

20. Dimcevski G, Kotopoulis S, Bjanes T, Hoem D, Schjott J, Gjertsen BT, Biermann M, Molven A, Sorbye H, McCormack E, et al. (2016) A human clinical trial using ultrasound and microbubbles to enhance gemcitabine treatment of inoperable pancreatic cancer. J Control Release 243:172-181. https://doi.org/10.1016/j.jconrel.2016.10.007

21. Kotopoulis S, Dimcevski G, Gilja OH, Hoem D, Postema M (2013) Treatment of human pancreatitc cancer using combined ultrasound, microbubbles and gemcitabine: a clinical case study. Medical Physics 40(7). https://doi.

org/10.1118/1.4808149]

22. Wang Y, Li Y, Yan K, Shen L, Yang W, Gong J, Ding K (2018) Clinical study of ultrasound and microbubbles for enhancing chemotherapeutic sensitivity of malignant tumors in digestive system. Chin J Cancer Res 30(5):553-563. https://doi.org/10.21147/j.issn.1000-9604.2018.05.09

23. Rix A, Piepenbrock M, Flege B, von Stillfried S, Koczera P, Opacic T, Simons N, Boor P, Thoroe-Boveleth S, Deckers R, et al. (2021) Effects of contrast-enhanced ultrasound treatment on neoadjuvant chemotherapy in breast cancer. Theranostics 11(19):9557-9570. https://doi.org/10.7150/thno.64767

24. Supsavhad W, Dirksen WP, Martin CK, Rosol TJ (2016) Animal models of head and neck squamous cell carcinoma. Vet J 210:7-16. https://doi.org/10.1016/j.tvjl.2015.11.006

25. Cannon C (2015) Cats, Cancer and Comparative Oncology. Veterinary Sciences 2(3):111-126. https://doi.org/10.3390/vetsci2030111

26. Wypij JM (2013) A naturally occurring feline model of head and neck squamous cell carcinoma. Patholog Res Int 2013:502197. https://doi.org/10.1155/2013/502197

27. Stebbins KE, Morse CC, Goldschmidt MH (1989) Feline Oral Neoplasia: A Ten-Year Survey. Vet Pathol 26:121-128.

28. Martin CK, Tannehill-Gregg SH, Wolfe TD, Rosol TJ (2011) Bone-invasive oral squamous cell carcinoma in cats: pathology and expression of parathyroid hormone-related protein. Vet Pathol 48(1):302-312. https://doi.org/10.1177/0300985810384414

29. Bostock DE (1972) The prognosis in cats bearing squamous cell carcinoma. J small Anim Pract 13:119-125.

30. Sabhlok A, Ayl R (2014) Palliative radiation therapy outcomes for cats with oral squamous cell carcinoma (1999-2005). Vet Radiol Ultrasound 55(5):565-570. https://doi.org/10.1111/vru.12157

31. Withrow SJ, Vail DM. Withrow and MacEwen's small animal clinical oncology. United States: Saunders Elsevier; 2007. 846 p.

32. Biller B, Berg J, Garrett L, Ruslander D, Wearing R, Abbott B, Patel M, Smith D, Bryan C (2016) 2016 AAHA Oncology Guidelines for Dogs and Cats. J Am Anim Hosp Assoc 52:181-204.

33. Hayes AM, Adams VJ, Scase TJ, Murphy S (2007) Survival of 54 cats with oral squamous cell carcinoma in United Kingdom general practice. J Small Anim Pract 48(7):394-399. https://doi.org/10.1111/j.1748-5827.2007.00393.x

34. Barabas K, Milner R, Lurie D, Adin C (2008) Cisplatin a review of toxicities and therapeutic applications. Veterinary and Comparative Oncology 6:1-18.

35. Tounekti O, Pron G, Belehradek J, Mir LM (1993) Bleomycin, an Apoptosis-mimetic Drug That Induces Two Types of Cell Death Depending on the Number of Molecules Internalized. Cancer Research 53:5462-5469.

36. Mir LM, Tounekti O, Orlowski S (1996) Bleomycin: revival of an old drug. Gen Pharmac 27(5):745-748.

37. Teissie J. Electropermeabilization of the cell membrane. In: Li S. CJ, Heller R., Teissie J., editor. Electroporation Protocols Methods in Molecular Biology (Methods and Protocols). 1121: Humana Press, New York, NY; 2014.

38. Spugnini EP, Baldi A (2019) Electrochemotherapy in Veterinary Oncology: State-of-the-Art and Perspectives. Vet Clin North Am Small Anim Pract 49(5):967-979. https://doi.org/10.1016/j.cvsm.2019.04.006

39. Spugnini EP, Pizzuto M, Filipponi M, Romani L, Vincenzi B, Menicagli F, Lanza A, De Girolamo R, Lomonaco R, Fanciulli M, et al. (2015) Electroporation Enhances Bleomycin Efficacy in Cats with Periocular Carcinoma and Advanced Squamous Cell Carcinoma of the Head. J Vet Intern Med 29(5):1368-1375. https://doi.org/10.1111/jvim.13586

40. Dotsinsky I, Nikolova B, Peycheva E, Tsoneva I (2012) New Modality for Electrochemotherapy of Surface Tumors. Biotechnology & Biotechnological Equipment 26(6):3402-3406. https://doi.org/10.5504/bbeq.2012.0098

41. Keller SB, Wang YN, Totten S, Yeung RS, Averkiou MA (2021) Safety of Image-Guided Treatment of the Liver with Ultrasound and Microbubbles in an in Vivo Porcine Model. Ultrasound Med Biol 47(11):3211-3220. https://doi.org/10.1016/j.ultrasmedbio.2021.07.003

42. Seiler GS, Brown JC, Reetz JA, Taeymans O, Bucknoff M, Rossi F, Ohlerth S, Alder D, Rademacher N, Drost T, et al. (2013) Safety of contrast-enhanced ultrasonography in dogs and cats: 488 cases (2002–2011). J Am Vet Med Assoc 242:1255-1259.

43. Streitberger A, Hocke V, Modler P (2013) Measurement of pulmonary transit time in healthy cats by use of ultrasound contrast media "Sonovue(R)": feasibility, reproducibility, and values in 42 cats. J Vet Cardiol 15(3):181-187. https://doi.org/10.1016/j.jvc.2013.05.001

44. de Brito M, Feliciano M, Coutinho LN, Uscategui RR, Simoes A, Maronezi MC, de Almeida VT, Crivelaro RM, Gasser B, Pavan L, et al. (2015) Doppler and Contrast-Enhanced Ultrasonography of Testicles in Adult Domestic Felines. Reprod Domest Anim 50(5):730-734. https://doi.org/10.1111/rda.12557

45. Streitberger A, Modler P, Haggstrom J (2015) Increased normalized pulmonary transit times and pulmonary blood volumes in cardiomyopathic cats with or without congestive heart failure. J Vet Cardiol 17(1):25-33. https://doi.org/10.1016/j.jvc.2014.09.005

46. Schweiger H, Ohlerth S, Gerber B (2015) Contrast-enhanced ultrasound of both kidneys in healthy, non-anaesthetized cats. Acta Vet Scand 57:80. https://doi.org/10.1186/s13028-015-0172-5

47. Stock E, Daminet S, Paepe D, Buresova E, Vandermeulen E, Smets P, Duchateau L, Saunders JH, Vanderperren K (2017) Evaluation of Renal Perfusion in Hyperthyroid Cats before and after Radioiodine Treatment. J Vet Intern Med 31(6):1658-1663. https://doi.org/10.1111/jvim.14852

48. de Maar JS, Rousou C, van Elburg B, Vos HJ, Lajoinie GPR, Bos C, Moonen CTW, Deckers R (2021) Ultrasound-

5

Mediated Drug Delivery With a Clinical Ultrasound System: In Vitro Evaluation. Front Pharmacol 12:768436. https://doi.org/10.3389/fphar.2021.768436

49.   Theilen GH, Madewell BR. Veterinary Cancer Medicine. 2 ed1979.

50.   Tatlock S, Gober M, Williamson N, Arbuckle R (2017) Development and preliminary psychometric evaluation of an owner-completed measure of feline quality of life. Vet J 228:22-32. https://doi.org/10.1016/j.tvjl.2017.10.005

51.   Dietrich CF, Averkiou MA, Correas JM, Lassau N, Leen E, Piscaglia F (2012) An EFSUMB introduction into Dynamic Contrast-Enhanced Ultrasound (DCE-US) for quantification of tumour perfusion. Ultraschall Med 33(4):344-351. https://doi.org/10.1055/s-0032-1313026

52.   Owen LN (Geneva 1980) TNM classification of tumours in domestic animals; World Health Organization. (First edition):23-24.

53.   Keller SB, Sheeran PS, Averkiou MA (2021) Cavitation therapy monitoring of commercial microbubbles with a clinical scanner. IEEE Trans Ultrason Ferroelectr Freq Control 68(4):1144-1154. https://doi.org/10.1109/TUFFC.2020.3034532

54.   van Wamel A, Kooiman K, Harteveld M, Emmer M, ten Cate FJ, Versluis M, de Jong N (2006) Vibrating microbubbles poking individual cells: drug transfer into cells via sonoporation. J Control Release 112(2):149-155. https://doi.org/10.1016/j.jconrel.2006.02.007

55.   Čemažar M, Miklavčič D, Serša G (1998) Intrinsic sensitivity of tumor cells to bleomycin as an indicator of tumor response to electrochemotherapy. Jpn J Cancer Res 89:328-333. https://doi.org/10.1111/j.1349-7006.1998.tb00566.x

56.   Emanuel AL, Meijer RI, van Poelgeest E, Spoor P, Serne EH, Eringa EC (2020) Contrast-enhanced ultrasound for quantification of tissue perfusion in humans. Microcirculation 27(1):e12588. https://doi.org/10.1111/micc.12588

57.   Jung EM, Weber MA, Wiesinger I (2021) Contrast-enhanced ultrasound perfusion imaging of organs. Radiologe 61(Suppl 1):19-28. https://doi.org/10.1007/s00117-021-00891-7

58.   Barrett EJ, Rattigan S (2012) Muscle perfusion: its measurement and role in metabolic regulation. Diabetes 61(11):2661-2668. https://doi.org/10.2337/db12-0271

59.   Snipstad S, Vikedal K, Maardalen M, Kurbatskaya A, Sulheim E, Davies CL (2021) Ultrasound and microbubbles to beat barriers in tumors: Improving delivery of nanomedicine. Adv Drug Deliv Rev 177:113847. https://doi.org/10.1016/j.addr.2021.113847

60.   Kikuchi M, Yamane T, Shinohara S, Fujiwara K, Hori SY, Tona Y, Yamazaki H, Naito Y, Senda M (2011) 18F-fluoromisonidazole positron emission tomography before treatment is a predictor of radiotherapy outcome and survival prognosis in patients with head and neck squamous cell carcinoma. Ann Nucl Med 25(9):625-633. https://doi.org/10.1007/s12149-011-0508-9

61.   Minchinton AI, Tannock IF (2006) Drug penetration in solid tumours. Nat Rev Cancer 6(8):583-592. https://doi.org/10.1038/nrc1893

62.   Jain RK (2001) Delivery of molecular and cellular medicine to solid tumors. Advanced drug delivery reviews 46:149-168.
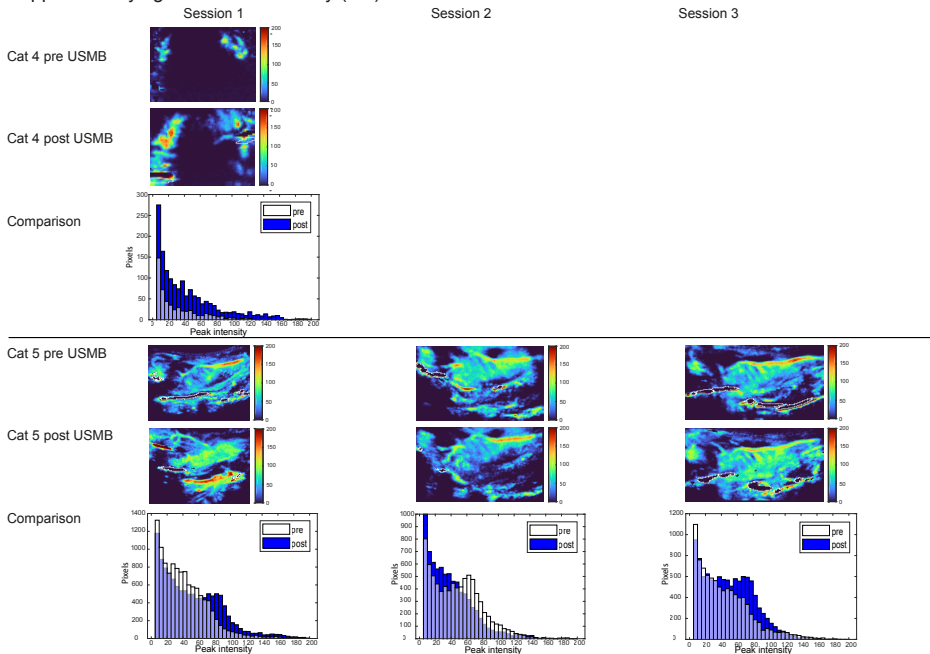
5

5

SUPPLEMENTARY MATERIALS
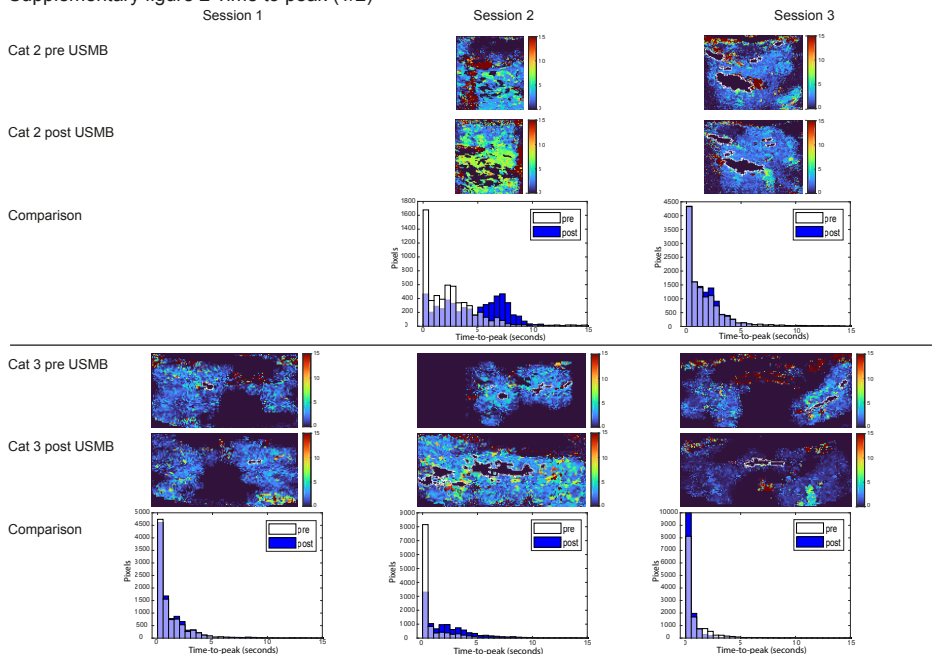
Supplementary figure 1 Peak intensity (1/2)
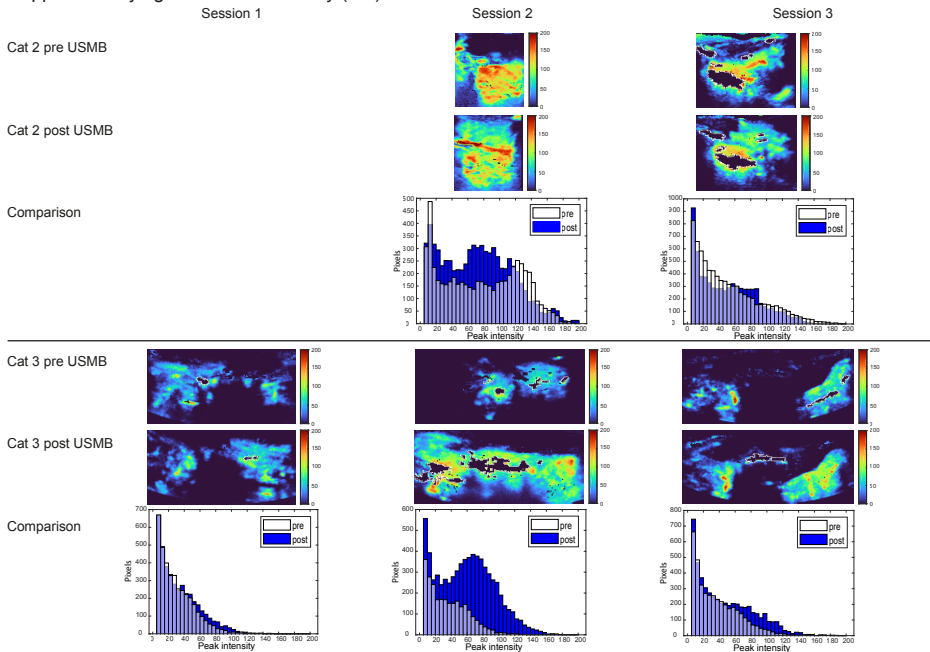
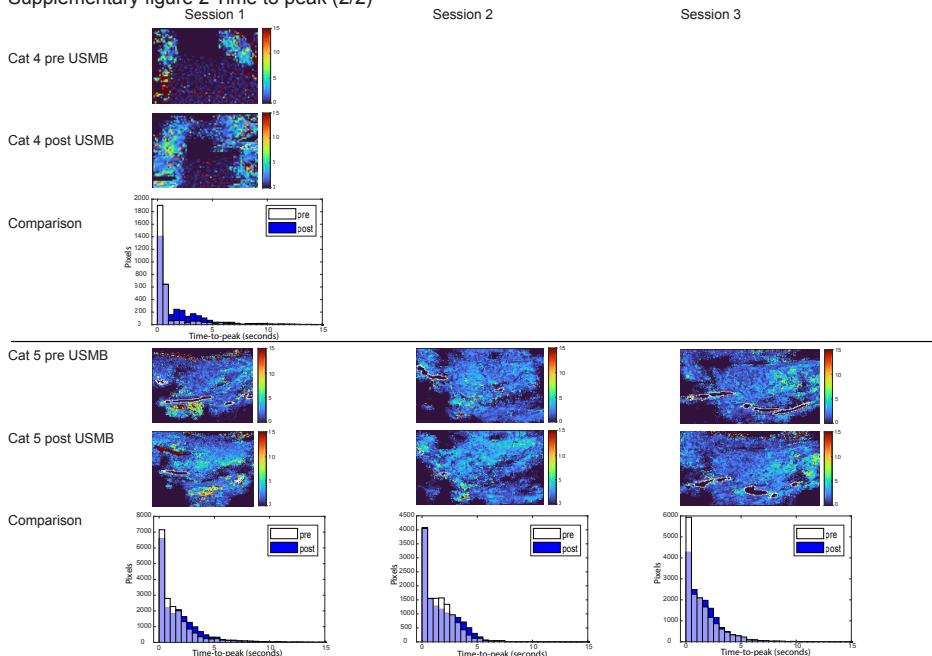## Supplementary figure 1 Peak intensity (2/2)

Supplementary figure 1 Contrast enhanced ultrasound (CEUS) parametric maps of cats 2-5, visualizing peak intensity (PI), before (top) and after (bottom) USMB therapy. For each cat the three treatment sessions are depicted from left to right. CEUS was available for nine treatment sessions. Pixels with high signal intensity before administration of microbubbles (e.g. regions containing bone) were set to zero and delineated with white dotted lines. Below the two maps PI is compared between before (white) and after (blue) USMB in a histogram, excluding pixels with a PI < 5. Note that the range of the y-axes differs between treatment sessions. ROIs pre and post USMB are identical in size within one treatment session and matched in position as much as possible. CEUS parameters were kept constant between treatment sessions, except in treatment session 2 of cat 3 when gain inadvertently changed from 45% (before USMB) to 49% (after USMB). Based on visual interpretation of the data PI increased in six out of nine treatment sessions.
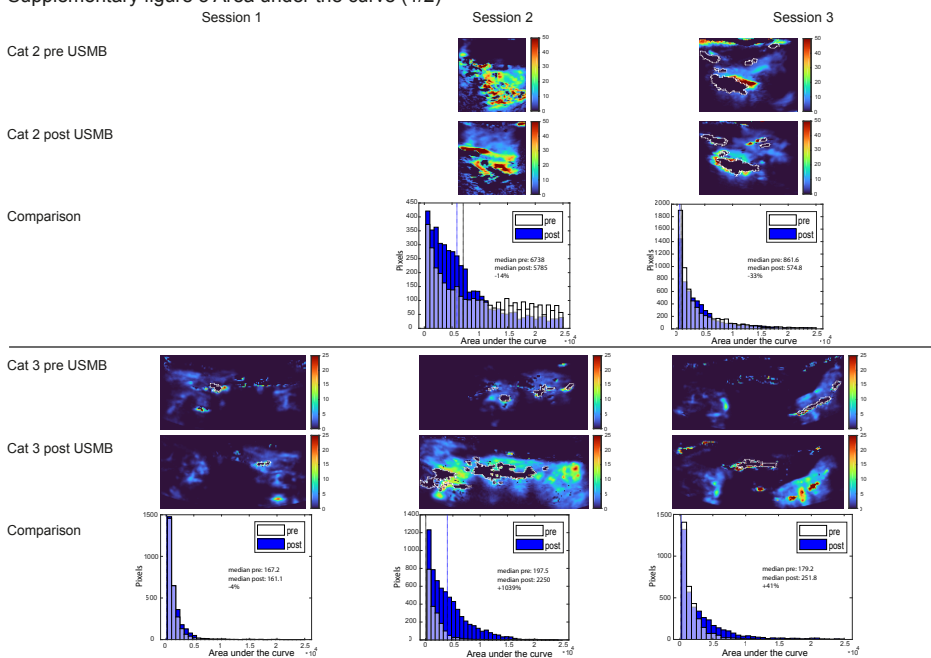
5

Supplementary figure 2 Time to peak (1/2)
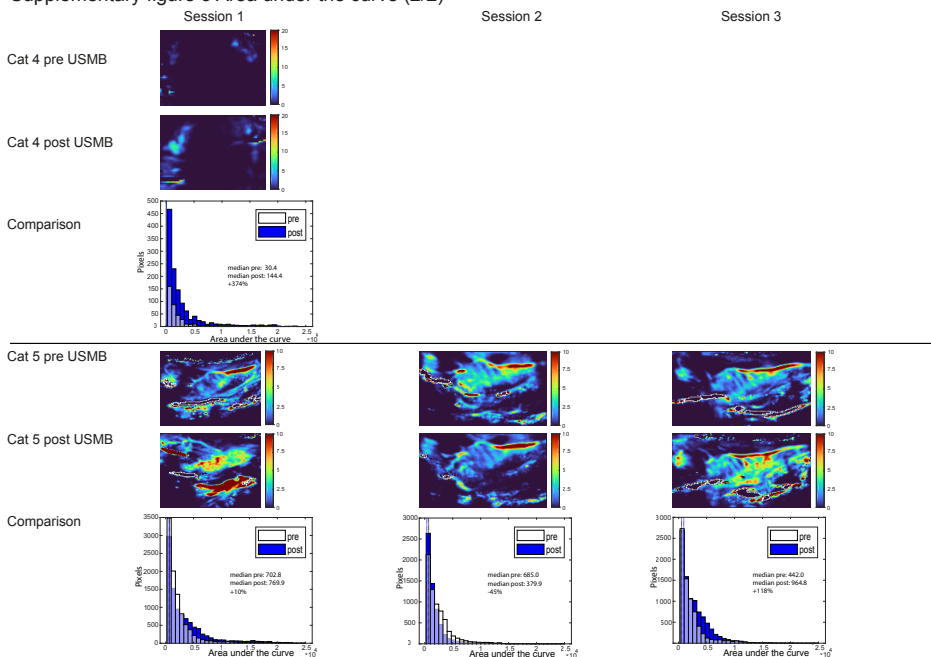

Supplementary figure 2 Time to peak (2/2)

Supplementary figure 2 Contrast enhanced ultrasound (CEUS) parametric maps of cats 2-5, visualizing time-to-peak (TTP), before (top) and after (bottom) USMB therapy. For each cat the three treatment sessions are depicted from left to right. CEUS was available for nine treatment sessions. Pixels with high signal intensity before administration of microbubbles (e.g. regions containing bone) were set to zero and delineated with white dotted lines. Below the two maps TTP is compared between before (white) and after (blue) USMB in a histogram. Note that the range of the y-axes differs between treatment sessions. ROIs pre and post USMB are identical in size within one treatment session and matched in position as much as possible. CEUS parameters were kept constant between treatment sessions, except in treatment session 2 of cat 3 when gain inadvertently changed from 45% (before USMB) to 49% (after USMB). Based on visual interpretation of the data we did not observe a trend in changes of TTP.

Supplementary figure 3 Area under the curve (1/2)

Supplementary figure 3 Area under the curve (2/2)

Supplementary figure 3 Contrast enhanced ultrasound (CEUS) parametric maps of cats 2-5, visualizing area under the curve (AUC), before (top) and after (bottom) USMB therapy. For each cat the three treatment sessions are depicted from left to right. CEUS was available for nine treatment sessions. Pixels with high signal intensity before administration of microbubbles (e.g. regions containing bone) were set to zero and delineated with white dotted lines. Below the two maps AUC is compared between before (white) and after (blue) USMB in a histogram, excluding pixels with an AUC < 250. Median AUC values before and after USMB and the relative difference are described in the histogram. Note that colour scales and the range of the y-axes differ between treatment sessions. ROIs pre and post USMB are identical in size within one treatment session and matched in position as much as possible. CEUS parameters were kept constant between treatment sessions, except in treatment session 2 of cat 3 when gain inadvertently changed from 45% (before USMB) to 49% (after USMB). The median AUC in the ROI decreased in four out of nine treatment sessions (mean decrease 24%, range-4 to-45%) while it increased in five out of nine treatment sessions (mean increase 316.4%, range 10 to 1039%).
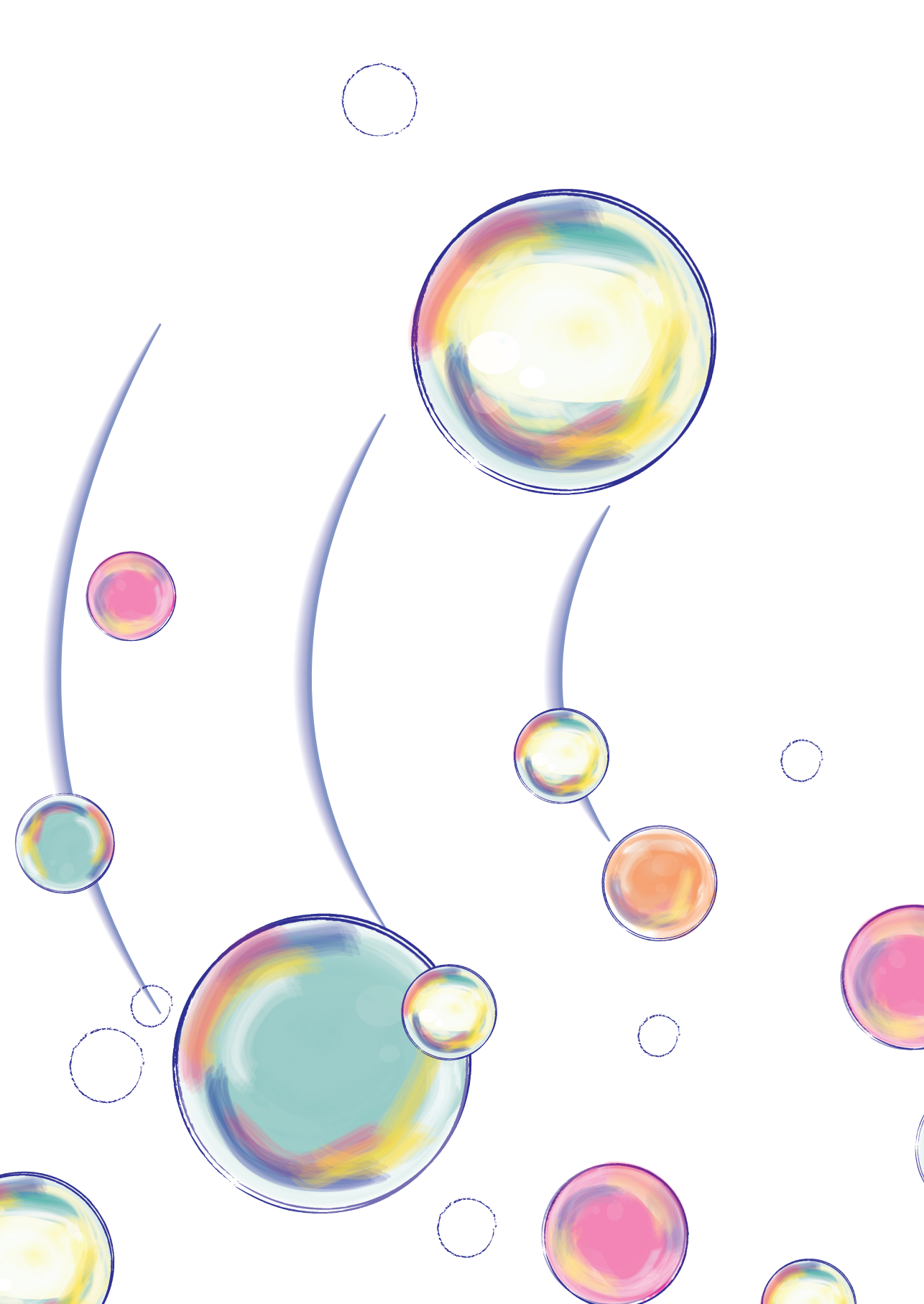
6

NEW DEVELOPMENTS IN IMAGING FOR SENTINEL LYMPH NODE BIOPSY IN EARLY-STAGE ORAL CAVITY SQUAMOUS CELL CARCINOMA

Rutger Mahieu [1], **Josanne S. de Maar [2,†]**, Eliane R. Nieuwenhuis [3,†], Roel Deckers [2], Chrit Moonen [2], Lejla Alic [3], Bennie ten Haken [3], Bart de Keizer [4] and Remco de Bree [1,*]

[1] Department of Head and Neck Surgical Oncology, University Medical Center Utrecht, University of Utrecht, 3584 CX Utrecht, The Netherlands; R.Mahieu@umcutrecht.nl

[2] Division of Imaging and Oncology, University Medical Center Utrecht, University of Utrecht, 3584 CX Utrecht, The Netherlands; J.S.deMaar@umcutrecht.nl (J.d.M.); R.Deckers-2@umcutrecht.nl (R.D.); C.Moonen@umcutrecht.nl (C.M.)

[3] Department of Magnetic Detection & Imaging, University of Twente, 7522 NB Enschede, The Netherlands; e.r.nieuwenhuis@utwente.nl (E.N.); l.alic@utwente.nl (L.A.); b.tenhaken@utwente.nl (B.t.H.)

[4] Department of Radiology and Nuclear Medicine, University Medical Center Utrecht, 3584 CX Utrecht, The Netherlands; B.deKeizer@umcutrecht.nl

[*] Correspondence: R.deBree@umcutrecht.nl; Tel.: +31-88-7550819

[†] Equally contributed.

ABSTRACT

Sentinel lymph node biopsy (SLNB) is a diagnostic staging procedure that aims to identify the first draining lymph node(s) from the primary tumor, the sentinel lymph nodes (SLN), as their histopathological status reflects the histopathological status of the rest of the nodal basin. The routine SLNB procedure consists of peritumoral injections with a technetium-99m [^{99m}Tc]-labelled radiotracer followed by lymphoscintigraphy and SPECT-CT imaging. Based on these imaging results, the identified SLNs are marked for surgical extirpation and are subjected to histopathological assessment. The routine SLNB procedure has proven to reliably stage the clinically negative neck in early-stage oral squamous cell carcinoma (OSCC). However, an infamous limitation arises in situations where SLNs are located in close vicinity of the tracer injection site. In these cases, the hotspot of the injection site can hide adjacent SLNs and hamper the discrimination between tracer injection site and SLNs (shine-through phenomenon). Therefore, technical developments are needed to bring the diagnostic accuracy of SLNB for early-stage OSCC to a higher level. This review evaluates novel SLNB imaging techniques for early-stage OSCC: MR lymphography, CT lymphography, PET lymphoscintigraphy and contrast-enhanced lymphosonography. Furthermore, their reported diagnostic accuracy is described and their relative merits, disadvantages and potential applications are outlined.

Keywords
Squamous cell carcinoma of head and neck; mouth neoplasms; lymphatic metastases; sentinel lymph node biopsy; diagnostic imaging; lymphatics; tracer

Simple Summary
In early-stage (cT1-2N0) oral cancer, occult lymph node metastases are present in 20–30% of patients. Accordingly, accurate staging of the clinically negative cervical nodal basin is warranted in these patients. Sentinel lymph node biopsy has proven to reliably stage the clinically negative cervical nodal basin in early-stage oral cancer. However, due to the limited resolution of conventional sentinel lymph node imaging, occult lymph node metastasis may be missed in particular circumstances. Therefore, technical developments are necessary to bring the diagnostic accuracy of sentinel lymph node biopsy, in early-stage oral cancer, to a higher level. This review evaluates novel sentinel lymph node imaging techniques for early-stage oral cancer, such as MR lymphography, CT lymphography, PET lymphoscintigraphy and contrast-enhanced lymphosonography. Their reported diagnostic accuracy is described and their relative merits, disadvantages and potential applications are outlined.

INTRODUCTION

In early-stage (cT1-2N0) oral squamous cell carcinoma (OSCC), occult lymph node metastases are present in 20–30% of patients, even when the status of the regional lymph nodes has been evaluated using combinations of advanced clinical diagnostic imaging modalities (i.e., ultrasound guided fine-needle aspiration (USgFNA), magnetic resonance imaging (MRI) and/or computed tomography (CT)) [1–3]. As watchful-waiting in these patients has been associated with a poor prognosis, especially when compared to those in whom the clinically negative neck was electively treated [1], two strategies for the clinically negative neck in early-stage OSCC are available: elective neck dissection (END) and sentinel lymph node biopsy (SLNB) [3–6]. Although END is the strategy of choice in the majority of medical centers globally [5], which has the benefit of being a single-stage procedure, SLNB is a less invasive procedure for the 70–80% of patients without metastatic neck involvement and has overall lower morbidity rates, better quality-of-life and lower health-care costs as compared to END [7–10].

The concept of SLNB is based on the premise that lymph flow from the primary tumor travels sequentially to the sentinel lymph node (SLN) and then on to the other regional lymph nodes. Hence, the SLN is the lymph node that has the highest risk of harboring metastasis [11].

The SLNB procedure aims to identify these first draining lymph node(s), as their histopathological status reflects the histopathological status of the rest of the nodal basin. Complementary nodal treatment (e.g., surgery, radiotherapy) should be performed in case of metastatic involvement of SLN(s). A negative SLNB, however, would justify a wait-and-scan policy [12].

In short, the routine SLNB procedure consists of preoperative peritumoral injections with a technetium-99m [^{99m}Tc; γ-emitter]-labelled radiotracer followed by planar dynamic and static lymphoscintigraphy including SPECT-CT (single photon emission computed tomography-computed tomography) imaging. Based on preoperative lymphoscintigraphy, the position of the SLN(s) is marked on the skin. The marked SLNs are surgically removed, using a portable γ-probe for intraoperative localization of SLNs. Subsequently, the harvested SLNs are subjected to meticulous histopathological assessment using step-serial-sectioning and immunohistochemistry [12–15].

SLNB has proven to reliably stage the clinically negative neck in early-stage OSCC with a pooled sensitivity and negative predictive value (NPV) of 87% and 94%, respectively [16]. However, an infamous limitation of the routine SLNB procedure arises in situations where SLNs are located in close vicinity of the tracer injection site. In these cases, the hotspot of the injection site can hide adjacent SLNs, which consequently hampers the discrimination between tracer injection site and SLNs (shine-through phenomenon; Figure 1). This shine-through phenomenon is particularly evident in patients with floor-of-mouth OSCC and sublingual, submental and submandibular SLNs, resulting in a

6

significantly lower accuracy of SLNB in floor-of-mouth tumors (sensitivity 63%; NPV 90%) compared to other oral cavity subsites (sensitivity 86%; NPV 95%) [4,17–21].
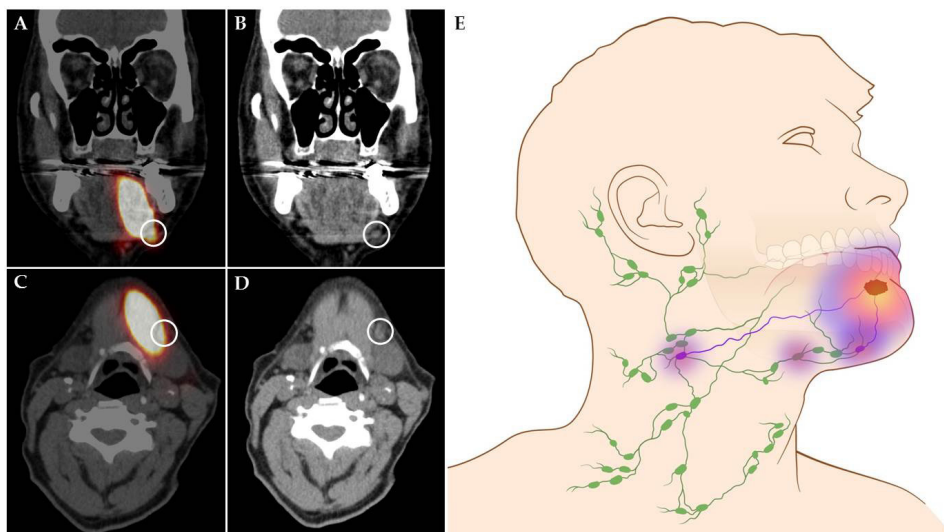

Figure 1. Shine-through phenomenon in 72-year-old patient with a cT1N0 floor-of-mouth carcinoma. (**A**,**C**) Coronal and axial SPECT-CT images: radiation flare of the tracer injection site over shines a sentinel lymph node located in cervical lymph node level Ib (white circle). (**B**,**D**) Coronal and axial low-dose CT images of same patient: (sentinel) lymph node located in cervical lymph node level Ib that could not be differentiated from the hotspot originating from tracer injection site on SPECT-CT (white circle). (**E**) Schematic illustration of shine-through phenomenon. (**A**–**D**) Informed consent has been obtained from this patient. (**E**) ©University Medical Center Groningen.

Therefore, technical developments are needed to bring the diagnostic accuracy of SLNB for all subsites of OSCC to the same high level. This review evaluates new developments in preoperative SLN imaging techniques for early-stage OSCC: MR lymphography, CT lymphography, PET lymphoscintigraphy and contrast-enhanced lymphosonography. Furthermore, this review describes their diagnostic accuracy as reported in literature and outlines their relative merits, disadvantages and potential applications.

RESULTS

A systematic literature search for new developments in preoperative SLN imaging techniques for early-stage OSCC resulted in a total of 452 PubMed indexed articles, of which 40 were considered relevant. Cross-reference led to 1 additional relevant study with healthy volunteers. Of these 41 articles, 27 were reviews (n = 1), animal or preclinical

studies (n = 26). In particular, 20 animal or preclinical studies used similar methods for SLN identification (i.e., imaging modality, tracer) as corresponding clinical studies.

Table 1 shows the range of reported diagnostic accuracy, in terms of sensitivity and NPV, and rate of patients in which SLNs were identified using the reviewed techniques. Figure 2 illustrates how both preoperative detection and intraoperative localization of SLNs was achieved, using the reviewed techniques, as described in literature.
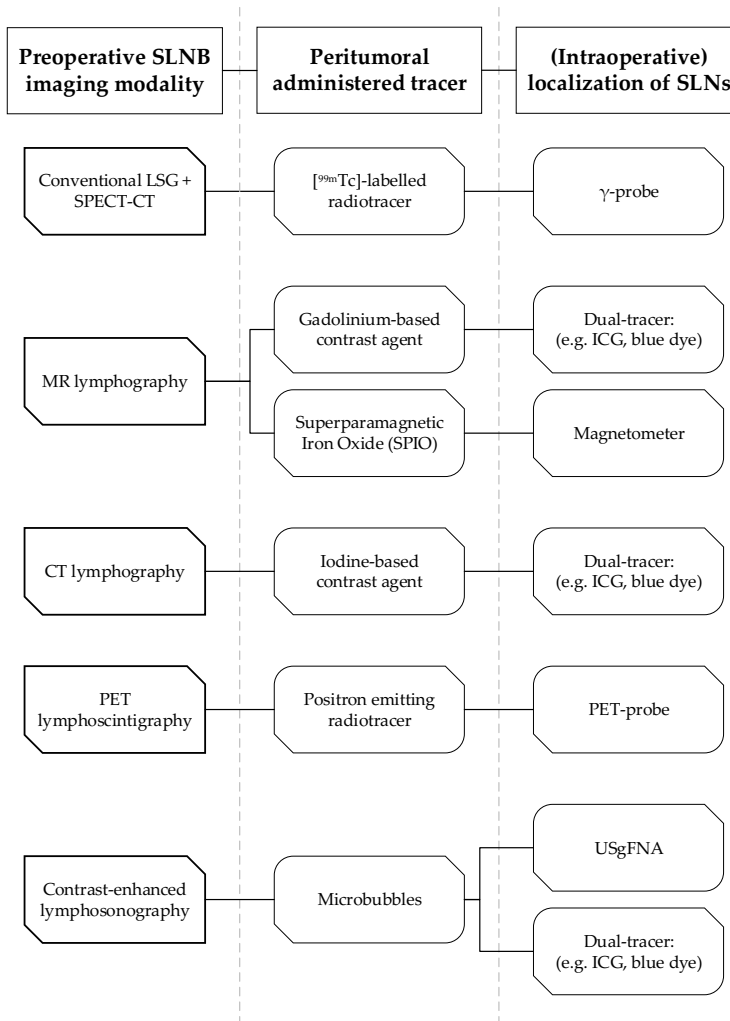
Figure 2. Overview of the reviewed preoperative SLN imaging techniques (column 1), the administered tracers for the corresponding techniques (column 2) and their intraoperative SLN localization techniques (column 3) as described in literature. SLNB; sentinel lymph node biopsy, LSG; lymphoscintigraphy, SPECT-CT; single photon emission computed tomography-computed tomography, MR; magnetic resonance, CT; computed tomography, PET; positron emission tomography, ICG; indocyanine green, USgFNA; ultrasound guided fine needle aspiration.

Table 1. Reported diagnostic accuracy and detection rate of sentinel lymph nodes per technique.

Technique	Source	Tracer	Number of studies	Sensitivity	NPV	SLN identification in (%) of patients
Conventional lymphoscintigraphy & SPECT-CT	γ-ray	γ-emitting [^{99m}Tc]-labelled radiotracer (e.g., [^{99m}Tc]-nanocolloid)	n = 66	87%[16]	94%[16]	–
MR Lymphography (Gd^{3+})	Radio-wave	Paramagnetic (Gd^{3+}) contrast agent (e.g., gadobutrol)	n = 1	91%[26]	93%[26]	100%[26]
MR Lymphography (SPIO)	Radio-wave	Superparamagnetic (iron oxide) contrast agent (e.g., Resovist, Magtrace)	n = 2	NR	NR	100%[37,40,41]
CT Lymphography	X-ray	Iodine contrast agent (e.g., iopamidol, lipiodol)	n = 6	56%–80% [54,55,57,58]	82%–96% [54,55,57,58]	89%–96%[54–59]
PET lymphoscintigraphy	β$^+$-decay (γ-rays)	Positron emitting isotope [^{89}Zr, ^{68}Ga, ^{18}F]-labelled radiotracer (e.g., [^{68}Ga]-tilmanocept)	n = 2	67%[71]	67%[71]	100%[71,73]
Contrast-enhanced lymphosonography	US-wave	Microbubbles (e.g., SonoVue, Sonazoid)	n = 2	NR	NR	80%–92%[80,81]

NPV; negative predictive value, SLN; sentinel lymph node, SPECT-CT; single photon emission computed tomography-computed tomography, ^{99m}Tc; technetium-99m, MR; magnetic resonance, Gd^{3+}; gadolinium, NR; not reported, CT; computed tomography, PET; positron emission tomography, ^{89}Zr; zirconium-89, ^{68}Ga; gallium-68, ^{18}F; fluorine-18, US; ultrasound.

Magnetic Resonance Lymphography

Magnetic resonance (MR) lymphography with peritumoral administration of a paramagnetic gadolinium [Gd^{3+}]-based contrast agent has been recently introduced in breast and cervical cancer, as an alternative method for preoperative visualization of SLNs and lymphatics [22–24]. These studies showed that paramagnetic gadolinium [Gd^{3+}]-based contrast agents, conventionally administered intravenously for contrast-enhanced MRI or MR angiography [25], are safe and useful for peritumoral administration and SLN mapping in humans.

To review MR lymphography for SLN detection using paramagnetic gadolinium-based contrast agents in early-stage OSCC, a systematic literature search was conducted. This led to retrieval of 53 PubMed indexed articles for MR lymphography; 7 were considered relevant [26–32]. Of these 7 articles, 6 were animal studies [27–32]. Cross-reference led to identification of 1 relevant study with healthy volunteers [33].

In the only study that performed MR lymphography with a gadolinium-based contrast agent (i.e., gadobutrol) in OSCC patients (n = 26) [26], SLNs were consistently visualized in all patients and lymph node vessels were visualized in the majority of patients (81%) (Figure 3). Following MR lymphography, identified SLNs were injected with 1% patent blue dye under sonographic guidance. Subsequently, primary tumor resection and ipsilateral elective neck dissection were performed in all patients. Blue stained SLNs were dissected, marked and sent separately for histopathological assessment.

Among the 11 patients with pathologically positive necks, SLNs containing metastases

were accurately identified by MR lymphography in 10 patients. In the remaining patient, MR lymphography depicted SLNs in ipsilateral neck level III. However, in the neck dissection specimen, 3 metastatic lymph nodes in ipsilateral neck level I were found, whereas no metastasis was found in level III. With histopathological assessment of the neck dissection specimen as reference standard, this approach reached a sensitivity of 90.9% with a NPV of 92.8%.

Another type of contrast agent that can be used for MR lymphography are superparamagnetic iron oxide nanoparticles (SPIO), which provide a negative contrast on MR lymphography as opposed to gadolinium-based contrast agents (Figure 4). Following peritumoral administration of SPIOs, transportation through the lymphatic system is mainly facilitated by macrophages, although unbound transport is seen as well [34]. SPIO accumulates primarily in lymph node sinuses and can be detected preoperatively on MRI and intraoperatively with a handheld magnetometer [34–38]. MR lymphography using SPIO has been investigated for several tumor types, including breast and prostate cancer [35,36].
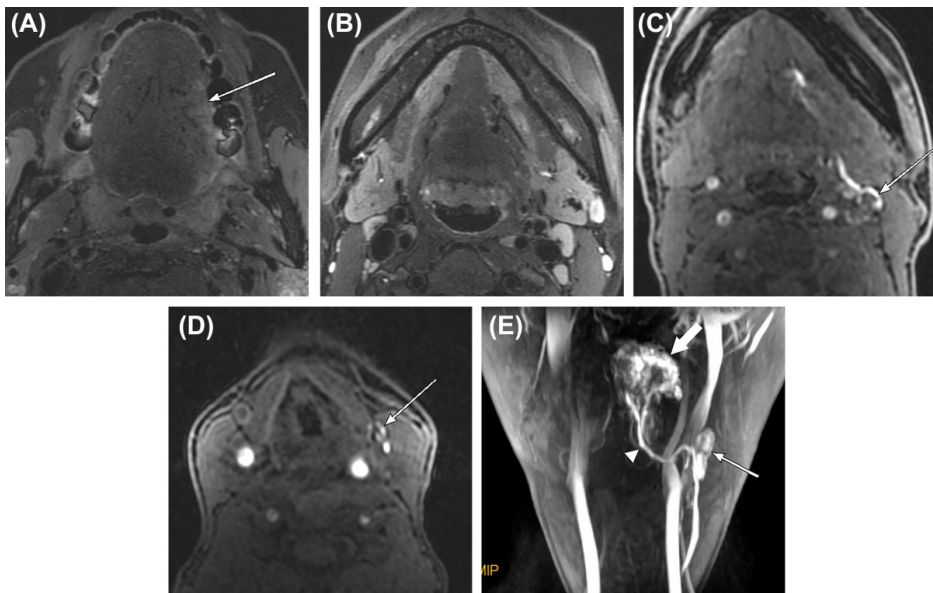
Figure 3. A 38-year-old woman with oral tongue cancer and palpably negative neck. (**A**,**B**) Fat-saturated T2-weighted MRI scans show a shallow infiltrative tumor on the left lateral surface of oral tongue (arrow) and several small lymph nodes in the submandibular areas. (**C**,**D**) After peritumoral injection of contrast, MR lymphography revealed two first-enhanced lymph nodes in left level IB and IIA (arrows) on the first phase of the dynamic scan, respectively. (**E**) The maximum intensity projection reconstruction image of MR lymphography shows the contrast injection site in the tongue (thick arrow), the assumed sentinel lymph node (thin arrow), and the lymph vessel connecting them (arrowhead). After neck dissection, the assumed sentinel lymph nodes observed on MR lymphography revealed no metastasis on histologic examination [26]. Figure used with permission of John Wiley and Sons©, permission license number 4807630108259.

The systematic literature search retrieved 116 PubMed indexed articles, of which 6 were considered relevant [32,37–41]. Of these 6 articles, 3 were animal studies [32,38,39]. Cross-reference did not lead to identification of additional relevant articles, resulting in a total of 3 included human studies [37,40,41]. One of these studies did not perform preoperative SPIO-enhanced MRI, but was the only study in early-stage OSCC patients that achieved intraoperative localization of SLNs with the magnetometer [37].

Mizokami et al. performed MR lymphography using SPIO in three tongue cancer patients (cT2N0), planned for tumor resection and ipsilateral elective neck dissection [40]. Seven days before surgery, patients received peritumoral injections with Resovist (Bayer Schering Pharma) of 0.1–0.3 mL, corresponding with 2.78–8.37 mg iron. MR lymphographic images were acquired at 10 min, 30 min and 24 h post-injection. On the day before surgery, [99mTc]-phytate was administered peritumorally, followed by planar lymphoscintigraphy. Intraoperatively, SLNs were localized using a conventional γ-probe and were submitted for individual histopathological assessment. All SLNs depicted on 10 min MR lymphography were in accordance with planar lymphoscintigraphy and γ-probe findings. MR lymphography at 30 min and 24 h post-injection showed more uptake of SPIO in SLNs. However, MR lymphography 24 h post-injection also visualized higher echelon nodes (HEN). Besides, on MR lymphography SPIO-induced streak artifacts were seen around the injection site, but did not prevent identification of SLNs in vicinity of the tracer injection site. Histopathological assessment confirmed presence of iron in all harvested SLNs. In one patient nodal metastases were found in a harvested SLN; no additional metastases were seen in the neck dissection specimen. No follow-up results were reported in this study. In two patients, tissue swelling was observed at the injection site after administration of SPIO, which was attributed to the volume of SPIO injected.

Maza et al. evaluated fusion of lymphoscintigraphic SPECT, SPIO MR lymphography and CT, for identification of SLNs in rather complex anatomical regions [41]. Fourteen patients were included of whom two diagnosed with tongue cancer; scheduled for tumor resection and ipsilateral elective neck dissection. A mixture of [99mTc]-nanocolloid and SPIO (Resovist), in total 0.5 mL, was peritumorally injected on the day before surgery. MR lymphography was acquired 2 h post-injection. Lymph nodes were assessed as SLN if they corresponded with SPECT images and exhibited signal loss on T2*-weighted sequences. SPECT-MRI fusion was successful in both OSCC patients and showed corresponding SLNs. Intraoperatively, SLNs were localized using a γ-probe and were sent for individual histopathological assessment. SLN metastases were found in the contralateral neck of one OSCC patient, leading to a complementary contralateral neck dissection. No (additional) lymph node metastases were found in the neck dissection specimens of both patients. No follow-up results were reported.
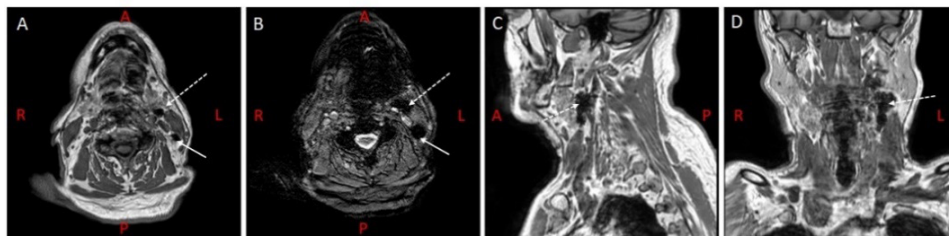
Figure 4. MR lymphography using superparamagnetic iron oxide nanoparticles in a 77-year-old man with oral tongue cancer and a clinically negative neck. (**A**) T1-weigted 3D fast-field echo (FFE) show uptake of SPIO in two SLNs in level IIa (dotted arrow) & level IIb (arrow) left. (**B**) T2-weighted FFE shows clear negative contrast in corresponding SLNs, as a result of SPIO uptake. (**C,D**) Sagittal and coronal reconstruction of (**A**) shows the SLN in level IIa left (dotted arrow). (**A–D**) Informed consent has been obtained from this patient.

CT Lymphography

Another approach for high-resolution lymphography regards computed tomography (CT) lymphography using peritumoral administered iodine-based contrast agents. The use of CT lymphography has been investigated in several tumor types including breast, lung, esophageal, gastric and skin cancer [42–53]. In these studies, CT lymphography provided high-resolution visualization of SLNs, lymphatic vessels and surrounding anatomical structures.

For reviewing the application of CT lymphography in early-stage OSCC, the systematic literature search led to retrieval of 112 PubMed indexed articles for CT lymphography, of which 17 were considered relevant [27,28,54–68]. Of these 17 articles, 11 were animal studies [27,28,60–68]. Cross-reference did not lead to any additional relevant articles.

The case report of Saito et al. [59] was the first article that described the application of CT lymphography in an early-stage OSCC patient. Using CT lymphography with peritumoral injection of iopamidol (2.0 mL), a right lateral lingual lymph node was identified as SLN from a cT2N0 right oral tongue tumor. Following partial glossectomy, without any management of the neck or extirpation of the SLN, the patient showed no evidence of disease after 14 months follow-up. This case-report demonstrated that CT lymphography is suitable for visualization of small SLNs located near the primary tumor, such as lingual lymph nodes.

The first series regarding CT lymphography in early-stage OSCC patients (n = 31; oral tongue) was reported by Honda et al. [58]. In this study, CT images were obtained 1, 3, 5, and 10 min after administration of 1.5 mL iopamidol mixed with 0.5 mL 1% lidocaine hydrochloride. Both contrast-enhanced lymph vessels draining the tumor injection site as well as SLNs were identified in 90.3% of patients. Identified SLNs were marked for biopsy using a lattice marker, combined with intraoperative peritumoral patent blue dye injection. All patients, except for those with T1N0 OSCC and negative frozen-section assessment of SLNs (n = 11), underwent selective neck dissection following tumor resection. Using histopathological examination of the neck dissection specimen and a

follow-up of 30 months as reference standard, this approach reached a sensitivity of 80% with a NPV of 95.8%.

In the sequel study of Honda et al., including 18 patients with cT1-2N0 oral tongue carcinoma, similar methods were used for CT lymphography, resulting in a preoperative SLN detection rate of 89% [57]. For intraoperative localization of SLNs, indocyanine green (ICG) and near-infrared imaging was used, instead of patent blue dye. In contrast to their previous study [58], only patients with advanced cT2N0 disease or positive frozen-section assessment of SLNs underwent selective neck dissection (*n* = 9). In the 16 patients with at least one detected SLN on CT lymphography, a sensitivity of 71.4% and NPV of 81.8% after 38 months median follow-up were reported.

More recently, Sugiyama et al. [56] performed CT lymphography in 20 early-stage OSCC patients. Following peritumoral administration of 2.0 mL iopamidol, SLNs and lymphatic vessels draining the injection site were detected in 95% and 90% of patients, respectively. Two lingual lymph nodes were identified as SLNs (5.4%). The optimal timing for CT scanning in this study was at both 2 and 5 min post-injection, visualizing all 37 contrast-enhanced SLNs. Intraoperative SLN detection was performed under ICG fluorescence guidance; the authors stated to have localized all CT lymphographic identified SLNs during surgery using intraoperatively administered ICG. Both number of patients with metastatic SLNs as well as follow-up results were not reported.

In the sequel study of Sugiyama et al. [54], preoperative CT lymphographic images were reevaluated in 32 early-stage OSCC patients with an approach similar to their previous study [56]. During follow-up 4/27 patients with negative SLNB (14.8%), based on CT lymphography, developed regional recurrence and 1/5 patients with SLN metastasis (20%) developed recurrence between primary tumor site and the neck. Accordingly, their approach reached a sensitivity of 55.6% and NPV of 85.2%. Reevaluation of CT lymphographic images showed a subtle increase in Hounsfield units (HU) of overlooked SLNs (*n* = 5) when compared to non-contrast CT images. Besides, their results showed that HU decreased at 10 min post-injection, indicating that iopamidol is only briefly retained in SLNs.

Figure 5 shows CT lymphographic images from a recent long-term follow-up study with early-stage OSCC patients (*n* = 27*; oral tongue*) [55]. In this study, SLNs were detected in 96.3% of patients using CT lymphography after peritumoral administration of 2.0 mL iopamidol. Intraoperatively, SLNs were localized using ICG and near-infrared imaging. In total, 5 patients had metastatic SLNs (18.5%) and 3 patients without SLN metastases developed regional recurrence (13.6%) after median follow-up of 76 months. This resulted in a sensitivity and NPV of 62.5% and 86.3%, respectively.
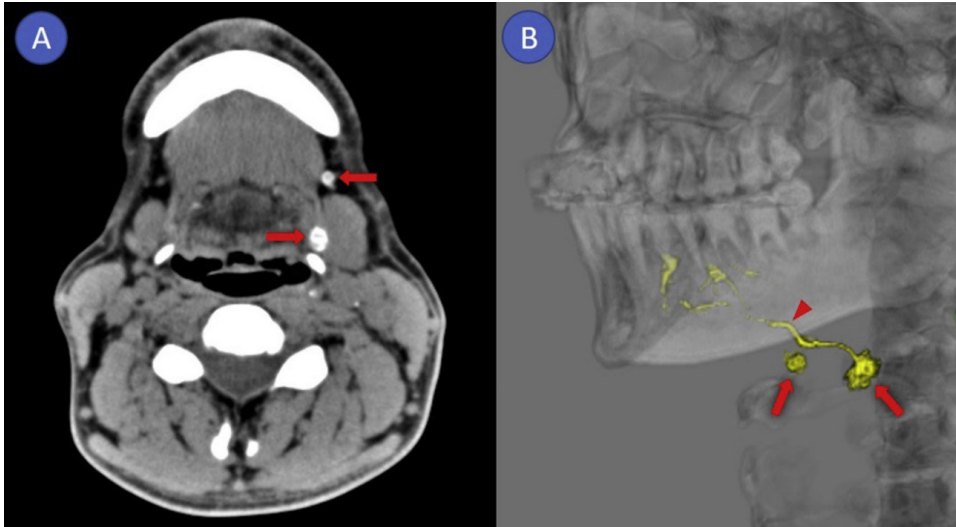
Figure 5. Computed tomographic lymphography: (**A**) axial image, (**B**) 3D image. Arrows: sentinel lymph node; arrowhead: lymphatics [55]. Figure used with permission of Elsevier©, permission license number: 4807630528815.

PET Lymphoscintigraphy

Alternatively, a potential nuclear imaging modality for improving the diagnostic accuracy of SLNB is positron emission tomography (PET). Since PET is able to detect and record a higher percentage of radioactive emitted events compared to SPECT, PET provides both higher spatial and temporal resolution (i.e., acquires higher number of frames per time unit for dynamic studies) [69]. Consequently, PET could be highly suitable for lymphoscintigraphy and may identify SLNs with higher precision than conventional lymphoscintigraphy with SPECT. Instead of a γ-emitter (e.g., [^{99m}Tc], [^{60}Co])-labelled radiotracer, generally used for conventional lymphoscintigraphy, PET lymphoscintigraphy requires a positron emitting isotope (e.g., [^{89}Zr], [^{68}Ga], [^{18}F])-labelled radiotracer [70].

A systematic literature search was conducted to review PET lymphoscintigraphy in early-stage OSCC. This led to retrieval of 64 PubMed indexed articles; 4 were considered relevant [71–74]. Of these 4 studies, 1 regarded an animal study [74] and 1 a review [72] that briefly discusses results from 2 of 3 included studies in our review [73,74]. Cross-reference did not lead to any additional relevant articles.

In 2013, Heuveling et al. were the first to perform dynamic and static PET lymphoscintigraphy in 5 patients with early-stage OSCC, following peritumoral administration of zirconium-89 [^{89}Zr]-labelled nanocolloid [73]. Subsequently, 7–9 days after PET lymphoscintigraphy, the routine SLNB procedure with [^{99m}Tc]-labelled nanocolloid was performed. The results of PET and SPECT lymphoscintigraphy were compared. PET lymphoscintigraphy was able to visualize all foci (n = 22) that were

identified on SPECT-CT and even visualized 5 additional foci that were considered to be SLNs; all of which were located near the injection site of the primary tumor (Figure 6). Of these 5 additional foci, considered to be SLNs, 2 regarded lingual lymph nodes. Furthermore, in 4 patients (80%) lymphatic vessels were visualized on dynamic PET lymphoscintigraphy. Intraoperatively, the additionally visualized PET foci close to the injection site could not be localized with the conventional portable γ-probe, due to difficulties in differentiating between SLN and injection site. In two patients metastatic SLNs were found, follow-up results were not reported.

In their sequel study, Heuveling et al. achieved both preoperative SLN detection with PET lymphoscintigraphy, as well as intraoperative SLN localization using a handheld PET-probe, after peritumoral administration of [^{89}Zr]-labelled nanocolloid [71]. This study included 5 OSCC patients who underwent tumor resection including neck dissection (i.e., clinically N1 disease or access of the neck was required for tumor resection or flap reconstruction). Preoperatively 13 SLNs were identified by PET lymphoscintigraphy, whereas the PET-probe detected 10 of 13 SLNs intraoperatively (77%). In this population, 3 patients (60%) had nodal metastases; in 1 patient the histopathologically positive SLN, found in the neck dissection specimen during histopathological assessment, was not localized with the PET-probe, although it was depicted on preoperative PET lymphoscintigraphy. None of the patients developed locoregional recurrence after a median follow-up of 25 months. With histopathological examination of the neck dissection specimen and follow-up as reference standard, this approach reached a sensitivity of 67% with a NPV of 67%. The authors concluded that PET lymphoscintigraphy using [^{89}Zr]-labelled nanocolloid may improve preoperative SLN detection, although it should be combined with other tracers for intraoperative localization.

Contrast-Enhanced Lymphosonography

In contrast-enhanced ultrasound (CEUS), echogenic particles such as microbubbles are administered to obtain information on vascularization or delineation of body cavities during ultrasound (US) imaging. FDA and EMA approved microbubbles consist of perfluorocarbons or sulfur hexafluoride (SF$_6$) gas surrounded by a thin biocompatible shell generally made of phospholipids or proteins [75,76]. Due to their compressibility and the large difference in acoustic impedance between gas and the surrounding liquid (i.e., blood or lymph) they strongly scatter ultrasound pulses. In addition, due to nonlinear microbubble oscillations, the scattered signal contains higher harmonic frequencies. These higher harmonic frequencies can be distinguished from the fundamental frequency scatter emitted by relatively incompressible tissue surroundings, consequently enhancing microbubble containing structures [75–77] (Figure 7).

Microbubbles are typically administered intravenously, but have more recently been proposed as a radiation-free tracer for lymphosonography. In breast cancer, studies reported SLN localization rates between 60–100%. For CEUS-guided SLNB a pooled

sensitivity of 54% (95% CI 47–61%) and a NPV of 83–92%, were reported [78]. Few to no adverse events of the procedure were registered; any minor adverse events consisted of localized redness, pain or bruising at the injection site [78,79].
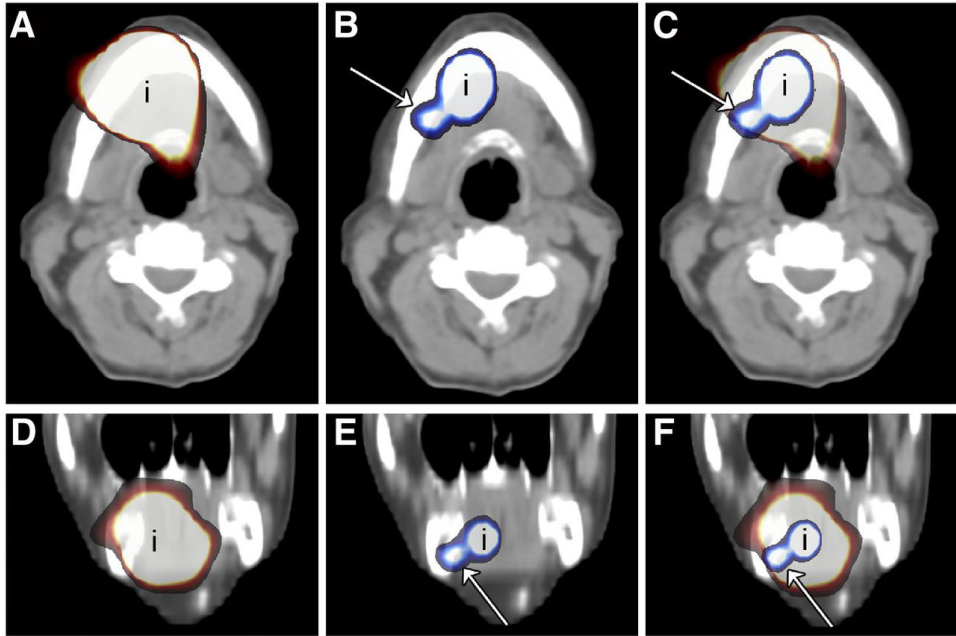
Figure 6. (**A**,**D**) Axial (**A**) and coronal (**D**) SPECT-CT image of injection site (i) of patient 1, i.e., floor of mouth, in which only a large hot spot from injection site could be visualized. (**B**,**E**) PET-CT image of injection site of same patient in which level IB lymph node (arrow) clearly could be identified. (**C**,**F**) Fused SPECT and PET-CT images showing that lymph node visualized on PET-CT is hidden behind large hot spot on SPECT-CT images [73]. This research was originally published in JNM [73]. Figure used with permission of original authors. ©SNMMI.

To review contrast-enhanced lymphosonography in OSCC, a systematic literature search was conducted, which led to retrieval of 107 PubMed indexed articles. A total of 6 studies were considered relevant (i.e., 2 clinical studies [80,81] and 4 large animal studies [82–85]). Cross-reference did not lead to identification of additional relevant articles.

Figure 7 illustrates the procedure used in the two clinical studies [80,81]. Gvetadze et al. [80] used sulfur hexafluoride (SF_6) phospholipid microbubbles (SonoVue; Bracco International B.V.) in 12 patients with T1-2cN0 oral tongue carcinoma and looked for lymph node enhancement after repetitive peritumoral injections. Fifteen SLNs were identified in 11/12 patients (91.7%). No attempt was made at intraoperative localization of identified SLNs and therefore the correlation between identified SLNs and histopathological assessment was lacking. In the second clinical study, Wakisaka et al.

[81] studied lymphosonography with perfluorobutane phospholipid (C_xF_y) microbubbles (Sonazoid; GE Healthcare, UK) in 10 patients with T1-4N0 oral or oropharyngeal carcinomas. Sonazoid was injected in four peritumoral locations. In 8/10 patients, 12 SLNs were identified. In one patient with a T4 tumor, Sonazoid had to be injected intratumorally and no SLNs were identified. SLN locations were marked on the skin. The next day indigo carmine blue dye was injected intraoperatively at the same injection sites. All lymph nodes marked during lymphosonography, which were not always dyed blue, were examined with frozen section analysis. Since frozen section analysis was negative in all cases, a less extensive neck dissection was performed. No metastatic lymph nodes were found during histopathological examination of neck dissection specimens. No follow-up results were reported for both studies. Contrast-related adverse events did not occur [80,81].
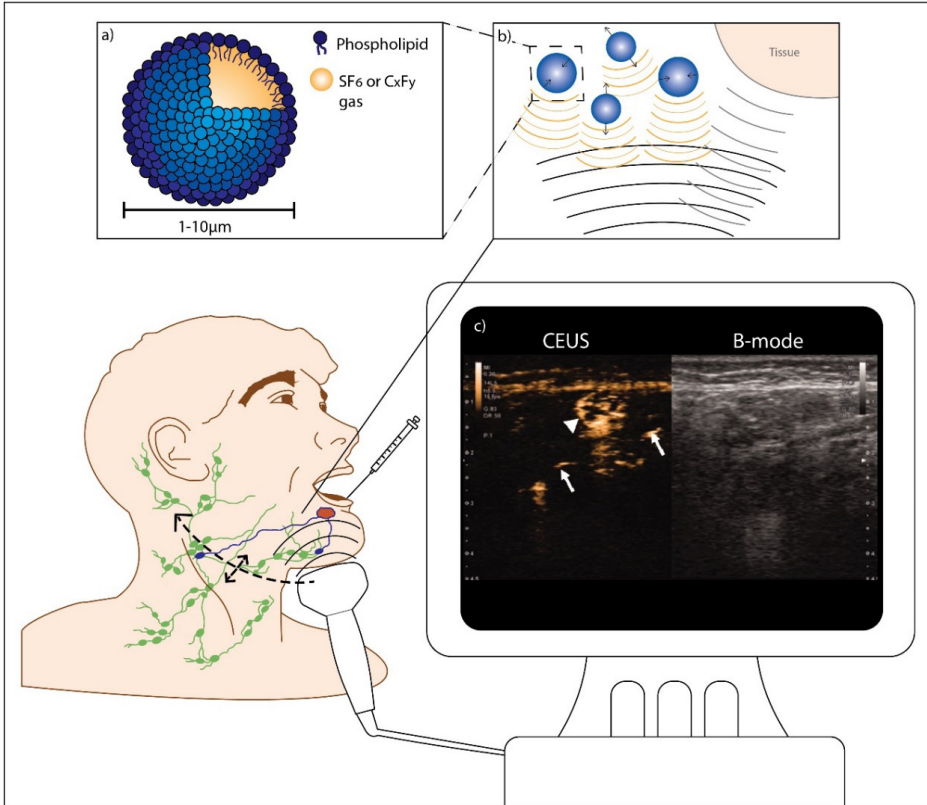
Figure 7. Contrast-enhanced lymphosonography in oral cancer. After microbubble injection at one or multiple peritumoral locations, contrast-enhancement of the injection site is visualized in ultrasound contrast mode. Using real-time imaging, the transportation of the microbubbles through lymphatic vessels may be followed until they accumulate in the sentinel lymph nodes. Subsequently, the neck is scanned for additional contrast-enhanced lymph nodes. Contrast-enhanced lymph nodes can be either marked for surgical resection or

directly subjected to biopsy or aspiration cytology. Peritumoral injections can be repeated if necessary. (**a**) Schematic representation of a microbubble; (**b**) Principle of contrast-enhanced ultrasound (CEUS): oscillating microbubbles produce strong nonlinear scattering which can be distinguished from scattering by the surrounding tissue; (**c**) Contrast-enhanced ultrasonography with Sonazoid. On the left half is a contrast-enhanced image, and on the right is the B-mode image. Contrast-enhancement of sentinel lymph nodes (SLNs) (arrowheads) was observed concomitant with lymphatic ducts (arrows) draining the nodes. (Adapted with permission from [81], copyright 2019 Taylor & Francis Group: license number: 4810090088685).

DISCUSSION

This paper reviewed new developments in preoperative SLN imaging techniques in patients with early-stage OSCC. None of the included clinical studies contradicted outcomes or clinical translation predictions from corresponding animal studies, in regard of SLN identification using these novel techniques [26,29–33,37–41,54–60,62,63,65–68]. The overall reported rate of patients in which SLNs were identified using the presented techniques ranged from 89–100%. The overall reported sensitivity ranged from 56–91%, with a NPV of 67–96% (Table 1).

Although the diagnostic accuracy of most presented techniques appears to be inferior to conventional lymphoscintigraphy including SPECT-CT, there are several promising advantages to the presented preoperative SLN imaging techniques which will be discussed individually in the subsections below. Accordingly, drawbacks of the presented techniques and methodology of the included studies will be discussed as well. While other (head and neck) tumor sites were not included in this review, the discussed strengths and flaws of performing SLNB using these techniques may also be relevant to other (head and neck) tumor sites. A summary of relative merits and disadvantages for each technique is listed in Table 2.

MR Lymphography

Bae et al. showed that MR lymphography using gadobutrol, is a promising technique for SLN detection in early-stage OSCC, with a sensitivity of 90.9%, a NPV of 92.8% and lymphatic vessel visualization in 81% of patients [26].

The high spatial resolution, high signal-to-noise ratio and few artifacts that MR lymphography with gadolinium-based contrast agents provides, even when compared to MR lymphography with SPIO, is the foremost asset of this technique [35,40,86–88]. These features result in accurate anatomical detail and facilitate visualization of lymphatic vessels, which is helpful in assessing whether a contrast-enhanced lymph node is a true SLN or a higher echelon node (HEN) [73]. Moreover, the high spatial resolution of MR lymphography eliminates the shine-through phenomenon, allowing identification of SLNs in vicinity of the tracer injection site. Additionally, MR lymphography is free of radiation exposure and does not require radioisotopes, which is of particular benefit if specific nuclear medicine facilities are unavailable [89,90].

6

Table 2. Merits and drawbacks per technique.

Technique	Advantages	Drawbacks
Conventional lymphoscintigraphy & SPECT-CT	Widely investigated and implemented Allows intraoperative localization of depicted SLNs Differentiation in intensity of radioactive signal Allows (intraoperative) differentiation between SLNs and HENs	Subject to shine-through phenomenon Requires nuclear facilities Low spatial resolution (~5 mm) Poor soft tissue contrast
MR Lymphography (Gd^{3+})	High spatial resolution (~1 mm) High signal-to-noise ratio and few artifacts Accurate anatomical detail Eliminates shine-through phenomenon Visualization lymphatic vessels May facilitate more targeted radiotherapy No nuclear facilities required Free of radiation exposure	Lacks intraoperative localization of depicted SLNs Rapid lymphatic transportation tracer No retention of tracer in SLNs Gd^{3+}based contrast agents not registered for lymphography
MR Lymphography (SPIO)	High spatial resolution (~1 mm) Accurate anatomical detail Allows intraoperative localization of depicted SLNs Eliminates shine-through phenomenon May facilitate more targeted radiotherapy No nuclear facilities required Free of radiation exposure	Limited clinical experience in OSCC Retention in SLNs depends on particle size Excess amounts of iron leads to signal voids Negative contrast may confound effectivity SLN detection Local inflammation following administration Metal elements interfere with magnetometer
CT Lymphography	High spatial resolution (~0.5 mm) High temporal resolution Eliminates shine-through phenomenon Visualization lymphatic vessels Visualization of lingual SLNs May facilitate more targeted radiotherapy No nuclear facilities required Widely available and low costs	Lacks intraoperative localization of depicted SLNs Rapid lymphatic transportation tracer No retention of tracer in SLNs Prone to artifacts Poor soft tissue contrast
PET lymphoscintigraphy	High spatial resolution (~2 mm) High temporal resolution Diminishes shine-through phenomenon Visualization lymphatic vessels Visualization of lingual SLNs Differentiation in intensity of radioactive signal Can be performed with known radiotracers Tri-model agent: IRD-800CW-[^{68}Ga]-[^{99m}Tc]-tracer Allows intraoperative localization of depicted SLNs	Requires nuclear facilities Poor intraoperative localization of SLNs with PET-probe Poor soft tissue contrast
Contrast-enhanced lymphosonography	Good safety profile of microbubbles High spatial resolution (~0.5mm) High temporal resolution and real-time imaging Eliminates shine-through phenomenon Possibly no uptake of microbubbles in HENs Can be combined with USgFNA May be extended to other head and neck sites Widely available and low costs Free of radiation exposure	Limited clinical experience in OSCC Suspected low reproducibility High operator dependency Rapid lymphatic transportation tracer Challenging to mark SLNs for biopsy

SPECT-CT; single photon emission computed tomography - computed tomography, SLN; sentinel lymph node, HEN; higher echelon node, MR; magnetic resonance, Gd^{3+}; gadolinium, SPIO; superparamagnetic iron oxide, OSCC; oral squamous cell carcinoma, CT; computed tomography, PET; positron emission tomography, IRD; infrared dye, ^{68}Ga; gallium-68, ^{99m}Tc; technetium-99m, USgFNA; ultrasound guided fine-needle aspiration.

Nevertheless, the low molecular weight of gadolinium-based contrast agents result in rapid lymphatic transportation, little retention in SLNs and rapid washout of the contrast agent [33,91]. This could increase the risk to overlook SLNs and of contrast-enhanced HEN(s) to erroneously being considered SLN(s). Since Bae et al. performed elective neck dissection in all patients, used only histopathological examination of the neck dissection specimen as reference standard and did not report any follow-up results (e.g., nodal recurrence), it is uncertain whether SLNs were overlooked with this technique [26]. Therefore, the diagnostic accuracy of SLNB using MR lymphography with gadolinium-based contrast agents in early-stage OSCC patients is yet to be established in larger studies with histopathological examination and follow-up as reference standard.

In addition, MR lymphography with gadolinium-based contrast agents cannot be performed when MRI or administration of these agents is contraindicated [89]. Besides, gadolinium-based contrast agents are not registered for lymphography and clinical trials on MR lymphography using these contrast agents are required before this technique can be implemented in routine clinical care.

Moreover, it is important to note that gadolinium-based contrast agents cannot be detected intraoperatively. The solution offered by Bae et al. [26], i.e., injection of identified SLNs with blue dye, is probably not reliable enough to assess whether the observed SLNs depicted on MR lymphography exactly matched the same nodes in the neck dissection specimen. A proposed alternative for intraoperative localization of SLNs is fluorescence guided surgery following peritumoral injection of ICG [92,93]. However, due to limited tissue penetration of the fluorescent signal and rapid flow through lymphatics of unbound ICG, matching of preoperative depicted SLNs and intraoperative fluorescent lymph nodes is challenging [90].

The inability to detect gadolinium intraoperatively, may be overcome by using SPIO for MR lymphography, as SPIO can be detected by both MRI and a handheld magnetometer [37,40]. Accordingly, SPIO may facilitate intraoperative localization of preoperative depicted SLNs, while maintaining benefits of MR lymphography over other imaging modalities (Table 2). Still, a correlation between preoperatively identified SLNs on MR lymphography and intraoperative localized SLNs with the handheld magnetometer has not yet been reported for early-stage OSCC patients.

The first results of MR lymphography using SPIO are auspicious, as all identified SLNs by MR lymphography corresponded with those identified by conventional lymphoscintigraphy [40,41]. Besides, adequate differentiation of SLN from injection site was seen [40] and precise anatomical information on SLN location was acquired when fused with SPECT [41]. However, some challenges for MR lymphography with SPIO remain. First of all, both ideal SPIO particle size and amount of iron administered are still under consideration. A hydrodynamic diameter of 59 nm was considered most suitable due to its fast uptake in lymphatics, retention in SLNs and its high accumulation when compared to SPIOs with a hydrodynamic diameter of 32 nm and 111 nm [38]. Hence, Resovist (45–60 nm) and

6

Magtrace (59 nm) may be fitting candidates [37,40,41]. With respect to the volume of SPIO administered with corresponding iron quantity, a considerable difference is seen among reports [37,40,41]. While a higher concentration may assist intraoperative localization of SLNs [37], excessive concentrations of SPIO can lead to disproportionate signal voids on MR lymphography and may hamper preoperative SLN identification [87]. Vice versa, a lower concentration may benefit preoperative SLN identification [40], but may impede intraoperative localization [35]. Furthermore, the negative contrast that SPIO provides on MR lymphography, which can be induced by other factors as well (i.e., dental implants, tissue interfaces, background noise, air), may confound the efficiency of detecting SLNs [41,87,88]. Moreover, in regard of intraoperative localization of SPIO-enhanced SLNs using the magnetometer, magnetic signals deriving from metal elements (e.g., pacemakers, prosthetics, surgical instruments) interfere with the magnetometer. This can instigate some logistical issues, such as requiring plastic surgical instruments, and can even lead to a contraindication for using the magnetometer in some cases (e.g., patients with pacemakers or prosthetics) [37]. Finally, concerns were addressed concerning swelling, local inflammation and pain of the injection site following administration of SPIO, which may depend on the volume of SPIO administered [37,40]. Some reports mention a higher number of identified SLNs on MR lymphography with SPIO when compared to conventional lymphoscintigraphy and SPECT-CT, due to the better resolution of MR lymphography [35,36]. It can be debated if the higher number of identified SLNs by MR lymphography with SPIO includes not only true SLNs, but HENs as well. Since Mizokami et al. showed more enhanced lymph nodes at 24 h post-injection, which were considered HENs, the timing of MR lymphography following SPIO administration seems to be pertinent in selecting the right contrast-enhanced lymph nodes for SLNB [40]. To distinguish true SLNs from HENs, visualization of lymphatic vessels may provide a solution. However, visualization of contrast-enhanced lymphatic vessels was not reported in any of the included studies [40,41]. To enable visualization of contrast-enhanced lymphatic vessels administration of smaller SPIOs is suggested, but is criticized by their faster migration through the lymphatic system [40].

Currently, the limited number of early-stage OSCC patients who underwent MR lymphography with SPIO prevents assessment of its diagnostic accuracy. Larger studies with adequate reference standards (i.e., histopathological assessment including follow-up) should be conducted to establish the diagnostic accuracy of MR lymphography with SPIO in OSCC patients.

In conclusion, MR lymphography using gadolinium-based contrast agents may currently not offer an alternative for conventional SLNB using radiotracers, mainly due to the lack of reliable intraoperative localization of preoperatively depicted SLNs. MR lymphography with SPIO may provide a solution, as it allows for intraoperative localization of SLNs with a magnetometer. However, MR lymphography with SPIO is subject to other limitations that may confound the efficiency of preoperative detection and intraoperative

localization of SLNs. Nonetheless, MR lymphography using either contrast agent can provide precise preoperative anatomical localization and identification of SLNs, particularly in situations with close spatial relation between injection site and SLN(s). Accordingly, MR lymphography might be a valuable addition to radiotherapy planning (e.g., higher radiation dose on SLNs), by performing MR lymphography as part of MRI that is increasingly used for radiotherapy planning in head and neck cancer [94]. MR lymphography-guided nodal irradiation may improve regional control, reduce acute and late radiation-related toxicity and enhance health-related quality-of-life [95].

CT Lymphography

CT lymphography has been proposed as a high potential alternative for conventional lymphoscintigraphy, with a sensitivity ranging from 56–80% and a NPV ranging from 82–96% [54,55,57,58]. Two series reported enhanced lymphatic vessel visualization in 90% of their patients [56,58]; in two studies lingual lymph nodes were identified as SLNs using CT lymphography [56,59].

CT lymphography shares several beneficial properties with MR lymphography: high spatial resolution, visualization of lymphatic vessels and elimination of shine-through phenomenon. The latter has been demonstrated by the identification of lingual lymph nodes as SLNs using CT lymphography [56,59]. Besides, CT lymphography does not require specific nuclear facilities and is easily implemented due to the wide availability of CT and iodine-based contrast agents [57,89]. Compared to MRI, CT has lower costs and is considered more comfortable for patients [89].

Yet, challenges for CT lymphography are similar to those in MR lymphography using gadolinium-based contrast agents. First of all, iodine-based contrast agents cannot be detected intraoperatively. Most authors used fluorescence guidance with intraoperatively administered ICG for SLN localization of preoperatively depicted SLNs by CT lymphography [54–57]. As previously mentioned, matching of preoperative depicted SLNs and intraoperative fluorescent lymph nodes is challenging [90]. Secondly, the rapid lymphatic transportation, limited retention in SLNs and rapid washout of iopamidol increases the risk to overlook SLNs and of contrast-enhanced HEN(s) to erroneously being considered SLN(s). This risk has been especially emphasized by Sugiyama et al., who showed that overlooked SLNs were only marginally contrast-enhanced on CT lymphography and that iopamidol was only briefly retained in SLNs [54].

Additional challenges arise for CT lymphography, especially when compared to MR lymphography, since CT has poor soft tissue contrast and is prone to artefacts from dental amalgam or orthopedic material, if present, which may hamper adequate visualization of SLNs. Besides, CT implies radiation exposure and, although only a low volume (2 mL) is used compared to regular intravenous use, iodine-based contrast agents may induce anaphylactic reactions, contrast-induced nephropathy or thyroid dysfunction [89]. However, contrast-related adverse events did not occur in any of the included studies

6

[54–59].

Further developments regarding CT lymphography should address these limitations (i.e., dual-tracer methods, high velocity lymphatic drainage tracer, limited retention of tracer in SLNs) to improve its diagnostic accuracy for SLNB.

As an alternative for iopamidol as CT lymphographic tracer, lipiodol might be worth considering. In contrast to iopamidol, lipiodol is oil-based with higher viscosity and is registered and widely used for lymphographic purposes [96]. The higher viscosity of lipiodol might result in increased retention in SLNs and delayed tracer wash-out, possibly improving preoperative SLN detection on CT lymphography. Moreover, lipiodol has been combined with ICG as a single emulsion, which could overcome the limitations of dual tracer methods, potentially enabling reliable intraoperative localization of preoperative depicted SLNs [97]. This has yet to be investigated in a clinical trial with an adequate reference standard (i.e., histopathological examination and follow-up).

Although CT lymphography requires some further developments, it has the potential for highly accurate identification of SLNs in early-stage OSCC patients. Especially in cases where SLNs are in close vicinity to the tracer injection site. Besides, analogous to MR lymphography, CT lymphography, performed concomitantly with conventional CT imaging for radiotherapy planning, may facilitate more targeted radiotherapy and consequently improve regional control, reduce acute and late radiation-related toxicity and enhance health-related quality-of-life [94,95].

PET Lymphoscintigraphy

Heuveling et al. demonstrated the high potential of preoperative PET lymphoscintigraphy using [^{89}Zr]-labelled nanocolloid for SLN detection in OSCC patients, by visualizing all foci identified on SPECT-CT and even detecting 5 additional SLNs in vicinity of the tracer injection site. Additionally, in 80% of patients, lymphatic vessels were visualized and 2 lingual lymph nodes (7%) were identified as SLNs [73].

In correspondence with MR-and CT lymphography, the high spatial resolution of PET lymphoscintigraphy enables identification of SLNs located close to the tracer injection site, which was demonstrated by detection of 2 lingual SLNs using PET lymphoscintigraphy. Moreover, PET lymphoscintigraphy provides both high temporal resolution as well as visualization of lymphatic vessels, contributing to better differentiation between true SLNs and HENs [73].

In contrast to the other presented techniques in this review, PET lymphoscintigraphy permits the use of commonly administered tracers for SLNB (e.g., nanocolloids, tilmanocept), whose kinetics have proven to be particularly suitable for SLNB [14,98]. Moreover, Heuveling et al. achieved reliable intraoperative localization of SLNs that were preoperatively identified by PET lymphoscintigraphy, using a handheld PET-probe [71]. Consequently, this method is unaffected by limitations of dual tracer methods.

Although intraoperative localization of SLNs using a handheld PET-probe was considered

feasible, some concerns were addressed [71]. First of all, the PET-probe detected only 12/15 SLNs as identified by PET lymphoscintigraphy, which was attributed to the PET-probe's limited sensitivity, resulting in a relatively low accuracy of the procedure (i.e., sensitivity 67%; NPV 67%). Secondly, a handheld PET-probe is relatively large in size because of features necessary for detection of high-energy photons from positron emitting isotopes [71,99]. Due to the limited sensitivity and large size of the PET-probe, wider skin incisions and exploration of the neck were required for SLN localization [71]. To overcome the problems with the use of a PET-probe, a radiotracer labelled with both [^{89}Zr] and a γ-emitter (e.g., [^{99m}Tc]) could allow high-resolution preoperative PET lymphoscintigraphy and intraoperative localization of SLNs using the conventional portable γ-probe. However, due to its half-life of 78.4 h, [^{89}Zr] will interfere with the [^{99m}Tc]-signal [100]. Therefore, a positron emitting isotope with a shorter half-life is required to enable detection of the [^{99m}Tc]-signal for intraoperative localization of SLNs using the conventional portable γ-probe.

Fluorine-18 [^{18}F] is considered the ideal radioisotope for PET imaging owing to the low positron energy (0.64 MeV), providing high-resolution images. Furthermore, [^{18}F] has a half-life of only 110 min [101]. However, [^{18}F] relies on C–F bond formation and is therefore difficult to label to currently used radiotracers for SLNB (e.g., nanocolloids or tilmanocept) [102]. Recently, PET lymphoscintigraphy with interstitially injected [^{18}F]-FDG has been investigated in patients with cervical or endometrial cancer and in healthy subjects [103,104]. Hypothesized was that the small size of the tracer allows passage through channels infiltrated with tumor cells, and that its molecular function allows uptake by tumor cells, which is not achieved by any of the currently used radiotracers for SLNB [103]. In the study with cervical or uterine cancer patients, SLN mapping was successful in 80% of patients [103]. In the study with healthy subjects however, PET lymphoscintigraphy using [^{18}F]-FDG was not considered feasible due to significant tracer washout to systemic capillaries [104].

Alternatively, gallium-68 [^{68}Ga] is a good candidate due to its half-life of only 68 min and its production with a [^{68}Ga]-generator, which provides an opportunity to prepare PET-radiopharmaceuticals on site when needed [100,105]. Moreover, its chemical properties allow labelling to various diagnostic molecules [106].

Whereas labelling of nanocolloids with [^{68}Ga] is complicated, mainly due to instability of the bond between [^{68}Ga] and nanocolloids [106], [^{68}Ga] has been successfully labelled to tilmanocept [107]. Moreover, fluorescent (IRD-800CW)-labelled tilmanocept can be radiolabelled with both [^{68}Ga] and [^{99m}Tc]. The resulting tri-modal agent provides high-resolution preoperative PET-images for SLN mapping and intraoperative localization of SLNs with both a conventional portable γ-probe and fluorescence imaging [108]. This tri-model agent has been successfully tested with reliable SLN identification in animal models [109,110]. Although PET lymphoscintigraphy using this tri-model agent might provide a solution to the issues addressed for SLNB in early-stage OSCC, it is indisputable

6

that first it has to be investigated in a clinical trial with adequate reference standards.

Contrast-Enhanced Lymphosonography

Compared to conventional lymphoscintigraphy, lymphosonography has many advantages (Table 2). Importantly, microbubbles are free of ionizing radiation and have a good safety profile, which was extensively documented for intravenous administration [111–113]. Secondly, lymphosonography is not affected by the shine-through phenomenon. Furthermore, none of the studies in humans or large animals found HEN enhancement [80–85]. It is possible that this is prevented by phagocytosis of microbubbles (which was histologically confirmed in animals for Sonazoid [85]) and the size of microbubbles compared to small-molecule dyes. Another advantage is the possibility to use lymphosonography preoperatively to improve lymph node selection for USgFNA. The sensitivity of USgFNA alone ranges from 45 up to 90% [114,115]. Adding lymphosonography could lead to more true positive patients, in whom the complex SLNB procedure may be omitted. A clinical trial using the combination of lymphosonography and USgFNA preceding SLNB will have to determine the value of this technique in head and neck oncological practice. Finally, ultrasound equipment is globally widely available and its mobility provides the option to use it in the operating room. Accordingly, lymphosonography may extend the application of SLNB from OSCC to less reachable sites of the head and neck (i.e., nasopharynx, oropharynx, larynx and hypopharynx), by allowing both peritumoral injection as well as SLN identification under general anesthesia.

However, lymphosonography has some disadvantages (Table 2). Foremost, the procedure is highly operator dependent and fast (a few seconds to minutes) transportation of microbubbles through the lymphatic system can make SLN identification challenging. Therefore, experienced staff will have to be appointed and trained. Future research will need to determine interobserver variability. Furthermore, if used without FNA it might be challenging to intraoperatively localize SLNs identified with preoperative lymphosonography; a reliable system to mark the exact location of SLNs is necessary. This drawback however is valid for several preoperative SLNB imaging techniques (i.e., CT lymphography, MR lymphography), and can be circumvented by combining lymphosonography with USgFNA or by performing lymphosonography intraoperatively. Besides, further research is needed to find out which CEUS imaging method and which microbubble are most suitable. The two clinical studies report a specific contrast imaging mode at a low mechanical index (MI), thus leaving the microbubbles intact [80–83,85]. Four animal studies performed lymphosonography in the head and neck region using Sonazoid, combined with either blue dye or ICG, in swine and rabbits without tumors [82,83,85] and with Definity in dogs with spontaneously arisen tumors [84]. The studies in swine added color flow Doppler at a high (microbubble destructing) mechanical index of 1.0 to confirm the presence of microbubbles [82,83]. In dogs power Doppler with a mechanical index of 1.3 was used primarily, which produces a color flair upon

microbubble destruction [84]. To select the most suitable microbubble, it is necessary to consider practicalities: using a microbubble that quickly reaches SLNs and is retained and detectable in the SLN for a long time might increase reproducibility. SonoVue consists of SF_6 phospholipid microbubbles with a mean bubble diameter of ~2.5μm [77], while Sonazoid consists of perfluorobutane phospholipid (C_xF_y) microbubbles with a mean bubble diameter ~2.1μm [116]. In most studies the time between peritumoral administration and lymph node enhancement (transit time) was described. Although no within-study comparisons have been made and clinical studies cannot be compared directly to preclinical studies, the transit time appears to be shorter for SonoVue (10–50 s post-injection [80]), than for Sonazoid (1–11 min post-injection [82,83,85]). Sonazoid enhancement seems to persist longer, namely ≥90 min [85], versus 2–4 min with SonoVue [80]. This could explain why multiple injections were necessary to identify SLNs in the clinical study using SonoVue [80]. However, Sonazoid has not yet been approved by FDA and EMA as a US contrast agent, which could complicate its application in clinical lymphosonography trials.

To conclude, lymphosonography is a promising method, but current clinical experience in OSCC is sparse. The two published clinical studies indicate that this technique is feasible, with SLN detection rates of 80 and 92% [80,81]. Unfortunately, correlation with histopathology is still lacking: in the only study that attempted this, no metastatic lymph nodes were detected [81]. Larger studies, preferably with histopathological examination and follow-up as reference standard, are needed to determine the diagnostic accuracy (i.e., sensitivity and NPV) of this technique for SLNB in OSCC and its place in the diagnostic workflow.

MATERIALS AND METHODS

A systematic literature search for relevant English written literature published up to 25 May 2020 was conducted in the PubMed database. Search syntaxes combined synonyms and medical subject headings (MeSH) terms for both OSCC and SLNB and was performed for all imaging techniques separately (i.e., MR lymphography, CT lymphography, PET lymphoscintigraphy and contrast-enhanced lymphosonography). Subsequently, title and abstract screening was performed by four authors (R.M, J.d.M., E.N and R.d.B.). The reference lists of included studies were screened to identify any additional relevant publications. No critical appraisal of the selected literature was performed. This review adheres to the PRISMA guidelines [117].

MR Lymphography
The following keywords and MeSH terms were included for MR lymphography: ("Mouth"[MeSH]) or ("Oral") or ("Head and Neck") and ("Sentinel lymph node"[MeSH])

6

or ("Lymph") and ("Node") or ("Sentinel") and ("Node") or ("Sentinel node") and ("Lymphography"[MeSH]) or ("Lymphography") or ("Lymphangiography") and ("Magnetic resonance imaging"[MeSH] or ("Magnetic") and ("Resonance") and ("Imaging") or ("Magnetic resonance imaging") or ("MRI") or ("MR").

For magnetic detection of SLNs using superparamagnetic iron oxide, the following keywords and MeSH terms were included: ("Mouth"[MeSH]) or ("Oral") or ("Head and Neck") and ("Sentinel lymph node"[MeSH]) or ("Lymph") and ("Node") or ("Sentinel") and ("Node") or ("Sentinel node") and ("Iron"[MeSH]) or ("Iron oxide") or ("SPIO") or ("SPION") and ("Magnetics"[MeSH] or ("Magnetic") or ("Superparamagnetic") or ("superparamagnetic iron oxide").

CT Lymphography

The following keywords and MeSH terms were included for CT lymphography: ("Mouth"[MeSH]) or ("Oral") or ("Head and Neck") and ("Sentinel lymph node"[MeSH]) or ("Lymph") and ("Node") or ("Sentinel") and ("Node") or ("Sentinel node") and ("Lymphography"[MeSH]) or ("Lymphography") and ("CT") or ("Computed Tomography") or ("Computed") or ("Tomographic").

PET Lymphoscintigraphy

The following keywords and MeSH terms were included for PET lymphoscintigraphy: ("Mouth"[MeSH]) or ("Oral") or ("Head and Neck") and ("Sentinel lymph node"[MeSH]) or ("Sentinel lymph node") or ("Sentinel") and ("Node") or ("Sentinel node") and ("Positron Emission Tomography Computed Tomography"[MeSH]) or ("Positron-Emission Tomography"[MeSH]) or ("PET") or ("Positron") or ("PET/CT") or ("PET-CT").

Contrast-Enhanced Lymphosonography

The following keywords and MeSH terms were included for contrast-enhanced ultrasound lymphography: ("Mouth"[MeSH]) or ("Oral") or ("Head and Neck") and ("Sentinel lymph node"[MeSH]) or ("Sentinel lymph node") or ("Sentinel") and ("Node") or ("Sentinel node") and ("Contrast-enhanced") or ("Contrast-assisted") or ("CEUS") or ("Microbubbles") or ("Sonovue") or ("Sonazoid") or ("Optison") or ("Levovist") or ("Imagent") or ("Imavist") or ("Definity") and ("Diagnostic Imaging") or ("Diagnostic") and ("Imaging") or ("Ultrasound") or ("Ultrasonography"[MeSH]) or ("Ultrasonography") or ("Ultrasonics"[MeSH]) or ("Ultrasonics").

CONCLUSIONS

Novel diagnostic imaging techniques for detection of SLNs have the potential to bring the diagnostic accuracy of SLNB to a higher level for all early-stage OSCC subsites.

However, technical improvements and further research of these novel techniques are required, if they are to replace the conventional SLNB procedure with [^{99m}Tc]-labelled radiotracers. Nevertheless, several of these novel techniques may already become valuable by facilitating more targeted radiotherapy; adjusting the radiation dose based on the tumor's individual lymphatic drainage pattern.

AUTHOR CONTRIBUTIONS

Conceptualization, R.M., B.d.K. and R.d.B.; methodology R.M., J.d.M., E.N. and R.d.B.; validation, B.d.K., R.d.B., R.D., C.M., L.A. and B.t.H.; formal analysis, R.M., J.d.M. and E.N.; investigation R.M., J.d.M. and E.N.; writing—original draft preparation, R.M., J.d.M., E.N., B.d.K. and R.d.B.; writing—review and editing, B.d.K., R.d.B., R.D., C.M., L.A. and B.t.H.; visualization, R.M., J.d.M., E.N. and B.d.K.; supervision B.d.K., R.d.B., R.D., C.M., L.A. and B.t.H.; project administration, R.M. and R.d.B. All authors have read and agreed to the published version of the manuscript.

FUNDING

CONFLICTS OF INTEREST

The authors declare no conflict of interest.

REFERENCES

1. D'Cruz, A.K.; Vaish, R.; Kapre, N.; Dandekar, M.; Gupta, S.; Hawaldar, R.; Agarwal, J.P.; Pantvaidya, G.; Chaukar, D.; Deshmukh, A.D.; et al. Elective versus Therapeutic Neck Dissection in Node-Negative Oral Cancer. *N. Engl. J. Med.* **2015**, *373*, 521–529, doi:10.1056/nejmoa1506007.

2. Abu-Ghanem, S.; Yehuda, M.; Carmel, N.-N.; Leshno, M.; Abergel, A.; Gutfeld, O.; Fliss, D.M. Elective Neck Dissection vs Observation in Early-Stage Squamous Cell Carcinoma of the Oral Tongue with No Clinically Apparent Lymph Node Metastasis in the Neck. *JAMA Otolaryngol. Neck Surg.* **2016**, *142*, 857–65, doi:10.1001/jamaoto.2016.1281.

3. De Bree, R.; Takes, R.P.; Shah, J.P.; Hamoir, M.; Kowalski, L.P.; Robbins, K.T.; Rodrigo, J.P.; Rodrigo, J.P.; Medina, J.E.; Rinaldo, A.; et al. Elective neck dissection in oral squamous cell carcinoma: Past, present and future. *Oral Oncol.* **2019**, *90*, 87–93, doi:10.1016/j.oraloncology.2019.01.016.

4. Toom, I.J.D.; Boeve, K.; Lobeek, D.; Bloemena, E.; Donswijk, M.L.; de Keizer, B.; Klop, W.M.C.; Leemans, C.; Willems, S.M.; Takes, R.P.; et al. Elective Neck Dissection or Sentinel Lymph Node Biopsy in Early Stage Oral Cavity Cancer Patients: The Dutch Experience. *Cancers* **2020**, *12*, 1783, doi:10.3390/cancers12071783.

5. Schilling, C.; Shaw, R.; Schache, A.G.; McMahon, J.; Chegini, S.; Kerawala, C.; McGurk, M. Sentinel lymph node biopsy for oral squamous cell carcinoma. Where are we now? *Br. J. Oral Maxillofac. Surg.* **2017**, *55*, 757–762, doi:10.1016/j.bjoms.2017.07.007.

6. Cramer, J.D.; Sridharan, S.; Ferris, R.L.; Duvvuri, U.; Samant, S. Sentinel Lymph Node Biopsy Versus Elective Neck Dissection for Stage I to II Oral Cavity Cancer. *Laryngoscope* **2018**, *129*, 162–169, doi:10.1002/lary.27323.

7. Schiefke, F.; Akdemir, M.; Weber, A.; Akdemir, D.; Singer, S.; Frerich, B. Function, postoperative morbidity, and quality of life after cervical sentinel node biopsy and after selective neck dissection. *Head Neck* **2009**, *31*, 503–512, doi:10.1002/hed.21001.

8. Murer, K.; Huber, G.F.; Haile, S.R.; Stoeckli, S.J. Comparison of morbidity between sentinel node biopsy and elective neck dissection for treatment of the n0 neck in patients with oral squamous cell carcinoma. *Head Neck* **2010**, *33*, 1260–1264, doi:10.1002/hed.21622.

9. Govers, T.M.; Schreuder, W.; Klop, W.; Grutters, J.P.C.; Rovers, M.; Merkx, M.A.W.; Takes, R. Quality of life after different procedures for regional control in oral cancer patients: Cross-sectional survey. *Clin. Otolaryngol.* **2016**, *41*, 228–233, doi:10.1111/coa.12502.

10. Govers, T.M.; Takes, R.P.; Karakullukcu, B.; Hannink, G.; Merkx, M.A.W.; Grutters, J.P.C.; Rovers, M. Management of the N0 neck in early stage oral squamous cell cancer: A modeling study of the cost-effectiveness. *Oral Oncol.* **2013**, *49*, 771–777, doi:10.1016/j.oraloncology.2013.05.001.

11. De Bree, R.; Nieweg, O.E. The history of sentinel node biopsy in head and neck cancer: From visualization of lymphatic vessels to sentinel nodes. *Oral Oncol.* **2015**, *51*, 819–823, doi:10.1016/j.oraloncology.2015.06.006.

12. Schilling, C.; Stoeckli, S.J.; Vigili, M.G.; de Bree, R.; Lai, S.Y.; Alvarez, J.; Christensen, A.; Cognetti, D.M.; D'Cruz, A.K.; Frerich, B.; et al. Surgical consensus guidelines on sentinel node biopsy (SNB) in patients with oral cancer. *Head Neck* **2019**, *41*, 2655–2664, doi:10.1002/hed.25739.

13. Alkureishi, L.W.T.; Burak, Z.; Alvarez, J.; Ballinger, J.; Bilde, A.; Britten, A.J.; Calabrese, L.; Chiesa, C.; Chiti, A.; de Bree, R.; et al. Joint Practice Guidelines for Radionuclide Lymphoscintigraphy for Sentinel Node Localization in Oral/Oropharyngeal Squamous Cell Carcinoma. *Ann. Surg. Oncol.* **2009**, *16*, 3190–3210, doi:10.1245/s10434-009-0726-8.

14. Giammarile, F.; Schilling, C.; Gnanasegaran, G.; Bal, C.; Oyen, W.J.G.; Rubello, D.; Schwarz, T.; Tartaglione, G.; Miller, R.N.; Paez, D.; et al. The EANM practical guidelines for sentinel lymph node localisation in oral cavity squamous cell carcinoma. *Eur. J. Nucl. Med. Mol. Imaging* **2018**, *46*, 623–637, doi:10.1007/s00259-018-4235-5.

15. Sandhu, S.V.; Dhawan, I.; Bhandari, R.; Sood, N.; Bhullar, R.K.; Sethi, N. Detection of cervical lymph node micrometastasis and isolated tumor cells in oral squamous cell carcinoma using immunohistochemistry and serial sectioning. *J. Oral Maxillofac. Pathol.* **2016**, *20*, 436–444, doi:10.4103/0973-029X.190946.

16. Liu, M.; Wang, S.J.; Yang, X.; Peng, H. Diagnostic Efficacy of Sentinel Lymph Node Biopsy in Early Oral Squamous Cell Carcinoma: A Meta-Analysis of 66 Studies. *PLoS ONE* **2017**, *12*, e0170322, doi:10.1371/journal.pone.0170322.

17. Boeve, K.; Schepman, K.; Schuuring, E.; Roodenburg, J.; de Bree, R.; Boorsma, R.; de Visscher, J.; Brouwers, A.; van der Vegt, B.; Witjes, M.J.H.; et al. High sensitivity and negative predictive value of sentinel lymph node biopsy in a retrospective early stage oral cavity cancer cohort in the Northern Netherlands. *Clin. Otolaryngol.* **2018**, doi:10.1111/coa.13107.

18. Toom, I.J.D.; Heuveling, D.; Flach, G.B.; van Weert, S.; Karagozoglu, K.H.; van Schie, A.; Bloemena, E.; Leemans, C.R.; Jansen, F. Sentinel node biopsy for early-stage oral cavity cancer: The VU University Medical Center experience. *Head Neck* **2014**, *37*, 573–578, doi:10.1002/hed.23632.

19. Alkureishi, L.W.T.; Ross, G.L.; Shoaib, T.; Soutar, D.S.; Robertson, A.G.; Thompson, R.; Hunter, K.D.; Sørensen, J.A.; Thomsen, J.B.; Krogdahl, A.; et al. Sentinel Node Biopsy in Head and Neck Squamous Cell Cancer: 5-Year Follow-Up of a European Multicenter Trial. *Ann. Surg. Oncol.* **2010**, *17*, 2459–2464, doi:10.1245/s10434-010-1111-3.

20. Pedersen, N.J.; Jensen, D.H.; Hedbäck, N.; Frendø, M.; Kiss, K.; Lelkaitis, G.; Mortensen, J.; Christensen, A.; Specht, L.; von Buchwald, C. Staging of early lymph node metastases with the sentinel lymph node technique and predictive factors in T1/T2 oral cavity cancer: A retrospective single-center study. *Head Neck* **2015**, *38*, E1033–E1040, doi:10.1002/hed.24153.

21. Stoeckli, S.J.; Huebner, T.; Huber, G.F.; Broglie, M.A. Technique for reliable sentinel node biopsy in squamous cell carcinomas of the floor of mouth. *Head Neck* **2016**, *38*, 1367–1372, doi:10.1002/hed.24440.

22. Li, C.; Meng, S.; Yang, X.; Zhou, D.; Hu, J.; Wang, J. Sentinel lymph node detection using magnetic resonance lymphography with conventional gadolinium contrast agent in breast cancer: A preliminary clinical study. *BMC Cancer* **2015**, *15*, 213, doi:10.1186/s12885-015-1255-4.

23. Lu, Q.; Hua, J.; Kassir, M.M.; DelProposto, Z.; Dai, Y.; Sun, J.; Haacke, M.; Hu, J. Imaging Lymphatic System in Breast Cancer Patients with Magnetic Resonance Lymphangiography. *PLoS ONE* **2013**, *8*, e69701, doi:10.1371/journal.pone.0069701.

24. Hong, Y.; Xiang, L.; Hu, Y.; Zhou, Z.; Yu, H.; Zhu, B. Interstitial magnetic resonance lymphography is an effective diagnostic tool for the detection of lymph node metastases in patients with cervical cancer. *BMC Cancer* **2012**, *12*, 360, doi:10.1186/1471-2407-12-360.

25. Scott, L.J. Gadobutrol: A Review in Contrast-Enhanced MRI and MRA. *Clin. Drug Investig.* **2018**, *38*, 773–784, doi:10.1007/s40261-018-0674-9.

26. Bae, S.; Lee, H.J.; Nam, W.; Koh, Y.W.; Choi, E.; Kim, J. MR lymphography for sentinel lymph node detection in patients with oral cavity cancer: Preliminary clinical study. *Head Neck* **2018**, *40*, 1483–1488, doi:10.1002/hed.25167.

27. Yang, Y.; Zhou, B.; Zhou, J.; Shi, X.; Sha, Y.; Wu, H. Assessment of lingual sentinel lymph nodes metastases using dual-modal indirect CT/MR lymphography with gold–gadolinium-based nanoprobes in a tongue VX2 carcinoma model. *Acta Oto-Laryngol.* **2018**, *138*, 727–733, doi:10.1080/00016489.2018.1441544.

28. Yang, Y.; Zhou, J.; Shi, X.; Sha, Y.; Wu, H. Long-term observation of indirect lymphography using gadolinium-loaded polyethylenimine-entrapped gold nanoparticles as a dual mode CT/MR contrast agent for rabbit lingual sentinel lymph node identification. *Acta Oto-Laryngol.* **2016**, *137*, 207–214, doi:10.1080/00016489.2016.1222550.

29. Mayer, M.N.; Kraft, S.L.; Bucy, D.S.; Waldner, C.L.; Elliot, K.M.; Wiebe, S. Indirect magnetic resonance lymphography of the head and neck of dogs using Gadofluorine M and a conventional gadolinium contrast agent: A pilot study. *Can. Vet. J.* **2012**, *53*, 1085–1090.

30. Nason, R.W.; Torchia, M.G.; Morales, C.M.; Thliveris, J. Dynamic MR lymphangiography and carbon dye for sentinel lymph node detection: A solution for sentinel lymph node biopsy in mucosal head and neck cancer. *Head Neck* **2005**, *27*, 333–338, doi:10.1002/hed.20173.

31. Torchia, M.G.; Misselwitz, B. Combined MR Lymphangiography and MR Imaging—Guided Needle Localization of Sentinel Lymph Nodes Using Gadomer-17. *Am. J. Roentgenol.* **2002**, *179*, 1561–1565, doi:10.2214/ajr.179.6.1791561.

32. Kitamura, N.; Kosuda, S.; Araki, K.; Tomifuji, M.; Mizokami, D.; Shiotani, A.; Shinmoto, H.; Fujii, H.; Ichihara, K. Comparison of animal studies between interstitial magnetic resonance lymphography and radiocolloid SPECT/CT lymphoscintigraphy in the head and neck region. *Ann. Nucl. Med.* **2012**, *26*, 281–285, doi:10.1007/s12149-011-0565-0.

33. Loo, B.W.; Draney, M.T.; Sivanandan, R.; Ruehm, S.G.; Pawlicki, T.; Xing, L.; Herfkens, R.J.; Le, Q.T. Indirect MR lymphangiography of the head and neck using conventional gadolinium contrast: A pilot study in humans. *Int. J. Radiat. Oncol.* **2006**, *66*, 462–468, doi:10.1016/j.ijrobp.2006.05.045.

34. Johnson, L.R.; Pinder, S.E.; Douek, M. Deposition of superparamagnetic iron?oxide nanoparticles in axillary sentinel lymph nodes following subcutaneous injection. *Histopathology* **2012**, *62*, 481–486, doi:10.1111/his.12019.

35. Pouw, J.; Grootendorst, M.R.; Bezooijen, R.; Klazen, C.; de Bruin, W.I.; Klaase, J.M.; Hall-Craggs, M.A.; Douek, M.; Haken, B.T. Pre-operative sentinel lymph node localization in breast cancer with superparamagnetic iron oxide MRI: The SentiMAG Multicentre Trial imaging subprotocol. *Br. J. Radiol.* **2015**, *88*, 20150634, doi:10.1259/bjr.20150634.

36. Winter, A.; Kowald, T.; Paulo, T.S.; Goos, P.; Engels, S.; Gerullis, H.; Schiffmann, J.; Chavan, A.; Wawroschek, F. Magnetic resonance sentinel lymph node imaging and magnetometer-guided intraoperative detection in prostate cancer using superparamagnetic iron oxide nanoparticles. *Int. J. Nanomed.* **2018**, *13*, 6689–6698, doi:10.2147/IJN.S173182.

37. Hernando, J.; Aguirre, P.; Aguilar-Salvatierra, A.; Leizaola-Cardesa, I.O.; Bidaguren, A.; Gómez-Moreno, G. Magnetic detection of sentinel nodes in oral squamous cell carcinoma by means of superparamagnetic iron oxide contrast. *J. Surg. Oncol.* **2019**, *121*, 244–248, doi:10.1002/jso.25810.

38. Pouw, J.J.; Ahmed, M.; Anninga, B.; Schuurman, K.; Pinder, S.E.; van Hemelrijck, M.; Pankhurst, Q.A.; Douek, M.; Haken, B.T. Comparison of three magnetic nanoparticle tracers for sentinel lymph node biopsy in an in vivo porcine model. *Int. J. Nanomed.* **2015**, *10*, 1235–1243, doi:10.2147/IJN.S76962.

39. Torchia, M.G.; Nason, R.; Danzinger, R.; Lewis, J.M.; Thliveris, J.A. Interstitial MR lymphangiography for the detection of sentinel lymph nodes. *J. Surg. Oncol.* **2001**, *78*, 151–156, doi:10.1002/jso.1139.

6

40. Mizokami, D.; Kosuda, S.; Tomifuji, M.; Araki, K.; Yamashita, T.; Shinmoto, H.; Shiotani, A. Superparamagnetic iron oxide-enhanced interstitial magnetic resonance lymphography to detect a sentinel lymph node in tongue cancer patients. *Acta Oto-Laryngol.* **2012**, *133*, 418–423, doi:10.3109/00016489.2012.744143.

41. Maza, S.; Taupitz, M.; Taymoorian, K.; Winzer, K.J.; Rückert, J.; Paschen, C.; Räber, G.; Schneider, S.; Trefzer, U.; Munz, D.L. Multimodal fusion imaging ensemble for targeted sentinel lymph node management: Initial results of an innovative promising approach for anatomically difficult lymphatic drainage in different tumour entities. *Eur. J. Nucl. Med. Mol. Imaging* **2006**, *34*, 378–383, doi:10.1007/s00259-006-0223-2.

42. Suga, K.; Ogasawara, N.; Okada, M.; Matsunaga, N. Interstitial CT lymphography-guided localization of breast sentinel lymph node: Preliminary results. *Surgery* **2003**, *133*, 170–179, doi:10.1067/msy.2003.17.

43. Tangoku, A.; Yamamoto, S.; Suga, K.; Ueda, K.; Nagashima, Y.; Hida, M.; Sato, T.; Sakamoto, K.; Oka, M. Sentinel lymph node biopsy using computed tomography–lymphography in patients with breast cancer. *Surgery* **2004**, *135*, 258–265, doi:10.1016/j.surg.2003.07.003.

44. Yamamoto, S.; Suga, K.; Maeda, K.; Maeda, N.; Yoshimura, K.; Oka, M. Breast sentinel lymph node navigation with three-dimensional computed tomography–lymphography: A 12-year study. *Breast Cancer* **2015**, *23*, 456–462, doi:10.1007/s12282-015-0584-0.

45. Nakagawa, M.; Morimoto, M.; Takechi, H.; Tadokoro, Y.; Tangoku, A. Preoperative diagnosis of sentinel lymph node (SLN) metastasis using 3D CT lymphography (CTLG). *Breast Cancer* **2015**, *23*, 519–524, doi:10.1007/s12282-015-0597-8.

46. Sugi, K.; Kitada, K.; Yoshino, M.; Hirazawa, K.; Matsuda, E.; Azuma, T.; Umemori, Y. New Method of Visualizing Lymphatics in Lung Cancer Patients by Multidetector Computed Tomography. *J. Comput. Assist. Tomogr.* **2005**, *29*, 210–214, doi:10.1097/01.rct.0000154241.22519.2f.

47. Takizawa, H.; Kondo, K.; Toba, H.; Kajiura, K.; Ali, A.H.K.; Sakiyama, S.; Tangoku, A. Computed tomography lymphography by transbronchial injection of iopamidol to identify sentinel nodes in preoperative patients with non–small cell lung cancer: A pilot study. *J. Thorac. Cardiovasc. Surg.* **2012**, *144*, 94–99, doi:10.1016/j.jtcvs.2012.03.040.

48. Hayashi, H.; Tangoku, A.; Suga, K.; Shimizu, K.; Ueda, K.; Yoshino, S.; Abe, T.; Sato, T.; Matsunaga, N.; Oka, M. CT lymphography-navigated sentinel lymph node biopsy in patients with superficial esophageal cancer. *Surgery* **2006**, *139*, 224–235, doi:10.1016/j.surg.2005.07.027.

49. Yuasa, Y.; Seike, J.; Yoshida, T.; Takechi, H.; Yamai, H.; Yamamoto, Y.; Furukita, Y.; Goto, M.; Minato, T.; Nishino, T.; et al. Sentinel Lymph Node Biopsy using Intraoperative Indocyanine Green Fluorescence Imaging Navigated with Preoperative CT Lymphography for Superficial Esophageal Cancer. *Ann. Surg. Oncol.* **2011**, *19*, 486–493, doi:10.1245/s10434-011-1922-x.

50. Filip, B.; Scarpa, M.; Cavallin, F.; Alfieri, R.; Cagol, M.; Castoro, C. Minimally invasive surgery for esophageal cancer: A review on sentinel node concept. *Surg. Endosc.* **2013**, *28*, 1238–1249, doi:10.1007/s00464-013-3314-8.

51. Lee, J.H.; Park, D.J.; Kim, Y.H.; Shin, C.M.; Lee, H.S.; Kim, H.-H. Clinical Implementations of Preoperative Computed Tomography Lymphography in Gastric Cancer: A Comparison with Dual Tracer Methods in Sentinel Node Navigation Surgery. *Ann. Surg. Oncol.* **2013**, *20*, 2296–2303, doi:10.1245/s10434-012-2855-8.

52. Kim, Y.H.; Lee, Y.J.; Park, J.H.; Lee, K.H.; Lee, H.S.; Park, Y.S.; Park, D.J.; Kim, H.-H. Early Gastric Cancer: Feasibility of CT Lymphography with Ethiodized Oil for Sentinel Node Mapping. *Radiology* **2013**, *267*, 414–421, doi:10.1148/radiol.12121527.

53. Yasuta, M.; Sato, S.; Ishida, T.; Kiyohara, T. Usefulness of CT-lymphography in sentinel lymph node navigation. *Int. J. Clin. Oncol.* **2013**, *19*, 557–562, doi:10.1007/s10147-013-0582-1.

54. Sugiyama, S.; Iwai, T.; Izumi, T.; Baba, J.; Oguri, S.; Hirota, M.; Mitsudo, K. Sentinel lymph node mapping of clinically N0 early oral cancer: A diagnostic pitfall on CT lymphography. *Oral Radiol.* **2020**, 1–5, doi:10.1007/s11282-020-00442-1.

55. Ishiguro, K.; Iwai, T.; Izumi, T.; Sugiyama, S.; Baba, J.; Oguri, S.; Hirota, M.; Mitsudo, K. Sentinel lymph node biopsy with preoperative CT lymphography and intraoperative indocyanine green fluorescence imaging for N0 early tongue cancer: A long-term follow-up study. *J. Cranio-Maxillofac. Surg.* **2020**, *48*, 217–222, doi:10.1016/j.jcms.2020.01.007.

56. Sugiyama, S.; Iwai, T.; Izumi, T.; Ishiguro, K.; Baba, J.; Oguri, S.; Mitsudo, K. CT lymphography for sentinel lymph node mapping of clinically N0 early oral cancer. *Cancer Imaging* **2019**, *19*, 72, doi:10.1186/s40644-019-0258-9.

57. Honda, K.; Ishiyama, K.; Suzuki, S.; Kawasaki, Y.; Saito, H.; Horii, A. Sentinel Lymph Node Biopsy using Preoperative Computed Tomographic Lymphography and Intraoperative Indocyanine Green Fluorescence Imaging in Patients with Localized Tongue Cancer. *JAMA Otolaryngol. Neck Surg.* **2019**, *145*, 735–740, doi:10.1001/jamaoto.2019.1243.

58. Honda, K.; Ishiyama, K.; Suzuki, S.; Oumi, E.; Sato, T.; Kawasaki, Y.; Saito, H.; Ishikawa, K. Sentinel lymph node biopsy using computed tomographic lymphography in patients with early tongue cancer. *Acta Oto-Laryngol.* **2015**, *135*, 507–512, doi:10.3109/00016489.2015.1010126.

59. Saito, M.; Nishiyama, H.; Oda, Y.; Shingaki, S.; Hayashi, T. The lingual lymph node identified as a sentinel node on CT lymphography in a patient with cN0 squamous cell carcinoma of the tongue. *Dentomaxillofacial Radiol.* **2012**, *41*, 254–258, doi:10.1259/dmfr/61883763.

60. Randall, E.K.; Jones, M.D.; Kraft, S.L.; Worley, D.R. The Development of an Indirect CT Lymphography Protocol for Sentinel Lymph Node Detection in Head and Neck Cancer and Comparison to Other Sentinel Lymph Node Mapping Techniques. *Vet. Comp. Oncol.* **2020**, doi:10.1111/vco.12585.

61. Shi, F.; Yang, Y.; Chen, J.; Sha, Y.; Shu, Y.; Wu, H. Dendrimer-Entrapped Gold Nanoparticles as Potential CT Contrast Agents for Localizing Sentinel Lymph Node via Indirect CT Lymphography on Rabbit Model. *BioMed Res. Int.* **2018**, *2018*, 1–6, doi:10.1155/2018/1230151.

62. Rossi, F.; Körner, M.; Suárez, J.; Carozzi, G.; Meier, V.; Roos, M.; Bley, C.R. Computed tomographic-lymphography as a complementary technique for lymph node staging in dogs with malignant tumors of various sites. *Vet. Radiol. Ultrasound* **2017**, *59*, 155–162, doi:10.1111/vru.12569.

63. Grimes, J.A.; Secrest, S.A.; Northrup, N.; Saba, C.F.; Schmiedt, C.W. Indirect computed tomography lymphangiography with aqueous contrast for evaluation of sentinel lymph nodes in dogs with tumors of the head. *Vet. Radiol. Ultrasound* **2017**, *58*, 559–564, doi:10.1111/vru.12514.

64. Yang, Y.; Shi, F.; Zhou, J.; Shi, X.; Sha, Y.; Wu, H. Short-Term Dynamic Observation of the Color Change and Enhancement Effect of Polyethylenimine-Entrapped Gold Nanoparticles used for Indirect Lymphography. *ORL* **2016**, *78*, 136–143, doi:10.1159/000446190.

65. Shu, Y.; Xu, X.; Wang, Z.; Dai, W.; Zhang, Y.; Yu, Y.; Sha, Y.; Wu, H. Assessment of cervical lymph node metastases using indirect computed tomography lymphography with iopamidol in a tongue VX2 carcinoma model. *J. Laryngol. Otol.* **2011**, *125*, 820–828, doi:10.1017/s0022215111000958.

66. Shu, Y.; Xu, X.; Chodara, A.M.; Regner, M.F.; Sha, Y.; Jiang, J.J.; Xiang, M.; Wu, H. Correlative study of indirect computed tomography lymphography using iopamidol and histopathology in a cervical lymph node metastasis model. *Laryngoscope* **2011**, *121*, 724–731, doi:10.1002/lary.21404.

67. Wu, H.; Ying, H.; Xi, X.; Shen, N.; Shu, Y.; Hoffman, M.R.; Rieves, A.; Sha, Y.; Zhou, L. Localization of the sentinel lymph node in tongue VX2 carcinoma via indirect CT lymphography combined with methylene blue dye injection. *Acta Oto-Laryngol.* **2009**, *130*, 503–510, doi:10.3109/00016480903253595.

68. Wu, H.; Xu, X.; Ying, H.; Hoffman, M.; Shen, N.; Sha, Y.; Zhou, L. Preliminary study of indirect CT lymphography-guided sentinel lymph node biopsy in a tongue VX2 carcinoma model. *Int. J. Oral Maxillofac. Surg.* **2009**, *38*, 1268–1272, doi:10.1016/j.ijom.2009.07.009.

69. Rahmim, A.; Zaidi, H. PET versus SPECT: Strengths, limitations and challenges. *Nucl. Med. Commun.* **2008**, *29*, 193–207, doi:10.1097/mnm.0b013e3282f3a515.

70. Wadsak, W.; Mitterhauser, M. Basics and principles of radiopharmaceuticals for PET/CT. *Eur. J. Radiol.* **2010**, *73*, 461–469, doi:10.1016/j.ejrad.2009.12.022.

71. Heuveling, D.A.; Karagozoglu, K.H.; van Lingen, A.; Hoekstra, O.S.; van Dongen, G.A.M.S.; de Bree, R. Feasibility of intraoperative detection of sentinel lymph nodes with 89-zirconium-labelled nanocolloidal albumin PET-CT and a handheld high-energy gamma probe. *EJNMMI Res.* **2018**, *8*, 15, doi:10.1186/s13550-018-0368-6.

72. Bluemel, C.; Rubello, D.; Colletti, P.M.; de Bree, R.; Herrmann, K. Sentinel lymph node biopsy in oral and oropharyngeal squamous cell carcinoma: Current status and unresolved challenges. *Eur. J. Nucl. Med. Mol. Imaging* **2015**, *42*, 1469–1480, doi:10.1007/s00259-015-3049-y.

73. Heuveling, D.A.; van Schie, A.; Vugts, D.J.; Hendrikse, N.H.; Yaqub, M.; Hoekstra, O.S.; Karagozoglu, K.; Leemans, C.R.; van Dongen, G.A.M.S.; de Bree, R. Pilot Study on the Feasibility of PET/CT Lymphoscintigraphy with 89Zr-Nanocolloidal Albumin for Sentinel Node Identification in Oral Cancer Patients. *J. Nucl. Med.* **2013**, *54*, 585–589, doi:10.2967/jnumed.112.115188.

74. Heuveling, D.A.; Visser, G.W.; Baclayon, M.; Roos, W.; Wuite, G.J.; Hoekstra, O.S.; Leemans, C.R.; de Bree, R.; van Dongen, G.A.M.S. 89Zr-Nanocolloidal Albumin-Based PET/CT Lymphoscintigraphy for Sentinel Node Detection in Head and Neck Cancer: Preclinical Results. *J. Nucl. Med.* **2011**, *52*, 1580–1584, doi:10.2967/jnumed.111.089557.

75. Chong, W.K.; Papadopoulou, V.; Dayton, P.A. Imaging with ultrasound contrast agents: Current status and future. *Abdom. Radiol.* **2018**, *43*, 762–772, doi:10.1007/s00261-018-1516-1.

76. Frinking, P.; Segers, T.; Luan, Y.; Tranquart, F. Three Decades of Ultrasound Contrast Agents: A Review of the Past, Present and Future Improvements. *Ultrasound Med. Biol.* **2020**, *46*, 892–908, doi:10.1016/j.ultrasmedbio.2019.12.008.

77. Greis, C. Technology overview: SonoVue. *Eur. Radiol. Suppl.* **2004**, *14*, P11–P15, doi:10.1007/s10406-004-0076-3.

78. Moody, A.N.; Bull, J.; Culpan, A.M.; Munyombwe, T.; Sharma, N.; Whitaker, M.; Wolstenhulme, S. Preoperative sentinel lymph node identification, biopsy and localisation using contrast enhanced ultrasound (CEUS) in patients with breast cancer: A systematic review and meta-analysis. *Clin. Radiol.* **2017**, *72*, 959–971, doi:10.1016/j.crad.2017.06.121.

79. Machado, P.; Stanczak, M.; Liu, J.; Moore, J.N.; Eisenbrey, J.R.; Needleman, L.; Kraft, W.K.; Forsberg, F. Subdermal Ultrasound Contrast Agent Injection for Sentinel Lymph Node Identification: An Analysis of Safety and Contrast Agent Dose in Healthy Volunteers. *J. Ultrasound Med.* **2017**, *37*, 1611–1620, doi:10.1002/jum.14502.

80. Gvetadze, S.R.; Xiong, P.; Lv, M.; Li, J.; Hu, J.; Ilkaev, K.D.; Yang, X.; Sun, J. Contrast-enhanced ultrasound mapping of sentinel lymph nodes in oral tongue cancer—a pilot study. *Dentomaxillofacial Radiol.* **2017**, *46*, 20160345, doi:10.1259/dmfr.20160345.

6

81.	Wakisaka, N.; Endo, K.; Kitazawa, T.; Shimode, Y.; Kato, K.; Moriyama-Kita, M.; Koda, W.; Ikeda, H.; Ishikawa, K.; Ueno, T.; et al. Detection of sentinel lymph node using contrast-enhanced agent, Sonazoid™, and evaluation of its metastasis with superb microvascular imaging in oral and oropharyngeal cancers: A preliminary clinical study. *Acta Oto-Laryngol.* **2019**, *139*, 94–99, doi:10.1080/00016489.2018.1535193.

82.	Curry, J.M.; Bloedon, E.; Malloy, K.M.; Cognetti, D.M.; Merton, D.A.; Goldberg, B.B.; Keane, W.M.; Rosen, D.; Pribitkin, E.A. Ultrasound-guided contrast-enhanced sentinel node biopsy of the head and neck in a porcine model. *Otolaryngol. Neck Surg.* **2007**, *137*, 735–741, doi:10.1016/j.otohns.2007.07.019.

83.	Curry, J.M.; Grindle, C.R.; Merton, D.A.; Goldberg, B.B.; Rosen, D.; Pribitkin, E.A. Lymphosonographic Sentinel node Biopsy of the Supraglottis in a Swine Model. *Otolaryngol. Neck Surg.* **2008**, *139*, 798–804, doi:10.1016/j.otohns.2008.08.029.

84.	Lurie, D.M.; Seguin, B.; Schneider, P.D.; Verstraete, F.J.; Wisner, E.R. Contrast-Assisted Ultrasound for Sentinel Lymph Node Detection in Spontaneously Arising Canine Head and Neck Tumors. *Investig. Radiol.* **2006**, *41*, 415–421, doi:10.1097/01.rli.0000201230.29925.95.

85.	Kogashiwa, Y.; Sakurai, H.; Akimoto, Y.; Sato, D.; Ikeda, T.; Matsumoto, Y.; Moro, Y.; Kimura, T.; Hamanoue, Y.; Nakamura, T.; et al. Sentinel Node Biopsy for the Head and Neck Using Contrast-Enhanced Ultrasonography Combined with Indocyanine Green Fluorescence in Animal Models: A Feasibility Study. *PLoS ONE* **2015**, *10*, e0132511, doi:10.1371/journal.pone.0132511.

86.	Choi, S.H.; Moon, W.K. Contrast-Enhanced MR Imaging of Lymph Nodes in Cancer Patients. *Korean J. Radiol.* **2010**, *11*, 383–394, doi:10.3348/kjr.2010.11.4.383.

87.	Liu, T.; Spincemaille, P.; de Rochefort, L.; Wong, R.; Prince, M.; Wang, Y. Unambiguous identification of superparamagnetic iron oxide particles through quantitative susceptibility mapping of the nonlinear response to magnetic fields. *Magn. Reson. Imaging* **2010**, *28*, 1383–1389, doi:10.1016/j.mri.2010.06.011.

88.	Lin, C.; Cai, S.; Feng, J. Positive Contrast Imaging of SPIO Nanoparticles. *J. Nanomater.* **2012**, *2012*, 1–9, doi:10.1155/2012/734842.

89.	Vogel, D.W.T.; Thoeny, H.C. Cross-sectional imaging in cancers of the head and neck: How we review and report. *Cancer Imaging* **2016**, *16*, 1–15, doi:10.1186/s40644-016-0075-3.

90.	De Bree, R.; Dankbaar, J.W.; de Keizer, B. New Developments in Sentinel Lymph Node Biopsy Procedure in Localized Oral Cancer. *JAMA Otolaryngol. Neck Surg.* **2019**, *145*, 741, doi:10.1001/jamaoto.2019.1342.

91.	Bisso, S.; Degrassi, A.; Brambilla, D.; Leroux, J.C. Poly(ethylene glycol)-alendronate coated nanoparticles for magnetic resonance imaging of lymph nodes. *J. Drug Target.* **2018**, *27*, 659–669, doi:10.1080/1061186x.2018.1545235.

92.	Nakamura, T.; Kogashiwa, Y.; Nagafuji, H.; Yamauchi, K.; Kohno, N. Validity of sentinel lymph node biopsy by ICG fluorescence for early head and neck cancer. *Anticancer. Res.* **2015**, *35*, 1669–1674

93.	Peng, H.; Wang, S.J.; Niu, X.; Yang, X.; Chi, C.; Zhang, G. Sentinel node biopsy using indocyanine green in oral/oropharyngeal cancer. *World J. Surg. Oncol.* **2015**, *13*, 1–7, doi:10.1186/s12957-015-0691-6.

94.	Wong, K.H.; Panek, R.; Bhide, S.; Nutting, C.M.; Harrington, K.J.; Newbold, K. The emerging potential of magnetic resonance imaging in personalizing radiotherapy for head and neck cancer: An oncologist's perspective. *Br. J. Radiol.* **2017**, *90*, 20160768, doi:10.1259/bjr.20160768.

95.	Mestdagh, P.D.D.V.; Walraven, I.; Vogel, W.V.; Schreuder, W.H.; van Werkhoven, E.; Carbaat, C.; Donswijk, M.L.; Brekel, M.W.V.D.; Al-Mamgani, A. SPECT/CT-guided elective nodal irradiation for head and neck cancer is oncologically safe and less toxic: A potentially practice-changing approach. *Radiother. Oncol.* **2020**, *147*, 56–63, doi:10.1016/j.radonc.2020.03.012.

96.	Pieper, C.C.; Hur, S.; Sommer, C.-M.; Nadolski, G.; Maleux, G.; Kim, J.; Itkin, M. Back to the Future. *Investig. Radiol.* **2019**, *54*, 600–615, doi:10.1097/rli.0000000000000578.

97.	Kim, H.; Kil Lee, S.; Kim, Y.M.; Lee, E.H.; Lim, S.J.; Kim, S.H.; Yang, J.; Lim, J.S.; Hyung, W.J. Fluorescent Iodized Emulsion for Pre- and Intraoperative Sentinel Lymph Node Imaging: Validation in a Preclinical Model. *Radiology* **2015**, *275*, 196–204, doi:10.1148/radiol.14141159.

98.	Wallace, A.M.; Hoh, C.K.; Ellner, S.J.; Darrah, D.D.; Schulteis, G.; Vera, D.R. Lymphoseek: A Molecular Imaging Agent for Melanoma Sentinel Lymph Node Mapping. *Ann. Surg. Oncol.* **2006**, *14*, 913–921, doi:10.1245/s10434-006-9099-4.

99.	Gulec, S.A. PET probe-guided surgery. *J. Surg. Oncol.* **2007**, *96*, 353–357, doi:10.1002/jso.20862.

100.	Kasbollah, A.; Eu, P.; Cowell, S.; Deb, P. Review on Production of 89Zr in a Medical Cyclotron for PET Radiopharmaceuticals. *J. Nucl. Med. Technol.* **2013**, *41*, 35–41, doi:10.2967/jnmt.112.111377.

101.	Couturier, O.; Vuillez, J.-P.; Rigo, P.; Hustinx, R. Fluorinated tracers for imaging cancer with positron emission tomography. *Eur. J. Nucl. Med. Mol. Imaging* **2004**, *31*, 1182–1206, doi:10.1007/s00259-004-1607-9.

102.	Ting, R.; Aguilera, T.A.; Crisp, J.L.; Hall, D.J.; Eckelman, W.C.; Vera, D.R.; Tsien, R.Y. Fast18F Labeling of a Near-Infrared Fluorophore Enables Positron Emission Tomography and Optical Imaging of Sentinel Lymph Nodes. *Bioconjugate Chem.* **2010**, *21*, 1811–1819, doi:10.1021/bc1001328.

103.	Mueller, J.J.; Dauer, L.T.; Murali, R.; Iasonos, A.; Pandit-Taskar, N.; Abu-Rustum, N.R.; Grimm, J. Positron Lymphography via Intracervical 18F-FDG Injection for Presurgical Lymphatic Mapping in Cervical and Endometrial Malignancies. *J. Nucl. Med.* **2020**, *61*, 1123–1130, doi:10.2967/jnumed.119.230714.

104.	Jensen, M.R.; Simonsen, L.; Lonsdale, M.N.; Bülow, J. Foot skin depots of 18F-fluorodeoxyglucose do not

6

enable PET/CT lymphography of the lower extremity lymphatic system in man. *EJNMMI Res.* **2013**, *3*, 17, doi:10.1186/2191-219X-3-17.

105. Martiniova, L.; de Palatis, L.; Etchebehere, E.; Ravizzini, G. Gallium-68 in Medical Imaging. *Curr. Radiopharm.* **2016**, *9*, 187–207, doi:10.2174/1874471009666161028150654.

106. Persico, M.G.; Marenco, M.; de Matteis, G.; Manfrinato, G.; Cavenaghi, G.; Sgarella, A.; Aprile, C.; Lodola, L. 99mTc-68Ga-ICG-Labelled Macroaggregates and Nanocolloids of Human Serum Albumin: Synthesis Procedures of a Trimodal Imaging Agent Using Commercial Kits. *Contrast Media Mol. Imaging* **2020**, *2020*, 1–11, doi:10.1155/2020/3629705.

107. Stroup, S.P.; Kane, C.J.; Farchshchi-Heydari, S.; James, C.M.; Davis, C.H.; Wallace, A.M.; Hoh, C.K.; Vera, D.R. Preoperative sentinel lymph node mapping of the prostate using PET/CT fusion imaging and Ga-68-labeled tilmanocept in an animal model. *Clin. Exp. Metastasis* **2012**, *29*, 673–680, doi:10.1007/s10585-012-9498-9.

108. Qin, Z.; Hoh, C.K.; Hall, D.J.; Vera, D.R. A tri-modal molecular imaging agent for sentinel lymph node mapping. *Nucl. Med. Biol.* **2015**, *42*, 917–922, doi:10.1016/j.nucmedbio.2015.07.011.

109. Lee, H.J.; Barback, C.V.; Hoh, C.K.; Qin, Z.; Kader, K.; Hall, D.J.; Vera, D.R.; Kane, C.J.; Zhengtao, Q.; Kareem, K.; et al. Fluorescence-Based Molecular Imaging of Porcine Urinary Bladder Sentinel Lymph Nodes. *J. Nucl. Med.* **2017**, *58*, 547–553, doi:10.2967/jnumed.116.178582.

110. Anderson, K.M.; Barback, C.V.; Qin, Z.; Hall, D.J.; Hoh, C.K.; Vera, D.R.; McHale, M.T. Molecular Imaging of endometrial sentinel lymph nodes utilizing fluorescent-labeled Tilmanocept during robotic-assisted surgery in a porcine model. *PLoS ONE* **2018**, *13*, e0197842, doi:10.1371/journal.pone.0197842.

111. Wei, K.; Mulvagh, S.L.; Carson, L.; Davidoff, R.; Gabriel, R.; Grimm, R.A.; Wilson, S.; Fane, L.; Herzog, C.A.; Zoghbi, W.A.; et al. The Safety of Definity and Optison for Ultrasound Image Enhancement: A Retrospective Analysis of 78,383 Administered Contrast Doses. *J. Am. Soc. Echocardiogr.* **2008**, *21*, 1202–1206, doi:10.1016/j.echo.2008.07.019.

112. Tang, C.; Fang, K.; Guo, Y.; Li, R.; Fan, X.; Chen, P.; Chen, Z.; Liu, Q.; Zou, Y. Safety of Sulfur Hexafluoride Microbubbles in Sonography of Abdominal and Superficial Organs: Retrospective Analysis of 30,222 Cases. *J. Ultrasound Med.* **2017**, *36*, 531–538, doi:10.7863/ultra.15.11075.

113. Miyamoto, Y.; Ito, T.; Takada, E.; Omoto, K.; Hirai, T.; Moriyasu, F. Efficacy of Sonazoid (Perflubutane) for Contrast-Enhanced Ultrasound in the Differentiation of Focal Breast Lesions: Phase 3 Multicenter Clinical Trial. *Am. J. Roentgenol.* **2014**, *202*, W400–W407, doi:10.2214/ajr.12.10518.

114. De Bondt, R.; Nelemans, P.; Hofman, P.; Casselman, J.; Kremer, B.; van Engelshoven, J.; Beets-Tan, R. Detection of lymph node metastases in head and neck cancer: A meta-analysis comparing US, USgFNAC, CT and MR imaging. *Eur. J. Radiol.* **2007**, *64*, 266–272, doi:10.1016/j.ejrad.2007.02.037.

115. Liao, L.J.; Hsu, W.L.; Wang, C.T.; Lo, W.C.; Lai, M.S. Analysis of sentinel node biopsy combined with other diagnostic tools in staging cN0 head and neck cancer: A diagnostic meta-analysis. *Head Neck* **2015**, *38*, 628–634, doi:10.1002/hed.23945.

116. Sontum, P.C. Physicochemical Characteristics of Sonazoid™, A New Contrast Agent for Ultrasound Imaging. *Ultrasound Med. Biol.* **2008**, *34*, 824–833, doi:10.1016/j.ultrasmedbio.2007.11.006.

117. Moher, D.; Liberati, A.; Tetzlaff, J.; Altman, D.G. Preferred Reporting Items for Systematic Reviews and Meta-Analyses: The PRISMA Statement. *J. Clin. Epidemiol.* **2009**, *62*, 1006–1012, doi:10.1016/j.jclinepi.2009.06.005.

6

SUMMARIZING DISCUSSION AND FUTURE PERSPECTIVES

NEDERLANDSE SAMENVATTING *(DUTCH SUMMARY)*

DANKWOORD *(WORD OF THANKS)*

CURRICULUM VITAE

SUMMARIZING DISCUSSION AND FUTURE PERSPECTIVES

While the results of cancer therapy continue to improve, not all patients diagnosed with cancer are cured and those who survive longer often have to live with long-term side effects. Heterogeneous drug distribution is one of the causes for ineffective cancer treatment: an effective drug is only effective when it reaches the right location at the right dose. Optimizing drug delivery to the target location aims to tilt the balance towards maximal effect and minimal side effects. In this thesis we discussed methods to optimize drug delivery using imaging and therapeutic ultrasound.

The review in **chapter 1** concludes that spatial heterogeneity in nanoparticle distribution occurs at all scales and can reduce efficacy of nanomedicine. A wide range of imaging modalities help visualize nanoparticle distribution or factors contributing to heterogeneous distribution, by imaging the drug, the nanoparticle and the tumour environment. Clinically, spatially heterogeneous distribution of therapeutic nanoparticles, creates a risk of both under- and overtreatment. While this review focuses on heterogeneity in distribution of nanomedicine, heterogeneity is of importance for any drug formulation [1-3]. Imaging drugs or nanoparticles in clinical studies can help predict treatment effect and therefore select which patients will benefit most and in which patients for example an adjusted dose or a different therapy are necessary. An alternative is to use imaging to select eligible patients for a combination treatment, such as the therapeutic ultrasound methods investigated in this thesis. Combining imaging of nanoparticle and drug distribution with imaging of characteristics of the tumour environment promises to help personalize treatment further. Choosing and combining imaging modalities wisely will hopefully lead to more successful applications of nanomedicine in the future.

Widespread clinical application of imaging drug distribution and heterogeneity can be hampered by costs (of the imaging method itself or for labelling nanoparticles and drugs), the anticipated burden on patients (e.g. long imaging procedures and extra hospital visits) safety or regulatory aspects (labelling slightly changes drug formulations) or the invasive nature of the procedure (for optical imaging and mass spectrometry imaging tissue samples are necessary). However, when evaluation of heterogeneity in drug distribution is omitted from clinical trials, effective drugs could wrongly be discarded as not effective, and an opportunity for personalized treatment could be missed. Future clinical researchers should therefore take into account which imaging method is most suitable to image heterogeneity on the scale of interest and for the nanoparticle/drug of interest. Ideally, future clinical studies should invest in imaging of both nanoparticle/drug distribution and heterogeneity of the tumour environment on multiple scales. Because the results could indicate predictive characteristics useful to select patients or adjust treatment for future patients, less extensive imaging might afterwards be suffi-

cient for a personalized treatment plan. Researchers should take feasibility and patient burden into account while designing such clinical studies; a recommendation would be to combine study procedures with standard-of-care imaging procedures and tumour sampling as much as possible. In this setting also retrospective studies with reanalysis of routinely collected images and tissue samples can be of great value for hypothesis generation, as we should try to learn as much as possible from each patient.

In **chapter 2** Dutch patients with *de novo* metastastic breast cancer (MBC) diagnosed between 2008 and 2018 were compared to a group of patients with metachronous MBC in the same period. We found differences in characteristics, treatment and survival, which highlight that these are two distinct subgroups and that the presence of a primary breast tumour is not the only difference. Compared to metachronous patients, patients with *de novo* metastatic breast cancer were more likely to be 70 years or older, to have invasive lobular carcinoma, clinical T3 or T4 tumours, loco-regional lymphnode metastases, HER2 positivity, bone only disease and to have received systemic therapy in the metastatic setting. They were less likely to have triple negative tumours and liver or brain metastases. Unlike patients with *de novo* MBC, many patients with metachronous MBC have already received systemic treatment in addition to loco-regional treatment following diagnosis of the primary tumour. Recurrence despite these previous systemic therapies could reflect 1) disadvantageous tumour-characteristics, 2) patient comorbidity / fitness and 3) primary or acquired therapy resistance. Patients with *de novo* metastases survived longer (median 34.7 months) than patients with metachronous metastases (median 24.3 months) and the hazard ratio (0.75) varied over time.
Future studies into the differences between patients with *de novo* and metachronous MBC would ideally also take into account indicators of fitness (such as performance score, comorbidity), indicators of metastatic burden (such as number and volume of metastases) and in more detail the type of systemic therapy administered. This would be helpful to make even more accurate prognosis possible for individual patients, which could help patients make informed treatment decisions. Furthermore, comparison of patients with *de novo* MBC with *all* patients diagnosed with metachronous MBC in the same period (regardless of metastasis free interval) would provide even more accurate results and the opportunity to compare changes over time as well.
The findings in this study could help clinicians better inform patients about their prognosis and to provide more personalized treatment. Moreover, it could facilitate design of *de novo* specific trials of innovative treatments such as the trial described in **chapter 3**.

In **chapter 3** we discussed the study design of the i-GO study. This is the first clinical trial that will investigate the combination of LTLD and MR-HIFU induced hyperthermia in breast cancer. We think that this combination leads to improved treatment of the primary tumour, without changing the systemic doxorubicin concentration and thus without

compromising effective treatment of metastases or increasing toxicity.

If this phase I trial demonstrates that safety, feasibility and tolerability are adequate, this approach could in the future lead to improved neoadjuvant treatment of the breast tumour in patients with stage II or III breast cancer, without increasing toxicity. It could lead to less extensive surgery or even in selected patients make surgery (and the associated burden and side effects) redundant.

Unfortunately, this trial has not yet included its first participant at the moment of publication of this thesis. We chose to position this trial in the palliative setting of *de novo* MBC to evaluate safety of the treatment first, before continuing in the neo-adjuvant setting, where the potential benefit for patients is expected. This limits the number of available study participants (circa 5% of all newly diagnosed breast cancer patients present with *de novo* MBC). In addition, it makes an altruistic motivation of the patient necessary, in patients who already have a lot to process after their diagnosis of metastatic breast cancer. Due to ongoing developments and new treatment options in the palliative setting, that arose between the first idea for the study and the start of accrual, the eligible study population became smaller than anticipated. One of these developments is the use of chemotherapy other than anthracycline containing or targeted regimens in the first, second and even third line of metastatic treatment. Amendments to the study design are currently being proposed to improve feasibility of patient recruitment, while still maintaining optimal safety for trial participants. We expect that determining safety and feasibility of LTLD plus MR-HIFU in this population will be possible and ethical, while changing the standard of care treatment (doxorubicin, cyclophosphamide and paclitaxel, AC-P) as little as possible.

For future applications of MR-HIFU hyperthermia and temperature sensitive liposomes the following conditions should be met for the treatment to be feasible and successful in providing a solution to a clinical need. First, there must be a need for a local treatment effect. This could arise with a primary tumour or a metastasis which is symptomatic, incurable with standard treatment, or can only be addressed by an intervention that induces significant morbidity (i.e. amputation of a limb or reduction of an organ). Improving local drug delivery could then provide better palliation, increase chance of survival or decrease treatment related toxicity. An advantage over other local treatment options such as radiotherapy or surgery would be that the treatment occurs simultaneously with systemic treatment and is not invasive. Future studies should incorporate quality of life assessments to determine if this indeed benefits patients. Sometimes standard of care local treatment options are suitable alternatives, but a patient could prefer a non-surgical treatment due to e.g. fear of surgical toxicity, change of body-image or risks of general anaesthesia. In any case, patient preference and shared decision making are very important when deciding between conventional local treatment options (surgery, radiotherapy) and enhanced local drug delivery using MR-HIFU plus LTLD. Second, there should be at least some suggestion that drug distribution with conventional systemic

treatment is sub-optimal in this patient or tumour type, or that reaching the desirable drug distribution with systemic treatment would lead to more side effects. Third, the tumour should be accessible for safe and feasible MR-HIFU (based on tissue type, tumour location and technical properties of the MR-HIFU system). Fourth, the tumour type should be sensitive to the envisioned drug when used in sufficient concentrations. For example, with LTLD the tumour type should be known to respond to anthracyclines. It should be noted that previous resistance may also have been caused by inadequate drug distribution. In tumour types resistant to anthracyclines, temperature sensitive liposomes with other drugs such as cisplatin or gemcitabin could be investigated, although these are less far in development [4].

Considering this, we expect MR-HIFU hyperthermia combined with LTLD could potentially provide a benefit for patients with soft tissue sarcomas (STS), as these tumours are known for their sensitivity to anthracyclines. STS often lead to painful local symptoms, and in the majority of patients extensive surgery is required to relieve symptoms, while standard-of-care chemotherapy is likely to lead to heterogeneous drug distribution due to heterogeneity in the tumour environment [5].

In addition to the application of MR-HIFU for hyperthermia in combination with temperature sensitive liposomes, other applications of MR-HIFU are currently being investigated as well. MR-HIFU ablation of small breast tumours could in the future provide the possibility to omit surgery in selected patients. A previous trial in our hospital showed that (deliberately partial) ablation of breast tumours is feasible and safe [6, 7], a trial evaluating feasibility of complete tumour ablation is currently ongoing (ClinicalTrials.gov Identifier: NCT02407613).

Moreover, MR-HIFU can be used not only to increase temperature, but also to mechanically fractionate part of the tumour, also known as histotripsy. HIFU histotripsy creates a sterile local inflammation and release of tumour associated antigens and danger-associated molecular patterns, which activate dendritic cells. Preclinical studies have shown that histotripsy can enhance the effect of immune checkpoint inhibition, by converting a non-immunogenic (cold) tumour into a (hot) tumour sensitive to immune checkpoint inhibition [8]. An important next step is to show that this combination can be used safely in patients with cancer. A phase I clinical trial is currently being designed.

Before implementing new treatment options, health technology assessments can help evaluate if the benefits of a technique outweigh its financial burden on our society and health care system[9]. Early evaluations showed that MR-HIFU ablation for breast cancer was more expensive than conventional breast conserving treatment [10]. MR-HIFU ablation as palliative treatment for painful bone metastases did seem cost effective compared to radiotherapy alone[11]. Formal health technology assessments for MR-HIFU plus LTLD to our knowledge have not yet been performed. At the moment, costs for MR-HIFU plus LTLD treatment are considerably higher than standard-of-care treatment with doxorubicin. However, costs are expected to decrease with increasing clinical expe-

rience and future studies will need to determine whether the benefits (including quality of life but also financial benefits of possibly reducing need for surgery) outweigh the costs.

In **chapter 4** we described *in vitro* experiments to evaluate the effect of ultrasound and microbubbles (USMB) therapy in combination with chemotherapy on a head and neck cancer cell line. Clinical translation of USMB therapy is currently compromised by the large variety of (non-clinical) US set-ups and US parameters that are used in preclinical studies, which are not easily translated to clinical practice. In this chapter we took a step towards facilitating clinical translation, by proving that USMB therapy, using a clinical ultrasound system in combination with clinically approved microbubbles, leads to efficient *in vitro* uptake of a drug mimicking fluorescent dye and enhanced effect of chemotherapy with bleomycin. In contrast to previous clinical studies that used B-mode and contrast mode [12] or power Doppler [13], we used the PW Doppler mode and performed an extensive evaluation of multiple transducers and available US settings. With the PW Doppler settings used, we were able to achieve similar or even higher intracellular uptake compared to the settings used on a dedicated system with optimized parameters [14]. Future studies should determine the safety and efficacy of our methods and US parameters in patients. To bridge the gap between *in vitro* application and the first clinical trial, we performed a veterinary trial, which is discussed in chapter 5.

Chapter 5 describes a small veterinary clinical trial, evaluating the combination of bleomycin chemotherapy and USMB therapy in cats with oral squamous cell carcinoma. In these cats, the USMB treatments were feasible and well tolerated. Adverse events were considered mild and related to anaesthesia, comorbidity or progressive tumour growth. Eventually, all cats had progressive disease. However, while the median overall survival is (historically) around 44 days with supportive care alone [15], survival in our (albeit small and uncontrolled) study was somewhat longer (46 - 85 days). Moreover, CEUS imaging immediately before and after USMB treatment in 4 of the cats indicated an increase in tumour perfusion, which may be beneficial for drug delivery.

This was a small feasibility study. An ideal veterinary clinical trial would include a larger number of patients and a control group of patients treated with bleomycin alone. Simultaneous cavitation-detection to monitor microbubble response during USMB therapy could further benefit safety and efficacy [16]. Blood samples would be taken to monitor pharmacokinetics of bleomycin in cats treated with and without USMB. Tumour biopsies before and after treatment would be used for imaging of bleomycin distribution throughout the tumour (for example using mass spectrometry imaging) and to quantify the amount of bleomycin in the tumours. Additionally, the tumour biopsies would be cultured as organoids and tested *in vitro* for bleomycin sensitivity, with and without USMB. In this way we could determine if non-responders were inherently resistant to

bleomycin or if the bleomycin still reached the target location in an insufficient dose *in vivo*. Finally, it would be interesting to continue the study treatment longer, perhaps a total number of 3 sessions was insufficient. Although this trial design would provide a wealth of information it is unlikely that it is feasible in the setting of veterinary patients. The advantage of the study design in **chapter 5** is that it was relatively simple and posed a small burden on the cats and their owners, which gave us the opportunity to include five patients.

In the future, we expect USMB therapy in combination with chemotherapy could provide a benefit in human patients with (for example) head and neck cancer. Based on previous *in vitro* results from our group, the effect of the standard-of-care chemotherapy or chemoradiotherapy with cisplatin could be improved by addition of USMB [17]. Furthermore, the combination of USMB therapy with radiotherapy in the absence of drug is promising, considering the effect of USMB on perfusion. Clinical studies are already ongoing (Clinicaltrials.gov NCT04431674, NCT04431648). Since we already used a clinical US system, and EMA/FDA approved microbubbles in this study, the step to a clinical trial in human patients can be taken in the near future. In other centres, early clinical trials using USMB in combination with chemotherapy in patients with various tumour types have already shown promising results or are still ongoing [12, 18, 19] (Clinical-Trials.gov Identifiers: NCT04146441, NCT04821284, NCT03477019 and NCT03458975, NCT03385200). As a first clinical trial in patients with head and neck cancer, I propose to evaluate safety and feasibility of USMB therapy to enhance tumour perfusion (without chemotherapy). USMB therapy could be performed before surgery and CEUS before and after USMB would be used to investigate the effect on perfusion. This type of trial would pose a small burden and low risk on the patient. When this is proven safe and feasible, USMB therapy could be evaluated in addition to standard of care chemo(radio)therapy (such as cisplatin and/or cetuximab) to improve drug delivery or in addition to radiotherapy (to enhance tumour perfusion and reduce hypoxia). In the future the combination of USMB therapy with a decreased dose of chemoradiotherapy could lead to similar efficacy while reducing local toxicity.

Chapter 6 is a review about preoperative sentinel lymph node imaging techniques which could help select which head and neck cancer patients, in particular patients with early stage oral cavity squamous cell carcinoma, need additional therapy to treat lymph node metastases. With improving the diagnostic accuracy of these techniques, invasive treatments of the neck could safely be omitted in more patients. Although diagnostic accuracy of most presented techniques is still inferior to conventional lymphoscintigraphy, each technique has its own strengths and flaws, and further development may in the future lead to better results.

Related to the topic of ultrasound and microbubbles, lymphosonography is a promising technique but clinical experience is currently still insufficient. A future trial combining

preoperative US guided fine needle aspiration (USgFNA) with lymphosonography, prior to the conventional sentinel node procedure would be very useful to determine if lymphosonography could increase the sensitivity of USgFNA [20, 21] and perhaps decrease the need for sentinel node procedures in the future.

To conclude**,** this thesis describes methods to optimize drug delivery using imaging and therapeutic ultrasound and focuses on ways to achieve personalized treatment with optimal effect and minimal side effects. It demonstrates the value of multidisciplinary collaboration between both technical and clinical researchers, radiologists and oncologists and veterinary and human clinicians. These collaborations will become increasingly important in the future. Future studies should be designed with both theoretical benefit and clinical feasibility in mind. In this way, clinical translation of promising techniques will hopefully benefit future patients.

REFERENCES

1. Minchinton AI, Tannock IF (2006) Drug penetration in solid tumours. Nat Rev Cancer 6(8):583-592. https://doi.org/10.1038/nrc1893

2. Tredan O, Galmarini CM, Patel K, Tannock IF (2007) Drug resistance and the solid tumor microenvironment. J Natl Cancer Inst 99(19):1441-1454. https://doi.org/10.1093/jnci/djm135

3. Garattini S, Fuso Nerini I, D'Incalci M (2018) Not only tumor but also therapy heterogeneity. Ann Oncol 29(1):13-18. https://doi.org/10.1093/annonc/mdx751

4. Kneidl B, Peller M, Winter G, Lindner LH, Hossann M (2014) Thermosensitive liposomal drug delivery systems: state of the art review. Int J Nanomedicine 9:4387-4398. https://doi.org/10.2147/IJN.S49297

5. Scalas G, Parmeggiani A, Martella C, Tuzzato G, Bianchi G, Facchini G, Clinca R, Spinnato P (2021) Magnetic resonance imaging of soft tissue sarcoma: features related to prognosis. Eur J Orthop Surg Traumatol 31(8):1567-1575. https://doi.org/10.1007/s00590-021-03003-2

6. Merckel LG, Knuttel FM, Deckers R, van Dalen T, Schubert G, Peters NH, Weits T, van Diest PJ, Mali WP, Vaessen PH, et al. (2016) First clinical experience with a dedicated MRI-guided high-intensity focused ultrasound system for breast cancer ablation. Eur Radiol 26(11):4037-4046. https://doi.org/10.1007/s00330-016-4222-9

7. Deckers R, Merckel LG, Denis de Senneville B, Schubert G, Kohler M, Knuttel FM, Mali WP, Moonen CT, van den Bosch MA, Bartels LW (2015) Performance analysis of a dedicated breast MR-HIFU system for tumor ablation in breast cancer patients. Phys Med Biol 60(14):5527-5542. https://doi.org/10.1088/0031-9155/60/14/5527

8. Eranki A, Srinivasan P, Ries M, Kim A, Lazarski CA, Rossi CT, Khokhlova TD, Wilson E, Knoblach SM, Sharma KV, et al. (2020) High-Intensity Focused Ultrasound (HIFU) Triggers Immune Sensitization of Refractory Murine Neuroblastoma to Checkpoint Inhibitor Therapy. Clin Cancer Res 26(5):1152-1161. https://doi.org/10.1158/1078-0432.CCR-19-1604

9. Grutters JPC, Govers T, Nijboer J, Tummers M, van der Wilt GJ, Rovers MM (2019) Problems and Promises of Health Technologies: The Role of Early Health Economic Modeling. Int J Health Policy Manag 8(10):575-582. https://doi.org/10.15171/ijhpm.2019.36

10. Knuttel FM, Huijsse SEM, Feenstra TL, Moonen CTW, van den Bosch M, Buskens E, Greuter MJW, de Bock GH (2017) Early health technology assessment of magnetic resonance-guided high intensity focused ultrasound ablation for the treatment of early-stage breast cancer. J Ther Ultrasound 5:23. https://doi.org/10.1186/s40349-017-0101-3

11. Simoes Correa Galendi J, Yeo SY, Grull H, Bratke G, Akuamoa-Boateng D, Baues C, Bos C, Verkooijen HM, Shukri A, Stock S, et al. (2022) Early economic modeling of magnetic resonance image-guided high intensity focused ultrasound compared to radiotherapy for pain palliation of bone metastases. Front Oncol 12:987546. https://doi.org/10.3389/fonc.2022.987546

12. Kotopoulis S, Dimcevski G, Gilja OH, Hoem D, Postema M (2013) Treatment of human pancreatitc cancer using combined ultrasound, microbubbles and gemcitabine: a clinical case study. Medical Physics 40(7). https://doi.org/10.1118/1.4808149]

13. Rix A, Piepenbrock M, Flege B, von Stillfried S, Koczera P, Opacic T, Simons N, Boor P, Thoroe-Boveleth S, Deckers R, et al. (2021) Effects of contrast-enhanced ultrasound treatment on neoadjuvant chemotherapy in breast cancer. Theranostics 11(19):9557-9570. https://doi.org/10.7150/thno.64767

14. Lammertink B, Deckers R, Storm G, Moonen C, Bos C (2015) Duration of ultrasound-mediated enhanced plasma membrane permeability. Int J Pharm 482(1-2):92-98. https://doi.org/10.1016/j.ijpharm.2014.12.013

15. Hayes AM, Adams VJ, Scase TJ, Murphy S (2007) Survival of 54 cats with oral squamous cell carcinoma in United Kingdom general practice. J Small Anim Pract 48(7):394-399. https://doi.org/10.1111/j.1748-5827.2007.00393.x

16. Keller SB, Sheeran PS, Averkiou MA (2021) Cavitation therapy monitoring of commercial microbubbles with a clinical scanner. IEEE Trans Ultrason Ferroelectr Freq Control 68(4):1144-1154. https://doi.org/10.1109/TUFFC.2020.3034532

17. Lammertink BH, Bos C, van der Wurff-Jacobs KM, Storm G, Moonen CT, Deckers R (2016) Increase of intracellular cisplatin levels and radiosensitization by ultrasound in combination with microbubbles. J Control Release 238:157-165. https://doi.org/10.1016/j.jconrel.2016.07.049

18. Dimcevski G, Kotopoulis S, Bjanes T, Hoem D, Schjott J, Gjertsen BT, Biermann M, Molven A, Sorbye H, McCormack E, et al. (2016) A human clinical trial using ultrasound and microbubbles to enhance gemcitabine treatment of inoperable pancreatic cancer. J Control Release 243:172-181. https://doi.org/10.1016/j.jconrel.2016.10.007

19. Wang Y, Li Y, Yan K, Shen L, Yang W, Gong J, Ding K (2018) Clinical study of ultrasound and microbubbles for enhancing chemotherapeutic sensitivity of malignant tumors in digestive system. Chin J Cancer Res 30(5):553-563. https://doi.org/10.21147/j.issn.1000-9604.2018.05.09

20. de Bondt RB, Nelemans PJ, Hofman PA, Casselman JW, Kremer B, van Engelshoven JM, Beets-Tan RG (2007) Detection of lymph node metastases in head and neck cancer: a meta-analysis comparing US, USgFNAC, CT

and MR imaging. Eur J Radiol 64(2):266-272. https://doi.org/10.1016/j.ejrad.2007.02.037

21. Liao LJ, Hsu WL, Wang CT, Lo WC, Lai MS (2016) Analysis of sentinel node biopsy combined with other diagnostic tools in staging cN0 head and neck cancer: A diagnostic meta-analysis. Head Neck 38(4):628-634. https://doi.org/10.1002/hed.23945

NEDERLANDSE SAMENVATTING

Optimale medicijnverdeling bij kanker met behulp van beeldvorming en therapeutisch ultrageluid

De laatste jaren is er veel vooruitgang geboekt op het gebied van de behandeling van kanker. In Nederland leven patiënten met kanker steeds langer [1]. Deze verbetering is helaas niet bij alle kankertypes even sterk, nog niet alle patiënten genezen van hun ziekte en daarnaast kunnen bijwerkingen van de behandelingen op de langere termijn veel problemen opleveren [2-5]. Eén van de oorzaken van niet-effectieve kankerbehandeling is een ongelijkmatige (heterogene) verdeling van de medicijnen tegen kanker. Verschillen in de verdeling van medicijnen tussen patiënten, maar ook tussen verschillende organen van een patiënt en zelfs tussen verschillende gebieden binnen een tumor dragen daaraan bij [6-8]. Een medicijn is alleen effectief wanneer het de juiste plek bereikt in de juiste hoeveelheid. In dit proefschrift beschrijven we twee behandelmethodes om medicijnafgifte zo optimaal mogelijk te maken. Deze methodes (die we hieronder toelichten) maken gebruik van therapeutisch ultrageluid:

1. **MR-HIFU hyperthermie** gecombineerd met **temperatuurgevoelige vetbolletjes** met chemotherapie
2. **Ultrageluid en microbellen behandeling**

Beide behandelingen hebben als doel om de medicijnverdeling zo optimaal mogelijk te maken. De meest optimale situatie is een máximaal effectieve behandeling die zorgt voor mínimale schade aan gezond weefsel (schade aan gezond weefsel wordt 'toxiciteit' of 'bijwerking' genoemd).

Beeldvorming (het maken van scans en beelden voorafgaand aan en tijdens een behandeling) kan ons meer informatie geven over de kenmerken van patiënten en zo helpen om de behandeling zo goed mogelijk te richten op de plek waar deze nodig is, de behandeling zo veilig mogelijk te maken en om de behandeling aan te passen aan de individuele patiënt (ook wel 'gepersonaliseerde behandeling' genoemd).

Deze Nederlandse samenvatting omschrijft de belangrijkste achtergrondinformatie en bevindingen van de hoofdstukken in dit proefschrift.

Ultrageluid

Ultrageluid staat bekend om haar toepassing bij het maken van beelden. In het Nederlands wordt dit onderzoek 'echografie' genoemd. Het meest bekend is de echo bij een zwangere, maar echografie kan informatie geven over vrijwel alle organen. Bij echografie worden ultrageluidsgolven door het echoapparaat uitgestuurd richting het lichaamsweefsel. Deze golven reflecteren op de overgangen tussen verschillende weefsels en worden

weer opgevangen door het echoapparaat, dat vervolgens een zwart-wit beeld van de weefsels maakt [9]. Bij een contrast-echografie worden daarnaast heel kleine gasbelletjes intraveneus (via het infuus) toegediend (dit worden ook wel 'microbellen' genoemd), deze zorgen voor een sterkere weerkaatsing van het ultrageluid. Dit kan bijvoorbeeld helpen om meer informatie te krijgen over de bloedvaten [9-11].

In dit onderzoek gebruiken we ultrageluid niet alleen voor het maken van beelden, maar ook als een behandeling om lokale medicijnverdeling te verbeteren. Daarom noemen we dit 'therapeutisch ultrageluid'. Twee voorbeelden van therapeutisch ultrageluid zijn MR-gestuurde hoge intensiteit gebundeld ultrageluid (MR-HIFU) en behandeling met ultrageluid in combinatie met microbellen (USMB behandeling).

Magnetische resonantie - gestuurde hoge intensiteit gebundeld ultrageluid (MR-HIFU)

MR-HIFU is een combinatie van MRI (magnetische resonantie beeldvorming) en HIFU (hoge intensiteit gebundeld ultrageluid), met als doel om weefsel (zoals een tumor) op te warmen of mechanische effecten te veroorzaken. HIFU bestaat uit sterke ultrageluidsgolven die in één punt worden gebundeld. Dit is vergelijkbaar met het bundelen van zonnestralen op één punt met een vergrootglas om zo vuur te maken. Afhankelijk van het doel van de behandeling kan het weefsel verwarmd worden tot 55-70°C ('thermale ablatie' [12-14] of tot 40-43°C ('hyperthermie' [15-17]. MR-gestuurd betekent dat we op basis van MRI beelden precies kunnen plannen welk gedeelte van de patiënt verwarmd wordt. Daarnaast kunnen we met MRI beelden tijdens de HIFU behandeling de temperatuur in de patiënt meten en volgen wat het effect van de behandeling is [18].

Nanomedicijnen zoals temperatuurgevoelige vetbolletjes met doxorubicine.

Om medicijnafgifte op de gewenste plek te verbeteren kan MR-HIFU hyperthermie gecombineerd worden met temperatuurgevoelige nanomedicijnen. Nanomedicijnen zijn kleine deeltjes (op nanometerschaal, ook nanodeeltjes genoemd) gebonden aan medicijnen of als verpakking voor medicijnen. Nanodeeltjes zijn gemaakt om deze medicijnen zoveel mogelijk af te leveren op de plek waar ze nodig zijn. Dit heeft als doel om de effectiviteit te verhogen (hogere hoeveelheden (concentraties) van medicatie in de tumor) en de toxiciteit te verlagen (beperken van schade aan het gezonde weefsel) [24]. In dit onderzoek hebben we het nanomedicijn ThermoDox onderzocht. Dit zijn temperatuurgevoelige vetbolletjes (liposomen) van circa 100 nanometer die bestaan uit een membraan met een dubbele laag fosfolipiden en binnenin verpakt het chemotherapiemiddel doxorubicine. Deze vetbolletjes worden in de bloedbaan toegediend en stromen door het lichaam terwijl de tumor wordt verwarmd. Alleen daar waar de vetbolletjes verwarmd worden (in de tumor), komt er snel een grote hoeveelheid doxorubicine vrij [25-27]. In de rest van het lichaam (op lichaamstemperatuur) lekken de vetbolletjes een beetje en komt er heel langzaam evenveel doxorubicine vrij als bij een behandeling met doxorubicine die niet is verpakt in een vetbolletje. Zo willen we het lokale effect van chemotherapie in de tumor versterken,

zonder dat er meer bijwerkingen en schade ontstaan in de rest van het lichaam. Er is al veel onderzoek gedaan bij patiënten naar de combinatie van ThermoDox met andere methoden van verwarming [28-32]. In dit proefschrift beschrijven we hoe we het willen onderzoeken in combinatie met MR-HIFU hyperthermie.

Ultrageluid en microbellen behandeling (USMB behandeling)
De tweede methode van therapeutisch ultrageluid die we toepassen in dit onderzoek is ultrageluid en microbellen (USMB) behandeling. Microbellen zijn zoals hierboven genoemd contrastmiddelen voor echografie. Het zijn kleine deeltjes van 1-10 micrometer doorsnede, gevuld met gas en omgeven met een laagje fosfolipiden of eiwitten [19, 20]. Naast de rol van microbellen bij het maken van beelden, biedt de combinatie van ultrageluid met microbellen ook de mogelijkheid om lokaal de werking van medicijnen te versterken. Afhankelijk van de gebruikte ultrageluid instellingen zoals frequentie en druk gaan microbellen trillen ('stabiele cavitatie') of kunnen ze kapot gaan ('inertiële cavitatie'). Beide soorten cavitatie kunnen biologische effecten veroorzaken in het omringende weefsel, zoals het maken van kleine gaatjes in celmembranen, het stimuleren van opname van stoffen door endocytose, het meer doorgankelijk maken van de bloedvatwand en het beperken of juist stimuleren van de bloedtoevoer. Alle effecten van behandeling met ultrageluid en microbellen die kunnen zorgen voor meer lokale afgifte van medicijn op de gewenste plek heten samen 'sonopermeatie'[21-23].

Patiëntengroepen in dit proefschrift
In dit proefschrift beschrijven we de toepassing van therapeutisch ultrageluid om medicijnverdeling te verbeteren in het kader van twee groepen patiënten:

1. Patiënten met '***de novo* uitgezaaide borstkanker'** voor de toepassing van MR-HIFU plus ThermoDox
2. Patiënten met **hoofd-halskanker** voor de toepassing van USMB behandeling plus chemotherapie

*Patiënten met de novo uitgezaaide borstkanke*r
Dit zijn patiënten bij wie bij het stellen van de diagnose borstkanker ook gelijktijdig uitzaaiingen buiten de borst (op afstand) worden gevonden. De diagnose borstkanker wordt in Nederland elk jaar bij ongeveer 14.500 nieuwe patiënten gesteld [33]. Ongeveer 5% van hen heeft op dat moment uitzaaiingen ergens anders in het lichaam [34]. Bij de meeste mensen met uitgezaaide borstkanker ('stadium IV') worden de uitzaaiingen ontdekt in de jaren na de diagnose en behandeling (zogenaamde 'metachrone uitzaaiingen'). Omdat mensen met *de novo* uitgezaaide borstkanker zowel een tumor in de borst hebben als uitzaaiingen op afstand is het mogelijk om het effect (lokaal in de borst en op afstand in de uitzaaiingen) én de bijwerkingen van de combinatie van ThermoDox

met MR-HIFU hyperthermie goed te onderzoeken. We hebben een fase 1 studie opgezet (de eerste fase van onderzoek bij mensen) om bij deze patiënten te onderzoeken of de combinatiebehandeling veilig en haalbaar is.

Patiënten met hoofd-halskanker

De diagnose 'hoofd-halskanker' wordt in Nederland elk jaar bij ongeveer 3.000 nieuwe patiënten gesteld [35]|6B. Het gaat om een groep van tumoren in het hoofd-hals gebied (bijvoorbeeld in de mond, neus, keelholte of strottenhoofd). De meeste patiënten hebben lokaal uitgebreide ziekte [36, 37], waarbij een operatie soms niet mogelijk is doordat de tumor niet volledig weggehaald kan worden of doordat de operatie onacceptabel veel omliggend weefsel zou beschadigen of lokale functies zou verminderen. Ondanks combinaties van behandeling (operatie, chemotherapie, bestraling, doelgerichte medicijnen en/of immuuntherapie) met veel bijwerkingen komt de tumor bij ongeveer de helft van de patiënten in het hoofd-halsgebied terug. De kanker is dan vaak niet meer genezen [38, 39]. Omdat dit kankertype zoveel lokale problemen kent, denken we dat een verbetering van lokale medicijnverdeling met behulp van therapeutisch ultrageluid bij deze patiënten zou kunnen helpen, door de effectiviteit van de behandeling te verbeteren, zonder voor meer bijwerkingen te zorgen.

Hoofd-hals kanker bij katten

De behandeling met ultrageluid en microbellen is al vaak onderzocht met celexperimenten in een laboratorium, dit noemen we '*in vitro*' (Latijn voor 'in glas', oftewel buiten een mens of dier, bijvoorbeeld in een kweekschaaltje of reageerbuis). Ook is het onderzocht bij levende proefdieren zoals ratten en muizen (*in vivo*). Vervolgens is er onderzoek gedaan bij kleine groepen mensen, maar nog niet specifiek bij patiënten met hoofd-halskanker. Om een stap verder te komen richting het toepassen van deze behandeling bij mensen, kan dieronderzoek helpen. In dit proefschrift hebben we niet gekozen voor proefdieronderzoek, maar voor een klinische studie bij huisdieren, namelijk katten. Deze katten zijn patiënten van een dierenarts, bij wie een behandeling veel kan lijken op die van menselijke patiënten. Hoofd-hals kanker komt vaak voor bij oudere katten en 10% van alle tumoren bij katten zitten in de bek [40]. Helaas overleven deze katten met alleen ondersteunende behandeling gemiddeld slechts 1,5 maand [41]. Er zijn veel overeenkomsten tussen hoofd-hals tumoren bij mensen en bij katten, en door de afmetingen van een kat kunnen dezelfde echoapparatuur en ultrageluidsinstellingen gebruikt worden als bij mensen [42-44]. Een onderzoek bij deze veterinaire patiënten kan ons daarom een stap vooruit brengen in het onderzoek bij mensen.

Overzicht van de hoofdstukken

Het review artikel in **hoofdstuk 1** geeft een overzicht van verschillende onderzoeken die laten zien dat nanodeeltjes en nanomedicijnen zich niet altijd op een gelijkmatige manier

verdelen. Er zijn verschillen in de verdeling tussen patiënten, tussen organen in één patiënt, tussen tumoren of binnen **één tumor**. Kortom, er is op elke schaal heterogeniteit in de verdeling van deze nanodeeltjes, terwijl we weten dat een medicijn alleen effectief is wanneer het de juiste plek bereikt in de juiste hoeveelheid.

Beeldvorming (het maken van scans) kan helpen om de verdeling van nanodeeltjes en factoren die bijdragen aan heterogeniteit in kaart te brengen. Hierbij zijn er beeldvormende technieken voor het afbeelden van de verdeling van het medicijn, het nanodeeltje dat het medicijn vervoert en de omgeving van de tumor waar het medicijn moet werken. Dit soort beeldvormende technieken kunnen in klinische studies helpen voorspellen welke patiënten het meeste baat hebben bij een behandeling en bij welke patiënten de behandeling aangepast moet worden. Ook zouden zo patiënten geselecteerd kunnen worden die baat hebben bij het toevoegen van een behandeling, met als doel de verdeling van de medicijnen te verbeteren, zoals therapeutisch ultrageluid.

In **hoofdstuk 2** vergelijken we Nederlandse patiënten die tussen 2008 en 2018 de diagnose *de novo* uitgezaaide borstkanker hebben gekregen met een groep patiënten bij wie in dezelfde periode (metachrone) uitzaaiingen van eerdere borstkanker zijn ontdekt. We vonden verschillen in de kenmerken, behandeling en overlevingsduur van deze patiënten. Dit benadrukt dat het twee aparte groepen zijn, waarbij de aanwezigheid van een tumor in de borst zeker niet het enige verschil is. Het feit dat de kanker bij de patiënten met metachrone uitzaaiingen is teruggekeerd ondanks de eerdere behandeling kan wijzen op: 1) ongunstige tumorkenmerken 2) minder fitte patiënten die meer andere ziektes hebben naast de borstkanker en 3) dat de tumor al resistent was of is geworden tijdens de behandeling. Patiënten met *de novo* uitgezaaide borstkanker overleven langer (mediaan 34.7 maanden na de diagnose) dan patiënten met metachrone uitzaaiingen (mediaan 24.3 maanden).

Dit onderzoek kan dokters helpen hun patiënten nog beter voor te lichten en de behandeling nog meer te personaliseren. Daarnaast kan het helpen om klinische studies te ontwerpen met innovatieve behandelingen specifiek voor *de novo* uitgezaaide borstkanker, zoals de studie in hoofdstuk 3.

In **hoofdstuk 3** bespreken we de opzet van de i-GO studie. Dit is de eerste klinische studie naar de combinatie van het nanomedicijn ThermoDox in combinatie met MR-HIFU hyperthermie bij patiënten met borstkanker.

We willen deze behandeling onderzoeken bij patiënten met *de novo* uitgezaaide borstkanker. In de studie wordt de standaard chemotherapie doxorubicine vervangen door het nanomedicijn ThermoDox (doxorubicine in temperatuurgevoelige vetbolletjes) in combinatie met verwarmen van de borsttumor met MR-HIFU. We verwachten dat deze combinatie leidt tot betere behandeling van de tumor in de borst, zónder dat er meer chemotherapie in de rest van het lichaam terecht komt, zodat de uitzaaiingen in de

rest van het lichaam net zo goed behandeld worden als anders en de bijwerkingen niet toenemen. Het hoofddoel van het onderzoek is om bij een klein aantal patiënten (6- 12) te beoordelen of de behandeling veilig en haalbaar is. Als dit zo is, kan verder onderzoek laten zien of het ook tot betere uitkomsten voor de patiënten leidt. In de toekomst hopen we dat deze combinatiebehandeling bij patiënten met borstkanker zonder uitzaaiingen leidt tot minder uitgebreide borstoperaties, of operatie zelfs helemaal niet meer nodig is.

Voor **hoofdstuk 4** hebben we celexperimenten gedaan (*in vitro*) om het effect van ultrageluid en microbellen (USMB) behandeling in combinatie met bleomycine chemotherapie op gekweekte hoofd-halskankercellen te onderzoeken. Bleomycine kan kankercellen pas doden wanneer het in de cel aanwezig is, maar omdat het een wateroplosbaar medicijn is komt het niet makkelijk door de celmembraan naar binnen. USMB behandeling kan cellen doorgankelijk maken en medicijnopname stimuleren (sonopermeatie) om zo het effect te versterken.

Eerdere onderzoeken gebruiken veel verschillende (zelfgebouwde) apparatuur en instellingen van het ultrageluid, die niet altijd makkelijk vertaald kunnen worden naar de toepassing bij mensen in het ziekenhuis. Daarom hebben we in dit onderzoek een klinisch echoapparaat en voor toediening aan mensen goedgekeurde microbellen gebruikt. USMB behandeling met een klinisch echoapparaat leidt tot opname van een fluorescerende kleurstof (als model voor een medicijn) in kankercellen. Ook versterkt de USMB behandeling zoals verwacht het effect van bleomycine chemotherapie. Om de stap van *in vitro* experimenten naar de eerste klinische studie bij patiënten met hoofd-halskanker te verkleinen hebben we in hoofdstuk 5 deze behandeling toegepast bij katten.

Hoofdstuk 5 gaat over een klinische studie bij vijf katten met plaveiselcelcarcinomen in de bek, die we hebben behandeld met de combinatie van bleomycine chemotherapie en USMB behandeling. Hierbij werd opnieuw een klinisch echoapparaat gebruikt en microbellen die zijn goedgekeurd voor toepassing bij mensen. De behandeling werd door de katten goed verdragen. De symptomen die ze hadden waren mild en hingen samen met de narcose, andere aandoeningen of groei van de tumor. Uiteindelijk groeiden helaas alle tumoren verder, maar was de overlevingsduur met 46- 85 dagen wel iets langer dan wat in eerder onderzoek beschreven was na alleen een ondersteunende behandeling (mediaan 44 dagen) [41]. Tijdens dit onderzoek deden we (zowel voor als na de behandeling met ultrageluid en microbellen) ook contrast-echografie. Hierbij viel op dat de doorbloeding (perfusie) van de tumoren na USMB behandeling in veel gevallen toenam. We denken dat dit ervoor kan zorgen dat chemotherapie zich beter verdeelt in tumoren en dat radiotherapie (bestraling) beter werkt omdat er meer zuurstof in het tumorweefsel komt. Waarschijnlijk speelde andere mechanismen van sonopermeatie in ons onderzoek maar een kleine rol, waardoor bleomycine (dat niet zozeer van perfusie afhankelijk is maar wel iets nodig heeft om de celwand door te gaan en in de cel werkzaam te zijn) maar

een beperkt effect had. In toekomstige studies raden we aan te onderzoeken wat de toegevoegde waarde van USMB behandeling is bij andere chemotherapie (zoals cisplatin of carboplatin) en/of radiotherapie bij patiënten met hoofd-halskanker. Omdat de USMB behandeling uitgevoerd kon worden met klinische echoapparatuur en microbellen die ook goedgekeurd zijn voor gebruik bij mensen, brengt deze veterinaire studie ons een stap dichter bij toepassing van USMB behandeling bij mensen.

Hoofdstuk 6 is een review artikel over technieken voor het in beeld brengen van de schildwachtklier bij patiënten met hoofd-halskanker. Een van deze technieken maakt gebruikt van ultrageluid en microbellen op een andere manier dan we hiervoor hebben beschreven.

De schildwachtklierprocedure heeft als doel te onderzoeken of kankercellen van de tumor waar ze zijn ontstaan (primaire tumor) naar de lymfeklieren zijn verspreid, zonder daarbij álle lymfeklieren te hoeven weghalen. Bij de schildwachtklier procedure wordt een stofje in of rondom de primaire tumor gespoten en vervolgens wordt gekeken in welke lymfeklier dit stofje als eerste terecht komt. Die eerste lymfeklier heet de schildwachtklier en de verwachting is dat eventuele kankercellen dezelfde route volgen en hier ook als eerste naartoe zouden gaan. Deze schildwachtklier wordt dan verwijderd en onderzocht onder de microscoop. Als hier geen kankercellen in blijken te zitten verwachten we dat dit ook in de rest van de lymfeklieren niet zo is en hoeven deze niet allemaal preventief verwijderd te worden. Zo kan de patiënt een extra operatie en de risico's daarvan bespaard blijven [45]. Dit review artikel beschrijft verschillende technieken van beeldvorming van de schildwachtklier voorafgaand aan een operatie, die verschillende voor- en nadelen hebben. Een van deze technieken is lymphosonografie waarbij microbellen in of rondom de primaire tumor worden gespoten en met echografie worden gevolgd tot ze via de lymfebanen uitkomen bij de schildwachtklier. Dit is een veelbelovende techniek, maar er is tot nu toe nog weinig ervaring mee in de kliniek.

Samenvattend beschrijft dit proefschrift methodes om medicijnverdeling zo optimaal mogelijk te maken, door gebruik te maken van beeldvorming en therapeutisch ultrageluid. Hierbij streven we naar gepersonaliseerde behandeling met een zo sterk mogelijk gewenst effect en zo min mogelijk bijwerkingen. Dit onderzoek laat daarnaast zien dat samenwerking tussen verschillende vakgebieden van grote waarde is, tussen technische en klinische onderzoekers, radiologen en oncologen en artsen en dierenartsen. Deze samenwerking zal in de toekomst alleen maar belangrijker worden, met als doel ervoor te zorgen dat zoveel mogelijk toekomstige patiënten profiteren van veelbelovende nieuwe technieken.

REFERENTIES

1. Siesling S, Visser O, Aarts MJ, Verhoeven RHA, Aben KKH, Dinmohamed AG, van Dijk B, van der Aa M, Louwman M, Lemmens VEPP (2019) [Fight against cancer in the Netherlands: current state of affairs] [Article in Dutch]. Ned Tijdschr Geneeskd 163:D4150.

2. Schmielau J, Rick O, Reuss-Borst M, Kalusche-Bontemps EM, Steimann M (2017) Rehabilitation of Cancer Survivors with Long-Term Toxicities. Oncol Res Treat 40(12):764-771. https://doi.org/10.1159/000485187

3. Haidinger R, Bauerfeind I (2019) Long-Term Side Effects of Adjuvant Therapy in Primary Breast Cancer Patients: Results of a Web-Based Survey. Breast Care (Basel) 14(2):111-116. https://doi.org/10.1159/000497233

4. Nilsen ML, Belsky MA, Scheff N, Johnson JT, Zandberg DP, Skinner H, Ferris R (2020) Late and Long-Term Treatment-Related Effects and Survivorship for Head and Neck Cancer Patients. Curr Treat Options Oncol 21(12):92. https://doi.org/10.1007/s11864-020-00797-x

5. Buchberger AMS, Strzelczyk EA, Wollenberg B, Combs SE, Pickhard A, Pigorsch SU (2021) Report on Late Toxicity in Head-and-Neck Tumor Patients with Long Term Survival after Radiochemotherapy. Cancers (Basel) 13(17). https://doi.org/10.3390/cancers13174292

6. Minchinton AI, Tannock IF (2006) Drug penetration in solid tumours. Nat Rev Cancer 6(8):583-592. https://doi.org/10.1038/nrc1893

7. Tredan O, Galmarini CM, Patel K, Tannock IF (2007) Drug resistance and the solid tumor microenvironment. J Natl Cancer Inst 99(19):1441-1454. https://doi.org/10.1093/jnci/djm135

8. Garattini S, Fuso Nerini I, D'Incalci M (2018) Not only tumor but also therapy heterogeneity. Ann Oncol 29(1):13-18. https://doi.org/10.1093/annonc/mdx751

9. Perera RH, Hernandez C, Zhou H, Kota P, Burke A, Exner AA (2015) Ultrasound imaging beyond the vasculature with new generation contrast agents. Wiley Interdiscip Rev Nanomed Nanobiotechnol 7(4):593-608. https://doi.org/10.1002/wnan.1326

10. Leen E, Averkiou M, Arditi M, Burns P, Bokor D, Gauthier T, Kono Y, Lucidarme O (2012) Dynamic contrast enhanced ultrasound assessment of the vascular effects of novel therapeutics in early stage trials. Eur Radiol 22(7):1442-1450. https://doi.org/10.1007/s00330-011-2373-2

11. Schinkel AF, Kaspar M, Staub D (2016) Contrast-enhanced ultrasound: clinical applications in patients with atherosclerosis. Int J Cardiovasc Imaging 32(1):35-48. https://doi.org/10.1007/s10554-015-0713-z

12. Kim YS, Keserci B, Partanen A, Rhim H, Lim HK, Park MJ, Kohler MO (2012) Volumetric MR-HIFU ablation of uterine fibroids: role of treatment cell size in the improvement of energy efficiency. Eur J Radiol 81(11):3652-3659. https://doi.org/10.1016/j.ejrad.2011.09.005

13. Hurwitz MD, Ghanouni P, Kanaev SV, Iozeffi D, Gianfelice D, Fennessy FM, Kuten A, Meyer JE, LeBlang SD, Roberts A, et al. (2014) Magnetic resonance-guided focused ultrasound for patients with painful bone metastases: phase III trial results. J Natl Cancer Inst 106(5). https://doi.org/10.1093/jnci/dju082

14. Hsiao YH, Kuo SJ, Tsai HD, Chou MC, Yeh GP (2016) Clinical Application of High-intensity Focused Ultrasound in Cancer Therapy. J Cancer 7(3):225-231. https://doi.org/10.7150/jca.13906

15. Chu W, Staruch RM, Pichardo S, Tillander M, Kohler MO, Huang Y, Ylihautala M, McGuffin M, Czarnota G, Hynynen K (2016) Magnetic Resonance-Guided High-Intensity Focused Ultrasound Hyperthermia for Recurrent Rectal Cancer: MR Thermometry Evaluation and Preclinical Validation. Int J Radiat Oncol Biol Phys 95(4):1259-1267. https://doi.org/10.1016/j.ijrobp.2016.03.019

16. Bing C, Patel P, Staruch RM, Shaikh S, Nofiele J, Wodzak Staruch M, Szczepanski D, Williams NS, Laetsch T, Chopra R (2019) Longer heating duration increases localized doxorubicin deposition and therapeutic index in Vx2 tumors using MR-HIFU mild hyperthermia and thermosensitive liposomal doxorubicin. Int J Hyperthermia 36(1):196-203. https://doi.org/10.1080/02656736.2018.1550815

17. Zhu L, Partanen A, Talcott MR, Gach HM, Greco SC, Henke LE, Contreras JA, Zoberi I, Hallahan DE, Chen H, et al. (2019) Feasibility and safety assessment of magnetic resonance-guided high-intensity focused ultrasound (MRgHIFU)-mediated mild hyperthermia in pelvic targets evaluated using an in vivo porcine model. Int J Hyperthermia 36(1):1147-1159. https://doi.org/10.1080/02656736.2019.1685684

18. de Poorter J (1995) Noninvasive MRI thermometry with the proton resonance frequency method: study of susceptibility effects. MRM 34:359-367.

19. Chong WK, Papadopoulou V, Dayton PA (2018) Imaging with ultrasound contrast agents: current status and future. Abdom Radiol (NY) 43(4):762-772. https://doi.org/10.1007/s00261-018-1516-1

20. Frinking P, Segers T, Luan Y, Tranquart F (2020) Three Decades of Ultrasound Contrast Agents: A Review of the Past, Present and Future Improvements. Ultrasound Med Biol 46(4):892-908. https://doi.org/10.1016/j.ultrasmedbio.2019.12.008

21. Deprez J, Lajoinie G, Engelen Y, De Smedt SC, Lentacker I (2021) Opening doors with ultrasound and microbubbles: Beating biological barriers to promote drug delivery. Adv Drug Deliv Rev 172:9-36. https://doi.org/10.1016/j.addr.2021.02.015

22. Snipstad S, Sulheim E, de Lange Davies C, Moonen C, Storm G, Kiessling F, Schmid R, Lammers T (2018) Sonopermeation to improve drug delivery to tumors: from fundamental understanding to clinical translation.

Expert Opin Drug Deliv 15(12):1249-1261. https://doi.org/10.1080/17425247.2018.1547279

23. Snipstad S, Vikedal K, Maardalen M, Kurbatskaya A, Sulheim E, Davies CL (2021) Ultrasound and microbubbles to beat barriers in tumors: Improving delivery of nanomedicine. Adv Drug Deliv Rev 177:113847. https://doi.org/10.1016/j.addr.2021.113847

24. Allen TM, Cullis PR (2004) Drug delivery systems: entering the mainstream. Science 303:1818-1822.

25. Al-Jamal WT, Al-Ahmady ZS, Kostarelos K (2012) Pharmacokinetics & tissue distribution of temperature-sensitive liposomal doxorubicin in tumor-bearing mice triggered with mild hyperthermia. Biomaterials 33(18):4608-4617. https://doi.org/10.1016/j.biomaterials.2012.03.018

26. Needham D, Anyarambhatla G, Kong G, Dewhirst MW (2000) A new temperature-sensitive liposome for use with mild hyperthermia: characterization and testing in a human tumor xenograft model. Cancer Res 60:1197-1201.

27. Needham D, Dewhirst MW (2001) The development and testing of a new temperature-sensitive drug delivery system for the treatment of solid tumors. Adv Drug Deliv Rev 53:285-305.

28. Zagar TM, Vujaskovic Z, Formenti S, Rugo H, Muggia F, O'Connor B, Myerson R, Stauffer P, Hsu IC, Diederich C, et al. (2014) Two phase I dose-escalation/pharmacokinetics studies of low temperature liposomal doxorubicin (LTLD) and mild local hyperthermia in heavily pretreated patients with local regionally recurrent breast cancer. Int J Hyperthermia 30(5):285-294. https://doi.org/10.3109/02656736.2014.936049

29. Poon RT, Borys N (2011) Lyso-thermosensitive liposomal doxorubicin: an adjuvant to increase the cure rate of radiofrequency ablation in liver cancer. Future Oncol 7(8):937-945.

30. Tak WY, Lin SM, Wang Y, Zheng J, Vecchione A, Park SY, Chen MH, Wong S, Xu R, Peng CY, et al. (2017) Phase III HEAT study adding Lyso-Thermosensitive Liposomal Doxorubicin to Radiofrequency Ablation in patients with unresectable hepatocellular carcinoma lesions. Clin Cancer Res 24(1):73-83. https://doi.org/10.1158/1078-0432.CCR-16-2433

31. Lyon PC, Gray MD, Mannaris C, Folkes LK, Stratford M, Campo L, Chung DYF, Scott S, Anderson M, Goldin R, et al. (2018) Safety and feasibility of ultrasound-triggered targeted drug delivery of doxorubicin from thermosensitive liposomes in liver tumours (TARDOX): a single-centre, open-label, phase 1 trial. Lancet Oncol 19(8):1027-1039. https://doi.org/10.1016/s1470-2045(18)30332-2

32. Gray MD, Lyon PC, Mannaris C, Folkes LK, Stratford M, Campo L, Chung DYF, Scott S, Anderson M, Goldin R, et al. (2019) Focused Ultrasound Hyperthermia for Targeted Drug Release from Thermosensitive Liposomes: Results from a Phase I Trial. Radiology 291(1):232-238. https://doi.org/10.1148/radiol.2018181445

33. IKNL (2021) Breast cancer in the Netherlands, trends 1989 - 2020 based on data from the Netherlands Cancer Registry [Flyer IKNL, title translated from Dutch]. https://iknl.nl/getmedia/fe459c3a-c561-40de-b740-fff15997f020/IKNL-Folder-Borstkanker-2020.pdf. Accessed 15 February 2022

34. Ruiterkamp J, Ernst MF, de Munck L, van der Heiden-van der Loo M, Bastiaannet E, van de Poll-Franse LV, Bosscha K, Tjan-Heijnen VC, Voogd AC (2011) Improved survival of patients with primary distant metastatic breast cancer in the period of 1995-2008. A nationwide population-based study in the Netherlands. Breast Cancer Res Treat 128(2):495-503. https://doi.org/10.1007/s10549-011-1349-x

35. IKNL (2022) Incidence head and neck cancer [Title translated from Dutch]. https://doi.org/https://iknl.nl/kankersoorten/hoofd-halskanker/registratie/incidentie. Accessed 1 April 2022

36. Braakhuis BJ, Leemans CR, Visser O (2014) Incidence and survival trends of head and neck squamous cell carcinoma in the Netherlands between 1989 and 2011. Oral Oncol 50(7):670-675. https://doi.org/10.1016/j.oraloncology.2014.03.008

37. van der Kamp MF, van Dijk BAC, Plaat BEC, van der Laan B, Halmos GB (2021) To what extent has the last two decades seen significant progress in the management of older patients with head and neck cancer? Eur J Surg Oncol 47(6):1398-1405. https://doi.org/10.1016/j.ejso.2021.01.014

38. Leeman JE, Li JG, Pei X, Venigalla P, Zumsteg ZS, Katsoulakis E, Lupovitch E, McBride SM, Tsai CJ, Boyle JO, et al. (2017) Patterns of Treatment Failure and Postrecurrence Outcomes Among Patients With Locally Advanced Head and Neck Squamous Cell Carcinoma After Chemoradiotherapy Using Modern Radiation Techniques. JAMA Oncol 3(11):1487-1494. https://doi.org/10.1001/jamaoncol.2017.0973

39. Rohde M, Rosenberg T, Pareek M, Nankivell P, Sharma N, Mehanna H, Godballe C (2020) Definition of locally recurrent head and neck squamous cell carcinoma: a systematic review and proposal for the Odense-Birmingham definition. Eur Arch Otorhinolaryngol 277(6):1593-1599. https://doi.org/10.1007/s00405-020-05953-5

40. Stebbins KE, Morse CC, Goldschmidt MH (1989) Feline Oral Neoplasia: A Ten-Year Survey. Vet Pathol 26:121-128.

41. Hayes AM, Adams VJ, Scase TJ, Murphy S (2007) Survival of 54 cats with oral squamous cell carcinoma in United Kingdom general practice. J Small Anim Pract 48(7):394-399. https://doi.org/10.1111/j.1748-5827.2007.00393.x

42. Supsavhad W, Dirksen WP, Martin CK, Rosol TJ (2016) Animal models of head and neck squamous cell carcinoma. Vet J 210:7-16. https://doi.org/10.1016/j.tvjl.2015.11.006

43. Cannon C (2015) Cats, Cancer and Comparative Oncology. Veterinary Sciences 2(3):111-126. https://doi.org/10.3390/vetsci2030111

44. Wypij JM (2013) A naturally occurring feline model of head and neck squamous cell carcinoma. Patholog Res Int 2013:502197. https://doi.org/10.1155/2013/502197

45. de Bree R, Nieweg OE (2015) The history of sentinel node biopsy in head and neck cancer: From visualization of lymphatic vessels to sentinel nodes. Oral Oncol 51(9):819-823. https://doi.org/10.1016/j.oraloncology.2015.06.006

DANKWOORD

DANKWOORD

Op 1 oktober 2016 begon ik aan dit avontuur en nu is het dan eindelijk zover: mijn proefschrift is af! Mijn promotietijd was er één om nooit te vergeten, met veel pieken en dalen, tegenvallers en opluchting. Met het uitbreiden van mijn capaciteiten en vaardigheden waarbij mijn comfort zone toch steeds weer wat groter bleek te zijn dan ik dacht, veel interessante gesprekken en discussies en ook veel gezelligheid in de samenwerking met zoveel mensen uit uiteenlopende disciplines. Hoewel ik zes jaar geleden een heel ander boekje voor mij zag ben ik ontzettend trots op het eindresultaat. Dit alles was mij nooit gelukt zonder de hulp van heel veel mensen die direct en indirect betrokken waren en die ik allemaal van harte wil bedanken. Een aantal mensen wil ik hier in het bijzonder noemen.

Ten eerste mijn fantastische promotoren prof. dr. Elsken van der Wall en prof. Chrit Moonen.

Lieve **Elsken**, jij was voor mij de ideale supervisor. Het is inspirerend hoe jij ervoor kunt zorgen dat iedere PhD-student het beste uit zichzelf haalt, en hoe jouw doel is om anderen in de spotlight te zetten. Onze afspraken, altijd met chocola, begonnen steevast met de vraag hoe het met mij ging en als ik me goed voelde was jij tevreden. Daarnaast wist je altijd de juiste vragen te stellen zodat ik op ideeën kwam om ons onderzoek te verbeteren en kwam ook zelf met nieuwe ideeën (zoals het IKNL-project) als ik het even echt niet meer wist. Bedankt dat jij voor mij een voorbeeld was (en altijd zult blijven) als dokter, wetenschapper en supervisor!
Beste **Chrit**, ik wil jou ook van harte bedanken voor de samenwerking! Door onze verschillende achtergronden heb ik in jouw MR-HIFU groep heel veel geleerd over de technische kant van de geneeskunde. Jouw enthousiasme bij onze gesprekken over nieuwe toepassingen van bijvoorbeeld de combinatie van histotripsie met immuun checkpoint inhibitie was erg aanstekelijk. Ik had altijd het gevoel dat mijn inbreng door jou erg gewaardeerd werd. Zelfs tijdens je pensioen blijf je betrokken en bereikbaar voor advies. Jouw voorstel om te solliciteren voor de opleiding tot radiotherapeut zie ik als een groot compliment en dat ik nu in opleiding ben tot internist betekent niet dat ik niet graag nog eens meedenk!

Mijn twee geweldige copromotoren, dr. Roel Deckers en dr. Britt Suelmann.

Beste **Roel**, zonder jou was dit proefschrift er nooit gekomen. We hebben samen veel tegenslagen meegemaakt, en steeds weer kwam je met ideeën voor nieuwe onderwerpen en onderzoeken. Ik had niet kunnen denken dat ik als klinische dokter bleomycine zou zitten te pipetteren, de finesses van de meest optimale ultrageluidsparameters met jou zou bediscussiëren, vlees zou koken in de MRI of een vijftal katten als mijn patiënten zou

beschouwen. Jij bent de reden dat ik mijn comfort zone zo heb kunnen uitbreiden en dat ik zo'n breed beeld van de wetenschap heb kunnen krijgen. Daarnaast heeft jouw feedback mijn artikelen naar een hoger niveau getild. Ik vond onze discussies over de klinische toepassing van nieuwe technieken altijd erg inspirerend en was het erg gezellig om samen te kliederen en klussen bij de praktische experimenten. Bedankt voor alles!

Lieve **Britt**, jouw tomeloze energie heeft mij keer op keer weer versteld doen staan. Niet alleen ben je een heel goede betrokken klinische dokter, ook stort je je steeds weer met hart en ziel op verschillende klinische studies. Jij bent bij uitstek degene die de vertaalslag kan maken van een idee naar de klinische toepassing voor de patiënt. Zelfs naast het afronden van je eigen promotieonderzoek en je drukke leven was je altijd beschikbaar voor advies en leefde je mee met mijn successen en tegenslagen, hiervoor wil ik je heel hartelijk bedanken!

Ik wil alle co-auteurs die hebben meegewerkt aan de artikelen van dit proefschrift van harte bedanken, in het bijzonder Marianne Luyendijk, Maurice Zandvliet en mijn paranimf Charis Rousou.

Lieve **Marianne**, bedankt voor alle hulp bij het analyseren en interpreteren van de IKNL data! Zonder jou was het artikel nooit afgekomen en zeker niet zo goed geworden. Bedankt dat je zoveel geduld had met mij, als relatieve epidemiologie- en absolute R-leek!

Beste **Maurice**, bedankt dat je de samenwerking met ons vanuit de diergeneeskunde bent aangegaan! Je hebt mij een kijkje gegeven in de wereld van de diergeneeskunde, die vaak niet eens zoveel verschilt van de ziekenhuiswereld die ik gewend ben (maar toch ook weer wel). Hier heb ik heel veel van geleerd en ik ben het meest trots op het multidisciplinaire karakter van onze kattenstudie. Ook bedankt dat je tijdens je drukke werkzaamheden steeds weer informatie en foto's van de katten voor mij bleef verzamelen voor de studie. Daarnaast wil ik alle andere medewerkers van de diergeneeskunde (waaronder **Mauricio** en **Stefanie**) bedanken voor hun hulp bij de studie, en alle patiënteigenaren die ons het vertrouwen hebben gegeven om hun katten te laten deelnemen aan het onderzoek.

Mijn paranimfen Charis Rousou en Milou Smit. Wat fijn dat jullie aan mijn zijde staan op 26 januari!

Dear **Charis**, I know you are pretty much fluent in Dutch now, but English still feels like 'our' language. Thank you so much for everything you did for me during my Phd. You introduced me into the wondrous world of *in vitro* experiments and taught me everything I know about cell culture. I will never forget your method to practice working in the flowhood (practice while you're cooking). You were always so patient with me and your smart comments helped me improve our work. I enjoyed working together during our experiments and the coffees, dinners and trips we had (remember when we were literally blown away in

Rotterdam). I am looking forward to your own PhD-defense!

Milou, lieve vriendin, bedankt dat je mijn paranimf wil zijn! We kennen elkaar al zo lang en hoewel we al op de middelbare school andere studierichtingen op zijn gegaan zijn we toch allebei in een promotietraject beland. Het is zo fijn dat we altijd al onze frustraties en ergernissen over onze PhD-perikelen met elkaar konden en kunnen delen. Ik weet zeker dat jij ook binnenkort succesvol je proefschrift zal verdedigen!

Ik wil ook graag de leden van de beoordelingscommissie bedanken voor de beoordeling van dit proefschrift: **Prof. dr. S.C. Linn, Prof. dr. S. Siesling, Prof. dr. H.J. Bloemendal, Prof. dr. R. de Bree en Prof. dr. ir. C.A.T. van den Berg.** De opponenten wil ik alvast hartelijk bedanken voor hun aanwezigheid op 26 januari, ik kijk uit naar een interessante discussie.

Daarnaast wil mijn (oud-) collega's uit het UMC Utrecht van harte bedanken:

Al mijn kamergenoten in de loop der tijd **Annemarie, Bianca, Dhabia, Esmée, Gerke, Liselore, Ludwike, Marcia, Mimount en Suzanne** en ganggenoten **Caren, Frans en Margot,** bedankt voor jullie empathie, hulp, interesse en gezelligheid bij alle koffiemomentjes, wandelingen en etentjes (met of zonder pannenkoeken)! Mede dankzij jullie heb ik een heel fijne promotietijd gehad!
Ook de andere collega's van de Epirad-groep: bedankt voor de gezelligheid en interessante presentaties **Ahmed, Atia, Carlo, Floor, Jonas, Justine, Martina, Nienke, Robbert, Wieke, Wouter, Sander en Sarah.**
Natuurlijk mijn opvolger **Mirjam** die zo stoer was om mijn klinische projecten over te nemen. Je kreeg nogal een klus overgedragen, bedankt voor al je inspanningen om mijn "kindje" de i-GO studie verder te brengen. Ik heb er alle vertrouwen in dat het je gaat lukken om patiënten te includeren!
Bedankt voor de mede-mamma-onderzoekers voor het samen coördineren van de MDO's en de gezelligheid bij bijeenkomsten, cursussen en congressen: **Bianca, Carmen, Erwin, Janine, Jeanine, Lieke, Liselore, Maureen, Marilot en Susana.**

Bedankt aan iedereen met wie ik heb samengewerkt om de klinische studies van de grond te krijgen en met wie ik interessante gesprekken heb gehad over mogelijke toekomstige studies: **de leden van de trialbureaus van oncologie en beeld** (onder wie **Roelien Kronemeijer**)**, researchverpleegkundigen oncologie** (onder wie **Heleen Klein Wolterink**)**, mammaverpleegkundigen, apothekers, internist-oncologen** (onder wie **Karijn Suijkerbuijk** en **Lot Devriese**), radiologen (in het bijzonder **Manon Braat** voor je expertise over en begeleiding van de MR-HIFU borstkanker studies), chirurgen (onder wie **Thijs van Dalen** en **Arjen Witkamp**), radiotherapeuten (onder wie **Desirée van den Bongard**).

Bedankt voor jullie samenwerking als onderdeel van de MR-HIFU groep **Annemiek, Beatrice, Clemens, Helen** (ook voor de gezellige etentjes!), **Isabel, Kim** (ook voor het FACS-en!), **Suzanne** en **Megan.**

Bedankt aan alle collega's die proefpersoon wilden zijn om het MR-HIFU apparaat te testen en de MR-HIFU laboranten **Greet, Jørgen en Niels.**

Bedankt aan iedereen voor het hartelijke ontvangst voor het uitvoeren van de celexperimenten in het David de Wiedgebouw (waaronder **Cristina, Joep, Louis, Mies en Roel**), LTO-lab en in de COVID-tijd het LKCH-lab waar ik in de avonden en weekenden mijn toevlucht kon zoeken. **Corlinda** bedankt dat ik jullie microscoop mocht gebruiken.

Alice, Colette en Judith bedankt voor alle praktische ondersteuning!

I would like to thank **Profound Medical** and **Celsion Coorporation** for their cooperation in preparation for the clinical trials using the MR-HIFU system and ThermoDox.

Voor het financieren van mijn onderzoek wil ik het **KWF** hartelijk bedanken. Voor het mede-financieren gaat mijn dank uit naar de **Vrienden UMC Utrecht & Wilhelmina Kinderziekenhuis** (waaronder het Dirkzwager-Assink Fonds, de Louise Vehmeijer Stichting, de Schumacher-Kramer Stichting) en **het Center for Translational Molecular Medicine** (binnen de projecten VOLTAVALO en HIFU-chem).

Alle (oud-)collega's in het Diakonessenhuis Utrecht en het Radboudumc Nijmegen met wie ik samen heb gewerkt als ANIOS en sinds korts als AIOS interne terwijl ik daarnaast mijn promotie probeerde af te ronden: bedankt voor jullie steun, interesse en begrip en voor het feit dat jullie mij weer hebben laten thuis voelen in de kliniek na mijn onderzoeksjaren.

Mijn lieve vriendinnen wil ik bedanken, **Esther, Lisanne, Majsa, Mei-Jhi, Menke** en **Seline**, die altijd voor mij klaar stonden als alles even tegen zat en die altijd geïnteresseerd waren in waar ik mee bezig was. Bedankt voor alle gezellige thee-, eet-, borrel- en kletsmomenten samen! Daarnaast mijn fijne (oud-) tennisteam **dames 1 van Metgensbleek** die mijn hele promotietijd hebben meegemaakt en altijd geïnteresseerd waren. Net als de **Game-nighters** (no spam, vrees niet) **Elisa, Jeroen** en **Michiel** die mij tijdens de gezellige spelletjesavonden tot diep in de nacht met Monsters en dobbelstenen konden afleiden van METC's en ThermoDox houdbaarheidsdata.

Ook zonder de steun van mijn familie was ik nooit zover gekomen.

Lieve mama, bedankt dat je mij altijd hebt gesteund en gestimuleerd om te doen wat ik wilde en waar ik goed in was. Mijn creatieve kant heb ik aan jou te danken. Toen ik 30 werd vertelde je in je speech dat ik als baby liever nieuwsgierig de wereld in keek dan tegen de borst gedrukt werd, misschien zat mijn promotieonderzoek er toen al aan te komen.

Bedankt voor alle steun en liefde die je mij geeft, voor de gezelligheid en voor jouw mooie jurkjes die ik altijd mag overnemen (wie weet weer eentje voor de verdediging?).

Lieve papa, bedankt voor je rotsvaste vertrouwen in mij, dat ik alles kan bereiken wat ik wil. En voor je verontwaardiging wanneer iemand anders dat even niet ziet. Nu treed ik in je voetsporen als dr. de Maar en als internist in opleiding, en daar ben ik heel trots op (opa Egbert was dat vast en zeker ook geweest). Bedankt voor de internistische en wetenschappelijke genen (of opvoeding?), je interesse in mij, voor alle liefde, spontane dansjes en stevige knuffels. Wie weet een dansje wagen op de volgende internistendagen? En natuurlijk veel dank aan Plasgoed B.V.!

Lieve Saskia en Frans, wat zijn jullie allebei geweldige partners voor papa en mama. Jullie ook bedankt voor alle liefde, gezelligheid en steun de afgelopen jaren.

Lieve **Eduard, Juliette** en **Felice**, mijn lieve brussen, bij jullie kan ik altijd aankloppen voor gezelligheid, liefde en steun. We zitten altijd op één lijn en voelen altijd aan wat we bedoelen. Lieve Edu, blijf maar vaak een weekendje Utrecht boeken want hoe druk ik het ook heb maak ik daar altijd graag tijd voor vrij! Lieve Juul, wat hebben we het altijd gezellig samen, jij weet altijd wat ik bedoel als er gedoe is met een patiënt of als er andere doktersdilemma's spelen. Jij bent nu onze drs. de Maar en een hele goede! En Felice, mijn grote kleine zusje! Veel dank voor je hulp bij het ontwerpen van de kaft van dit boekje! Wat ben je toch creatief en wat was het gezellig om hier samen aan te werken!

De rest van mijn **familie** wil ik ook hartelijk bedanken voor alle geïnteresseerde vragen en ondersteunende woorden en daden inclusief mijn schoonouders **Albertina** en **Erik** en schoonopa **Jon** en-oma **An**. In het bijzonder mijn **lieve oma José** die altijd het meest trots van iedereen over haar borst strijkt bij elke mijlpaal. En mijn lieve nicht **Anouk**, we hebben het altijd zo gezellig samen en je bent altijd oprecht geïnteresseerd hoe het met mij gaat. Jouw scherpe maar liefdevolle psychologische analyses laten zelfs mij inzien dat het niet alleen aan mijzelf ligt wanneer ik niet op waarde wordt geschat.

Mijn liefste **Ron**, jij bent in al die jaren natuurlijk degene die dit promotietraject het meest intensief met mij heeft meegeleefd. Alle tegenslagen hebben we samen beleefd en alle mijlpalen hebben we samen gevierd. Zonder jouw steun weet ik niet hoe ik dit had moeten afronden, want jouw slimme en geïnteresseerde vragen, kalmerende woorden, liefdevolle knuffel en "komt wel goed schatje" zorgen dat ik altijd weer de zonnige kant kan zien. Bedankt dat je mijn momenten van stress en frustratie hebt geaccepteerd en altijd vertrouwen in mij hebt gehouden. Let maar op: nu krijgen we zeeën van vrije tijd!
Ik hou heel veel van je en ik kijk uit naar de rest van ons leven samen!

CURRICULUM VITAE

Josanne de Maar was born on March 3rd 1992 in Groningen, the Netherlands.

In 2009 she graduated cum laude from her pre-university education at Praedinius Gymnasium and started studying Medicine at University of Groningen.

After receiving her medical degree in 2015, she started working as a resident not in training (ANIOS) at the department of internal medicine of the Meander Medical Center in Amersfoort. In 2016 she started her PhD at the UMC Utrecht Division of Imaging and Oncology, focusing on optimizing drug delivery in oncology using imaging and therapeutic ultrasound, under supervision of professor Elsken van der Wall, professor Chrit Moonen, dr. Roel Deckers and dr. Britt Suelmann.

After working as a resident not in training (ANIOS) at the departments of internal medicine of the Diakonessenhuis in Utrecht and the Radboudumc in Nijmegen, she started her specialization in internal medicine in July 2022 at the Radboudumc in Nijmegen.

Josanne lives in Utrecht together with her partner Ron van Doorne.